

**PERFORMANCE OF GEOGRID REINFORCED GEO-  
BASE ISOLATION SYSTEM FOR SEISMIC  
PROTECTION OF LOW-RISE BUILDINGS**

*A THESIS*

*submitted by*

**DHANYA J S**

*for the award of the degree*

*of*

**DOCTOR OF PHILOSOPHY**



**GEOTECHNICAL ENGINEERING DIVISION  
DEPARTMENT OF CIVIL ENGINEERING  
INDIAN INSTITUTE OF TECHNOLOGY MADRAS**

**AUGUST 2019**

**Dedicated to**

*The Almighty*

*&*

*My mother*

## THESIS CERTIFICATE

This is to certify that the thesis titled “**PERFORMANCE OF GEOGRID REINFORCED GEO-BASE ISOLATION SYSTEM FOR SEISMIC PROTECTION OF LOW-RISE BUILDINGS**”, submitted by **Ms. DHANYA J S**, to the Department of Civil Engineering, Indian Institute of Technology Madras, Chennai, for the award of the degree of **Doctor of Philosophy** is a bona fide record of research work carried out by her under our supervision. The contents of this thesis, in full or in parts, have not been submitted and will not be submitted to any other Institute or University for the award of any degree or diploma.

**Dr. Boominathan A.**

Research Guide

Professor

Department of Civil Engineering

Indian Institute of Technology Madras

Chennai - 600 036, India

**Dr. Subhadeep Banerjee**

Research Guide

Associate Professor

Department of Civil Engineering

Indian Institute of Technology Madras

Chennai - 600 036, India

Chennai, India

**August, 2019**

## ACKNOWLEDGEMENTS

I thank IIT Madras for the great opportunity given to me to pursue doctoral studies in the GT division. I express my feelings of gratitude to Prof. Boominathan A and Dr. Subhadeep Banerjee for their motivating ideas, constant support, immense patience for long discussions, thoughtful feedback, meticulous comments, and their invaluable guidance throughout the research program.

With great respect, I express my thanks to Prof. G. Dodagoudar, Prof, S. R Gandhi, Prof. K Rajagopal, Prof. R. G. Robinson, Dr. T. Thyagaraj, Dr. Vidya Bhusham Maji, Dr. Dali Naidu Arnepalli, Dr. Ramesh Kannan K and Dr. Tarun Naskar for their constructive criticisms, suggestions, encouragement, and for inculcating a sense of responsibility and values in me during the various stages of this research program.

I would like to express my gratitude to my Doctoral Committee members Dr. Rupen Goswami, for his constant support and refreshing insights about this research program, Dr. Arun Menon for his valuable comments and words of encouragement during seminars and Prof. Sujatha C for her support and suggestions about the research. I express my sincere thanks to the present Head, Department of Civil Engineering, Prof. K. Ramamurthy, and the former heads Prof. A. Meher Prasad and Prof. S.R. Gandhi for facilitating my academic needs during the pursuit of my Ph.D. program.

I express my sincere thanks to all the lab staff, especially to Mr. Aravind Raj, Mr. Om Prakash K, Mr. Suresh P and Mr. Soundarapandian, for their inestimable help in the experimental work and test set-ups. The support from the Civil Engineering office is gratefully acknowledged. I thank Project Staff Mr. Sarvesh for his help during experimental work.

I am grateful to Ms. Dhanya Jaya and Ms. Daphne R for their care, moral support, technical guidance and encouragement in several ways and helping in making a better version of myself in the journey of friendship. My sincere gratitude to Ms. Anu Jose for her immense help from the start of course work till the end of the research.

My sincere appreciation to all my lab mates and friends at IIT Madras, Ms Vineetha , Mr Senthin Amuthan, Mr Ramon Varghese, Ms Vijaya Ramanathan, Ms Priya Beena Sudevan, Ms. Jyothsna, Mr. Prasanna and all other research scholars for the discussions and help rendered during different stages of my research work making my stay at IIT Madras memorable.



I thank my friends Mr. Siva Kumar, Mr. Sivaguru Prabhakaran, Ms. Surya, Ms. Sabrina and Mr. Maxwell for their constant motivation and support. I would also like to thank Ms. Anu Rachel and Ms. Anu V for their goodwill and motivation for the research. I would also like to thank Dr. Jayachandran K, Dr. Prabha Mohandoss, Mr. Nikhil John, Mr. Sunil Mohapatra, Mr. Nithin, Mr. Sowmyaranjan Mishra, Mr.Subramanyam and Mr. Ramesh for their technical support and guidance during the research.

My sincere appreciation to all my friends and fellow researchers at IIT Madras, Ms. Malavika, Ms. Swagathika, Mr. Sundaravel, Mr. Ashok, Ms. Reshma, Ms. Syamala, Mr. kumar, Mr. Sriram, Mr. Deepak Kamade and Mr. Suraj, for the discussions and help rendered during different stages of my research work. I am very delightful to acknowledge the support from the intern students, especially Angel Jessee and Prithika for their valuable contributions to this research study.

With deep respect, I express gratitude to my beloved mother Ms. Sunanda Kumari Thankachy for believing in my capabilities and her understanding and motivational words of courage to complete the research program. I want to thank everyone who ever said anything positive to me or taught me something.

**Dhanya J S**

## ABSTRACT

**Keywords:** Geo-base isolation, Sand rubber mixture, Geogrid, Model test, Finite element analysis, SSI, Seismic settlement, Interstorey drift.

Earthquakes can bring devastating effects to life and structures. Earthquake damages to the buildings can be minimized by incorporating engineering interventions that could improve the flexibility of the building. Introducing base isolation systems like laminated rubber bearings, elastomeric bearing and friction pendulum can reduce the intensity of earthquake waves reaching the superstructure of the building to a great extent. Although in developed nations such seismic isolation systems are quite commonly used for building structures in the seismic prone areas, in case of developing countries, base isolation is limited mostly to important buildings such as hospitals, schools, etc. However, ordinary residential and commercial buildings remain vulnerable to the destructive effects of ground motions. The common masses of developing and underdeveloped nations necessarily need a method and means to protect their houses from the earthquakes given that the existing seismic isolation systems are expensive and need skilled installation. On the other side, the generation of scrap rubber tyres and its disposal is a severe environmental problem. A single shot solution to the above issues of earthquake hazard, unavailability of an affordable & effective seismic isolation system, rapid generation of scrap rubber tyres would be by incorporating an engineered layer made of sand scrap tyre rubber mixed with sand below the foundation level acting as a simple alternative to conventional base isolation system. The novel seismic isolation system made of the sand-rubber mixture (SRM) hereafter called as Geo-Base Isolation (GBI) system acts as a seismic filter medium below the building foundation reducing the intensity of seismic waves passing through it by energy dissipation and damping.

The present study explores the performance of GBI under static and dynamic loading using laboratory tests, scaled model tests and FEM-based numerical studies for its application for low-rise buildings considering geogrid reinforced and unreinforced conditions. In the first part of this study, the static and dynamic characterization of SRM was carried out to assess its suitability for seismic base isolation of low-rise buildings. The scrap rubber tyre tailored to fine size were mixed with poorly graded sand in various gravimetric proportions. The static shear strength is determined using direct shear test and monotonic triaxial shear tests under consolidated drained & undrained conditions while the dynamic shear properties were assessed using cyclic triaxial tests under consolidated undrained conditions. The results of laboratory tests show that SRM with 30% rubber (gravimetric) mixtures possess adequate static and

dynamic properties required for seismic isolation of low-rise buildings. However, the settlement of SRM arising due to initial compressibility of rubber could pose a problem for building foundations.

The GBI system should possess adequate dynamic stiffness and damping properties, as well as enough shear strength to resist both static and seismic loads. To address the settlement issue of SRM geogrid reinforcement was introduced within the GBI system. The second part of the study focuses on the use of geogrid reinforcement to improve the bearing capacity, settlement and rotational aspects of shallow foundation resting on GBI layer under static loading. Load tests were carried out on a model footing resting on GBI layer with and without geogrid reinforcement in a sand-bed tank setup. A finite element based numerical modelling of the footing on the GBI system with geogrid was also carried out and the computed results were compared with that measured from the experiments. Parametric studies were carried out using the developed finite element model to arrive at an optimum thickness of GBI layer, number of geogrid layers, depth of placement of first geogrid and length of geogrids. The results from the study indicate that the bearing capacity of GBI layer can be increased up to three times by providing double layered geogrid reinforcements with a substantial reduction in settlement.

Once the static performance of geogrid reinforced GBI system was found to be satisfactory, 2D FE analysis was carried out to explore the seismic performance of a two-storied building supported on raft footing resting on geogrid reinforced GBI system. The typical soil profile and seismic loads recommended by design codes for the seismically active Indo-Gangetic plain region of India was considered. The seismic response of the GBI layer under free field condition and with the building structure was studied. Effect of various factors such as the thickness of GBI layer, frequency content & peak ground acceleration of earthquake input motions on the seismic performance of the framed structure resting on geogrid reinforced GBI system was investigated. From the analysis, the double layered geogrid system with a spacing of  $0.05B$  (where  $B$  is the footing width) was found to be effective for settlement reduction of GBI layer under static and seismic loading conditions. It was found that for the geogrid reinforced GBI system with a thickness of  $0.1B$  to  $0.2B$ , an overall 30% to 40% reduction of peak ground acceleration can be achieved. Furthermore, the shear force and interstory drift developed in the building decreased by around 50% and 20% respectively, for the geogrid reinforced GBI layer compared to the non-isolated system. Based on the study, a novel geosynthetic reinforced GBI layer is proposed for base isolation of symmetric low-rise framed building in the seismically active Indo-Gangetic plain region of India.

## TABLE OF CONTENTS

<b>ACKNOWLEDGEMENTS.....</b>	<b>I</b>
<b>ABSTRACT .....</b>	<b>III</b>
<b>TABLE OF CONTENTS.....</b>	<b>V</b>
<b>LIST OF FIGURES.....</b>	<b>XI</b>
<b>LIST OF TABLES.....</b>	<b>XIX</b>
<b>NOTATIONS AND ABBREVIATIONS.....</b>	<b>XXI</b>
<b>1. INTRODUCTION .....</b>	<b>1</b>
1.1. BACKGROUND .....	1
1.2. EARTHQUAKE DAMAGES IN INDIA .....	3
1.3. CONCEPTS OF BASE ISOLATION.....	4
1.4. CRITERIA FOR BASE ISOLATION .....	7
1.5. CONVENTIONAL BASE ISOLATION .....	8
1.6. GEO-BASE ISOLATION .....	9
1.7. SIGNIFICANCE OF THE STUDY .....	11
1.8. OBJECTIVES AND SCOPE.....	12
1.9. RESEARCH METHODOLOGY .....	13
1.10. ORGANIZATION OF THE THESIS.....	13
<b>2. LITERATURE REVIEW .....</b>	<b>16</b>
2.1. INTRODUCTION .....	16
2.2. SAND RUBBER MIXTURES FOR GEOTECHNICAL APPLICATIONS.....	16
2.3. CONVENTIONAL BASE ISOLATION SYSTEMS.....	18
2.3.1. Background.....	18
2.3.2. Base isolation systems .....	19
2.4. BASIC PROPERTIES OF SAND-RUBBER MIXTURES.....	21
2.4.1. Environmental implications of scrap tyre.....	22

2.4.2.	Basic properties of scrap tyre derived materials .....	23
2.5.	SHEAR STRENGTH RESPONSE OF SAND RUBBER MIXTURES .....	26
2.5.1.	Effect of rubber inclusion .....	31
2.5.2.	Effect of confining pressure.....	32
2.5.3.	Effect of size/type of rubber .....	33
2.6.	SEGREGATION OF SAND RUBBER MIXTURE.....	34
2.7.	DURABILITY AND DEGRADATION OF TYRE SHREDS AND CREEP .....	34
2.8.	DYNAMIC PROPERTIES OF SAND RUBBER MIXTURE .....	36
2.8.1.	Measurement of dynamic properties by low strain tests .....	36
2.8.2.	Measurement of dynamic properties by medium and high strain tests ...	39
2.8.3.	Liquefaction susceptibility of sand rubber mixtures .....	42
2.9.	GEO-MATERIALS IN VIBRATION ISOLATION.....	43
2.10.	EXPERIMENTAL STUDIES ON DYNAMIC RESPONSE OF FOOTINGS RESTING ON SAND RUBBER MIXTURE LAYER.....	45
2.11.	NUMERICAL STUDIES ON SEISMIC SSI ANALYSIS OF BUILDINGS ON SAND RUBBER MIXTURE LAYER.....	47
2.12.	GEOSYNTHETIC REINFORCED SOIL FOUNDATIONS .....	52
2.13.	SUMMARY .....	56
<b>3.</b>	<b>CHARACTERISATION OF MATERIALS USED .....</b>	<b>58</b>
3.1.	INTRODUCTION .....	58
3.2.	MATERIALS .....	59
3.2.1.	Soil .....	59
3.2.2.	Scrap rubber tyre.....	60
3.2.3.	Sand rubber mixture (SRM) .....	61
3.3.	DRY UNIT WEIGHT .....	62
3.3.1.	Minimum dry unit weight.....	63
3.3.2.	Maximum dry unit weight .....	63
3.3.3.	Relative density .....	67
3.3.4.	Segregation check .....	68
3.4.	SHEAR STRENGTH .....	69

3.4.1. Direct shear test .....	70
3.4.2. Monotonic Triaxial Test .....	76
3.5. CYCLIC TRIAXIAL TEST .....	84
3.5.1. Test setup and procedure .....	84
3.5.2. Cyclic behaviour of SRM .....	85
3.6. GEOGRIDS .....	89
3.7. SUMMARY .....	92
<b>4. STATIC RESPONSE OF FOOTING ON GEOGRID REINFORCED GBI SYSTEM.....</b>	<b>94</b>
4.1. INTRODUCTION .....	94
4.2. MODEL TEST .....	95
4.2.1. Scale factor for geometry and materials .....	95
4.2.2. Experimental setup .....	97
4.2.3. Sample preparation .....	98
4.2.4. Test procedure and test program.....	101
4.2.5. Behaviour of footing resting on geo-base isolation layer .....	103
4.2.6. Behaviour of footing resting on geogrid reinforced geo-base isolation layer .....	103
4.3. FE MODELLING AND ANALYSIS .....	107
4.3.1. Model description .....	107
4.3.2. Element type .....	108
4.3.3. Constitutive models .....	109
4.3.4. Interface modelling.....	111
4.3.5. Boundary conditions and modelling procedure .....	112
4.4. VALIDATION OF FE RESULTS WITH EXPERIMENTAL RESULTS .....	113
4.5. PARAMETRIC STUDIES .....	114
4.5.1. Effect of depth of placement of top geogrid .....	115
4.5.2. Effect of length of geogrid.....	116
4.5.3. Effect of number and spacing of reinforcement .....	117
4.5.4. Strain distribution across the geogrids.....	119

4.5.5. Surface deformation in the reinforced GBI system .....	120
4.5.6. Effect of embedment depth of footing .....	121
4.6. SUMMARY .....	123

## **5. DYNAMIC FE MODELLING AND ANALYSIS OF A LOW-RISE**

### **BUILDING RESTING ON GEOGRID REINFORCED GBI SYSTEM.....124**

5.1. INTRODUCTION .....	124
5.2. PROBLEM STATEMENT .....	125
5.2.1. Seismicity of the region considered .....	126
5.2.2. Geotechnical properties .....	128
5.2.3. Superstructure details .....	128
5.2.4. Foundation details .....	130
5.3. FE MODELLING AND ANALYSIS .....	131
5.3.1. FE meshing and element types .....	132
5.3.2. Constitutive models and material properties .....	132
5.3.3. Damping mechanism .....	138
5.3.4. Boundary conditions .....	139
5.3.5. Input motion .....	140
5.3.6. Analysis .....	142
5.4. VALIDATION OF THE NUMERICAL ANALYSIS WITH 1G SHAKE TABLE STUDIES (BANDYOPADHYAY ET AL. 2015) .....	143
5.5. SEISMIC SETTLEMENT OF GBI SYSTEM WITH GEOGRID REINFORCEMENT .....	144
5.6. SEISMIC RESPONSE OF FRAMED STRUCTURE RESTING ON GEOGRID REINFORCED GBI LAYER .....	147
5.6.1. Free field response .....	148
5.6.2. Framed structure response .....	153
5.6.3. Shear force and inter-storey drift .....	163
5.7. SUMMARY .....	165

<b>6. CONCLUSIONS AND RECOMMENDATIONS .....</b>	<b>168</b>
6.1. SUMMARY .....	168
6.2. CONCLUSIONS .....	169
6.2.1. Static and cyclic response of SRM .....	169
6.2.2. Static response of model footing resting on geogrid reinforced GBI layer .....	170
6.2.3. Seismic response of a low-rise building resting on geogrid reinforced GBI system .....	171
6.3. RECOMMENDATIONS FOR FUTURE STUDIES .....	172
 <b>REFERENCES .....</b>	 <b>174</b>
<b>LIST OF PUBLICATIONS BASED ON THIS THESIS .....</b>	<b>199</b>
<b>DOCTORAL COMMITTEE .....</b>	<b>200</b>
<b>CURRICULUM VITAE .....</b>	<b>201</b>





## LIST OF FIGURES

<b>Figure 1.1</b> Seismicity map of India from 2474 BC to 2012 AD (Raghukanth and Kavitha 2014).....	2
<b>Figure 1.2</b> Building collapse in Ahmedabad due to Bhuj earthquake 2001 (source: <a href="https://www.nicee.org/Bhuj.php">https://www.nicee.org/Bhuj.php</a> ) .....	4
<b>Figure 1.3</b> Base isolation principle <b>(a)</b> Conventional building <b>(b)</b> Isolated building (Mayes and Naeim 2001) .....	5
<b>Figure 1.4</b> Base isolation effects on <b>(a)</b> period lengthening <b>(b)</b> relative displacement between ground and structure and damping (Naeim and Kelly 1999).....	6
<b>Figure 1.5</b> Effects of base isolation for different soil conditions (Ealangi 2010) .....	7
<b>Figure 1.6</b> Typical base isolation below buildings(source: <a href="https://en.wikipedia.org/wiki/Base_isolation">https://en.wikipedia.org/wiki/Base_isolation</a> ).....	9
<b>Figure 1.7</b> Geo-base isolation below foundation for earthquake protection .....	11
<b>Figure 1.8</b> Flowchart showing the research methodology adopted.....	15
<b>Figure 2.1</b> Typical elastomeric bearing system with force-displacement relationship (Li et al. 2013).....	19
<b>Figure 2.2</b> Advanced elastomeric systems with high damping <b>(a)</b> Lead rubber bearing (Yazici 2014) <b>(b)</b> High damping rubber bearing (Bridgestone catalogue) ....	20
<b>Figure 2.3</b> Schematic of <b>(a)</b> Flat sliding bearing system <b>(b)</b> friction pendulum isolator bearing (Ealangi 2010) .....	21
<b>Figure 2.4</b> Influence of rubber content on the shear strength of sand matrix (Zornberg et al. 2004).....	27
<b>Figure 2.5</b> Consolidated drained triaxial test on SRM (55% relative density) <b>(a)</b> deviatoric stress–strain response <b>(b)</b> volumetric strain response (Zornberg et al. 2004).....	28
<b>Figure 2.6</b> Zonation of SRM based on rubber content <b>(a)</b> Mashiri et al. (2015) <b>(b)</b> Perez et al. (2016).....	31

<b>Figure 2.7</b> Peak deviatoric stress at failure for varying rubber content as reported in the literature (Perez et al. 2016) .....	32
<b>Figure 2.8</b> Segregation of tire chips and sand due to high gradation gap (Mashiri 2014).....	35
<b>Figure 2.9</b> Variation of shear modulus and damping ratio with shear strain for SRM with different rubber content at confining pressure of 345 kPa (Feng and Sutter 2000) .....	36
<b>Figure 2.10</b> The effect of sand fraction (sf) on the low strain shear modulus ( $G_{max}$ ) of SRM (Lee et al. 2007) .....	37
<b>Figure 2.11</b> Shear modulus and damping curves for SRM (5% rubber content) at different confining pressures (Senetakis et al. 2012) .....	39
<b>Figure 2.12</b> Variation of damping ratio with shear strain for SRM with different rubber contents (Nakhaei et al. 2012) .....	40
<b>Figure 2.13</b> Effect of rubber content (RF) on the damping ratio for SRM with different $D_{50, rubber}/D_{50, sand}$ ratio for a confining pressure of 50 kPa (Li et al. 2016).....	41
<b>Figure 2.14</b> Foundation isolation using smooth synthetic liner (Yegian and Kadakal, 2004).....	44
<b>Figure 2.15</b> Schematic view of the shake table setup using SRM isolator (Xiong and Li 2013) .....	46
<b>Figure 2.16</b> Shake table tests on model footing resting on SRM layer (Bandyopadhyay et al. 2015).....	47
<b>Figure 2.17</b> Direct method configuration for modelling of SSI system (Gharehbaghi et al. 2012).....	49
<b>Figure 2.18</b> Normalized footing horizontal acceleration time histories (Tsang et al. 2007).....	50
<b>Figure 2.19</b> Finite element model of the soil–foundation–structure system (Tsang et al. 2012).....	51

<b>Figure 2.20</b> FE model of the soil–structures systems (Pitilakis et al. 2015) .....	52
<b>Figure 2.21</b> Model test setup of geosynthetic reinforced soil footing (Abu-Farsakh et al. 2013).....	54
<b>Figure 2.22</b> Numerical model of geosynthetic-reinforced cushioned pile (Xu and Fatahi 2018b).....	56
<b>Figure 3.1 (a)</b> Mechanical sieve shaker used for grain size analysis <b>(b)</b> Particle size distribution curve of sand and granulated tyre .....	60
<b>Figure 3.2</b> Samples of <b>(a)</b> Sand <b>(b)</b> Granulated rubber <b>(c)</b> SRM.....	62
<b>Figure 3.3</b> Vibratory table test setup with surcharge .....	64
<b>Figure 3.4</b> Variation in maximum dry unit weight with surcharge increment .....	65
<b>Figure 3.5</b> Calibration chart for relative density of sand using pluviation technique .....	68
<b>Figure 3.6</b> Segregation checks before and after subjected to vibration .....	69
<b>Figure 3.7</b> Experimental setup for the direct shear test.....	71
<b>Figure 3.8</b> Variation of shear stress with horizontal displacement for sand/SRM (normal stress=50 kPa; relative density=65%). .....	72
<b>Figure 3.9</b> Variation of volumetric strain with horizontal displacement for sand/SRM (normal stress=50 kPa; relative density=65%). .....	73
<b>Figure 3.10</b> Influence of rubber content on the shear strength of SRM (relative density- 80%) .....	74
<b>Figure 3.11</b> Influence of relative density on the shear strength of SRM .....	75
<b>Figure 3.12</b> Sample preparation <b>(a)</b> tools used <b>(b)</b> spit mould & rubber membrane to hold the sample.....	79
<b>Figure 3.13 (a)</b> Prepared SRM sample <b>(b)</b> No evidence of segregation .....	79
<b>Figure 3.14</b> Triaxial test setup.....	80
<b>Figure 3.15</b> Deviator stress-axial strain curves of sand and SRM (30% rubber) for drained conditions .....	81

<b>Figure 3.16</b> Volume change behaviour of sand and SRM (30% rubber) under different confining pressures.....	82
<b>Figure 3.17</b> Deviator stress-axial strain curves of SRM (30% rubber) for undrained conditions .....	83
<b>Figure 3.18</b> Excess pore water pressure curves under different confining pressures for SRM (30% rubber).....	83
<b>Figure 3.19</b> Cyclic triaxial test setup.....	85
<b>Figure 3.20</b> Hysteresis loop of SRM for different cycles of loading (30% rubber content).....	86
<b>Figure 3.21</b> Shear modulus and damping ratio calculation from hysteretic loop (Kramer 1996).....	87
<b>Figure 3.22</b> Shear modulus degradation curve for different proportions of SRM .....	88
<b>Figure 3.23</b> Damping curves for different proportions of SRM .....	88
<b>Figure 3.24</b> Geogrid reinforcement used for the study .....	90
<b>Figure 3.25</b> SRM-geogrid interaction study using direct shear test.....	91
<b>Figure 3.26</b> Variation of shear stress with horizontal displacement for sand/SRM with geogrids .....	91
<b>Figure 4.1</b> Photograph of the test setup.....	97
<b>Figure 4.2</b> Schematic of the experimental setup .....	98
<b>Figure 4.3 (a)</b> Model footing on GBI layer <b>(b)</b> Aluminium sheet box used to prepare the GBI layer .....	100
<b>Figure 4.4</b> Geogrid reinforcement used for the GBI system .....	101
<b>Figure 4.5</b> GBI layer and sand bed with the model footing .....	102
<b>Figure 4.6</b> Bearing Pressure-Settlement ratio response for footing with and without GBI layer .....	104

<b>Figure 4.7</b> Bearing pressure-settlement ratio curve for geogrid reinforced GBI system ( $T_{GBI}=0.5B$ ).....	104
<b>Figure 4.8</b> Variation of bearing capacity factor ( $I_f$ ) with settlement ratio for geogrid reinforced-GBI system .....	105
<b>Figure 4.9</b> Variation of strain developed in the geogrids with depth of GBI.....	106
<b>Figure 4.10</b> Finite element model showing geometry and boundary conditions of geogrid reinforced GBI system .....	108
<b>Figure 4.11. (a)</b> 4-node reduced integration elements <b>(b)</b> 2-node beam elements (ABAQUS, 2014).....	109
<b>Figure 4.12 (a)</b> Drucker-Prager yield surface in the stress space (Cervera et al. 2015) <b>(b)</b> Typical yield surface for the Drucker Prager model in the deviatoric plane (ABAQUS, 2014) .....	111
<b>Figure 4.13</b> Typical Surface to surface interface configuration (ABAQUS, 2014).....	112
<b>Figure 4.14</b> Comparison of bearing pressure to settlement ratio as obtained from numerical study with experimental results.....	114
<b>Figure 4.15</b> Effect of the depth of placement of first geogrid on bearing capacity improvement factor ( $I_f$ ) .....	115
<b>Figure 4.16</b> Effect of length of geogrid on the bearing capacity improvement factor ( $I_f$ ) .....	117
<b>Figure 4.17</b> Effect of number of layers ( $N$ ) and spacing of geogrid on bearing capacity improvement factor ( $I_f$ ) .....	118
<b>Figure 4.18</b> Effect of number of layers ( $N$ ) and spacing of geogrid on bearing capacity improvement factor ( $I_f$ ) .....	119
<b>Figure 4.19</b> Variation of surface heave with settlement for GBI layer and sandy layer .....	121
<b>Figure 4.20</b> Influence of embedment depth on the bearing capacity .....	122
<b>Figure 5.1</b> Schematic of the soil-structure system with geogrid reinforced GBI layer..	126

<b>Figure 5.2</b> Indo-Gangetic plain region (source: www.iitk.ac.in/gangetic/intro_gallerie/subsurface_indo-gang) .....	127
<b>Figure 5.3</b> Details of typical soil profile for the Indo-Gangetic plain region .....	129
<b>Figure 5.4</b> Details of the building structure-footing system.....	129
<b>Figure 5.5.</b> Details of the framed structure analysis.....	130
<b>Figure 5.6</b> Finite element model of the soil-structure system with the proposed GBI layer .....	133
<b>Figure 5.7</b> Modulus reduction curves for non-plastic soils under varying confining pressure (Ishibashi 1992) .....	134
<b>Figure 5.8</b> FE mesh for triaxial test simulation.....	136
<b>Figure 5.9</b> Hyper-elastic model validations for SRM (30% rubber content) under varying confining pressure .....	136
<b>Figure 5.10</b> Constitutive model adopted for geogrid behaviour .....	137
<b>Figure 5.11 (a)</b> Geometry of typical infinite element (Bettess 1980) <b>(b)</b> Infinite element used in ABAQUS 2D model .....	139
<b>Figure 5.12</b> Acceleration-time histories of earthquakes <b>(a)</b> 2015 Nepal ( $M_w=7.8$ ) <b>(b)</b> 2009 Andaman ( $M_w=7.8$ ) <b>(c)</b> 2011 Sikkim ( $M_w=6.9$ ) <b>(d)</b> 2001 Bhuj ( $M_w=7.7$ ) <b>(e)</b> 2016 Myanmar ( $M_w=6.9$ ) .....	142
<b>Figure 5.13</b> Comparison of response spectra as obtained in the present study with that reported by Bandyopadhyay et al. (2015) for <b>(a)</b> GBI layer <b>(b)</b> sand layer. ....	145
<b>Figure 5.14.</b> Seismic settlement of the footing subjected to the 2015 Nepal earthquake motion ( $M_w=7.8$ ; PGA=0.14g) .....	146
<b>Figure 5.15</b> Maximum mobilized tensile force along the top geogrid layer (2015 Nepal earthquake, $M_w=7.8$ ; PGA=0.14g).....	147
<b>Figure 5.16</b> Schematic of different points considered for the analysis output.....	148

<b>Figure 5.17</b> Acceleration-time history <b>(a)</b> below GBI layer at $R$ <b>(b)</b> middle of GBI layer at $Q$ <b>(c)</b> ground surface at $P$ <b>(d)</b> ground surface at $P$ for GBI with geogrids (2015 Nepal earthquake, $M_w=7.8$ ; PGA=0.14g) .....	150
<b>Figure 5.18</b> Transfer functions: <b>(a)</b> below GBI layer at $R$ , <b>(b)</b> middle of GBI layer at $Q$ , and <b>(c)</b> ground surface at $P$ (2015 Nepal earthquake, $M_w=7.8$ ; PGA=0.14g).....	152
<b>Figure 5.19</b> Response spectra at the ground surface at $P$ for the 2015 Nepal earthquake ( $M_w=7.8$ ; PGA= 0.14g).....	153
<b>Figure 5.20</b> Acceleration time history at the footing top for the 2015 Nepal earthquake ( $M_w=7.8$ ; PGA= 0.14g) .....	154
<b>Figure 5.21</b> Response spectra at the footing top for the 2015 Nepal earthquake ( $M_w=7.8$ ; PGA= 0.14g) .....	155
<b>Figure 5.22</b> Hysteresis loop for GBI isolated and non-isolated system: <b>(a)</b> $T_{GBI}$ of 0.05B <b>(b)</b> $T_{GBI}$ of 0.1B (2015 Nepal earthquake) .....	157
<b>Figure 5.23</b> Response spectra at the top of footing for unreinforced natural soil and reinforced GBI system <b>(a)</b> low & medium frequency earthquakes <b>(b)</b> high frequency earthquakes (scaled PGA=0.24g).....	160
<b>Figure 5.24</b> Response spectra at the top of footing for different PGA (2009 Andaman earthquake, $M_w=7.8$ ) .....	162
<b>Figure 5.25</b> Base shear ratios for different earthquakes for the building (scaled) .....	163





## LIST OF TABLES

<b>Table 2.1</b> Classification of shredded tyre in civil engineering (ASTM D6270-08 2012).	23
<b>Table 2.2</b> Basic properties of SRM from the past studies .....	25
<b>Table 2.3</b> Comments on the shear strength of SRM from past studies .....	29
<b>Table 3.1</b> Properties of sand and rubber tyre .....	62
<b>Table 3.2.</b> Details of minimum unit weight of the materials .....	63
<b>Table 3.3</b> Maximum dry unit weight values obtained from different methods.....	67
<b>Table 3.4</b> Details of maximum unit weight of the materials.....	67
<b>Table 3.5</b> Summary of the direct shear test results for sand and SRM .....	76
<b>Table 3.6</b> Properties of geogrid .....	90
<b>Table 4.1</b> Scale factors used for the model test (Wood, 2004; Viswanadham and Konig, 2004) .....	96
<b>Table 4.2.</b> Details of model tests carried out.....	102
<b>Table 4.3</b> Material properties used in the FE analysis .....	110
<b>Table 5.1.</b> Effect of thickness of GBI layer on peak spectral acceleration and predominant period (Scaled 2015 Nepal earthquake, $M_w=7.8$ ; PGA= 0.24g) .....	156
<b>Table 5.2.</b> Effect of peak acceleration on predominant frequency of input motions (scaled PGA=0.24g) at the top of the footing .....	161
<b>Table 5.3.</b> Effect of peak spectral acceleration on predominant frequency of input motions (scaled PGA=0.24g) at the top of the footing .....	161
<b>Table 5.4.</b> Maximum inter-storey drift of the building for different earthquake motions.....	164
<b>Table 5.5.</b> Rotation of the building .....	165



## NOTATIONS AND ABBREVIATIONS

$B$	width of the footing (m)
$b_{\text{GBI}}$	width of the GBI layer (m)
$C$	damping matrix
$c$	cohesion
$d$	deformation at the surface
$d_j, d_{j+1}$	lateral deflection in the $j^{\text{th}}$ & $(j+1)^{\text{th}}$ storey of the building
$E$	Young's modulus
$E_{\text{slip}}$	tolerance parameter
$F$	yield function
$f$	predominant frequency
$\text{GBI}_r$	reinforced geo-base isolation
$\text{GBI}_{ur}$	unreinforced geo-base isolation
$H$	building storey height
$I_f$	bearing capacity improvement factor
ID	inter-storey drift
$K$	stiffness matrix
$k$	stress ratio at the yield point
$L$	length of geogrid
$N$	number of geogrid layers
$M$	mass matrix
$M_w$	moment magnitude of earthquake

$N$	number of blows from SPT
$SIF_a, SIF_{sa}$	seismic isolation factors
$P$	first invariant of stress
$q$	Von Mises equivalent stress
$q_o$	bearing pressure of the unreinforced soil foundation
$q_r$	bearing pressure of the reinforced soil foundation
$r$	third invariant of deviatoric stress
$S_{ur}$	natural soil
$s$	settlement of footing
$T_{GBI}$	thickness of GBI layer (m)
$V_s$	shear wave velocity (m/sec)
$u$	depth of placement of first geogrid below the footing
$x$	distance from footing
$\mu$	interaction friction coefficient
$\sigma$	normal stress
$\tau$	shear strength
$D^{el}$	tangent elasticity matrix
$d\varepsilon^{el}$	rate of change of elastic strain
$\varepsilon^{el}$	elastic strain
$I_1, I_2$ and $I_3$	strain invariants
$\sigma_i$	principal Cauchy stresses
$\lambda_i$	principal stretch ratio
$p$	hydrostatic stress
$\alpha, \beta$	Rayleigh coefficients

$\zeta$	damping ratios
$\omega_i$	frequencies for different modes
$\phi$	angle of internal friction
$\Omega$	electrical resistance

# CHAPTER 1

## INTRODUCTION

### 1.1. BACKGROUND

Earthquake is an unpredictable catastrophe, the consequence of which brings loss of lives and properties on an immense scale. Developing nations bear the aftermaths for a longtime to recover from the socio-economic damages. Globally, most of the seismic activities occur in and around the Pacific belts, the Mid-Oceanic Ridge belts and the Alpine Himalayan belts. The Alpine-Himalayan belt which is the collision boundary between the Indian plate and the Eurasian plate runs from Indonesia through the mountains of south-east Asia including the Himalayan belt via Iran and joins the Atlantic Ocean. South Asian countries like India, Pakistan, Nepal, Bhutan and Bangladesh are highly seismic prone due to the tremendous stress held in the Alpine-Himalayan belt and the Indo-Burmese Andaman Arc, which is a subduction boundary.

The Indian subcontinent, with its complex geology, can be subdivided into the Himalayas, the Indo-Gangetic plain, and the peninsular region wherein more than 60% of the country falls under moderate to high seismic zones (Jain 2016). The Himalayan region formed by the collision between Eurasian and Indian tectonic plate is the melting pot of prolific seismicity with two major earthquakes of magnitude ( $M_w$ ) above 8 (1934 Nepal-Bihar earthquake,  $M_w=8.4$ ; 1950 Assam-Tibet earthquake,  $M_w=8.6$ ) and six earthquakes of magnitude range 7  $M_w$  to 8  $M_w$  of which two occurred in 2015 since the 1900s (Bilham 2019). The Himalayan frontal thrust and main central thrust consisting of potential seismic zones could trigger future earthquakes (Kattri 1987; Bilham and England 2001). Besides, extensive liquefaction was reported in the north-eastern part of India during the 1950 Assam earthquake (Raghukanth 2008).

The Indo-Gangetic plains, with its proximity to the Himalayas and a dense population, falls under zone IV and V (IS 1893 Part 1 2016) posing a severe seismic risk for impending earthquake in the future making it one of the biggest concerns for the engineering society in India. The past earthquakes in the Indo-Gangetic plain and the surrounding Himalayan regions, such as the 1905 Kangra ( $M_w=8.6$ ), 1950 Assam ( $M_w=8.7$ ), 1988 Bihar-Nepal ( $M_w=6.9$ ), 2005 Kashmir ( $M_w=7.6$ ), 2015 Hindu Kush ( $M_w=7.5$ ), etc. show the seismicity of the region. The peninsular region of India, the major part of which falls under zone II and III (IS 1893 Part 1 2016) shows relatively less

seismic activity. However, the region has witnessed devastating earthquakes like the 1967 Koyna ( $M_w=6.6$ ), 1993 Latur ( $M_w=6.2$ ) and the 2001 Bhuj ( $M_w=7.7$ ) earthquakes in the past. Figure 1.1 shows the seismicity map of India from 2474 BC to 2012 AD, as reported by Raghukanth and Kavitha (2014). Lately, earthquakes such as the 2015 Nepal earthquake ( $M_w=7.8, 7.3$ ), 2015 India-Pakistan earthquake ( $M_w=7.8$ ), 2011 Gangtok-Sikkim earthquake ( $M_w=7.8$ ), have raised the alarm about the severity of seismic activities taking place in the Indian subcontinent. The movement of Indian tectonic plates at a rate of 47 mm/year towards the Eurasian plate further shows the inevitability of mega earthquakes the area in the coming future.

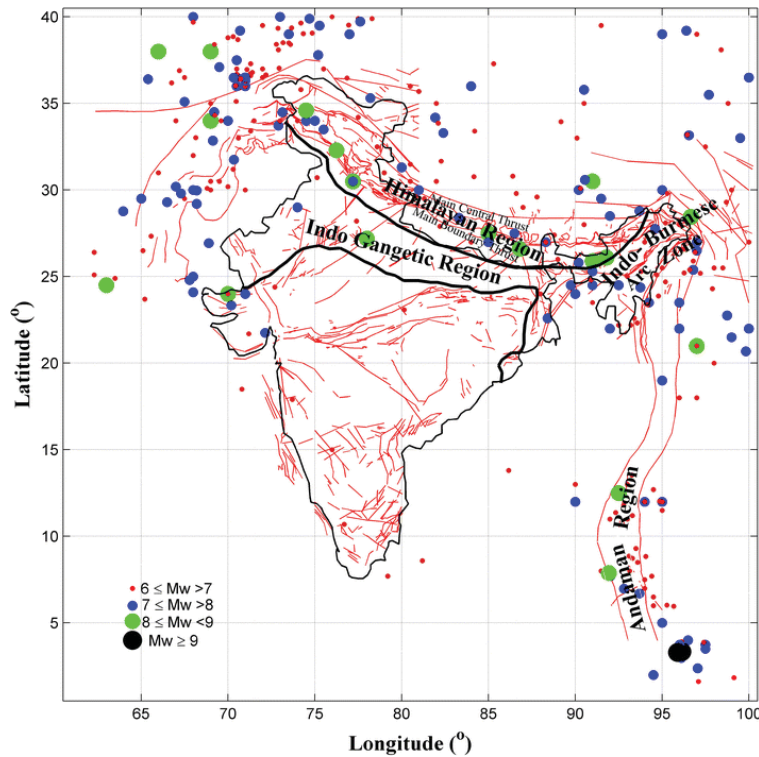


**Figure 1.1** Seismicity map of India from 2474 BC to 2012 AD (Raghukanth and Kavitha 2014)

Demographically, India is the second largest population the world with 1.3 billion people, with more than half the population living in the Indo-Gangetic plain region comprising of cities like New Delhi (second most populous city in the world) and Kolkata. A massive population of about 125 million in the Indo-Gangetic plain region ([www. censusindia.gov](http://www.censusindia.gov).) with a high rate of population growth together with active seismic faults (Dasgupta et al. 1987; Goswami et al. 2009) and proximity to the Himalayan seismicity means high seismic risk. Besides, the basin effect arising from thick soil sediments increases the ground amplification potential in the region (Bagchi



and Raghukanth 2019). Furthermore, buildings poorly adhering to earthquake design practices further add to the vulnerability to earthquake hazards, inevitably leading to huge loss of life and property in the event of an earthquake. Consequently, it is essential to look into the seismic protection of buildings through efficient and low-cost engineering interventions against earthquake disaster.

## **1.2. EARTHQUAKE DAMAGES IN INDIA**

Though the extent of the damage for any earthquake primarily depends on the earthquake input motion characteristics, characteristics of soil and the building add to the seismic vulnerability. The earthquake-related casualties are very high in developing nations due to building collapse. The 2015 Nepal earthquake ( $M_w=7.8$ ) in the Himalayan belt caused a casualty of around 9000 people with more than 600,000 houses usually made of brick fully damaged. The 2001 Bhuj earthquake ( $M_w=7.7$ ) is important for the earthquake engineering community in India, due to the high death involved (13,805 persons) with the collapse of rural buildings made of the masonry wall. Further, Ahmedabad (230 km from the epicenter of Bhuj earthquake) experienced around 130 such buildings collapse of multi-storey reinforced concrete frame buildings (Figure 1.2). The 1993 Latur earthquake ( $M_w=6.2$ ) killed around 7635 persons wherein 52 villages having houses made of rubble masonry and heavy roofs wholly razed to the ground. In all the above cases, it is underlined that the poor construction practice and lack of earthquake safety measures are the primary reason for building damage.

An estimated 330 million housing units exist in India as per the 2011 Census of India of which about two-thirds of the housing are low-rise buildings in the rural area. About 30% of these rural houses are located in earthquake zones IV and V as per BMTPC (2019). The aftermaths of 2001 Bhuj earthquake and the 2015 Nepal earthquake has helped to create awareness to the local population for the need of earthquake safety by reconstruction initiatives and training classes to engineers and masons by government and NGOs towards a safer building. Though countries like Japan and the US have gone a long way in earthquake resilient structures, in India, the focus is still on providing earthquake resistant construction practices. There exist a huge gap and potential for the country to implement the advanced techniques/ concepts for building safety. However, the practicality of implementation in rural India and cost efficiency is the biggest challenge.



**Figure 1.2** Building collapse in Ahmedabad due to Bhuj earthquake 2001 (source: <https://www.nicee.org/Bhuj.php>)

### **1.3. CONCEPTS OF BASE ISOLATION**

Over the past few decades, much emphasis is given on the construction of earthquake-resistant buildings based on structural control concepts. Seismic resistant structures were designed through increasing the strength and stiffness of structural elements to withstand earthquake-generated inertial forces on the building. Though the strengthening method leads to safeguarding the structure from collapse at, the functionality of the structure after an earthquake cannot be guaranteed due to excessive damages. An alternative strategy is to decouple the structure from the footing to minimize the intensity of the strong earthquake vibrations transmitted into the structure (Webster 1994) through base isolation techniques. Seismic base isolation systems reduce the magnitude of energy transferred to the structure by shifting the natural period of the structure such that the peak earthquake spectral acceleration value zone is crossed. Further, base isolation increases the damping of the system through the process of energy dissipation by which the spectral displacement also gets reduced (Christopoulou and Filiatrault 2006).

The fundamental concept of base isolation is to decouple the structure from the footing to minimize the intensity of the earthquake vibrations transmitted into the structure (Kelly 2002). Base isolation system ideally introduces energy dissipating flexible elements between the superstructure and foundation to lower the effect of ground motions on the superstructure. In a conventional and rigid

system where the superstructure is fixed to the foundation (zero period), when subjected to ground motion, the structure experiences a displacement equal to the ground displacement and acceleration equal to the ground motion acceleration thereby forcing the structure to experience considerably large inertial force. However, in the isolated base system, ground displacement and accelerations are reduced to a high degree enabling the protection of the structural elements above the isolation plane (Booth and Key 2006). The basic performance of the conventional building and base isolated building in an earthquake event is depicted in Figure 1.4. In the base isolated system, the reduction in the seismic demand limits the shear deformation as well as inter-storey drift developed in the building.

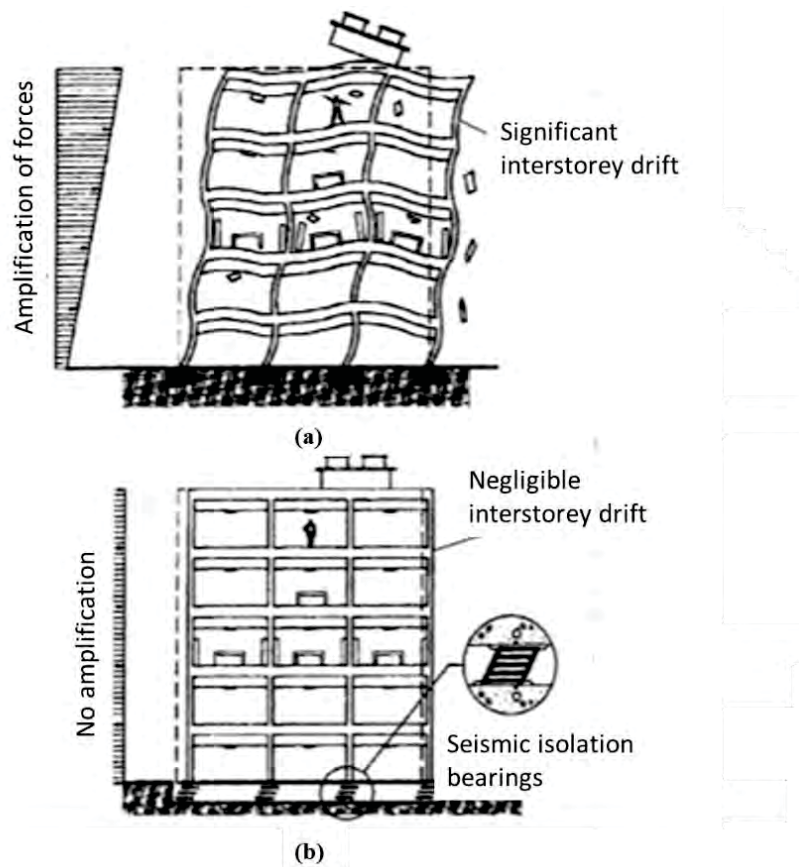


**Figure 1.3** Base isolation principle (a) Conventional building (b) Isolated building (Mayes and Naeim 2001)

Seismic isolation systems reduce the magnitude of energy transferred to the structure by shifting the natural period of the structure beyond the peak earthquake spectral acceleration zone, as shown in Figure 1.5a. The natural period of the isolated system thus becomes higher than that of the fixed-

base system (Naeim and Kelly 1999). The shift in the natural frequency of the structure was induced by the low horizontal stiffness of base isolation elements installed between the structure and the foundation. The increased natural period due to base isolation results in reduced seismic force and spectral acceleration on the structure. Further, seismic isolation increases the damping of the system through the process of energy dissipation for typical earthquake shaking (Christopoulos and Filiatrault 2006), as shown in Figure 1.5b. It should be noted that though the increase in the period increases the lateral displacement of the structure, increasing the damping of the isolation system can bring down the lateral displacement significantly.

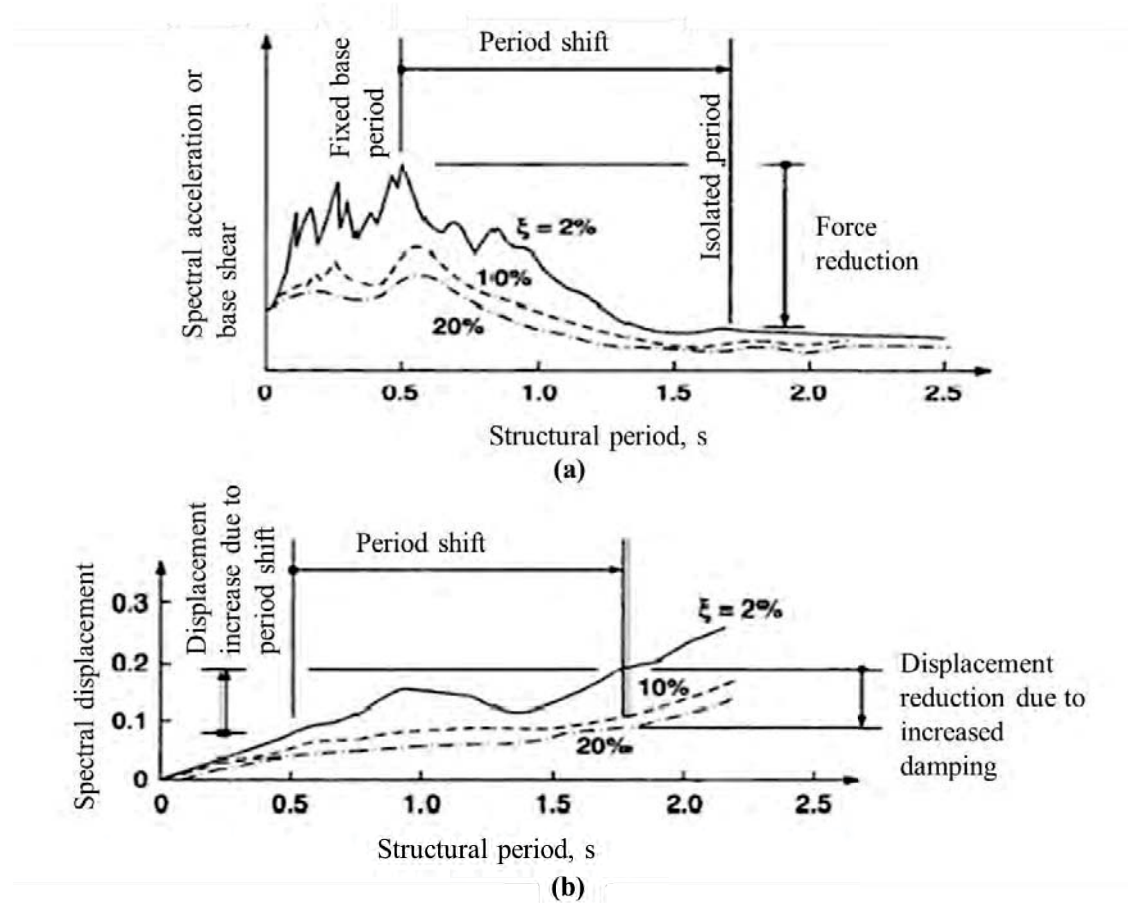


**Figure 1.4** Base isolation effects on (a) period lengthening (b) relative displacement between ground and structure and damping (Naeim and Kelly 1999)

Further, the performance of the base isolation system is influenced by the type of supporting soil medium. Base-isolated structures are usually designed neglecting the soil-structure interaction (SSI) effects. Studies have found that the SSI effect has a significant influence on the dynamic

characteristics of base isolated structures, which in turn affect its seismic response and isolation efficiency (Novak and Henderson 1989; Kelly 1991). Typically, base isolation systems are ideal for buildings supported on stiff soils. In soft soils, the period lengthening of base isolators results in increased seismic demand due to the influence of SSI (Ealangi 2010) as shown in Figure 1.6.

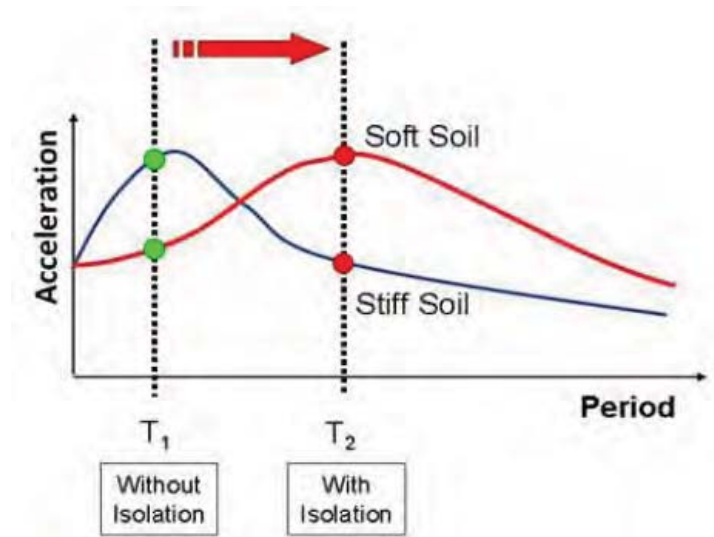


**Figure 1.5** Effects of base isolation for different soil conditions (Ealangi 2010)

#### 1.4. CRITERIA FOR BASE ISOLATION

The base isolation systems should satisfy four major criteria for its effective performance in the field conditions as follows (Booth and Key 2006):

- a) Horizontal flexibility for period lengthening of the building without compromising on the vertical stiffness
- b) Sufficient damping to reduce relative deformations beyond the capacity of the isolator bearings at the plane of isolation
- c) Adequate stiffness to resist wind loads
- d) Minimal residual horizontal deflection of the building relative to the ground after the earthquake shaking.

The horizontal flexibility is induced to the building system by providing rubber bearings and sliding bearings at the isolation plane. The reduction in horizontal stiffness increases the natural period of the system such that amplification of ground motion and seismic forces in the building is reduced, thereby minimizing structural and non-structural damages. The horizontal flexibility at

the foundation level ensures that the structure experience rigid body motion above the isolation plane, enabling the functionality of the building after an earthquake. Practically, base isolation systems provide only partial isolation since the building should have adequate lateral stiffness to resist wind loads. In any case, the vertical stiffness of the system should be high enough to limit static deformations. Generally, damping is included in the isolation system in the form of hysteresis damping, Coulomb friction damping and viscous damping. The high damping enables the base isolator to absorb the seismic energy reducing the energy transmission beyond the isolation plane along with controlling large lateral displacements. In addition, an ideal isolation system should have enough restoring force to recover from plastic deformations. The rubber bearings such as the conventional laminated rubber bearings and high damping rubber bearings are endowed with the self-centring capacity limiting the permanent displacement and residual deformations after an earthquake even (Medeot et al. 2004).

## **1.5. CONVENTIONAL BASE ISOLATION**

In general, the base isolation systems are classified into two categories, namely the elastomeric bearing systems and sliding bearing systems. The widely used elastomeric bearings involve the use of natural rubber bearings, lead rubber bearings and high-damping rubber bearings. Base isolation system that uses rubber bearings bifurcates the foundation and structure by introducing flexibility and damping, which in turn absorbs the high amount of seismic waves (Derham et al. 1985). In this approach, a layer of low horizontal stiffness is interposed between the structure and the foundation to decoupled it from the horizontal components of the earthquake ground motion (Figure 1.3). This layer gives the structure a fundamental frequency that is much lower than its fixed-base frequency and also much lower than the predominant frequencies of the ground motion. Such isolation works when the system is linear and even when undamped; however, some damping is beneficial to suppress any possible resonance at the isolation frequency. The second basic type of isolation system is the sliding and frictional system that works by limiting the transfer of shear across the isolation interface. Such gravity-based isolation systems like the popular friction-pendulum system use unique interfacial materials sliding on stainless steel. The sliding mechanisms usually adopt a concave siding surface acting as a natural restoring mechanism. The energy dissipaters placed under the structure can reduce the earthquake force by 40-60% (Zhou et al. 1990). Further, the base isolation system can be coupled with dampers (oil, steel or rubber) for



energy dissipation within the structural elements. Advanced techniques of base isolation are successful and ensure seismic protection and sustainability to buildings.



**Figure 1.6** Typical base isolation below buildings(source:[https://en.wikipedia.org/wiki/Base\\_isolation](https://en.wikipedia.org/wiki/Base_isolation))

The era of seismic isolation buildings started after the devastating 1995 Kobe earthquake ( $M_w=6.9$ ) in Japan. Ever since, developed nations like the USA, China, Russia, Italy and New Zealand frequently started to implement base isolation systems to avoid casualties arising from earthquake damages to buildings. Unlike the developed nations where this practice is highly successful, in developing countries, seismic isolation techniques are implemented only to bridges and structures of strategic importance. The production complexity, costly installation procedures and high degree of preciseness and massive weight is a significant challenge in its implementation of such base isolation systems for ordinary construction. Most of the low and medium raised residential buildings have been left to be seismically vulnerable due to poor construction practices and limited seismic protection methods even in highly seismic active zones pushing the need for a low-cost alternative for seismic protection of buildings.

## **1.6. GEO-BASE ISOLATION**

A simple and robust alternative to conventional base isolation can be attained by incorporating damping into the soil up to a certain depth. By this method, the partial energy dissipation happens within the soil itself before the vibrations reach the foundation and the superstructure. Compacted sand layers are often used as an energy dissipating layer (Xiao et al. 2004). However, as the availability of sand for the construction industry is reducing lately, green and eco-friendly

utilization of industrial leftovers, waste tyres from vehicles and other polymeric waste materials have found interesting applications in the civil engineering field. Generation of scrap rubber tires and their free disposal is a severe environmental problem. Annual waste tyre generation in the world is about 13.5 million tons out of which only a subtle percentage is recycled. Recycled and shredded scrap tyres are used in the geotechnical field for embankment fill, retaining walls backfill and as drainage layer in landfills.

One of the main applications of scrap tyre with rubber as its principal component is its utility in vibration isolation (Hazarika et al. 2008, Kaneko et al. 2013). A possible solution to the above problems of earthquake hazard, unavailability of an affordable, effective seismic isolation system, rapid generation of scrap rubber tyres and exploiting the excellent damping property of rubber tires, would be to consider sand-rubber tire shred mixtures as a vibration mitigation solution. The present study aims to utilize a control proportion of sand and rubber tyre scrap mixture as a possible base isolation material below building foundation hereafter referred to as Geo-Base Isolator (GBI) system. This novel seismic isolation layer acts similar to conventional base-isolators in attenuating the intensity of earthquake waves reaching the structure in the foundation level itself, as shown in Figure 1.7. The bulk reuse of scrap tyre would also reduce the pollution hazards related to stockpiling of scrap tyres.

The potential use of the sand-rubber mixture (SRM) as geotechnical seismic isolation layer beneath building foundations was proposed by Tsang (2007). Use of shredded scrap tyre-sand mixtures placed below the foundation as earthquake protection layer was found to partially dissipate earthquake energy before it propagates to the foundation (Tsang et al. 2012; Xiong and Li 2013; Pitilakis et al. 2015). Apart from reducing the level of shaking in the horizontal direction, the distinctive advantage of the method is that it also significantly reduces the shaking level in the vertical direction Tsang et al. (2007). Similar studies on the use of sandbags and synthetic liners as energy-absorbing layers for seismic protection underneath foundation were carried out by Yegian et al. (2004), Jain et al. (2004) and Ansari et al. (2011) confirming lesser accelerations experienced by the structure as compared to the fixed base structures. Pitilakis et al. (2015) noted that the effectiveness of SRM layers is predominant for mid-rise buildings in terms of reduction in design shear force and displacement. Limited studies on shaking-table experiments conducted by Xiong and Li (2013) and Bandyopadhyay et al. (2015) with shredded rubber–soil mixtures (SRM) as isolation material placed below concrete block further confirms the suitability of SRM for



seismic isolation. Previous studies have reported the increase in damping ratio of SRM with increment in rubber content (Hazarika et al. 2010; Anastasiadis et al. 2012; Senetakis et al. 2012) and low liquefaction potential (Hazarika et al. 2007; Kaneko et al. 2013; Mashiri et al. 2016). The high elastic nature of rubber present in SRM combined with high durability and non-biodegradability makes it a sustainable alternative for costly base isolation techniques.

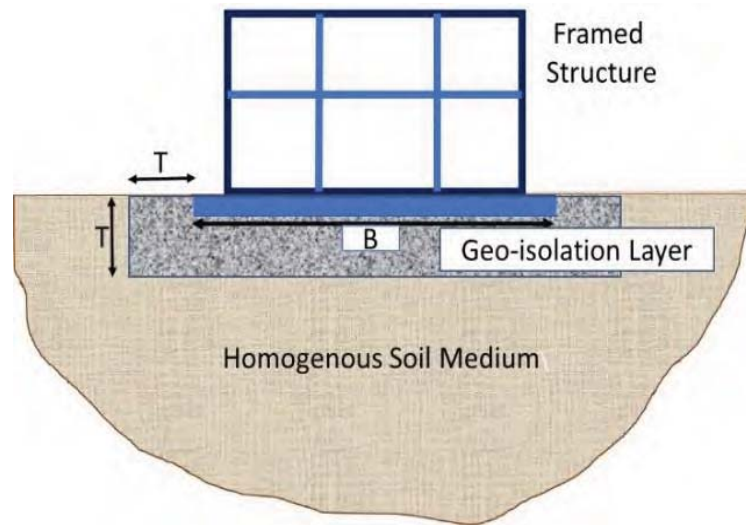


**Figure 1.7** Geo-base isolation below foundation for earthquake protection

## 1.7. SIGNIFICANCE OF THE STUDY

The existing works on SRM focus on the laboratory characterization of material with varying amount and size of the rubber. However, there is no conclusive study on the optimum percentage of sand-rubber shreds mixture which gives reasonable shear modulus with a satisfactory damping ratio for a wide range of strain ideal for its application as seismic isolation material. Limited studies reported on the use of SRM as a vibration-absorbing layer for buildings focus on idealized soil conditions with little emphasis on site-specific cases considering earthquakes of varying peak ground acceleration (PGA) and frequency content (Tsang et al. 2012; Xiong and Li 2013; Pitilakis et al. 2015). The static performance of buildings placed on the GBI system was also not addressed well. Further, the settlement problems posed by the low stiffness of SRM were not given adequate attention. Additionally, the influence of Soil-Structure Interaction (SSI) on the performance of the base-isolated building was not satisfactorily considered in most of the studies. Though few researchers carried out SSI studies on footing resting on SRM layer in the homogeneous soil

medium, studies on the influence of SSI on the performance of such seismic-isolated buildings for multi-layered soil system were limited.

In view of this, it is essential to conduct laboratory investigations to identify the static and dynamic response of SRM. Experimental studies needed to be carried out for arriving at the optimum percentage of SRM that has enough stiffness and energy dissipation capacities. Similarly scaled model tests can give a clear idea about the performance of footing resting on GBI systems. Settlement aspect of foundation on SRM layer may be of primary concern. Use of geosynthetic reinforcement in improving the bearing capacity and settlement performance of GBI was not studied in the past. Further, numerical tools can give better clarity about the various factors influencing the performic of GBI systems. A rigorous dynamic analysis using the advanced FEM tools and extensive parametric studies need to be carried out to quantify the behaviour of geogrid reinforced GBI system considering the loading and materials factors along with characteristics of earthquake input motion, GBI layer and stratification of the ground.

## **1.8. OBJECTIVES AND SCOPE**

The main objectives of the present research are:

- 1) To study the bearing capacity-settlement response of shallow foundation resting on GBI layer with and without geogrid reinforcement
- 2) To study the seismic SSI response of low-rise building supported on raft foundation resting on GBI layer with and without geogrid reinforcement

The scopes of the work are limited to:

- 1) Characterization of SRM using routine lab tests, monotonic and cyclic triaxial tests
- 2) Laboratory model tests on footing resting on GBI layer with and without geogrid reinforcement subjected to static loading
- 3) 2D FE modelling of footing resting on GBI layer with and without geogrid reinforcement subjected to static load using ABAQUS
- 4) 2D Dynamic FE modelling of a typical low-rise building (A-4 type as per NBC, 2016) resting on GBI layer with and without geogrid reinforcement using ABAQUS considering SSI

- 5) Parametric studies on various factors affecting the static and seismic response of geogrid reinforced GBI system using developed FE models

## **1.9. RESEARCH METHODOLOGY**

The research methodology is designed to meet the objectives formulated for the study using laboratory tests and numerical analysis, as shown in Figure 1.8. Initially, the material properties of SRM were studied using laboratory tests to identify the optimum proportion of SRM suitable for seismic isolation purpose. Direct shear tests and monotonic triaxial tests were carried out to understand the static response of SRM while cyclic triaxial tests were carried out to explore the dynamic material characteristics of SRM. Laboratory model tests and numerical studies were later carried out to understand the static performance of an isolated model footing resting on the proposed GBI layer with and without geosynthetic reinforcement. Finite element based numerical studies were carried out considering the various parameters of geosynthetic reinforcement to achieve maximum bearing capacity with a reduced settlement for the footing. Further numerical studies were undertaken to explore the dynamic soil-structure interaction response of a typical low-rise building resting on the geosynthetic reinforced GBI system. The seismic settlement analysis was carried out to optimize the geosynthetic reinforcement parameters, and the seismic response of framed structure resting on geosynthetic reinforced GBI system was analyzed considering various factors affecting its performance. The experimental programs that are developed to achieve the research objectives are discussed in Chapters 3 and 4, while the numerical studies carried out are presented in Chapters 4 and 5.

## **1.10. ORGANIZATION OF THE THESIS**

This PhD thesis is organized into six chapters. The present chapter provides an introduction to the research problem highlighting the significance and need for the study based on which the objective and scope of the work were framed. An overview of the research methodology was also discussed.

Chapter 2 provides a detailed overview of the general concepts and trends in base isolation systems and the applicability of seismic isolation using SRM. A critical review of the previous work done on the engineering and dynamic material properties of SRM was also carried out. The available literature on the scaled model studies and numerical studies of SRM as geo-base isolation material

was analyzed to identify the challenges and research gaps in the utilization of SRM for seismic isolation purpose. Further, the past studies the performance of geosynthetics as a reinforcing material and was also explored to identify its applicability with SRM

In this context, Chapter 3 discusses the material characterization of SRM using basic laboratory test. The maximum and minimum density of the material for different proportions of SRM was also detailed. The static response was identified using direct shear test to arrive at optimum rubber content. The monotonic response of SRM was identified using and triaxial test while the dynamic response was studied using cyclic triaxial test. Further, the basic properties of geogrids utilized were also studied.

Chapter 4 focuses on the laboratory-based model tests that were carried out to study the load-settlement behaviour of footing resting on geogrid reinforced GBI layer. Numerical simulation of the response of the footing resting on geogrid reinforced GBI layer was carried out using finite element (FE) code ABAQUS 6.14 (2014). Validation of the numerical procedure was done by comparing the numerical results with that of experimental results. A detailed FE analysis was carried out to establish the optimum parameters of the geosynthetic reinforcement, to achieve adequate bearing capacity and settlement characteristics of the footing resting on the GBI system.

In Chapter 5, to comprehend the seismic response of the geogrid reinforced GBI system, SSI based FE model was developed using ABAQUS 6.14 (2014) considering a conventional low-rise building-foundation system resting on soil/GBI layer. The accuracy of the numerical modelling procedure was confirmed by comparing the FE results with the results of laboratory shake table tests on SRM by Bandyopadhyay et al. (2015). The seismic settlement aspect of GBI system with and without the presence of geogrid reinforcement was explored initially. Parametric studies were carried out to address the influence of the thickness of GBI layer, frequency content and PGA of earthquake input motions on the seismic response of the structure placed on the geogrid reinforced GBI layer.

Chapter 6 summarizes the conclusions of each objective drawn from this study along with recommendations and scope for future research.

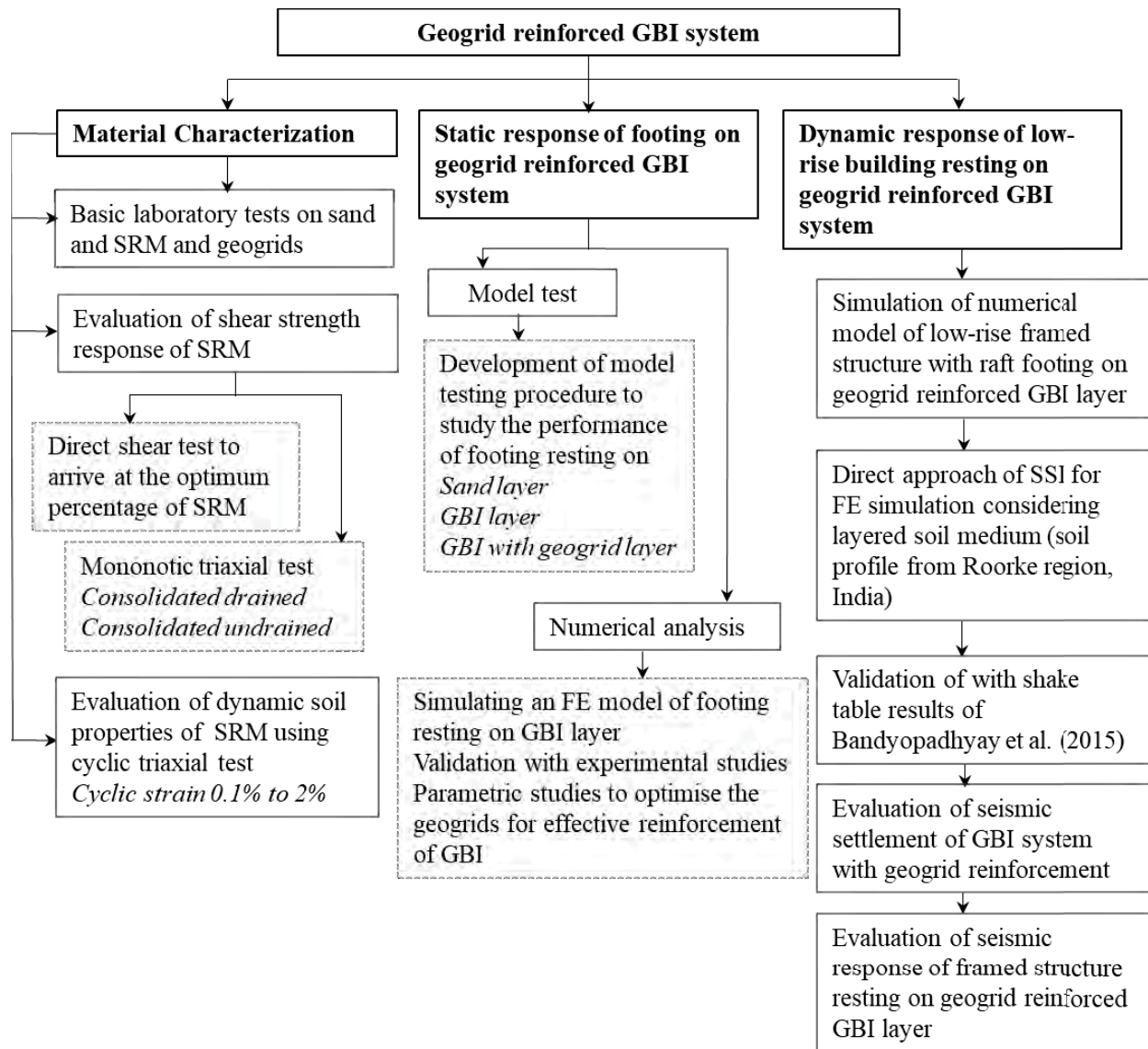


**Figure 1.8** Flowchart showing the research methodology adopted

## **CHAPTER 2**

### **LITERATURE REVIEW**

#### **1.1. INTRODUCTION**

In the current chapter, a critical review of the seismic isolation mechanism using Sand Rubber Mixture (SRM) was explored by discussing the static and dynamic response of the material along with recent trends on the applicability of SRM for seismic isolation purposes. Initially, the typical base isolation systems widely used for earthquake protection of structures were discussed. The two significant aspects of SRM, namely the engineering properties and the dynamic properties were reviewed in detail. Previous research on the static behaviour of SRM was assessed considering the index properties, shear strength, compressibility, monotonic behaviour and durability of SRM. The dynamic aspect of SRM was then discussed considering the low & high strain cyclic behaviour of the material along with probable liquefaction susceptibility. Following this, a review on the past research on the general application of geomaterials, including SRM in vibration mitigation was carried out. The existing numerical and shake table studies and its limitations on the utilization of SRM as a seismic isolator for building problems were then reviewed from the past and recent literature. Finally, the general application of geosynthetic reinforcement for foundation problems and the factors influencing its performance under static and dynamic loading were discussed. Recent studies on the interaction mechanism between geosynthetics and SRM were also discussed in this chapter.

#### **1.2. SAND RUBBER MIXTURES FOR GEOTECHNICAL APPLICATIONS**

For the past three decades, ground improvement techniques using engineered soils have gained much attention in the research community and field applications. Industrial by-product wastes, building demolition debris, industrial pollutants like flyash & pondash and plastic wastes were quite commonly used to create the engineered soil with better strength properties. The engineered soil acts as a way of disposing of the otherwise environmentally problematic pollutants into the ground. The scrap tyre products such as tyre shreds, chips and aggregates have found its way into the civil engineering field since the 1990s (Humphrey and Manion 1992). By and large, the unrecycled scarp tyre known as ‘black pollutant’ (Xiong and Li 2013) poses global pollution due

to its sheer volume. However, the scrap tyres were found to be an excellent additive to soil mainly due to its non-biodegradability.

In the geotechnical field, the tyre derived geomaterials have witnessed rapid growth in applications such as lightweight landfills, backfilling of retaining walls, buried pipeline and as ground improvement material for highway embankments (Humphrey and Manion 1992; Ahmed and Lovell 1993; Edil and Bosscher 1994; Bosscher et al. 1997; Masad et al. 1996; Rowe and McIsaac 2005; Karmokar 2007; Hazarika et al. 2010; Li et al. 2016). Lately, scrap tyre aggregates were used in concrete due to high durability and lightweight of rubber (Adamu and Uche 2014). The low unit weight of tyre derived engineered soil helps in minimising the lateral earth pressure exerted on retaining walls (Humphrey and Sandford 1993, Kaneda et al. 2007, Tsoi and Lee 2011) and reduces settlement in buried pipelines, caisson walls & embankments (Bosscher et al. 1997, Edeskar 2006; Hazarika et al. 2006). The high hydraulic conductivity of tyre derived aggregates enables utilization as filter layers for drainage purposes (Reddy and Saichek 1998). Further, the reinforcement property of tyre shreds is beneficial for slope stability and landslide problems (Poh and Broms 1995; Garga and O'Shaughnessy 2000; Abichou et al. 2004; Uchumira et al. 2007).

One of the main applications of scrap tyre with rubber as its principal component is its utility in vibration isolation (Hazarika et al. 2008, Kaneko et al. 2013). In recent times, aggregates derived from scrap tyres have been used in railways for vibration mitigation (Esmaeili et al. 2016). Since the 2000s, several studies were conducted on the use of scrap tyre for earthquake protection in the form of tunnel linings and synthetic liners below footing (Konagai and Kim 2001; Hazarika et al. 2007, 2008). Use of tyre derived geomaterials mixed with sand for earthquake protection of buildings has been the topic of interest in the recent years (Tsang et al. 2012; Xiong and Li 2013; Pitilakis et al. 2015). The high damping and liquefaction resistance of scrap tyre mixed with sand (Hyodo et al. 2007; Senetakis et al. 2009; Hazarika et al. 2010; Mavronicola et al. 2010; Senetakis et al. 2012; Kaneko et al. 2013; Senetakis and Anastasiadis 2015; Mashiri et al. 2016) points out its promising potential for seismic isolation of buildings below the foundation level itself. Nevertheless, very limited discussions were carried out to evaluate the performance of this geotechnical vibration absorbing mechanism for its practical applications and efficiency on par with the conventional base isolators for buildings.



### **1.3. CONVENTIONAL BASE ISOLATION SYSTEMS**

#### **1.3.1. Background**

Seismic isolation technique is derived from the idea of reducing the magnitude of the earthquake force coming to the structure instead of increasing the capacity of the building to withstand the entire earthquake force. The history of base isolation traces back to 550 BC with the Tomb of Cyrus being built with a layer of blocks without any mortar such that it can slide during an earthquake. The modern-day seismic isolation study was started by a British Scientist John Milne in 1885, wherein balls made of cast-iron plates with saucer-like edges placed at the pile heads were used. In 1969, the first application of rubber bearings isolator was implemented in a 3-story reinforced concrete elementary school building (Kelly 2002). In 1976, Pacific Engineering Research Centre (PEER), the University of California at Berkeley, was established to study the feasibility of using raw rubber bearings as base isolators. By 1980s, seismic isolation gained worldwide popularity, and significant research and initiatives were made to implement this concept in buildings. Japan started tremendous progress in the field of seismic isolation, followed by the 1995 Kobe earthquake. Initially, high damping rubber bearings were used which was followed by elastomeric bearing and lead-rubber bearings. Sliding bearings gain popularity in the 1990s and structures now days are isolated using primarily elastomeric, lead-rubber, and friction pendulum family of bearings (sliding).

Considering the Indian scenario, though earthquake engineering institute was set up in the 1950s (IIT Roorkee), the formation of National Information Centre of Earthquake Engineering (NICEE) in 1999 and the following 2001 Bhuj earthquake (7.7 Mw) at Gujarat started the earthquake engineering activities in the country (Jain 2016). The base isolation concept was introduced only in 2003 following the 2001 Bhuj earthquake with the help of the New Zealand government for a hospital building. Ever since, despite the proven effectiveness of seismic isolation, the technology is highly restricted to very few structures like hospitals, bridges and buildings of strategic importance in the country and are very limited in number. In the current scenario, the earthquake safety measures for the buildings are more focused on increasing its strength aspect based on seismic demands. Hence, there exists a high scope for the implementation of the seismic isolation systems in India following the success step in seismic safety by countries like Japan, USA, New Zealand and China.

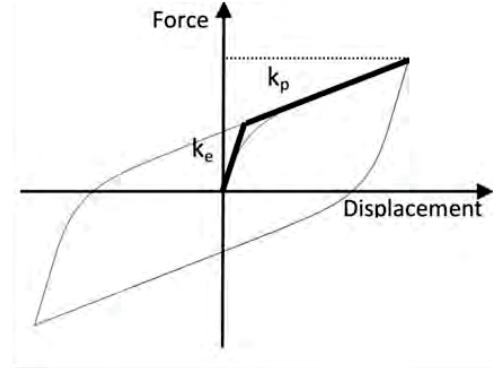
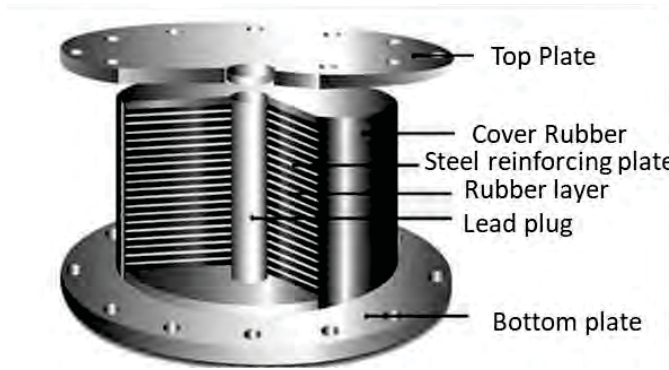


### 1.3.2. Base isolation systems

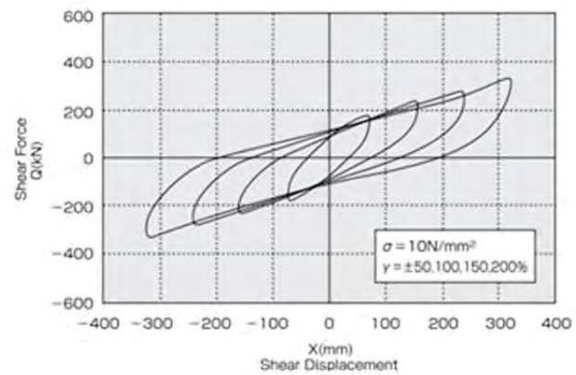
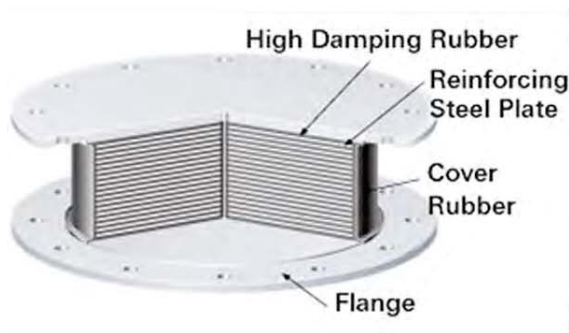
Natural rubber bearings were the first modern-era seismic isolation device developed in the New Zealand Department of Scientific and Industrial Research (Skinner, 1993). The rubber bearings quickly got updated to the modern elastomeric rubber bearings composed of rubber and steel layers alternately bonded together through vulcanisation. Figure 2.1 shows the typical elastomeric isolation bearing made of rubber and steel sheets. While the rubber layers provide horizontal flexibility, the steel layers enhance the vertical stiffness of the isolator besides controlling the bulging deformations of rubber layers under axial loading (Roeder et al. 1990). The elastomeric bearings exhibit low damping resistance in the order of 2% to 3% of critical viscous damping. A further improvement of elastomeric bearing came in the form of lead-rubber bearings wherein a lead plugs were inserted into the elastomeric bearings as shown in Figure 2.2a. The lead plugs act as supplemental energy dissipation mechanism by yielding under high lateral load, thereby reducing the lateral stiffness (Naeim and Kelly 1999). The lead rubber bearing generates hysteric damping varying from 15% to 30% and is commonly adopted worldwide for mid-rise buildings (Skinner 1993). Besides, high damping rubber bearings are also widely used as an alternative to standard elastomeric bearing where the energy absorption capacity was increased with the addition of fillers like carbon black (Figure 2.2b). The high damping rubber bearings also exhibits high vertical stiffness and horizontal flexibility, making it an ideal seismic isolator (Thompson 1998).



**Figure 2.1** Typical elastomeric bearing system with force-displacement relationship (Li et al. 2013)



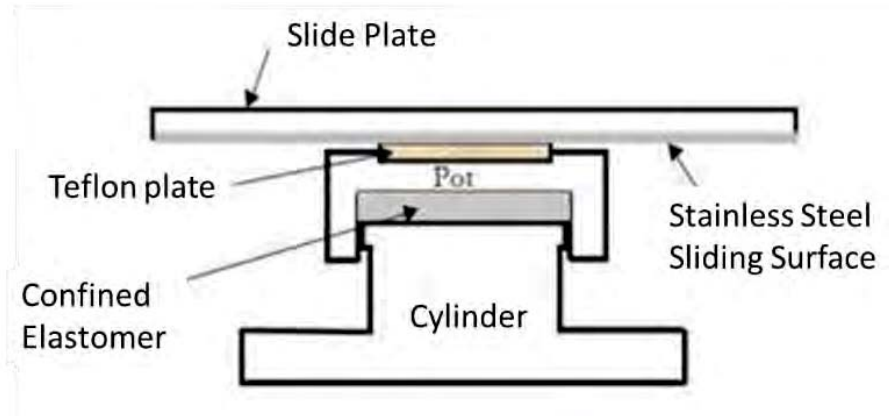
(a)



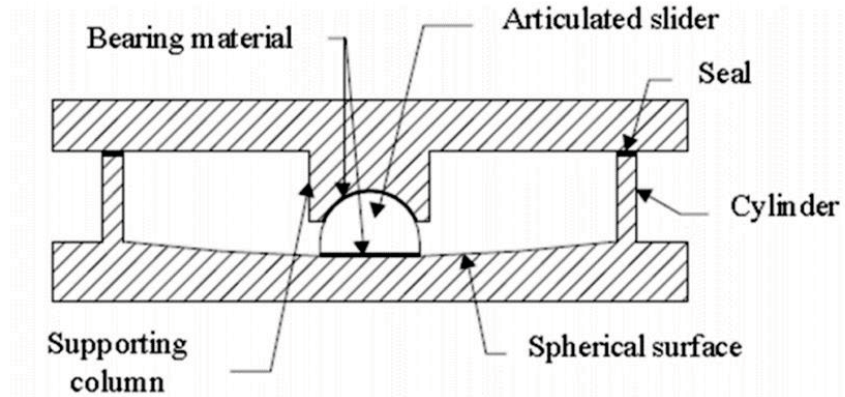
(b)

**Figure 2.2** Advanced elastomeric systems with high damping **(a)** Lead rubber bearing (Yazici 2014) **(b)** High damping rubber bearing (Bridgestone catalogue)

Flat sliding bearing systems were introduced in the late 1980s (Figure 2.3) which exhibit high damping (Coulomb damping induced by friction), vertical stiffness and perfectly plastic hysteresis behaviour. The advanced form of flat sliding bearing is the friction pendulum bearings which use gravity as the restoring force due to its concave sliding surface (Zayas 1987) and is widely used for buildings and bridges (Mokha et al.1991; Calvi et al. 2004). In addition to existing bearing systems, supplemental damping devices were also included in the base isolation system to enhance the lateral force resistance and to recenter the structure after an earthquake. Commonly used supplemental damping to reduce the internal strains arising from earthquake shaking involves the friction dampers made of metals, fluid dampers/viscous dampers, viscoelastic dampers (with friction pads and polymer pads), and hysteretic dampers/yielding dampers with ductile metal elements which are designed to yield under lateral loading (Torunbalci 2004).



(a)



(b)

**Figure 2.3** Schematic of (a) Flat sliding bearing system (b) friction pendulum isolator bearing (Ealangi 2010)

#### 1.4. BASIC PROPERTIES OF SAND-RUBBER MIXTURES

There exists a broader gap for implementing base isolation techniques to most of the developing nations due to costly installation procedures and preciseness involved. Rubber is an essential component of typical base isolation systems and rubber from scrap tyre are widely used for vibration mitigation in geotechnical applications such as landfills and retaining walls backfills. Hence, a simple alternative solution for the conventional base isolation is the use of an engineered layer of sand-rubber tyre shred mixture placed between the base of the building foundation and the supporting soil medium to attenuate the incoming earthquake waves. Limited studies on the use of shredded scrap tyre-sand mixtures placed below the foundation also point out its potential

as an earthquake protection layer (Tsang et al. 2012; Xiong and Li 2013; Pitilakis et al. 2015). The damping capacity of the engineered layer thus increases due to the energy dissipative nature of rubber present in it (similar to the rubber bearings of base isolators) limiting the amplification of earthquake waves below foundation level itself (Tsang et al. 2012). The Sand-Rubber Mixture (SRM) bed below building footing is hereafter referred to as Geo-Base Isolator (GBI) for the present study.

#### **1.4.1. Environmental implications of scrap tyre**

An estimated 13.5 million tonnes weight of scrap tyre is disposed of every year around the world. The annual scarp tyre discard quantities are approximately 4.4 million tons in the United States; 3.4 million tons in the European Union and 5.7 million tons by the rest of the world (Genan Business and Development A/S 2012). The increase in the population, along with rapid economic growth in developing countries, may further accelerate the rate of scrap tyre generation in the coming years. The stockpiling of waste tyres creates environmental pollution, illegal dumping issues, fire hazards resulting in toxic fumes, mosquito breeding and are hence a major health hazard for humans (Attom 2006). Recycling of waste tyre using pyrolysis and devulcanization techniques and bulk reuse in landfills and tyre derived fuel production were explored in recent years.

The recovery rate of scrap tyres is upto 60% in countries like US and European Union (European Tyre and Rubber Manufacturers' Association, 2012); 36% in Australia (Australian Government, 2011) and below 10% in developing countries. For the Indian scenario, waste tyre generation is around 6 % to 7% of world production accounting to around 112 million scrap tyre per year (Rao and Dutta 2006). Since the pyrolysis process is under rigid monitoring by the Indian government due to environmental degradation issues, bulk reuse of scrap tyre in the civil engineering applications like landfills and road construction have gained momentum currently. The high durability and non-biodegradable nature of scrap tyre open up its large-scale reuse as an alternate material in geotechnical engineering, thereby reducing its environmental pollution hazards. Further, this acts as a sustainable and eco-friendly remedy to address the scarcity of natural resources like sand, gravel and aggregates in the construction industry.

#### **1.4.2. Basic properties of scrap tyre derived materials**

Due to the broad applications of scrap tyre in civil engineering applications, the American Society of Testing and Materials (ASTM) has published ASTM D 6270-08 (2012) as a guideline for the

standard practice, properties and testing on scrap tyre. Table 2. 1 shows the designations and the classification of the processed tyre based on their size that will be used throughout the literature review section to avoid confusion in terminologies.

**Table 2.1** Classification of shredded tyre in civil engineering (ASTM D6270-08 2012)

Scrap tyre classification	Terminology	Size range
Particulate rubber (Scrap tyre with the wire removed and mechanically reduced in size into non-spherical particles using a shredding machine)	Powdered rubber	Below 425 $\mu\text{m}$
	Ground rubber	425 $\mu\text{m}$ – 2 mm
	Granulated rubber	425 $\mu\text{m}$ – 12 mm
Tyre derived aggregates (Scrap tyre cut into pieces ranging in size from 12 mm to 305 mm with most of the wire removed having a basic geometrical shape)	Tyre chip	12 mm – 50 mm
	Tyre shred	50 mm – 305 mm
	Rough shred	50 mm $\times$ 50 mm $\times$ 50 mm to 762 mm $\times$ 50 mm $\times$ 100 mm
Rubber fines (By-product of ground rubber obtained during the shredding process in the form of tiny particles)		Not specified

Since early 90s extensive laboratory studies were carried out to understand the fundamental response of pure tyre chips/shreds/granules and its combed response with soil to fulfil the demands of geotechnical engineering applications. One of the first such studies were carried out on tyre chips as a lightweight fill by Humphrey and Manion (1992) which showed that unlike sand, the effect of compactive energy and water content negligibly affects the resulting dry unit weight of SRM and 60% of standard Proctor energy itself would be sufficient for its field compaction. Subsequent studies by Humphrey et al. (1993) using large shear box pointed out the initial compressive nature of SRM which stabilises after the first cycle of loading along with its capacity to endure higher axial strains wherein the shear strength increases even at strain values beyond 10%.

Ahmed (1993) later investigated the basic properties of SRM for highway embankment applications using 1D compression tests and found that the compressive response of SRM is predominantly affected by rubber content in the mixture while the size of the rubber and compactive effort has little impact. The study reports that the compression mechanism of SRM was governed by particle rearrangement and sliding and the void ratio/density of SRM ideal for applications where a large settlement could pose an issue was observed for rubber content less than 38%. Humphrey and Sandford (1993) later found that the elastic deformation and bending of tyre chips are recoverable after unloading and that increasing the overburden/confining pressure on SRM can ideally reduce the compression of the material. Similar results were reported by Bosscher et al. (1993), who indicates that after the first load application, the compressibility of the material decreases considerably.

One of the distinct characteristics of SRM is its ability to maintain high levels of permeability, even under high vertical compression. For instance, Edil and Bosscher (1994), Karmokar (2007) and Hazarika et al. (2010) reported that pure tyre chips exhibit the permeability as high as granular soil thereby enabling high drainage to the base material to which it is blended. Subsequently, the excess pore pressure dissipation and liquefaction resistance of SRM increases, making it ideal for dynamic loading problems (Uchimura et al. 2007). However, the size of the rubber plays a major role since SRM with  $D_{50, \text{rubber}} / D_{50, \text{sand}}$  less than 0.25 may bring detrimental effects to the permeability contrary to the popular findings (Li et al. 2016).

The average unit weight of tyre chips was reported to be around 1.22 (Edil and Bosscher 1994), which in turn reduces the density of SRM depending on rubber content. Typically, the vibratory table method was used to find the maximum density of SRM similar to granular materials (Ahmed and Lovell 1993; Bali Reddy et al. 2016; Mashiri 2014). Conversely, Edil and Bosscher (1994) reported that the vibratory table method is not suitable for rubber-sand mixtures because of the vibration absorbent nature of the rubber. Hence proper approach should be adopted to represent the dry density of SRM while conducting laboratory studies. Table 2.2 summarises a few important findings on the fundamental properties of SRM found in the literature.



**Table 2.2** Basic properties of SRM from the past studies

<b>Property</b>	<b>Comments</b>	<b>Reference</b>
Density	The unit weight of SRM is primarily dependent on the rubber content in the mixture and the method of compaction. The influence of compactive effort and moulding water content are negligible in the unit weight of the mixture.	Humphrey and Manion (1992), Bosscher et al. (1993), Ahmed and Lovell (1993).
Permeability	The hydraulic conductivity of the material improves due to rubber inclusion for both granulated tyre and tyre chips. The permeability of sand improved by four times with 15% rubber chips inclusion. For granulated tyre, the permeability of SRM was higher than that of granular aggregates. Though overburden pressure reduces the permeability of SRM, a relatively high hydraulic conductivity in the order of 0.1 cm/sec or more can still be obtained for drainage purposes.	Ahmed and Lovell (1993); Edil and Bosscher (1994); Wiszniewski and Cabalar (2016).
Compaction	Vibratory compaction method is inadequate for effective compaction due to energy adsorption by rubber particles in the mixture. Tamping and mini-compaction methods are more suitable for SRM.	Bosscher et al. (1993), Ahmed and Lovell (1993), Senthin Amuthan et al. (2018).
Compressibility	Compressibility of SRM can be reduced by preloading and confinement. Typically, a soil cap of around 0.6 m to 1.8 m can reduce settlement due to traffic loads in embankments. While 30%-40% of rubber content in SRM is optimum from compressibility perspective, the type of rubber was found to have less significance on the compression behaviour of SRM. Though rubber inclusion decreases the constrained modulus of sand due to the reduced stiffness/softening effect of rubber, the residual strain of the mixture increases after unloading due to rubber inclusion.	Humphrey and Manion (1992), Humphrey and Sandford (1993), Bosscher et al. (1993), Edil and Bosscher (1994), Bosscher et al. (1997), Sheikh et al. (2013), Fu et al. (2017), Asadi et al. (2018).

## 1.5. SHEAR STRENGTH RESPONSE OF SAND RUBBER MIXTURES

Ahmed (1993) was among the earliest to present the shear strength response of SRM with tyre chips of varying size and gradation using triaxial tests. He reported that SRM exhibit strain hardening behaviour wherein the material stiffness keeps increasing at higher axial strains. The behaviour of SRM is sand-like at low chip/soil ratios and pure rubber-like at higher low chip/soil ratios. Further, confining pressure was found to be the primary factor controlling the shear strength response with the shear strength of the material increasing at higher confining pressure. In essence, SRM exhibits bulging at low confining pressure and high vertical compression with a negligible lateral bulge at high confining pressure. At higher confining pressures, the resilient modulus of soil was found to decrease with increase in rubber content. The author also acknowledges that tyre chip size and compactive effort have insignificant effects on shear strength of SRM. The study proposes an optimum mix proportion of 39% for maximum shear strength increment for its application as a lightweight material.

Edil and Bosscher (1994) studied the frictional behaviour of SRM using a large direct shear box and found that shear strength increment was evident at 10% rubber inclusion itself. The strength envelope for SRM showed bilinear response with a high friction angle of  $55^\circ$  up to 40 kPa normal stress and  $41^\circ$  after that. Besides, SRM was found to show high plastic deformation due to the initial porosity as reported by Humphrey et al. (1993) previously. Edil and Bosscher (1994) further extended the studies on SRM to randomly distributed tyre shreds, which was found to reinforce the sand to a considerable extent resulting in high friction angle and a stronger lightweight material. The findings by Edil and Bosscher (1994) were backed by Foose et al. (1996) using large-scale direct shear tests on SRM with tire shred further indicating that the shear strength was primarily controlled by tyre shred content, normal stress and unit weight of the sand matrix.

Zornberg et al. (2004) undertook large-scale triaxial experiments on SRM with tyre shreds (width 12.7 mm, 25.4 mm; aspect ratio-1 to 8). They reported that the addition of tyre shreds provides excess composite shear strength to sand above the baseline shear strength. In addition to the reinforcing effect of tyre shreds, the interaction mechanism between the individual tyre shred and the sand particles plays a dominant role in contributing to the excess shear strength of sand. The behaviour of SRM changes from sand-like to rubber-like at a rubber content of approximately 35%, as shown in Figure 2.4. Further, tyre shred inclusion was found to bring in an increased



apparent cohesion to sand as reported by Rao and Dutta (2006) from triaxial test as well as Ghazavi and Sakhi (2005) from direct shear test thereby contributing to shear strength increment.

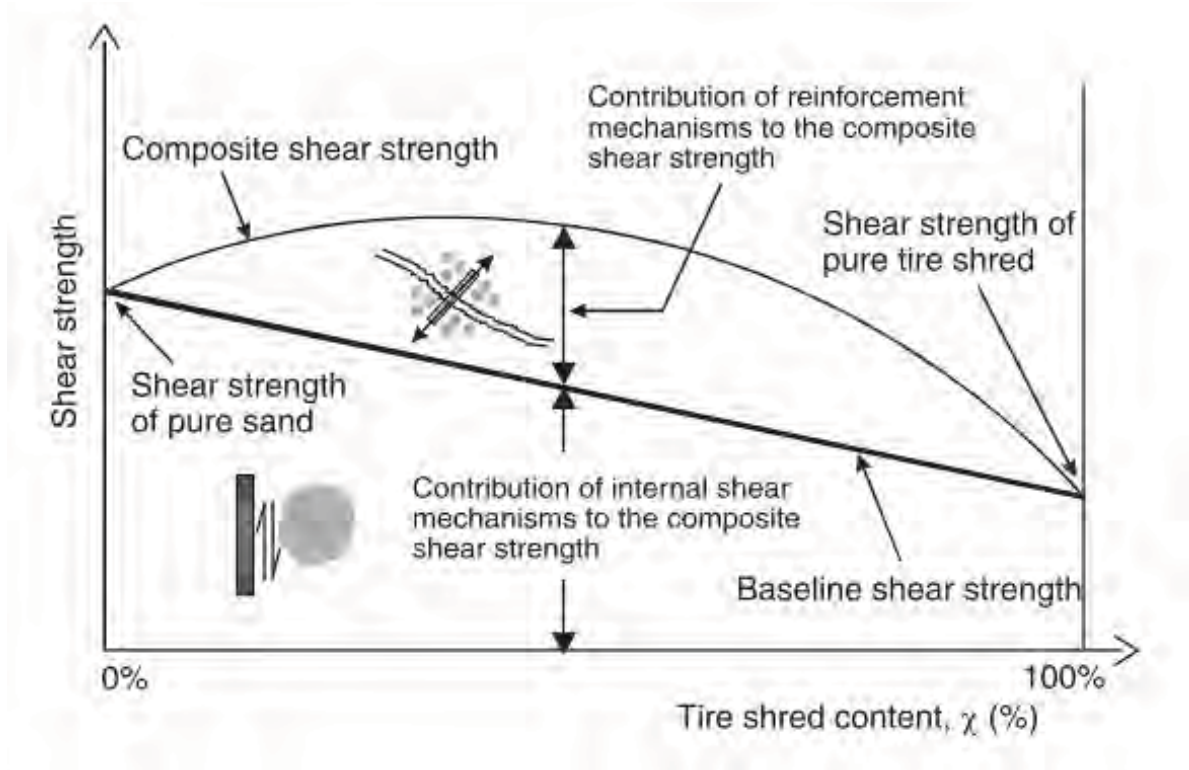


**Figure 2.4** Influence of rubber content on the shear strength of sand matrix in SRM (Zornberg et al. 2004)

In general, the deviatoric stress-strain response of SRM exhibits ductile behaviour with a reasonably well-defined peak shear strength at lower rubber content while for higher rubber content the shear strength keeps increasing even to axial strains of 15% to 22% (Lee et al. 1999; Youwai and Bergado 2003; Zornberg et al. 2004; Rao and Dutta 2006; Mashiri et al. 2015). The volumetric strain response of SRM exhibits dilatant behaviour for lower rubber content which changes to full contraction for higher rubber contents (Wu et al. 1997; Youwai and Bergado 2003; Zornberg et al. 2004). Figure 2.5 shows the typical deviatoric stress-strain and the volumetric response of SRM as reported by Zornberg et al. (2004). Table 2.3 shows a few of the typical shear strength characteristics of SRM as reported by different researchers in the literature.

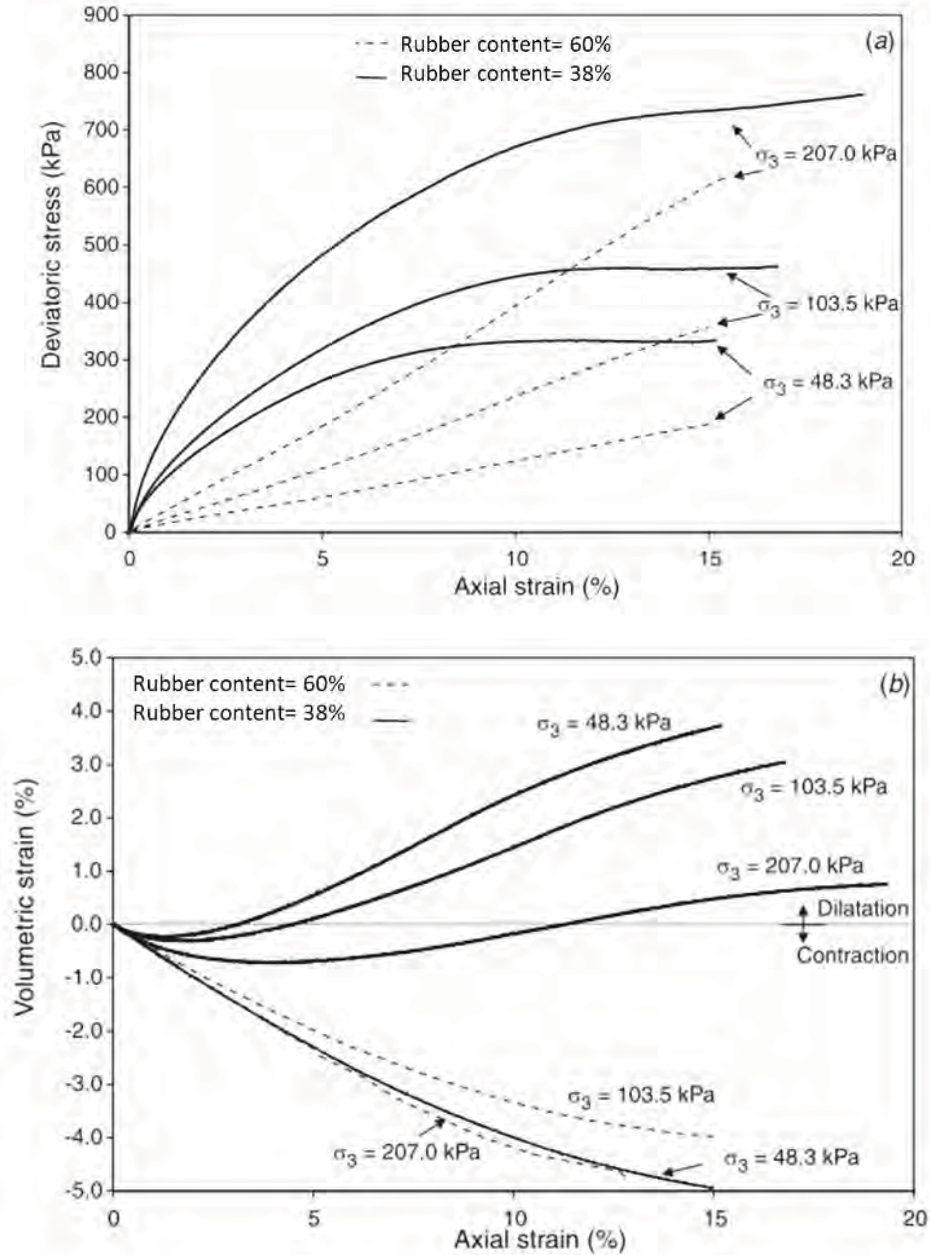


**Figure 2.5** Consolidated drained triaxial test on SRM (55% relative density) **(a)** deviatoric stress–strain response **(b)** volumetric strain response (Zornberg et al. 2004)

The use of smaller sized rubber such as the granulated rubber SRM started gaining attention due to the proximity in the mean particle size of base material and the rubber leading to homogeneity/lesser segregation along with ease of carrying out testing in standard sized testing equipment. Masad et al. (1996) used granulated tyre of size less than 4.75 mm and found that rubber inclusion in SRM (50% rubber content) brings in negligible shear strength improvement

irrespective of the confining pressure (150 kPa to 350 kPa). Similar results were also reported from triaxial tests by Youwai and Bergado (2003) using rubber granules with  $D_{10}$  of 5 mm. They reported decrement in shear strength of SRM with the addition of rubber granules mostly due to lack of reinforcing effects unlike the case of tyre chips as reported by Edil and Bosscher (1994) and Foose et al. (1996). Sheik et al. (2013) compared the response of two types of tyre granules having  $D_{50}$  of 1.39 and 2.2. It was concluded that, for a rubber content of 10%, at any given confining pressure, tyre granules with the bigger size exhibited higher shear strength compared to the smaller sized samples which indicate that gradation of the material can positively affect the shear strength of SRM comprehensively.

**Table 2.3** Comments on the shear strength of SRM from past studies

Reference	Sand type/grading	Rubber specifications	Testing type	Primary observations
Edil and Bosscher (1994)	Uniform graded	Tyre chips specific gravity 1.15 mean size 50 mm x 75 mm Rubber content 0%- 25%	Large size direct shear	Tyre chips provide reinforcement effect to SRM. Noted shear strength increment in SRM with dense sand and 10% rubber content
Foose et al. (1996)	Uniform graded $D_{50}=0.58$ mm	Tyre shreds Length 5 cm to 15 cm	Direct shear	Shear strength increment due to rubber addition to dense sand. Bilinear strength envelope was observed for SRM. Pure tyre chips exhibit friction angle as high as $39^\circ$ , whereas SRM in dense sand exhibit friction angle of $67^\circ$ .
Zornberg et al. (2004)	Uniform graded $D_{50}= 0.4$ mm	Tyre shreds width 12.7 mm & 25.4 mm thickness 2.16 mm to 3.23 mm aspect ratios 1, 2, 4, and 8	Large size triaxial	The high aspect ratio of tyre shreds increases the shear strength of SRM due to the increased pullout resistance  Below 35% tyre content the volumetric response of SRM is initially dilatant followed by full

				compression. Due to the strain hardening of SRM, the peak shear strength is achieved at axial strain as high as 15% for SRM with high rubber content.
Youwai and Bergado (2003)	Poorly graded $D_{10} = 0.27$	Granulated tyre $D_{10} = 5 \text{ mm}$	Triaxial	Due to the high deformation of the tyre chips, the initial dilatancy keeps increasing even at high confining stresses.
Ghazavi and Sakhi (2005)	Uniform sand $D_{50} = 1.2 \text{ mm}$	Rectangular tire chips 2cm, 3cm and 4cm aspect ratio 1 to 7	Direct shear and CBR	Mohr-Coulomb envelope was nonlinear for SRM irrespective of the rubber content. The optimum lengths of tire chips for peak shear strength was found to be 10 cm, 12 cm and 8 cm for the respective widths of 2 cm, 3 cm and 4 cm.
Rao and Dutta (2006)	Poorly graded $D_{50} = 0.42 \text{ mm}$	Rectangular tyre chips 10 mm x 10 mm, 10 mm x 20 mm and 20 mm x 20 mm	Triaxial	Maximum shear strength of SRM was obtained at 20% rubber content for tyre chips with an aspect ratio of 2. A maximum cohesion intercept of 18 kPa was also reported for SRM with 20% rubber content.
Sheikh et al. (2013)	Poorly graded $D_{50} = 0.34 \text{ mm}$	Granulated rubber $D_{50} = 1.39 \text{ \& } 2.20$	Triaxial	Reduction in shear strength of SRM was noted due to the addition of rubber. Larger sized granulated rubber can lessen the reduction in shear strength significantly.
Mashiri et al. (2015)	Poorly graded $D_{50} = 0.35 \text{ mm}$	Rectangular tyre chips of maximum width 8mm aspect ratio 2.8	Triaxial	Shear strength increased with the increase in relative density and confining pressure. Dilatancy of the mixture increased with relative density increment and vice versa with confining pressure. An optimum rubber content of 35% was reported.

### 1.5.1. Effect of rubber inclusion

For pure tyre chips, Humphrey and Sandford (1993) & Bernal et al. (1996) reported a friction angle of  $19^{\circ}$ – $35^{\circ}$  and a cohesion intercept of 4.3 kPa –11.5 kPa using large sized direct shear tests. Addition of tyre shreds to dense sand increased the apparent friction angle upto  $67^{\circ}$  as reported by Foose et al. (1996). Triaxial tests conducted on pure tyre chips by Wu et al. (1997) reported a friction angle of  $40^{\circ}$ . For SRM, Tatlisoz et al. (1998) reported a peak shear strength improvement at a rubber content of 30% volumetrically. Mashiri et al. (2015) identified a matrix zone for SRM wherein there exists mutual contribution by sand and rubber towards load transfer mechanism based on the void ratio of the material (Figure 2.6a). According to them, up to a rubber content of 18%, sand forms the matrix skeleton exhibiting sand-like behaviour. The SRM binary skeleton (dual response of sand and rubber) exists for a rubber content of 18% to 35% beyond which rubber-like behaviour predominates. Similar results were reported in the past by Ahmed (1993) and Zornberg et al. (2004). More recent evidence by Perez et al. (2017) using macro and particle scale results highlights the binary skeleton wherein the rubber- sand interplay zone exists between 20% to 50% rubber content as a function of  $D_{50, \text{rubber}}/D_{50, \text{sand}}$  ratio as shown in Figure 2.6b. Together, these studies outline that the optimum rubber inclusion for SRM lies anywhere between 20% to 40 % as evident from Figure 2.7.

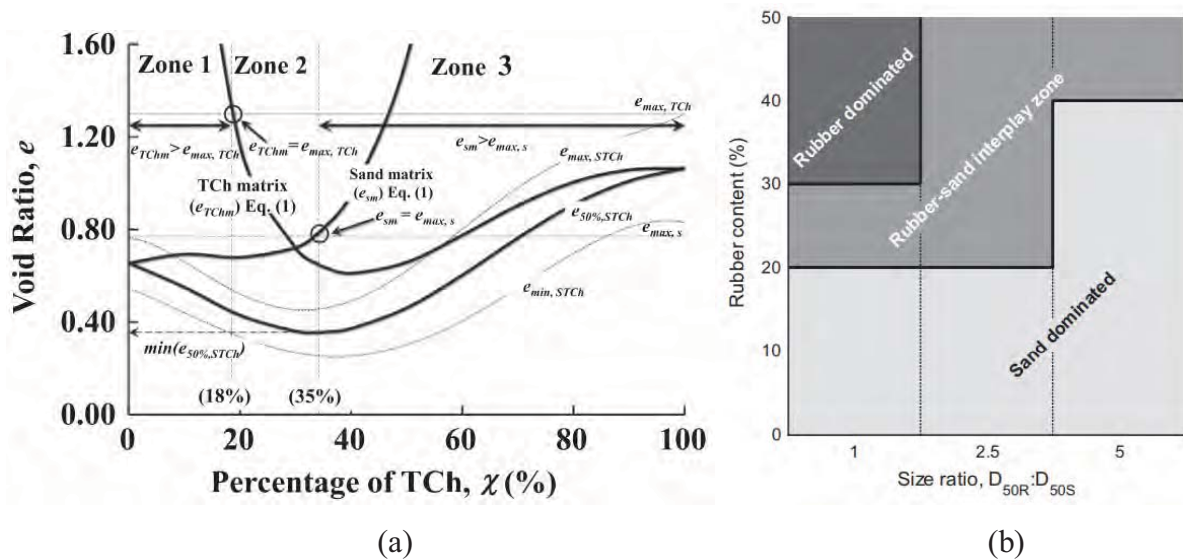


**Figure 2.6** Zonation of SRM based on rubber content **(a)** Mashiri et al. (2015) **(b)** Perez et al. (2016)



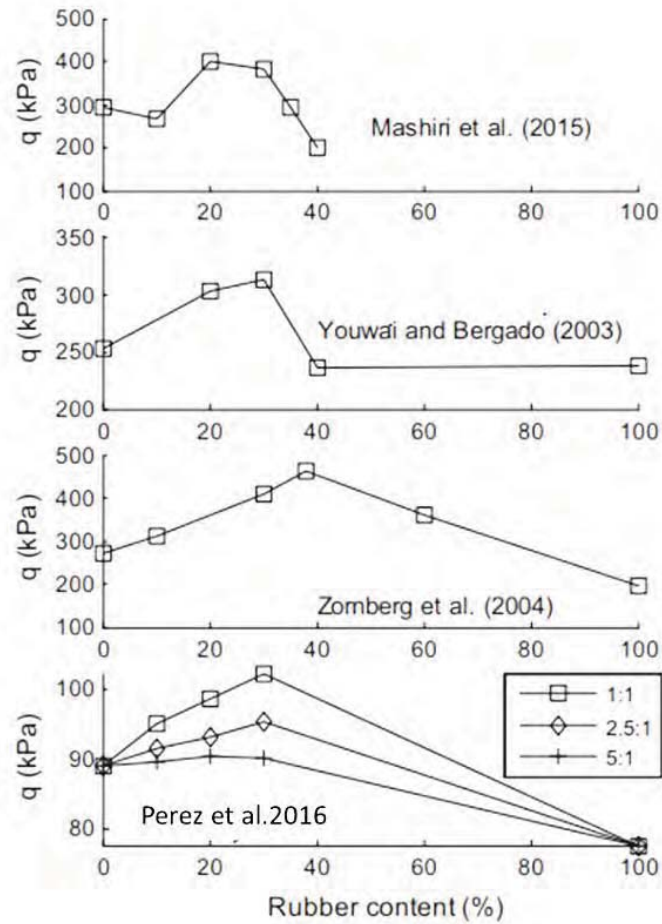


**Figure 2.7** Peak deviatoric stress at failure for varying rubber content as reported in the literature (Perez et al. 2016)

### 1.5.2. Effect of confining pressure

Zornberg et al. (2004) reported that the maximum shear strength increment for SRM was observed at low confining pressure, especially for dense sand. At higher confining pressure, the reduction in shear strength was chiefly due to the low contribution of reinforcement mechanism and high compressibility of the material (Gotteland 2005; Bałachowski and Gotteland 2007). Affirming the above findings, Anvari et al. (2017) attributed the shear strength decrement of SRM at high normal stress to the low interface friction angle between sand to granulated rubber particles using direct shear test. Contrary to the above observations, Masad et al. (1996) reported that while pure rubber granules show no shear strength improvement with confining pressure, SRM with 50% rubber exhibits shear strength increment at a higher confining pressure (Masad et al. 1996). Collectively, at high confining pressure, for SRM with granulated rubber and rubber shreds, the peak shear

strength and the corresponding axial strain was found to increase due to the increased stiffness of sample as shown in Figure.2.5 (Youwai and Bergado 2003; Mashiri et al. 2015). Besides, the increase in confining pressure reduces the dilation response of SRM and extends the strain at which transition from contractive to dilative volumetric behaviour of SRM occurs (Masad et al. 1996; Youwai and Bergado 2003; Mashiri et al. 2015).

### **1.5.3. Effect of size/type of rubber**

A major problem with the characterisation of SRM is the conflicting results in the literature regarding the shear strength of SRM due to the variation in size and aspect ratio of the rubber used (Youwai and Bergado 2003; Bergado et al. 2005; Zornberg et al. 2004; Edinçliler and Ayhan 2010). It was well reported that SRM with tyre chips/shreds of high aspect ratio exhibit improved shear strength (Ahmed 1993; Edil and Bosscher 1994; Foose et al. 1996; Zornberg et al. 2004; Gazhavi and Sakhi 2005; Rao and Dutta 2006).). However small-sized tyre chips/shreds and granules typically are found to have little to a negative influence on the shear strength of the mixture (Masad et al. 1996; Youwai and Bergado 2003; Kawata et al. 2007; Lee et al. 2007). Further, the influence of gradation of sand and rubber in SRM was demonstrated using discrete element studies by Perez et al. (2016). They concluded that SRM exhibits decrease in shear modulus with the addition of rubber when the  $D_{50, \text{rubber}}/D_{50, \text{sand}}$  ratios lie between 1.0 and 2.5 (ideal for settlement reduction) while for  $D_{50, \text{rubber}}/D_{50, \text{sand}}$  beyond 5, the shear strength was found to increase (sand dominated response).

More recent studies now focus on the influence of host sand in the shear strength behaviour of SRM (Fu et al. 2014, 2017). Studies of SRM at the micromechanical level by Li et al. (2019) reports that smooth and non-breakable sand exhibits higher friction angle at the critical state with rubber inclusion while rough and breakable sands show a decrease in the friction angle. The latter response was due to the low interface friction angle of the sand-rubber interface while the former response was due to high interparticle friction of sand-rubber. Further, Fu et al. (2017) pointed out that the friction angle at the critical state is independent of rubber content up to 30% rubber by weight.

Overall, the shear strength of SRM is highly dependent on factors such as rubber size/gradation, rubber content and confining pressure. However, there exists considerable disagreement regarding the shear strength of SRM depending on the specifications of rubber used in the mixture. Though

the high shear strength induced on the sand by tyre chips were well established, as one move towards the grey area of rubber size similar or slightly higher than that of sand (say 2 mm to 15 mm mean size), the evidence on shear strength is not conclusive. Hence laboratory tests should be carried out for the SRM before assuming the popular outcomes. Further, the purpose of SRM application should be kept in mind while choosing the rubber size; for instance, in vibration applications, the segregation and liquefaction aspects should be considered in addition to the shear strength for better performance of the mixture.

## **1.6. SEGREGATION OF SAND RUBBER MIXTURE**

While mixing two materials of different density and gradation, the ingredients may showcase segregative nature resulting in heterogeneity during the transportation, placing or compaction stages. While few findings hint that SRM may exhibit segregation when tyre chip/shred content greater than 30% was used (Zornberg et al. 2004), other studies point out that the segregative nature becomes explicit at rubber content above 50% in the mixture (Edil and Bosscher 1994; Anastasiadis et al. 2012; Mashiri 2014; Umashankar et al. 2014). Studies by Kim and Santamarina (2008) on large rubber chips in SRM ( $D_{50, \text{rubber}}/D_{50, \text{sand}}=10$ ) claims that segregation was induced when the volume fraction of rubber exceeds 70%. Besides, Mashiri et al. (2014) highlight that gradation gap and high contrast in shape/density of the ingredients in SRM primarily influences the segregation. Figure 2.8 shows the segregative nature of SRM with tyre chips. Typically, segregation of SRM resulting from vibrations leads to rubber layer coming to the top due to its low density. Unlike tyre chips, the high segregation resistance of granulated rubber mixed with soil and bottom ash were reported by Kim and Kang (2011) using flow testing due to the smaller gradation gap between sand and rubber in the mixture. More recent argument by Wang et al. (2018) using digital image processing and angle of repose tests highlights that higher interparticle friction can act as the controlling factor in minimizing segregation in SRM irrespective of the material stiffness.

## **1.7. DURABILITY AND DEGRADATION OF TYRE SHREDS AND CREEP**

Studies by Ab-Malek and Stevenson (1986) on the properties of rubber tyres immersed in seawater for 42 years (recovered from a sunken ship) showed that water absorption by tyre in the 42 years



duration was only 4.7%. Moreover, no adverse effect on the strength properties of tyres and inner tubes were noted based on tensile and tear test conducted on the samples. Chemical evaluation of the rubber condition by studying free sulphur and sulphide also showed that the chemical composition of rubber is not much altered due to severe exposure to alkaline conditions. Tyre shreds showed high durability under normal foundation engineering conditions based on investigations on old tyres by Edeskar (2004). Studies on the use of tyre sheds mixed with concrete also confirm the high durability of tyre shreds (Sukontasukkul and Tiamlom 2012; Adamu and Uche 2014). Humphrey and Manion (1992) studied the creep behaviour of tyre shreds of size 5mm to 76 mm for a period of 25 days, maintaining vertical stress of 50 kPa. The creep rate observed was 1%. Heimdahl and Drescher (1998) observed that the creep behaviour of tire shreds are significant only upto a period of 330 days. Strain rates observed on tyre shreds subjected to vertical stress of 83 kPa suggest that from day 60 to 330, the average strain-rate was 0.036 % per week and from day 330 to 360 days the average strain-rate reduced to 0.0093 % per week under confined conditions. Similar trends were also reported by Ngo and Valdes (2007) indicating that the initial and creep strains are proportional to the rubber content in SRM

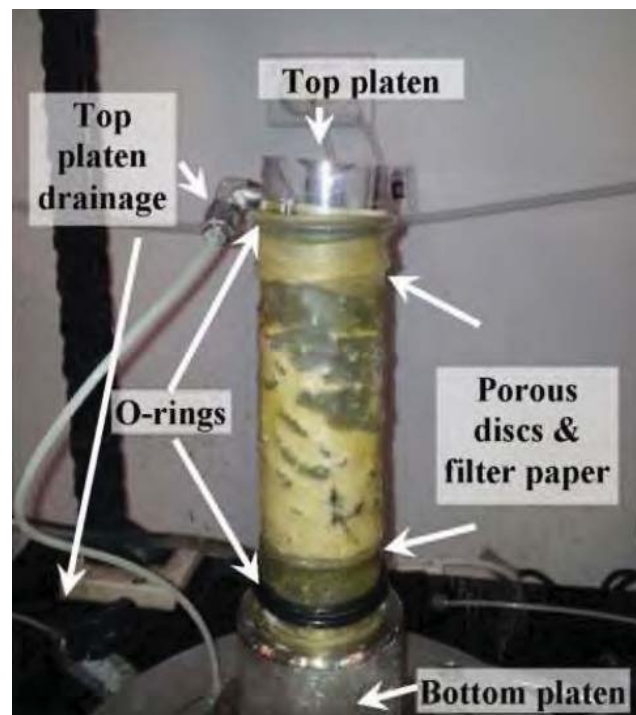


**Figure 2.8** Segregation of tire chips and sand due to high gradation gap (Mashiri 2014)

## 1.8. DYNAMIC PROPERTIES OF SAND RUBBER MIXTURE

### 1.8.1. Measurement of dynamic properties by low strain tests

A comprehensive study on the dynamic properties of SRM was initiated since the past decade due to its extensive application for geo-structures (Garga and Shaughnessy 2000; Humphrey 2004; Kaneda et al. 2007; Shrestha et al. 2016). Feng and Sutter (2000) carried out small strain resonant column test on SRM samples with granulated rubber ( $D_{50, \text{rubber}}/D_{50, \text{sand}} \approx 6$ ) for rubber content varying from 0 to 100% under confining pressure of 70 kPa to 480 kPa. For pure granulated rubber, increase in confining pressure increased the shear modulus. However, at high confining pressure, a slight increment in the damping ratio was observed quite the opposite to soil behaviour primarily due to the high interparticle contacts due to the presence of rubber granules. The rubber content in SRM was found to have a significant influence on the strain-dependent modulus and damping ratio curves of SRM (Figure 2.9). The increase in rubber content in the soil leads to an increased damping ratio and reduced shear stiffness for a given confining pressure. Further, it was found that the reference strain concept by Hardin et al. (1972) can be extended to predict the shear modulus of SRM. On the contrary, Pamukcu and Akbulut (2006) reported from their resonant column tests carried out on SRM ( $D_{50, \text{rubber}}/D_{50, \text{sand}} = 1$ ) that, upto a rubber content of 30% (volumetric) in the mixture, shear stiffness increases with a simultaneous increase in damping ratio, while beyond 30% rubber content the shear stiffness reduces. The addition of rubber content was also found to induce a systematic increment in the small-strain damping mechanism of SRM owing to the elastic and thermoelastic enhancement effects at the soil-rubber interfaces of the mixture.

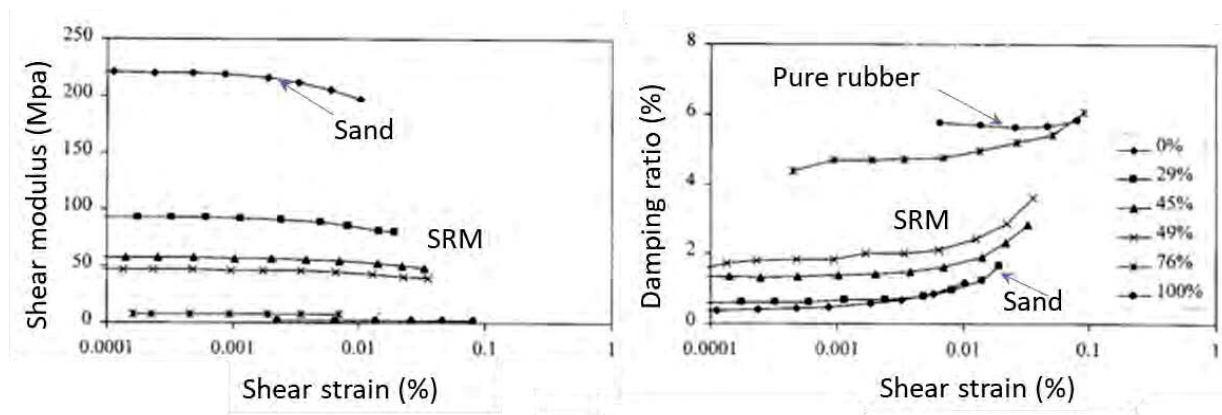
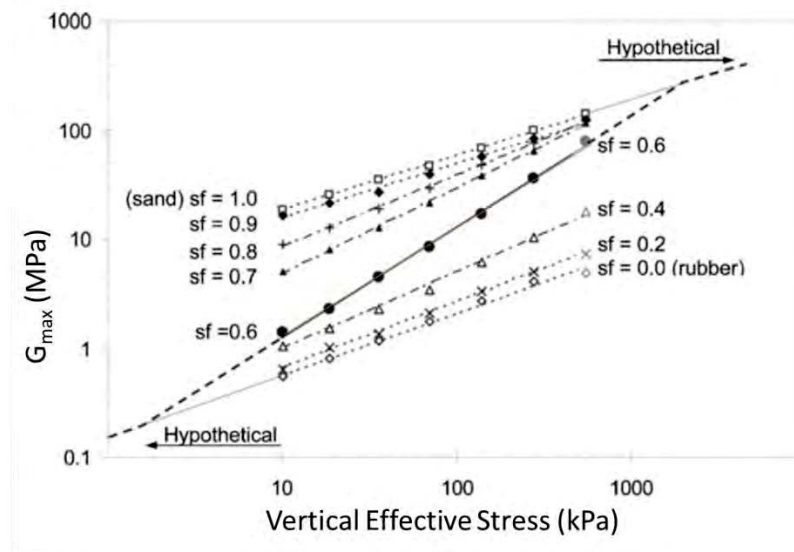


Figure 2.9 Variation of shear modulus and damping ratio with shear strain for SRM with different rubber content at confining pressure of 345 kPa (Feng and Sutter 2000)

Lee et al. (2007) conducted a wave propagation study to examine the small-strain dynamic response of SRM ( $D_{50, \text{rubber}}/D_{50, \text{sand}} < 1$ ) using bender-elements test in a modified oedometer cell instrument. For smaller rubber granules, the authors hint that, below a threshold rubber content of 40%, SRM shows a high shear modulus and sand-like response while for rubber content above 40%, rubber-like response and low shear moduli were observed. The threshold SRM mixture (rubber content of 40%) was found to be stress-sensitive exhibiting rubber-like behaviour at low confining stress due to the low stiffness of the mixture and more sand-like response at high confining stresses as a result of dense packing of rubber particle in the voids. Besides, the maximum shear modulus trends of SRM were reported to increase sharply at a sand fraction of 0.6 and above, as shown in Figure 2.10.



**Figure 2.10** The effect of sand fraction (sf) on the low strain shear modulus ( $G_{\max}$ ) of SRM (Lee et al. 2007)

Kim and Santamarina (2008) extended the studies by Lee et al. (2007) using large-sized rubber inclusions ( $D_{50, \text{rubber}}/D_{50, \text{sand}} = 10$ ). In this case, the maximum shear wave velocity was observed at a rubber content of 20% (volumetric fraction). Beyond a rubber content of 40%, the shear wave velocity trends decreased drastically. At a higher rubber content (above 50%), the closer rubber particles create a low-pass filtering effect, leading to the detection of S-wave with only long wavelengths. The larger rubber particles at low rubber content tend to float within the sand skeleton due to the gradation gap. The effect of confinement on the response of SRM is trivial, especially for rubber content of 40% and 50% unlike reported by Lee et al. (2007) for SRM with smaller

rubber particles. However, the larger rubber particles tend to get squeezed at a higher confining pressure.

Anastasiadis et al. (2012) carried out resonant column tests on SRM samples with  $D_{50, \text{rubber}}/D_{50, \text{sand}}$  ratio varying from 5:1 to 10:1 for confining pressures of 25 kPa to 400 kPa. For pure rubber, the shear modulus and damping ratio trends were similar to that of Feng and Sutter (2000). At low strain levels, pure rubber exhibited a damping ratio approximately ten times higher than that of sand. The reduction in shear modulus and increment in damping ratio of SRM was pronounced at 10% rubber content itself. The study also reports that, at any given rubber content, increase in  $D_{50, \text{rubber}}/D_{50, \text{sand}}$  soil leads to a decrease in shear modulus due to the gradual transition of the sand-rubber matrix to rubber-like behaviour. This dependence of shear modulus to the relative particle size ratio was also confirmed from the findings of Senetakis et al. (2012) based on resonant column testing on SRM with rubber granules ( $D_{50, \text{rubber}} = 0.34 \text{ mm to } 2.8 \text{ mm}$ ). Senetakis et al. (2012) also specified that confining pressure, rubber content, grain-size characteristics, dynamic properties of the base soil and  $D_{50, \text{rubber}}/D_{50, \text{sand}}$  ratios are the governing factors affecting the response of SRM. The modulus degradation and damping ratio curve trends of SRM were similar to that of clean granular sand. Typically, the shear modulus increased with increase in confining pressure and decrease in rubber content, whereas the opposite trend is observed for damping ratio, as shown in Figure 2.11. For a given shear strain amplitude, the increase of mean confining pressure linearly increases the shear modulus of SRM by virtue of the flexibility of specimens and higher rubber to rubber interfaces. Further, Senetakis et al. (2012) and Anastasiadis et al. (2012) proposed empirical relationships to predict the small-strain shear modulus of SRM.

Further, Okur and Umu (2018) extensively studied the dynamic response of SRM with granulated rubber having a mean size ( $D_{50, \text{rubber}}$ ) varying from 0.1 mm to 3 mm using a torsional resonant column test. It was observed that a larger particle size of rubber increases the void ratio leading to an insufficient coupling between the sand and rubber, thereby causing degradation in stiffness of SRM. However, a smaller particle size of rubber results in filling the voids and making the mixture denser with higher stiffness as reported by Lee et al. (2007). Contrary to normal soil, the strain-dependent damping response of SRM was least affected by the size of the rubber particles and confining pressure in this case for 10% and 15% rubber content.

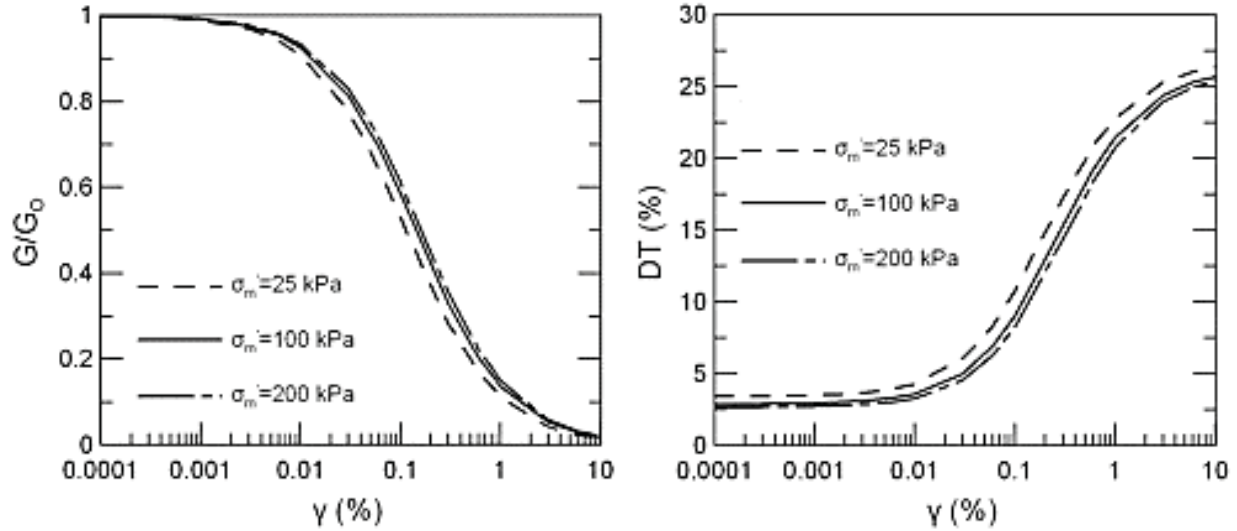


**Figure 2.11** Shear modulus and damping curves for SRM (5% rubber content) at different confining pressures (Senetakis et al. 2012)

### 1.8.2. Measurement of dynamic properties by medium and high strain tests

Initially, Edinçliler et al. (2004) carried out cyclic triaxial test on tyre buffings having diameter ranging from 1 mm to 4 mm and length varying from 2 mm to 40mm for confining pressures of 20,40 and 80 kPa. Similar to the small-strain response reported by Feng and Sutter (2000), the shear modulus of SRM under medium-strain also increased with increment in confining pressure. Addition of 10% rubber to sand increased the damping ratio by three times due to the high friction between the fibre shaped tyre buffings and sand. Afterwards, Hazarika et al. (2011) conducted a series of cyclic undrained triaxial tests and cyclic direct shear tests on specimens of tyre chips having different particle size (3 mm to 26 mm) using conventional and large-scale testing apparatus. It was found that the effect of the size of the tyre (scale effect) does not have much influence on the material strength parameters. Furthermore, the rate of modulus degradation of tyre chips with increasing shear strain is significantly less in comparison to the conventional geomaterials such as sand and clay. The damping ratio of tyre chips showed about 5% increment compared to the conventional geomaterials.

Nakhaei et al. (2012) performed large-scale consolidated undrained cyclic triaxial tests on SRM with  $D_{50, \text{rubber}}/D_{50, \text{sand}} \approx 1$ . The rubber content was varied from 0 to 14% for confining pressures ranging from 50 kPa to 300 kPa. The study substantiates that the confining pressure and rubber content are the governing factors affecting the dynamic behaviour of SRM. At any given confining



pressure, shear modulus of SRM decreases with the increase in rubber content due to the low stiffness of rubber comparable to the findings of Feng and Sutter (2000). Irrespective of the rubber content, shear modulus increases with increase in confining pressure due to increase in intergranular friction, although at high rubber content the rate of shear modulus increment comes down. One interesting observation is that for confining pressures of 50 kPa and 100 kPa, the damping ratio decreased with rubber inclusion while the opposite response is observed at a high confining pressure of 200 kPa and 300 kPa. The authors attribute this behaviour to the predominant elastic strain and deformation capacity of SRM at low confining pressure and increase in the relative displacement of the grains coupled with high plastic strain at higher confining pressure. The influence of rubber content on the damping ratio increment in SRM is shown in Figure 2.12. Hyperbolic law proposed by Hardin and Drnevich (1972) was found to fit for the modulus reduction curves of SRM as inferred by Feng and Sutter (2000) based on which the authors further proposed an empirical model to predict the  $G_{max}$  of SRM for various confining pressures and rubber percentage. The author points out that, in the medium to large-strain domain, SRM with rubber content of 10%–30% exhibited a damping ratio of 18%–25%.

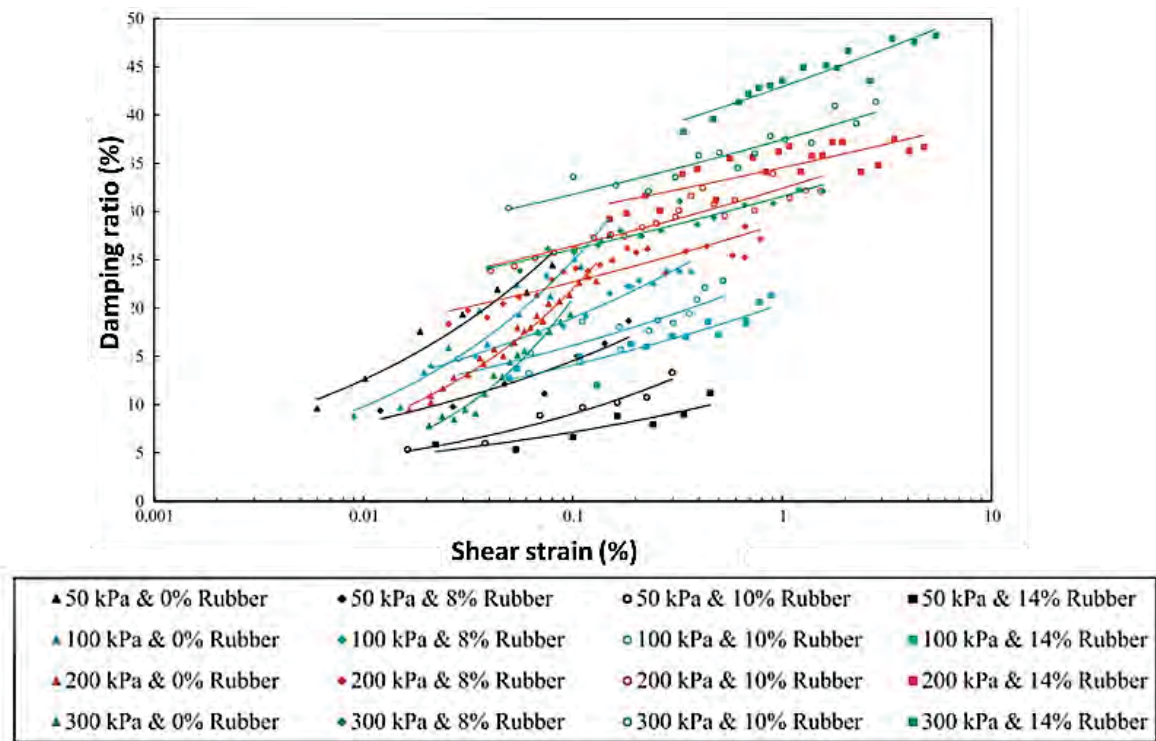


**Figure 2.12** Variation of damping ratio with shear strain for SRM with different rubber contents (Nakhaei et al. 2012)

Recently, studies by Ehsani et al. (2015) on SRM with granular rubber, using cyclic triaxial and resonant column tests also confirmed influence of rubber content, confining pressure and  $D_{50, \text{rubber}}/D_{50, \text{sand}}$ , rubber ratio on the response of SRM. It was reported that the increase in  $D_{50, \text{rubber}}/D_{50, \text{sand}}$ , rubber ratio causes the mixture to exhibit more rubber-like behaviour and higher damping ratios. Further, the use of coarser rubber particles was found to lower the shear modulus reduction, specifically in the large shear strain amplitude range.

Later, the combined small-strain and medium/high strain response of SRM with granulated rubber can be seen from the studies of Li et al. (2016) using the resonant column as well as cyclic triaxial tests. SRM with  $D_{50, \text{rubber}}/D_{50, \text{sand}} \approx 0.25$  & 1 were investigated. In the small-strain range, the shear modulus of SRM with smaller rubber particles was higher than that of SRM with large particle size due to high contact mechanism. However, the damping ratio remained the same irrespective of the size of the rubber. Whereas in the medium to large-strain range, the influence of rubber particle size is less significant on shear modulus since fabric change of SRM is dominant here. The damping ratio was higher for SRM with larger particle size compared to the mixture with smaller particles, especially at low confining pressure. However, at high confining pressure, this difference is negligible. Figure 2.13 shows the effects of rubber content on the damping ratio response of SRM having different particle size.

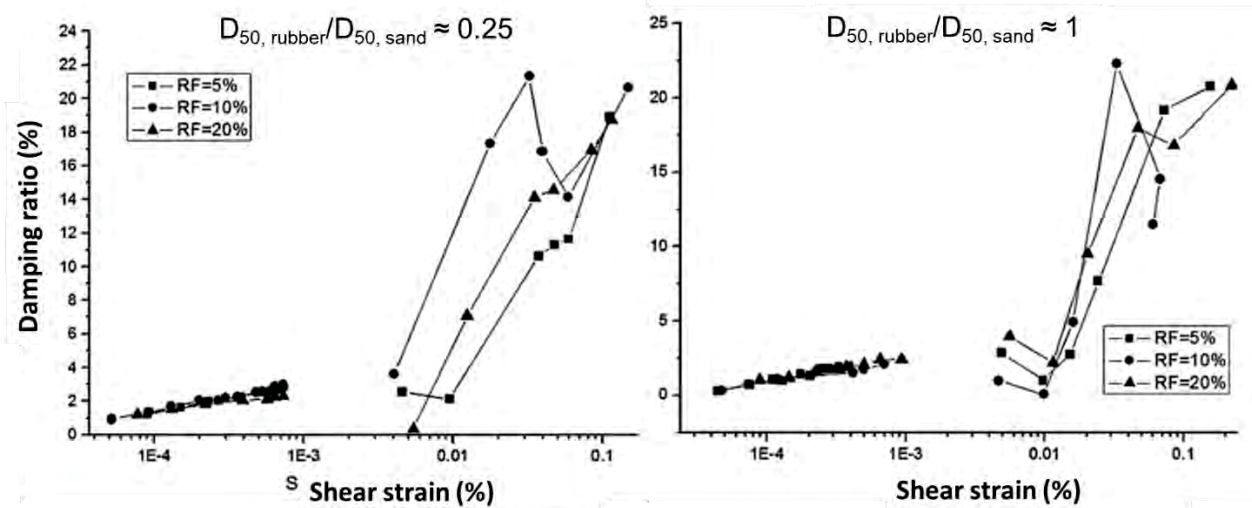


**Figure 2.13** Effect of rubber content (RF) on the damping ratio for SRM with different  $D_{50, \text{rubber}}/D_{50, \text{sand}}$  ratio for a confining pressure of 50 kPa (Li et al. 2016)

### **1.8.3. Liquefaction susceptibility of sand rubber mixtures**

Earlier studies by Masad et al. (1996) on the engineering properties of SRM reports an increase in the cohesion intercept value (apparent cohesion) due to rubber inclusion. It was found that the deformable nature of tire chips, along with the increased cohesion intercept in SRM contributed to a reduction in excess pore water pressure development. Based on a series of undrained cyclic triaxial test on SRM, Hyodo et al. (2007) reported that the presence of rubber content in SRM significantly reduce the liquefaction susceptibility of the material. Their study indicated that the reinforcement effect of tyre chips could aid in preventing liquefaction in loose sandy backfill soil. However, Promputthangkoon and Hyde (2007) report that the liquefaction resistance in SRM is limited to a rubber content of 15% (volumetrically). The findings of Hyodo et al. (2007) was backed by Hazarika et al. (2007) based on model shake table studies pointing out that upto a rubber content of 50% in SRM occurrence of liquefaction was prevented. Even at a high rubber content and relative density as low as 50%, there was no clear evidence of liquefaction. Further, Okamoto et al. (2008) used the results of monotonic triaxial shear tests to confirm the influence of tire chips in controlling the excess pore pressure generation during shearing in SRM.

Later, several researchers began to investigate the liquefaction potential of SRM for field applications. For example, Uchimura et al. (2008) studied the liquefaction response of tyre chips ( $D_{50, \text{rubber}} = 7.15 \text{ mm}$ ) mixed with sand as backfill for buried pipeline using element test and model shake table studies. While pure sand specimens liquefied at 3<sup>rd</sup> cycle of loading in cyclic triaxial testing, SRM specimens showed a gradual increment in pore water pressure, thereby liquefying only at the 18<sup>th</sup> cycle. The shake table studies indicated that SRM prevented the liquefaction induced uplift of pipes considerably.

Further, model shake table test by Hazarika et al. (2010) on caisson type quay wall with SRM as backfill also confirms the liquefaction resistance of the material for a rubber content 50% and less. Kaneko et al. (2013) numerically investigated the pseudo-dynamic liquefaction response of rubber layers alternatively placed between sand layers subjected to earthquake input motions. Though in general, poorly graded sand is vulnerable to liquefaction the tyre chips layers helped in a significant reduction of liquefaction potential and attenuation of seismic waves in the upper saturated sandy layer.



More recently, Li et al. (2016) pointed out that smaller sized rubber granules ( $D_{50, \text{rubber}}/D_{50, \text{sand}} \approx 0.25$ ) can negatively affect the liquefaction resistance of SRM. Ideally, rubber granules of size  $D_{50, \text{rubber}}/D_{50, \text{sand}} > 1$  notably improve the liquefaction resistance of the sand. Furthermore, Mashiri et al. (2016) reported that addition of 20% to 40% of tyre chips to sand is optimal for reducing the liquefaction potential of sand.

Hence, the above discussions confirm the high damping ratio of SRM rendered by the high elasticity of rubber compared to the soil, making it ideal for its application as seismic isolation material. However, the damping ratio increment in SRM highly depends on the shear strain amplitude. Further, the shear modulus of SRM was influenced by the rubber content, relative mean-size of the particles, and confining pressure. Overall, rubber content between 20% to 40% is deemed to exhibit sand-rubber matrix behaviour with adequate shear stiffness and damping ratio. Moreover, SRM was found to exhibit the high liquefaction resistance compared to natural soil making its applications suitable for geotechnical structures subjected to dynamic loading. However, most of the studies on the dynamic properties of SRM are non-conclusive and complicates the understanding regarding the parameters and factors to be considered for geotechnical problems. Hence laboratory studies should be carried out exclusively for the chosen gradation of SRM under cyclic loading to identify the modulus degradation, and damping response of SRM for the required strain ranges and confining pressures for effective use of SRM layer for base isolation of low-rise buildings.

## **1.9. GEO-MATERIALS IN VIBRATION ISOLATION**

The concept of vibration screening of surface waves for building structures was initially proposed by Woods (1968). In the past, materials such as rubber, fibreglass, asphalt pads, elastomer, elastomeric foam, rock wool, cork and other visco-elastic were commonly used as vibration isolators. The isolation system should necessarily have distinct means of providing adequate stiffness to serve as resilient support and sufficient damping for vibration separation, as a single unit or using or auxiliary damping mechanisms (Harris 1991). Konagai and Kim (2001) studied the seismic isolation effect of tunnel linings made of a thin layer of asphalt and rubber. According to the study, for augmenting the seismic isolation effect, compressible materials with low Poisson's ratio and low shear modulus are ideal, especially for reducing deformation in an earthquake.

Yegian and Kadakal (2004) conducted studies on foundation isolation for seismic protection using a smooth synthetic liner placed underneath foundations of building structures, as shown in Figure 2.14. Experimental studies conducted by the authors using shaking table & cyclic triaxial apparatus proved that high strength, nonwoven geotextile placed over an ultrahigh molecular weight polyethylene geotextile works well for seismic isolation. The energy absorption, in this case, was achieved through the sliding mechanism. Hazarika et al. (2007 and 2008) proposed the use of tyre chips for waterfront retaining structures as a cushion layer between soil backfill and a caisson quay wall. They performed a series of large-scale underwater shaking table tests on a gravity type model caisson protected by the tyre chips cushioning technique. They reported a substantial reduction in the seismic load against the caisson wall along with reduced residual displacement induced by seismic loading. Further, Kirzhner et al. (2006) proposed to replace soil by a more elastic material (including rubber or rubber soil mixture) surrounding tunnel for noise and vibration absorption.

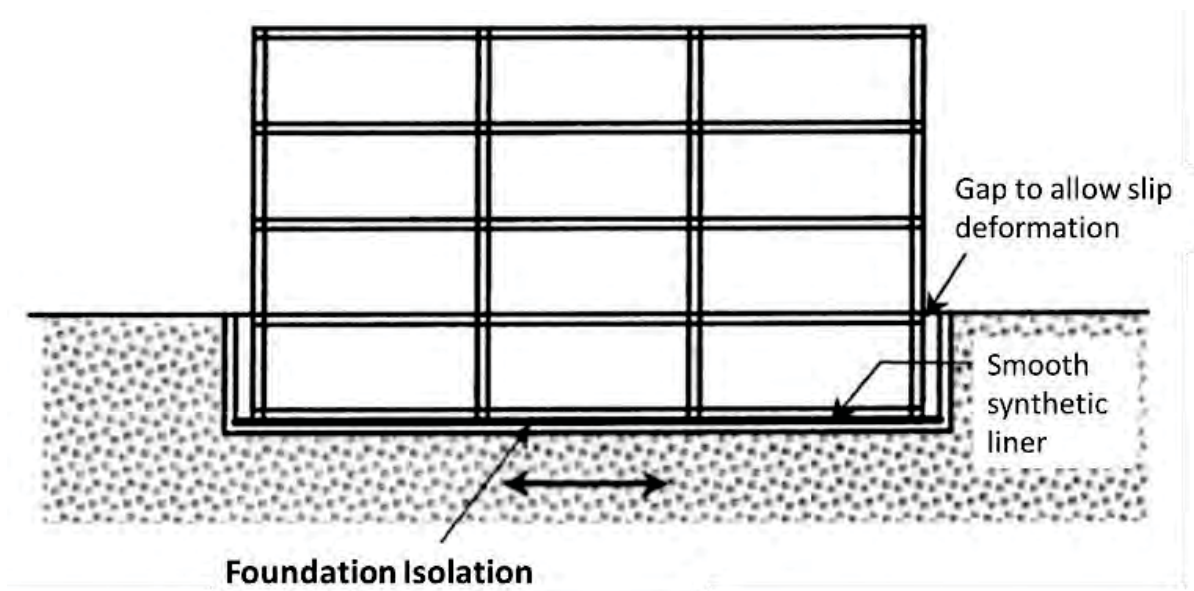


**Figure 2.14** Foundation isolation using smooth synthetic liner (Yegian and Kadakal, 2004)

The use of low acoustic impedance materials such as the compressible geofoam as seismic buffers was initially explored by Bathurst et al. (2007) for dampening of dynamic waves against retaining walls. They reported a dynamic force attenuation of about 30% by geofoam buffers using shake table studies on a model retaining wall. Later, ground vibration isolation studies by Zarnani and Bathurst (2008) and Murillo et al. (2009) also confirmed the high seismic buffer effects of geofoam barriers. Furthermore, studies on soil bags typically used as reinforcement for soft soil below

building foundations were found to reduce the traffic-induced ground vibrations. The vibration damping by soil bags was achieved through the frictional movement of the soil particles within the bag in addition to the contraction and expansion of the bag (Matsuoka et al. 2005; Nakagawa et al. 2009; Liu et al. 2014).

Recently, tyre derived aggregates are widely applied for vibration mitigation problems. For example, Lee and Roh (2007), used tire chip mixtures as backfill for culvert walls to reduce the dynamic earth pressure induced by construction loading. Ahn and Cheng (2014) used tyre aggregates for seismic protection of retaining walls and evaluating its dynamic performance on a full-scale shake table test subjected to simulated earthquakes. They confirmed the drastic reduction in dynamic pressure exerted by tyre aggregates. Lately, tyre aggregates have found its way as a potential vibrating mitigation option for railway tunnels (Cheng 2016).

#### **1.10. EXPERIMENTAL STUDIES ON DYNAMIC RESPONSE OF FOOTINGS RESTING ON SAND RUBBER MIXTURE LAYER**

Due to the lack of field data on buildings/foundations isolated using SRM during earthquakes, model tests can give a fair idea about the seismic performance of SRM as an isolation layer. Typically, 1g shake table tests on model footings are used to understand the actual nonlinear soil response and foundation rocking in the energy absorption mechanism of SRM isolators. However, limited shake table studies are reported in the literature on this topic wherein few researchers validated the performance of model footing/building isolated using SRM layer (Xiong and Li 2013; Bandyopadhyay et al. 2015) using shake table studies.

Shaking-table experiments were conducted by Xiong and Li (2013) with shredded SRM as isolation material placed below concrete block (1700 mm x 1700 mm x 300 mm) to simulate the actual vertical pressure of a rural building on the subsoil as shown in Figure 2.15. Sinusoidal, ambient, and El Centro waves were used as ground excitations in the shake table tests and tests were carried out for 100 and 200mm thickness of SRM layer (rubber content 35% and 50%). It was observed that the isolation effects are more significant for 200 mm thickness of RSM layer. Further, it was reported that an SRM layer with 35% rubber content caters to both seismic protection and the bearing capacity demands and can attenuate the structural response, in terms of the maximal output acceleration, by 30–50%.

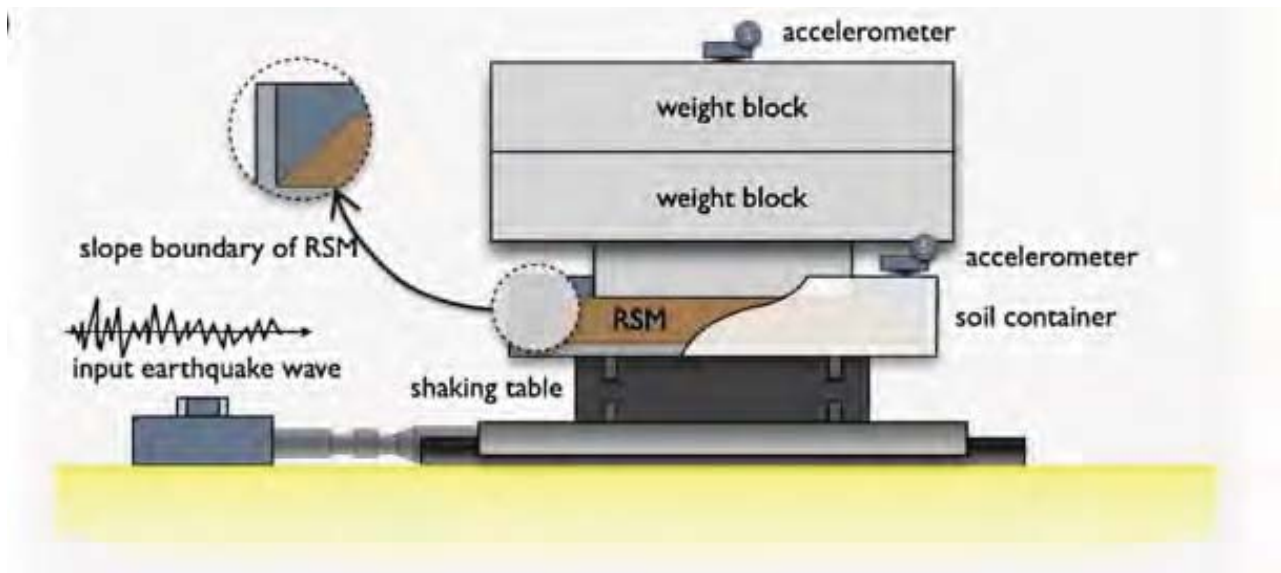


**Figure 2.15** Schematic view of the shake table setup using SRM isolator (Xiong and Li 2013)

The influence of frequency and peak amplitude of input motion on the performance of a model footing resting on SRM layer were investigated by Bandyopadhyay et al. (2015) using model shake table studies. They used rigid glass block (200 mm x 200 mm size; 40 mm thickness) with surcharges to simulate the loading of a two-story residential building in a shake table setup (1 m x 1 m x 0.5 m) filled with sand (Figure 2.16). The footing was placed on SRM layer of size 250 mm x 250 mm and 20 mm depth (variable) for a broader range of rubber content (10% to 50%). Sinusoidal excitations with acceleration amplitude of 0.15 g to 1 g at frequencies of 1.5 Hz to 4.5 Hz were applied during shaking while the output accelerations were measured at the model footing top. The effectiveness of sand as an isolation medium was noted only at high amplitudes of base motion greater than 0.6g. However, SRM exhibited high energy dissipation and damping as well as a significant reduction in the output acceleration response on the model footing even at the smaller amplitudes of base motion. SRM with 50% rubber content was found to be performing well in terms of damping the base motion beyond which foundation rocking starts to appear. Besides, increment in the surcharge load was found to reduce the acceleration amplification capacity of SRM isolator further. Nonetheless, the effect of frequency of input motion is not conclusive in this study.

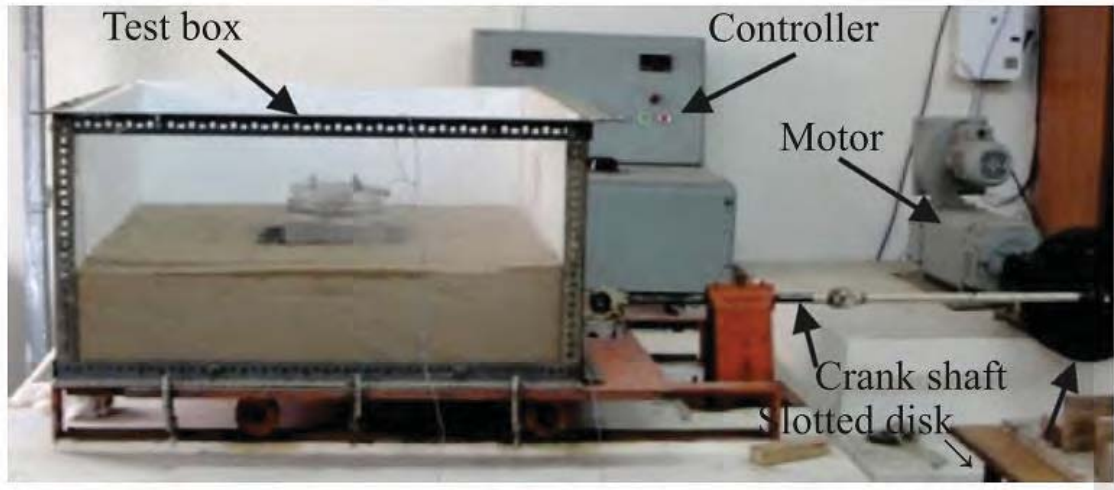


**Figure 2.16** Shake table tests on model footing resting on SRM layer (Bandyopadhyay et al. 2015)

### **1.11. NUMERICAL STUDIES ON SEISMIC SSI ANALYSIS OF BUILDINGS ON SAND RUBBER MIXTURE LAYER**

The literature abounds with methods to practically model the soil and foundation systems. These methods vary widely in complexity and applicability. Shallow foundations are often approximated with lumped springs with an assumption that the foundation is supported by a homogeneous, elastic, semi-infinite medium (Gazetas, 1991; Wolf, 1997). The application of these methods to the seismic analysis of a building/structure requires determining the equivalent elastic properties and fundamental frequency of the structure. However, the above methods may not accurately model the foundation soil system in the case of multi-layered soil system. Therefore, the most comprehensive approach to solve the SSI problem is through an FE analysis in which complex structural configurations and soil layers can be explicitly modelled. SSI analysis plays a vital role in the study of response of base isolator structures. The base isolation system works well for stiff soil conditions (Ealangi, 2010). However, when soft soils or soil with low stiffness are encountered for base isolated buildings, the effects of soil-structure interaction become predominant.

The two basic methods involved in the solution of soil-structure interaction (SSI) problems are the direct method and the substructure method.

#### ***a) Substructure method***

In this method, the foundation and structure are considered separately and are analysed using the principle of superposition. This approach has the advantage that soil can be considered separately

as an unbounded medium while structure can be considered and analysed separately as bounded discrete systems. In a substructure analysis, the soil-foundation-structure-interaction problem is broken down into three distinct parts that are combined to formulate the complete solution. This involves evaluation of a foundation input motion (FIM) and determination of the impedance function. The final step involves the dynamic analysis of the structure supported on a compliant base represented by the impedance function and subjected to a base excitation consisting of the FIM (Kramer and Stewart, 2004). The substructure approach is advantageous if the foundation is rigid, as the soil system can be approximated as a set of frequency-dependent equivalent springs (Kramer, 1996). Since the substructure method relies on the principle of superposition; the soil medium is considered as linear and equivalent linear elastic medium, but at a high intensity of shaking, soil behaves highly non-linear and true non-linear models should be considered.

***b) Direct method***

The direct method of SSI analysis accounts for the inertial and kinematic interactions simultaneously with the entire soil-structure system modelled as a finite element model. The approach can be used for both time- and frequency-domain analysis. The direct approach requires fewer assumptions than other simplified procedures in the modelling of near-field soil around a structure. However, there are a few key issues that need to be considered in the direct approach: the infinite boundary of the soil domain, mesh size of the soil, the domain size, the stability of the numerical integration scheme, the time step of the integration scheme and material damping of the soil. In the direct approach, the boundary of the entire soil system to be properly defined. There are several techniques that can consider infinite soil medium for dynamic FE analysis: viscous energy-absorbing boundary (Lysmer and Kuhlemeyer, 1969), the perfectly matched layer (PML) method (Basu and Chopra, 2003) and various kinds of infinite elements (Zienkiewicz et al. 1985; Chadwick et al. 1990; Kim and Yun, 2000).

Gharehbaghi et al. (2012) used the direct approach to simulate the SSI response of an RCC structure using FE software OpenSees. In this method, the entire soil-foundation-structure is modelled and analysed in a single step, as shown in Figure 2.17. Usually, the infinite soil medium is truncated using artificial boundaries using absorbing or transmitting boundary conditions or by placing the structure at a sufficient distance from the boundary, so that wave reflection effects at the boundary are minimized. In this study, the standard viscous boundary proposed by Lysmer and Kuhlemeyer (1969) is used. Since the direct method involves solving the entire soil and structural



response together, it is so much time consuming and requires more storage space, especially when iterations are required for calculation.

The effects of SSI on the seismic base-isolated buildings founded on different types of soil were studied by Alavi and Alidoost (2012). Mathematical models were used for simulating the base isolated structure and soil system. The foundation and structure were modelled using lump mass and the soil characteristics beneath of the buildings are modelled using half-space cone model theory. Four different base isolated building having 2, 4, 7, and 10 stories were used in the analysis. It was found that SSI effects are predominant on softer soils irrespective of the stiffness and natural period of the building. By increasing the aspect ratio  $H/r$  (height to equivalent radius) of the foundation, the effects of rocking action and SSI were found to increase.

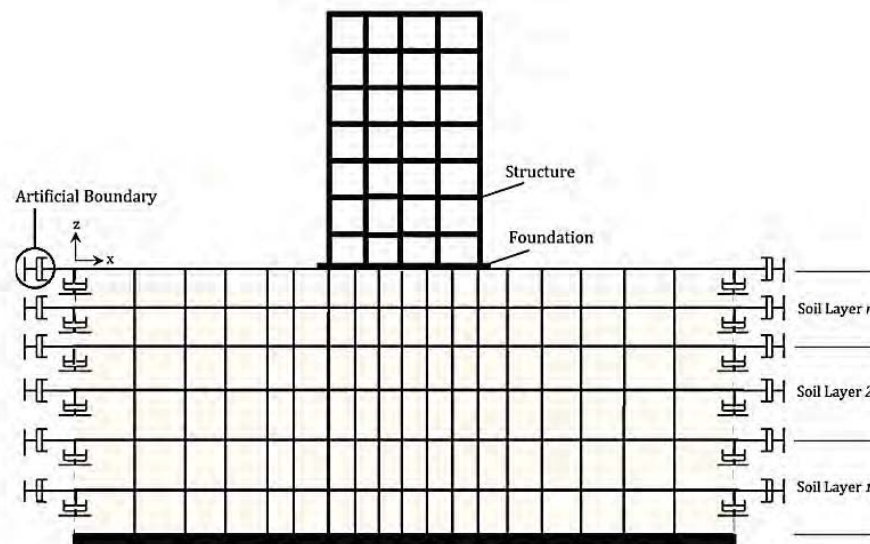


**Figure 2.17** Direct method configuration for modelling of SSI system (Gharehbaghi et al. 2012)

Past numerical studies on the dynamic responses of soil–foundation–structure system usually considered equivalent linear method was to incorporate the non-linearity of the materials. Tsang et al. (2007) and Xu et al. (2009) studied the time-domain dynamic response of soil–foundation–structure having SRM cushion for seismic isolation using 2D FE code QUAD4M. Parametric studies were carried out by Tsang et al. (2007) for 5 & 15 storeyed buildings for  $T/H$  (thickness of SRM/width of footing) ratio of 0.25 and peak ground acceleration varied from 0.45 g to 3.6 g. The typical time history of normalized acceleration response obtained for a 15-storey building is shown

in Figure 2.18. It was found out peak acceleration got reduced by 40–60% due to the placement of the SRM layer.

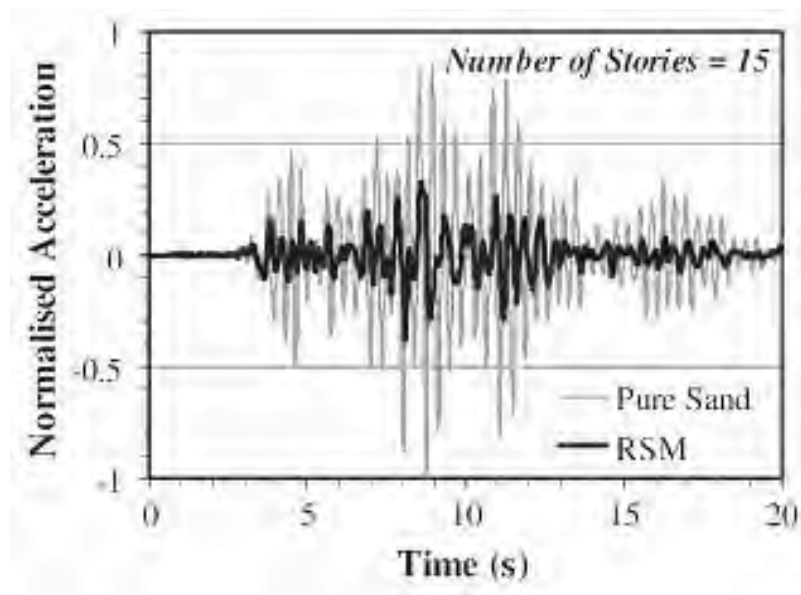


**Figure 2.18** Normalized footing horizontal acceleration time histories (Tsang et al. 2007)

Abdelhaleem (2012) studied the site response of a layer of SRM placed within the replacement soil of a landfill. The soil was modelled using an equivalent linear constitutive model. Earthquake motions having predominant period  $T_p$  greater than (0.92 s) and lesser than (0.13 s) that of the natural period of the site ( $T_{site}=0.5$  s) was considered in the study. The depth of placement and the thickness of the SRM layer was varied from 2 m to 6 m. The study identified that higher the natural period of the structure, deeper the sand/rubber layer needed to be placed for effective isolation. It was also found that period shifting and damping of spectral acceleration were predominant when RSM layer was placed at a greater depth.

Tsang et al. (2012) studied the time-domain dynamic response of a soil–foundation–structure system having isolation system made of granulated rubber–soil mixtures. 2D frame elements are used to model the superstructure as shown in Figure 2.19, and linear model analysis was carried out for superstructure. Newmark method was used to solve the governing dynamic equations. Four-Node quadrilateral plane-strain elements were used in the modelling of footing and soil materials. Rayleigh method was used for considering the material damping. Viscous boundaries were assumed as the boundary condition to cater to the non-reflective effects of infinite soil. It was



observed that the SRM isolation is more effective for low raised buildings and also, thicker the SRM layer higher would be the damping of waves.

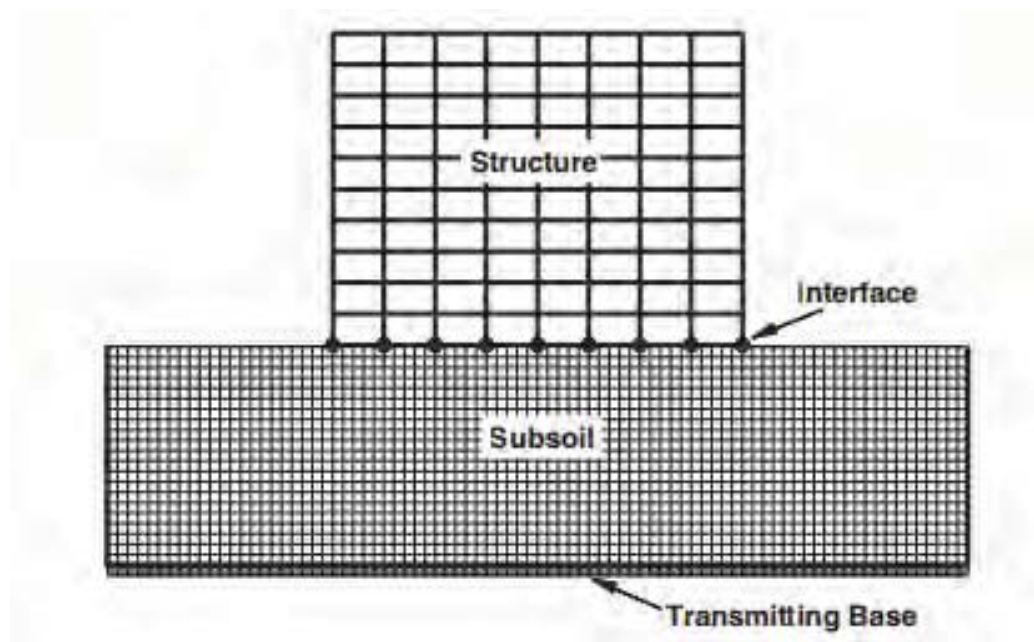


**Figure 2.19** Finite element model of the soil–foundation–structure system (Tsang et al. 2012)

The frequency-dependent response of the foundation stiffness and damping were well explored in the recently by Pitilakis et al. (2013). They used an equivalent linear approach to account for the non-linearity in soil behaviour for determining the impedance coefficients using boundary element formulation. Further, Pitilakis et al. (2015) carried out dynamic FE analysis of the soil–structure systems with isolation medium of SRM using FE code OpenSees. Dynamic analyses of the numerical model were performed for RC framed structure considering different SRM layer thickness and building's height. The soil was modelled as an elastoplastic material and continuous raft foundation is modelled as an elastic beam-column element (Figure 2.20). The thickness of RSM layer was taken as 3 and 6m. Earthquake input motions with predominant period varying from 0.18 s to 0.74 s was used. The study points out that the effectiveness of SRM layers is predominant for mid-rise and high-rise buildings in terms of reduction in design shear force and displacement. However, the settlement response of the building with SRM layer is not reported in these studies.

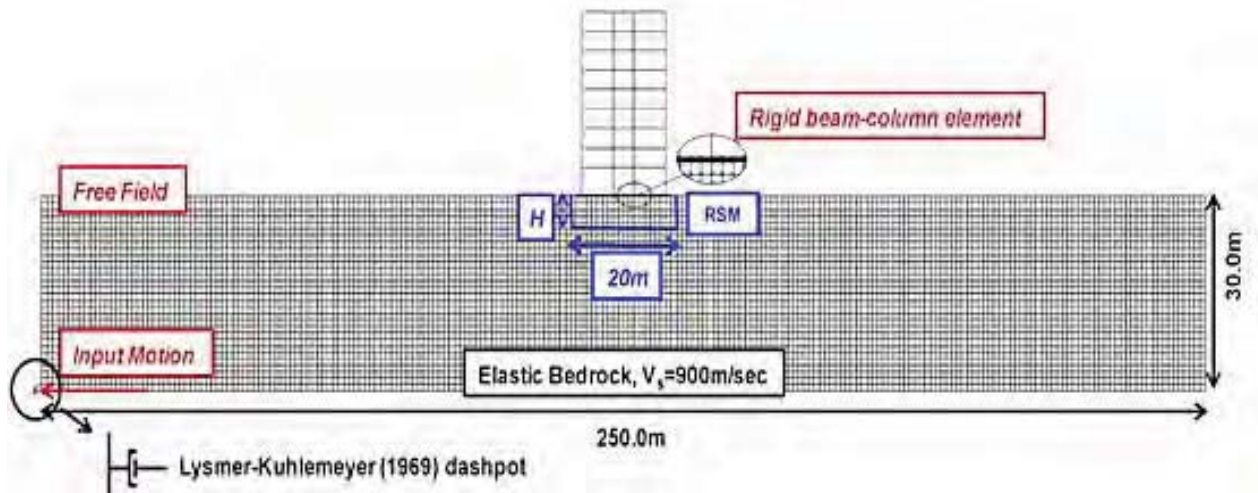


**Figure 2.20** FE model of the soil–structures systems (Pitilakis et al. 2015)

Almost all the researchers mentioned above had acknowledged the potential use of SRM as an effective seismic isolation layer for building/ foundation problems. However, most of the studies explore a very narrow range of predominant frequency and peak acceleration of earthquake input motion. Consequently, further studies need to be carried out to explore the influence of input motion characteristics for low rise building in a broader range. In addition, the focus is on idealized soil conditions with little emphasis on site-specific cases, which may affect the performance of the structure. Importance of the crucial issue of deformation and settlement posed by the low stiffness of SRM, which could adversely affect the building safety was also not given enough consideration. Finally, there are extremely limited cases available on the response of the foundation/building system supported on SRM layer with due consideration to the SSI effects.

## 1.12. GEOSYNTHETIC REINFORCED SOIL FOUNDATIONS

As discussed in the earlier sections, the low stiffness and high compressibility of SRM raises a concern about the bearing capacity and settlement of foundation (Youwai and Bergado, 2003; Sheikh et al. 2013). The bearing capacity of shallow foundations resting on weaker soils can be improved by adopting the concept of soil reinforcement, which is also found to decrease the soil settlement. In the past three decades, several researchers have carried out experimental and analytical studies on geosynthetic reinforced soil mass underlying shallow footings for different types of soils (Biquet and Lee 1975; Guido et al. 1986; Bathurst and Jarrett 1988; Das et al. 1994; Yetimoglu et al. 1994; Shin et al. 2002; Latha et al. 2009; Lavasan et al. 2017; Cicek et al. 2018).

Binquet and Lee (1975) distinguished three possible modes of failure in a geosynthetic reinforced soil-foundation system. The first mode of failure occurs through pull out of reinforcement due to sliding in the soil while the second mode occurs through rupture arising from the tensile failure. The third mode is inherent to small-scale tests where the sliding of reinforcement occurs due to the slippage of the soil below. Typically, the ultimate tensile force developed in the reinforcement is the sum of mobilized resistance in the soil as well as the reinforcement (Jewell 1984). The relative displacement between soil and the geosynthetic reinforcement leads to the development of frictional force at the soil– geosynthetic interface leading to improved lateral confinement. The increase in bearing capacity of the reinforced soil-foundation system can be attributed to two mechanisms namely: deep footing effect and wide-slab mechanism depending on the length of geosynthetics (Huang and Tatsuoka1990).

Commonly adopted geosynthetic materials include geotextile, geogrid and geocells. Geogrids are frequently adopted for footing problems, as it has been found to have interlocking properties with soil which in turn increases the soil stiffness and shear resistance around the geogrid (Jewel et al. 1984). Various researchers attempted to evaluate the bearing capacity of foundations on soils with geogrid reinforcement (Khing et al. 1993; Omar et al. 1993; Yetimoglu et al. 1994; Chen et al. 2007; Ghazavi and Lavasan, 2008; Prasad et al. 2016). The interlocking mechanism of geogrids limits the soil particles movement within the grid apertures leading to aperture deformation and additional lateral stress exerted by the grid ribs to the soil. Restraining, the lateral deformation of the reinforced soil, thus results in improved lateral confinement, which eventually improves the compressive strength of the soil. This way, the vertical deformation in the soil is reduced.

Further, the membrane effect provided to the reinforcement by the downward movement of soil further enhances the bearing capacity. According to Huang and Tatsuoka (1990), the membrane effect can develop only when the length of reinforcement is adequate to resist pullout failure with sufficient tensile strength. In addition to central vertical loading, the geogrids also increase the ultimate bearing capacity of soil under eccentric and normal loading conditions arising due to wind and earthquake loads (Badakhshan and Noorzad 2015; Xu and Fatahi 2018a, b).

The bearing capacity evaluation of soil with geosynthetic reinforcement is usually performed in the laboratory using scaled model tests to examine the load–settlement response of the footing (Shin et al. 2002; Chen et al. 2007; El-Sawwaf 2007; Tafreshi and Dawson 2010; Demir et al.2014). A typical model test setup of the footing resting on geosynthetic reinforced soil and the

associated instrumentation such as pressure cells and strain gauges used for laboratory testing by Abu-Farsakh et al. (2013) is shown in Figure 2.21.

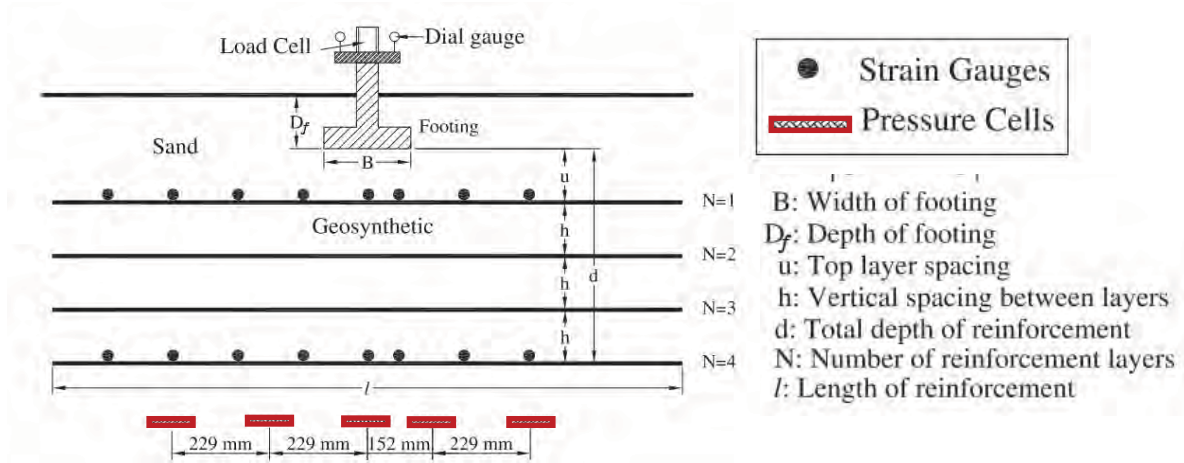


**Figure 2.21** Model test setup of geosynthetic reinforced soil footing (Abu-Farsakh et al. 2013)

Most of the above researches were focused on the primary parameters and factors that are crucial for obtaining the optimal bearing capacity improvement by geosynthetic inclusion in soil. Though there is a difference in specifications by various researches, most of the literature agrees to a narrow range of optimal values for the parameters. For example, the optimal depth of placement of the first reinforcement layer from the bottom of the footing is typically  $0.2B-0.5B$  (where  $B$  is the width of footing) while the optimal length of the reinforcement lies between  $2B$  to  $8B$ . Similarly, the contribution of reinforcement in bearing capacity improvement is primarily within the depth of the influence zone of the footing. While most of these results are for natural soils, to the knowledge of the authors, the influence of geogrid reinforcement for SRM on the foundation response is not explored in the past. Further, the effect of earthquake loading on the above combination of materials also needs to be taken into consideration since the focus of the present research is particularly on seismic isolation.

The beneficial effects of geosynthetics in the protection of structures such as foundations, retaining walls and soil walls subjected to dynamic loading were well established by Murali and Madhavi (2012), Kuwano et al. (2014) and Han et al. (2015). Recently, studies on the application of geosynthetics for seismic protection of mid-rise buildings on shallow/deep foundations by Xu and Fatahi (2018a, b) found that geosynthetic reinforcement reduces the shear forces, lateral displacement and inter-storey drifts that develop in a superstructure due to the seismic forces

(Figure 2.22). Geosynthetic reinforced soil aids in reducing the rocking response of foundations when subjected to seismic loading, thereby preventing failure of the reinforced soil bed (Taha et al. 2015; Xu and Fatahi 2018a, b). The confinement and membrane effects offered by the reinforcement layers can contribute to reducing soil deformations under lateral loading (Xu et al. 2015; Xiao et al. 2016).

Studies on the dynamic properties of geosynthetic reinforced soil have proved that geosynthetic inclusion could increase the damping ratio of the system (Vercueil and Cordary 1997; Pamukcu and Akbulut 2006; Akbulut and Pamukcu 2010). The higher damping ratio can further contribute to the reduction in vibration transmissions due to energy dissipation, which is beneficial while designing a seismic isolation system. Furthermore, the liquefaction resistance of granular materials reinforced with geosynthetics was well established (Krishnaswami and Isaak 1995; Boominathan and Hari 2002; Altun et al. 2008; Mittal and Chauhan 2013). Shake table studies by Maheshwari et al. (2012) reported the liquefaction resistance of geogrid reinforced poorly graded sand due to the reduction in pore pressure build-up time.

The sand/SRM-reinforcement interaction mechanisms play a vital role in the performance of geosynthetic reinforced soil -footing system. While considering numerical modelling, the soil/SRM geogrid interface modelling needs to be given due attention. One method involves modelling the soil and reinforcement grouped as an equivalent homogeneous continuum media (Yamamoto and Otani 2002) while the other method involves modelling the soil and geosynthetics separately as different elements (Latha and Somwanshi 2009; Kalpakci et al. 2018). The interaction properties are usually evaluated using direct shear and pull-out tests. Pull-out test on tyre chip with geogrids reveals that interaction coefficient gets reduced for soil due to the addition of rubber (Bernal et al. 1996, 1997) since in small-scale testing, the shearing areas surrounding the geogrids are not fully able to mobilise the maximum shear stress in the geogrid interface. Tatlisoz et al. (1998) reported that interaction coefficients between geosynthetics and SRM to be higher than 1, while Youwai et al. (2004) reports an interaction coefficient of 0.85 between wire mesh and tyre chip. Similarly, Tanchaisawat et al. (2010) reported an interaction coefficient of 0.87 between geogrid and tyre chip–sand backfill indicating efficient bond between the fill and the geosynthetic reinforcement.



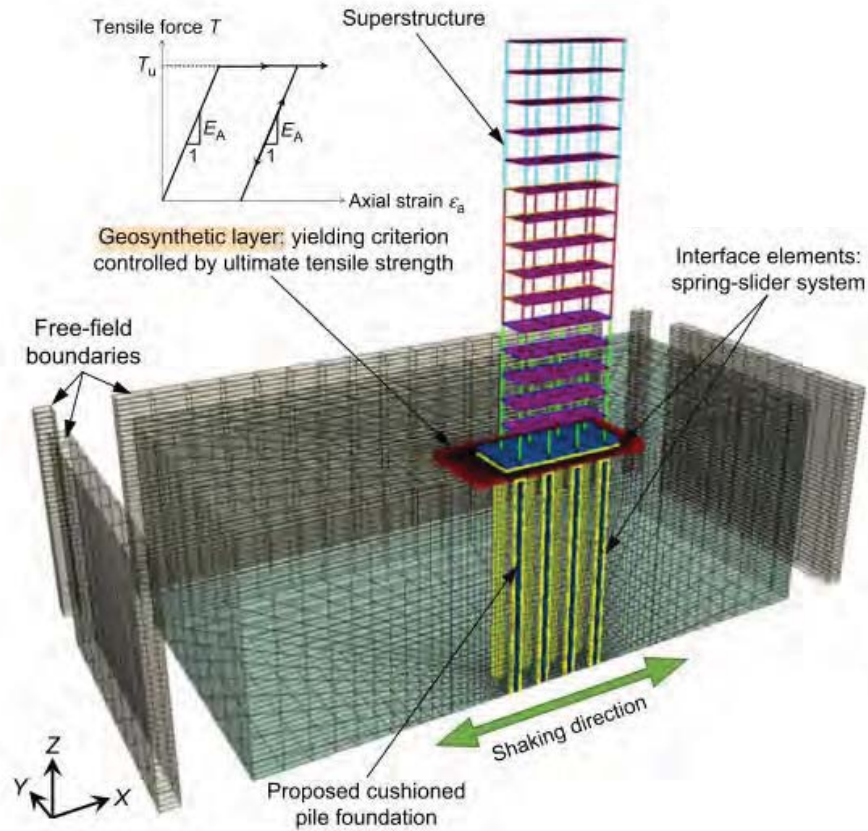


**Figure 2.22** Numerical model of geosynthetic-reinforced cushioned pile (Xu and Fatahi 2018b)

### 1.13. SUMMARY

Sand-tyre mixture is found to be a good seismic isolation material due to its energy dissipation properties. Most of the studies related to sand-tyre isolators are focused on material characterisation, which suggests that the performance of sand-tyre isolators is primarily dependent on rubber content and confining pressure. However, considerable disagreement exists regarding the shear strength of SRM depending on the specifications of rubber used in the mixture. Similarly, most of the studies on the dynamic property of SRM shows the high damping ratio of SRM with rubber content between 20% to 40% is deemed to exhibit sand-rubber matrix behaviour with adequate shear stiffness and damping ratio. Experimental studies needed to be carried out exclusively for the chosen gradation of SRM under static and cyclic loading for arriving at the optimum percentage of soil-rubber mixture that has enough stiffness and energy dissipation capacities for its application as seismic isolation material below building foundations. Further,

SRM was found to exhibit the high liquefaction resistance compared to natural soil as well as segregation resistance upto a rubber content of 50% making it suitable for vibration applications. In addition, the static performance of buildings placed on the GBI system and the settlement problems posed by the low stiffness of SRM was not given adequate attention from past studies. The possible use of geosynthetic reinforcement in improving the performance of geo-isolation layer made of SRM was not studied in the past.

Numerical studies on the field application of soil-tyre isolators are limited and much information is not available on the performance of the isolator under different earthquake conditions and for layered soil mediums. Limited studies reported on the use of SRM as a vibration-absorbing layer for buildings focus on idealized soil conditions with little emphasis on site-specific cases. The response of structure supported on a sand-tyre isolation layer depends on the performance of the isolator as well as the SSI interaction effects. Minimal studies are carried out to understand the influence of SSI effects on the performance of such base isolated buildings in a multi-layered soil system.

A rigorous dynamic analysis using the advanced FEM based tools is required to understand the effect of soil-rubber inclusion in reducing shaking intensity. The objective of this study is to investigate the behaviour of low-rise building with shallow foundation resting on GBI layer with and without geogrid reinforcement subjected to static and seismic loads and to carry out parametric studies to understand various factors influencing the performance of geogrid reinforced GBI system for isolation of typical low-rise building.

## CHAPTER 3

### CHARACTERISATION OF MATERIALS USED

#### 3.1. INTRODUCTION

From the preceding literature review, it was observed that while using SRM for geo-base isolation, the performance of the system is highly affected by the combined response of sand and rubber matrix present in the mixture. The shear strength properties of the material along with the dynamic properties of the material are the two important factors considered in the static and seismic behaviour characterization of SRM. While some literatures report the improvement in shear strength of the base soil with addition of tyre shreds/chips (Foose et al. 1996; Zornberg et al. 2004; Rao and Dutta 2006), other studies show the decrease in shear strength with addition of the tyre shreds (Masad et al. 1996; Cabalar 2011; El-Sherbiny et al. 2013). The variation in the properties was primarily due to the size of tyre chips/shreds relative to the base material as well the relative density of the material (Ghazavi and Sakhi 2005; Gotteland 2005). Similar variations were reported in the dynamic properties of the SRM by various researchers for granulated tyre rubber (Feng and Sutter 2000; Anastasiadis et al. 2012; Senetakis et al. 2012), tyre chips (Mashiri 2014) and tyre crumbs (Madhusudhan et al. 2017). Hence it is essential to undertake a proper experimental study to understand the engineering and dynamic properties of the SRM. This chapter discusses in detail the various experimental investigations carried out to determine the index property and shear strength characteristics of sand and SRM along with the monotonic and cyclic behaviour of the material.

The initial part of the chapter is focused on the determination of the index properties of the sand and SRM. Sieve analysis was carried out for gradation and classification of the materials. Different compositions of rubber were gravimetrically mixed with sand to compare and identify the basic response of different mixtures. The maximum and minimum unit weight of the sand and different proportions of SRM were discussed in this chapter. The suitability of various techniques used to calculate the maximum dry densities was also examined. The relative density technique was adopted as the control factor for uniformity check of the materials in the study. Segregation check was undertaken to ensure the homogenous distribution of rubber & sand in SRM throughout the experimental study. Further, the shear strength response of sand and different composition of SRM



using direct shear test was investigated. The results from the study serve as a valuable baseline reference for assessing the choice of the SRM. The shear strength and volumetric response were identified for different normal stresses and relative density of the material. Further, the shear strength parameters were reported for various combinations of SRM in the chapter.

Further, the monotonic response of the sand/SRM was explored using triaxial testing equipment. The sample preparation for sand/SRM and testing procedures were discussed in detail in this chapter. The response of sand/SRM under consolidated drained as well as the consolidated undrained conditions were explored to understand the strength and deformation response of SRM. To understand the dynamic response of the SRM, cyclic triaxial tests were conducted under consolidated drained conditions. The dynamic material properties such as shear modulus and damping ratio were obtained from the studies. The material properties of geogrids adopted for the model test in Chapter 4 was investigated in the current chapter using basic tensile strength tests and direct shear tests.

## **3.2. MATERIALS**

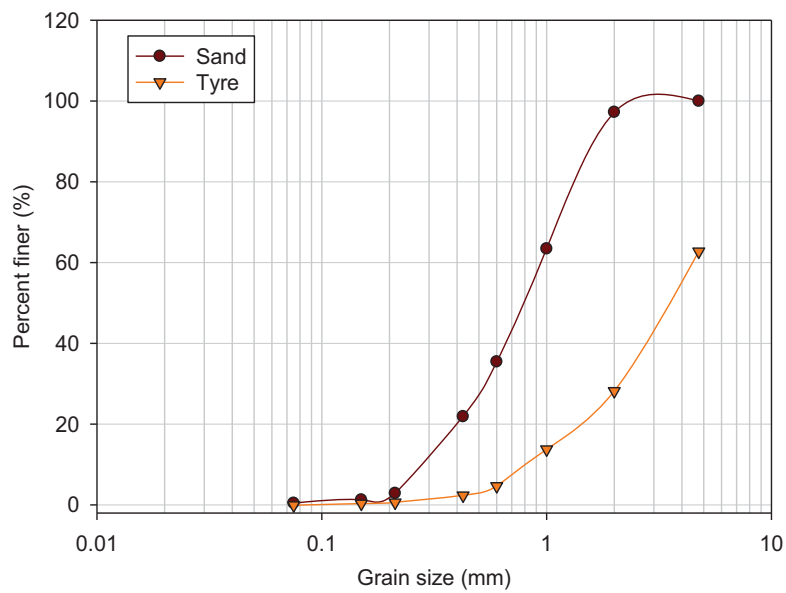
The experimental program to determine the engineering properties of the pure sand and SRM along with its classification was carried out by conducting routine laboratory tests. Initially, the gradation of soil and the shredded rubber from the waste tyre used for the testing were carried out using sieve analysis. The index properties of the material such as the specific gravity, minimum dry unit weight, maximum dry unit weight and relative density were obtained from laboratory tests following basic relationships, as discussed in the following sections.

### **3.2.1. Soil**

In the present investigation, locally available river sand collected from Chennai city (India) was used. The sand is relatively uniform with angular shaped grains. Grain size analysis using mechanical shakers (Figure 3.1a) was utilized to identify the gradation of the materials. The materials were classified as per the Indian standard classification system (IS: 1498 1970). The grain size distribution curve obtained for sand is shown in Figure 3.1b. The soil has a mean grain size ( $D_{50}$ ) of 0.8 mm, coefficient of uniformity ( $C_u$ ) of 3.4 and a specific gravity of 2.65. The soil is classified as poorly graded Sand (SP) as per IS: 1498 (1970).



(a)



(b)

**Figure 3.1 (a)** Mechanical sieve shaker used for grain size analysis **(b)** Particle size distribution curve of sand and granulated tyre

### 3.2.2. Scrap rubber tyre

Scrap rubber tyre used in the study was obtained from a local scrap tyre-recycling unit where the steel reinforcements inside the automobile tyres were removed. The tyre base material used for the study is from heavy-duty automobiles such as lorry/trucks which have a higher proportion of

natural rubber compared to other non-rubber ingredients like steel and fibres. The final shredded tyre samples are metal and textile fibre-free. Further, these tyres will have higher abrasion and wear resistance together with high durability compared to low duty automobiles. The scrap tyres were fragmented into angular shaped granulated tyres of size less than 4.75 mm using the shredding machine from the tyre-recycling unit. The tyre particles passing 4.75mm size sieve was used in the preparation of sand-rubber tyre mixture samples. The rubber tyre material used in this study is classified as granulated rubber tyre according to ASTM D 6270-08 (2012) since the particle size lies in the range of 425  $\mu\text{m}$  – 12 mm. The tyre granules used in this study are displayed in Figure 3.2. The gradation procedure same as that of sand is followed for the granulated tyre and the corresponding particle size distribution curve is presented in Figure 3.1. Coefficient of uniformity ( $C_u$ ) of 5.17 and a specific gravity of 1.1 was obtained for the tyre. The granulated tyre for the present study was classified as an equivalent of poorly graded sand (SP) as per IS: 1498 (1970). The physical properties of sand and the granulated rubber tyre are presented in Table 3.1.

### **3.2.3. Sand rubber mixture (SRM)**

Tyre granules passing 4.75 mm size sieve were mixed with sand in fixed proportions for the preparation of SRM samples for laboratory studies in the current chapter and scaled model studies in the next chapter. For the present study, SRM with rubber content of 0% to 50% by dry weight of sand were uniformly hand mixed to achieve a homogenous mixture. Gravimetric proportioning is adopted rather than the volumetric proportioning for the rubber/sand content in the SRM to attain better control and uniformity in the mixture.

Figure 3.2 shows the SRM samples used for the study. While considering the gradation of materials for the study, it is essential to assess the liquefaction potential of the materials chosen. Though in general, poorly graded sand in the study is vulnerable to liquefaction, the presence of rubber content in the SRM reduces the liquefaction susceptibility of the material (Hyodo et al. 2007). Further, the medium particle size ratio ( $D_{\text{rubber}}/D_{\text{sand}}$ ) of the individual materials in the mixture serves as an indicator of liquefaction. In this study, medium particle size ratio is greater than 1, which indicates the higher liquefaction resistance of the material (Li et al. 2016). Figure 3.2 shows the typical samples of sand, rubber and SRM used for the study.



**Figure 3.2** Samples of (a) Sand (b) Granulated rubber (c) SRM

**Table 3.1** Properties of sand and rubber tyre

Property	Sand	Granulated rubber tyre
D <sub>10</sub> , mm	0.28	0.87
D <sub>30</sub> , mm	0.51	1.95
D <sub>60</sub> , mm	0.95	4.5
Coefficient of uniformity (C <sub>u</sub> )	3.40	5.17
Coefficient of curvature (C <sub>c</sub> )	0.98	0.97
Specific gravity (G <sub>s</sub> )	2.6	1.47
Classification	SP	Equivalent of SP

### 3.3. DRY UNIT WEIGHT

This section evaluates the maximum and minimum unit weight of sand and SRM using suitable methods. Since the granulated rubber present in SRM exhibits elastic deformation and high compressibility especially at low normal stress (Bosscher et al. 1997), selecting an appropriate technique to achieve the maximum unit weight needs to be addressed. Besides, the compressibility of SRM shifts from granular material like to rubber-like behaviour as the rubber content in the mixture increases which in turn affects the density variation for different proportions of the mixture (Mashiri et al. 2015). The study considers sand and SRM with rubber content of 0%, 10%, 20%, 30%, 40%, 50% & 100%.

### 3.3.1. Minimum dry unit weight

The minimum dry unit weight for sand and SRM was obtained using the dry placement method (Mashiri et al. 2014), which is ideal for maintaining the homogeneity of the mixture. A cylindrical mould of inside diameter 15 cm, height 17 cm, and volume of 3004 cm<sup>3</sup> was used for the testing. The sand was poured into the cylinder of known volume using a funnel, maintaining a height of fall not higher than 2 cm such that the sand is in its loosest state with the maximum void ratio. To maintain uniform height while filling, the sand was poured in a circular path from the sides of the mould towards the centre. The top surface of the sand is levelled once the sample reaches the mould height.

The sample inside the mould is weighed from which the minimum dry unit weight is calculated, as shown in Table 3.2. For the SRM, the sand and rubber are well mixed using hand for each proportion of the mixture and is poured into the mould using a scoop (Mashiri et al. 2014) such that there is no segregation of materials. The height of placement of sample is not greater than 2 cm in this case also and the same procedure as that of sand is repeated for unit weight calculation. For each composition of SRM, three series of trial tests were carried out, and the average value is chosen for the minimum unit weight. It could be seen from Table 3.2 that as the proportion of rubber increased the mixture, the minimum unit weight decreases, which was expected since the unit weight of the tyre granules are lesser than that of the soil.

**Table 3.2.** Details of minimum unit weight of the materials

Properties	Sand	Sand-rubber mixture					Rubber
		10%R	20%R	30%R	40%R	50%R	
Minimum dry unit weight (kN/m <sup>3</sup> )	14.75	13.35	12.62	11.85	10.73	9.85	7.40

### 3.3.2. Maximum dry unit weight

The maximum unit weight for sand was obtained using dry placement technique using the vibratory table method. However, for SRM which contains two materials of different unit weight, along with the vibratory table method, compaction method is also carried out for calculating the maximum dry unit weight of SRM.

#### ***a) Vibratory table method***

The vibratory table testing procedure is commonly used to calculate the dry unit weight of cohesionless soils as per ASTM D4253 (2016). A calibrated cylindrical metal mould with an inner diameter of 15 cm and a height of 17 cm was used for the study. The mould is attached to a collar assembly using clamps. The sample of sand/SRM was homogeneously mixed and poured into the cylinder using a scoop. The mould was filled with the sample and the top surface is levelled using a straight rod. The sides of the mould were tamped a few times to unblock any huge voids present. The surcharge base plates were placed on the surface of the sample and were gently twisted a few times to ensure proper contact with the sample. Details of the test setup are presented in Figure 3.3.



**Figure 3.3** Vibratory table test setup with surcharge

Prior to testing, the mould is assembled at the centre of the vibratory table, which is then firmly attached to the table. A surcharge load of  $13.8 \pm 0.1$  kPa as per the ASTM D4253 (2016) guidelines was placed on the surcharge base plate. The surcharge was increased for each test to observe the change in the dry unit weight of the samples. The vibratory table was set into vibration for  $12 \frac{1}{4}$  min until no further densification can happen. The additional surcharge was incremented in the order of 2.35 kPa upto five equal increments. A maximum of 25.5 kPa total surcharge was used for the study. Following the testing, the final height of the sample was noted before as well as after the removal of surcharge cum base plates from which the sample settlement can be calculated. The difference in heights before and after the removal of surcharge indicates about the rebound height of the material. Following the test, the weight of the sample in the mould was carefully measured.



The final volume of the sample before and after the removal of surcharge was then calculated from which the maximum dry unit weight was determined for both the cases from the vibratory table test.

Figure 3.4 shows the percentage variation of dry unit weight of the material for different surcharge pressures. For sand, the dry unit weight remains nearly the same irrespective of surcharge load. ASTM D4253 (2016) recommends a standard surcharge of 13.8 kPa to calculate the dry unit weight of the materials from the vibratory table test. Further, the rebound height of sand is very small. Hence for sand, dry unit weight of was calculated to be  $17.5 \text{ kN/m}^3$  as per the standard procedure. For SRM and pure rubber, as expected the rebound of the material once the loading is removed due to the high elastic and deformable nature of rubber results in a slight difference in maximum dry unit weight before and after the removal of surcharge. Besides, the SRM/rubber exhibit different densities depending on the surcharge weight. This could be due to particle rearrangement between sand and rubber with the rubber granules filling up the voids even in the angular edges of the sand due to surcharge pressure. In the present case of SRM/rubber, the maximum dry unit weight is considered with the presence of surcharge, since SRM is used below footing with building loading which is discussed in the next chapters. The maximum dry unit weight obtained for sand and SRM from the above study is reported in Table 3.3.

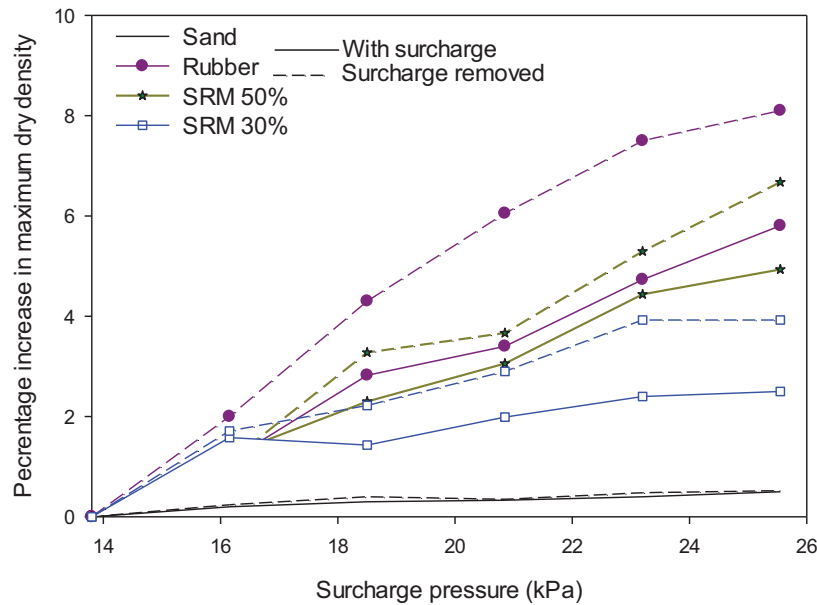


**Figure 3.4** Variation in maximum dry unit weight with surcharge increment



### ***b) Compaction method***

Though vibratory compaction technique is effective for sand, few studies suggest that it may not be an ideal option to induce compaction for determining the maximum dry unit weight of SRM since SRM tends to dilate at rubber content beyond 50% (Ahmed and Lovell 1992; Bosscher et al. 1993). The commonly adopted compaction methods such as the standard Proctor/modified Proctor compaction were found to be of less advantage to the SRM mixture (Humphrey and Manion 1992). The rebound of hammer resulting from the immediate deformation recovery by the high elasticity of the rubber present in the mixture, especially for higher rubber content is a common problem with the Proctor compaction method (Senthen Amuthan et al. 2018). On the other hand, the mini compaction method was deemed to be a suitable compaction technique to evaluate the maximum dry unit weight for SRM samples with granulated rubber (Sridharan and Sivapullaiah 2005; Senthen Amuthan et al. 2018). In this technique, an energy transferring iron prop of 36.5 mm diameter and 125 mm height was used to impart energy from the hammer impact to the material. The zero contact between the sample and hammer prevents the rebound of the material while applying the blows. The sample was placed in a mould of 38.1 mm diameter and 100 mm height. The standard mini compaction test was adopted in the study.

Initially, the energy transferring prop was placed above the material and the hammer (weight 1 kg). About 160 cm height of fall was maintained to compact three equal layers of the sample with 36 blows for each layer. Compaction energy of about  $1420 \text{ kN-m/m}^3$  was imparted in this process. The maximum dry unit weight obtained from this technique for sand and different proportions of SRM are presented in Table 3.3. It can be seen from the table that the standard mini compaction method provides higher value for the maximum dry unit weight compared to the vibratory method. An increase in the maximum dry unit weight of 7% to 12% was noted for the SRM using the mini compaction method. Overall, it can be stated that to achieve maximum unit weight, the vibratory compaction method is ideal for sand. While, for SRM, factors such as rubber content (which in turn influences the rebound of the hammer) and surcharge pressure plays a vital role. Hence under field conditions, the above factors should be due considered while adopting compaction techniques for SRM. The final maximum unit weight values arrived from the study is listed in Table 3.4.

**Table 3.3** Maximum dry unit weight values obtained from different methods

Sample	Maximum dry unit weight (kN/m <sup>3</sup> )		
	Vibratory table		Mini compaction
	Standard surcharge	Maximum surcharge	
Sand	17.68	17.67	17.66
SRM 10%	14.38	14.5	15.90
SRM 20%	13.02	13.5	13.93
SRM 30%	12.95	13.25	15.50
SRM 40%	10.3	10.7	11.5
SRM 50%	9.97	10.34	10.52
Rubber	6.20	6.58	7.75

**Table 3.4** Details of maximum unit weight of the materials

Properties	Sand	Sand-rubber mixture					Rubber
		10%R	20%R	30%R	40%R	50%R	
Maximum dry unit weight (kN/m <sup>3</sup> )	17.66	15.90	13.93	15.50	11.5	10.52	7.75

### 3.3.3. Relative density

Throughout the laboratory study in this chapter and model tests in the next chapter, the relative density approach was used for sample preparation for both sand as well as SRM of different rubber content. The relative density relation with respect to the maximum and minimum void ratio of the materials, as shown in equation 3.1 & 3.2 is adopted as follows.

$$\text{Relative Density} = \frac{e_{\max} - e_s}{e_{\max} - e_{\min}} \times 100 \quad (3.1)$$

where,  $e_{\max}$ ,  $e_{\min}$  &  $e_s$  are the maximum, minimum and sample void ratios respectively. The equation can be rewritten in terms of dry unit weight

$$\text{Relative Density} = \frac{1/\gamma_{\min} - 1/\gamma_s}{1/\gamma_{\max} - 1/\gamma_{\min}} \times 100 \quad (3.2)$$

where,  $\gamma_{\max}$ ,  $\gamma_{\min}$  &  $\gamma_s$  are the maximum, minimum and sample dry densities respectively. For SRM, the compaction effort necessary to achieve the desired relative densities while sample preparation, is pre-calculated depending upon the weight of tamping rod/plate used and no. of blows required. However, for sand with silt content less than 20%, the concept of air pluviation technique proposed by Cresswell et al. (1999) can be used to produce samples of desired relative density. In this technique, the drop height of sand samples was controlled depending on the density requirement. The dry/ air pluviation technique is adopted for sand specimen preparation all through the present study. Samples of sand were poured from a fixed height using a funnel to a mould of known volume and the corresponding density was calculated. The test is repeated for different drop heights and the density was calculated in each case. Figure 3.5 shows the calibration chart for relative density calculation based on the height of fall method for sand used for the study.

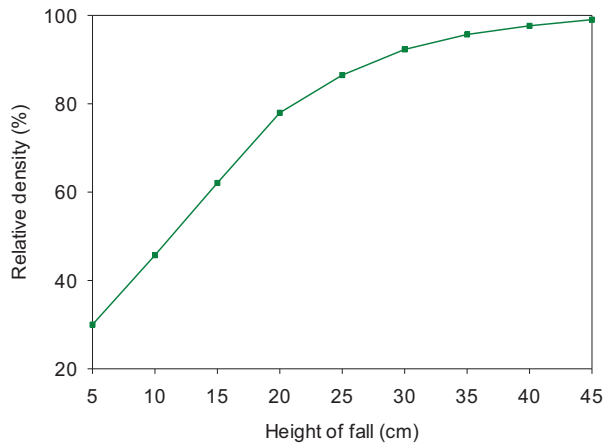


**Figure 3.5** Calibration chart for relative density of sand using pluviation technique

#### 3.3.4. Segregation check

Segregation resistance of materials is essential while placing the material under field conditions. The segregated nature of SRM was reported for mixtures of higher rubber content (greater than 50%) containing tyre chips of size 12 mm to 50 mm (Edil and Bosscher 1994; Anastasiadis 2011;

Mashiri 2014; Umashankar et al. 2014). In the present study, to understand the segregation of SRM, the same vibratory table method which was adopted in the previous section for calculating the dry unit weight (ASTM D4253, 2016) can be followed except that the surcharge loading was removed in this case. Free vibration is enabled for the cylindrical mould filled with sample and the top base plate upto a duration of 10 min following which the mixture is checked visually for any visible segregation. Figure 3.6 shows that there is no visible segregation for the mixture before and after the testing for 30% rubber content. Similar observations were obtained upto 50% rubber content. Past studies by Kim and Santamarina (2008) points out that the closer the maximum size of the sand particles and rubber, lesser the chance of segregation. In the present study, the maximum particle size of sand and SRM are close by due to the use of the granulated tyre, thereby preventing segregation even at higher rubber content.



**Figure 3.6** Segregation checks before and after subjected to vibration

### **3.4. SHEAR STRENGTH**

The shear strength characteristics of the SRM is of paramount importance especially for its use as geo-base isolation material below the building foundation since the mixture should have an adequate bearing capacity which in turn is dependent on the shear strength characteristics of the material. As discussed in the previous chapter, there has been some disagreement concerning the shear strength of SRM. Several studies report that mixing of the base soil with tyre shreds/chips improves its shear strength characteristics (Foosse et al. 1996; Tatlisoz et al. 1998; Zornberg et al. 2004; Ghazavi and Sakhi 2005; Rao and Dutta 2006). However, other studies by Masad et al.

(1996), Youwai and Bergado (2003), Cabalar (2011), El-Sherbiny et al. (2013) and Sheikh et al. (2013) have reported that the shear strength of soil decreases due to the addition of tyre crumbs contradicting some of the preceding studies. Hence, before optimizing the mix proportion of SRM for geo-base isolation, it is essential to study the shear strength response of the SRM used for the study since the gradation of the material and shred size influences the shear strength response of the mixture (Zornberg et al. 2004; Youwai and Bergado 2003; Mashiri et al. 2015). In this section, the shear strength response of SRM for varying rubber content using direct shear test are discussed. Further, monotonic triaxial tests were also carried out to understand the shear strength behaviour of the material under drained and undrained conditions.

#### **3.4.1. Direct shear test**

The direct shear test is carried out on a standard apparatus with a shear box of 60 mm x 60 mm size and thickness of 30 mm. The shear box is attached to a loading unit through which normal stress is transferred to the sample. The applied shear load taken by the soil is recorded by a proving ring of capacity 200 kg, while the deformations and volume changes were measured using a dial gauge. Strain-controlled direct shear testing is carried out at a constant rate of strain of 0.625 mm/min using a motor attached to the loading frame. Tests were conducted based on the procedure described in IS 2720 Part 13 (1986). The test setup used for direct shear testing for the study is shown in Figure 3.7. In the current direct shear test program, along with sand samples, SRM having rubber content of 10%, 20%, 30%, 40% and 50% were adopted to assess the shear strength and volumetric behaviour of the materials. The tests were conducted at relative densities of 30%, 65% and 80%.

While preparing the sample in the direct shear test box, appropriate criteria should be adopted to achieve the desired compaction degree for sand as well as SRM. For sand samples, the height of fall technique (air pluviation technique) was used to achieve the required relative density of the sample. The relative density is cross-checked from the dry unit weight of the sample by measuring the weight of the sample in the test box and the volume of the sample (60 mm x 60 mm x 30 mm). For SRM samples, initially, the mixture is prepared for the required gravimetric proportion of rubber followed by hand mixing to get a homogenous sample. The under-compaction method using tamping proposed by Ladd (1978) was used for the sample preparation of SRM. In this method, initially the weight of the sample to fill the test box was pre-calculated depending upon

the required relative density. The sample of the particular mixture was divided into three equal parts such that there is negligible segregation during sample preparation. Each part was transferred in the test box and subjected to tamping to achieve desired dry unit weight. Each layer was scarified before placing the top layer to prevent loss of bonding. The number of tamping required to achieve a particular relative density was calculated using a series of trials. The number of tamping increases as the relative density of the mixture required increases. It should be noted that the relative density reported in the study is initial relative density before the application of normal pressure. The test is carried out at normal pressure of 50, 100 & 150kPa.

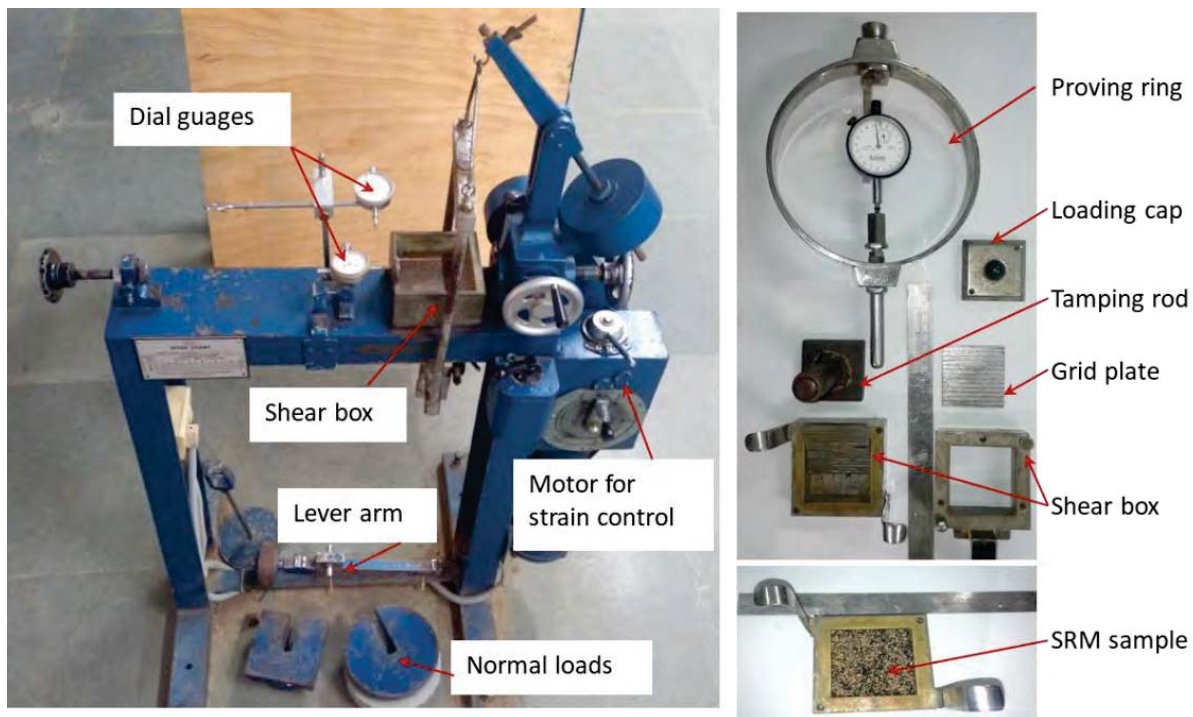


**Figure 3.7** Experimental setup for the direct shear test

Figure 3.8 illustrates the typical variation of the shear stress with horizontal displacement for sand as well as SRM of different rubber content for constant normal stress of 50 kPa compacted at a relative density of 65%. For the sand sample, Figure 3.8 shows a clear peak associated with failure followed by strain softening, which is indicative of typical medium dense/dense sand behaviour of brittle nature. A high initial stiffness could also be observed for sand. The curve gets flat and becomes constant at a horizontal displacement of about 5 mm for sand. On the contrary, SRM exhibits strain hardening behaviour without distinct failure peaks. In this case, the shear strength becomes constant beyond a horizontal displacement of about 8 mm. The gradual increase in shear



strain in SRM along with strain hardening indicates the ductile nature of SRM which could be associated with the densification of materials as well as high interlocking between sand and SRM during shear displacement (Anvari et al. 2017). It can be noted that, at given normal stress, and medium dense relative density, the ultimate shear resistance of the SRM is lower than that of the sand specimen overall. Also, the ultimate shear strength of SRM decreases with increase in rubber content. For rubber content upto 30%, the ultimate strength of SRM is closer to the ultimate response of sand. For relatively low rubber content of SRM (below 30% rubber), the reduction in initial stiffness compared to sand is less. At high rubber content of 50%, a steady drop in the initial stiffness and shear strength of SRM can be observed. This could be because the rubber to rubber interaction strength is lower than sand to rubber interaction strength (Choobbasti and Kutanaei, 2015).

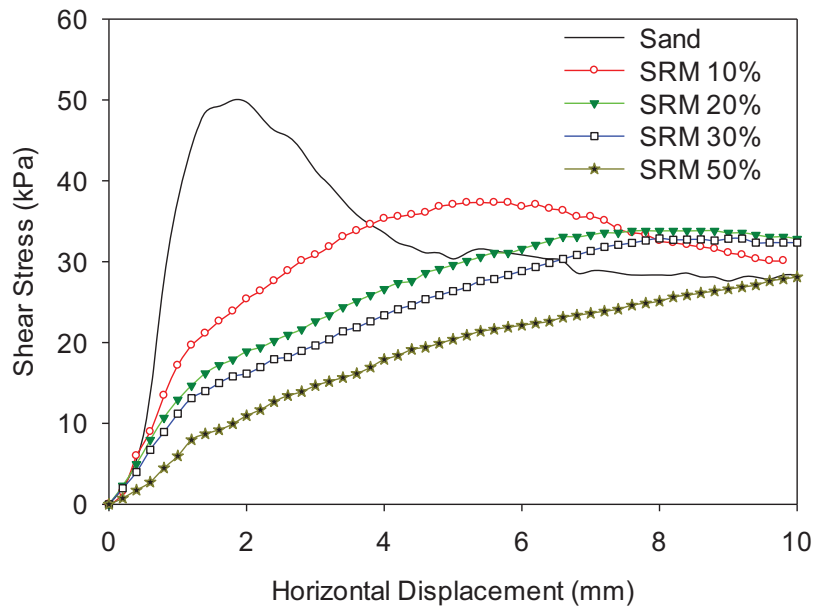


**Figure 3.8** Variation of shear stress with horizontal displacement for sand/SRM (normal stress=50 kPa; relative density=65%).

The typical volumetric change of sand and SRM samples throughout the shearing process is illustrated in Figure 3.9 for varying rubber content (normal stress = 50 kPa; relative density = 60%). It can be observed that the pure sand initially exhibits compression followed by dilation as is expected in case of medium dense sand. However, for SRM samples, compression is the primary response leading to the densification of the material. The increase in rubber content in the mixture



decreases the dilatancy behaviour of the material. SRM with rubber content upto 30% exhibits dilation at higher horizontal displacement. In the case SRM with high rubber content of 50%, high shear displacement is required to overcome the compressive response. The findings are in agreement with earlier investigations on SRM by Gotteland (2005) & Rao and Dutta (2006).

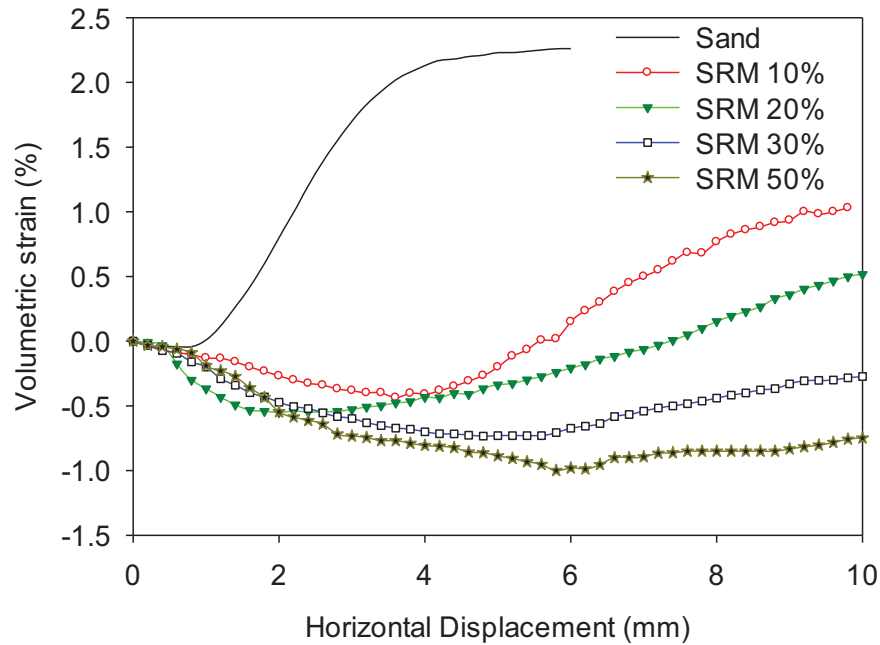


**Figure 3.9** Variation of volumetric strain with horizontal displacement for sand/SRM (normal stress=50 kPa; relative density=65%).

To get a better insight into the effect of rubber content on the shear strength response of the mixture, the shear strength of the mixture was normalized with respect to sand for a given relative density. Figure 3.10 shows the normalized shear strength plots for a relative density of 80. It can be seen that the decrease in peak shear strength is gradual upto 30% rubber content, beyond which there is a steep decrease in the strength characteristics. For SRM with rubber content less than 30%, reduction in peak shear strength of upto 20% was observed compared to sand. Similarly, for 50% rubber content of SRM, a 40% reduction in shear strength was observed for all normal stresses. Further, increase in normal stress was found to increase the shear strength of the mixture, this could be due to redistribution of rubber within the voids of sand particles thereby increasing the contact surface and interlocking friction between sand and rubber particles (Foosse et al., 1996; Asadi et al., 2018).

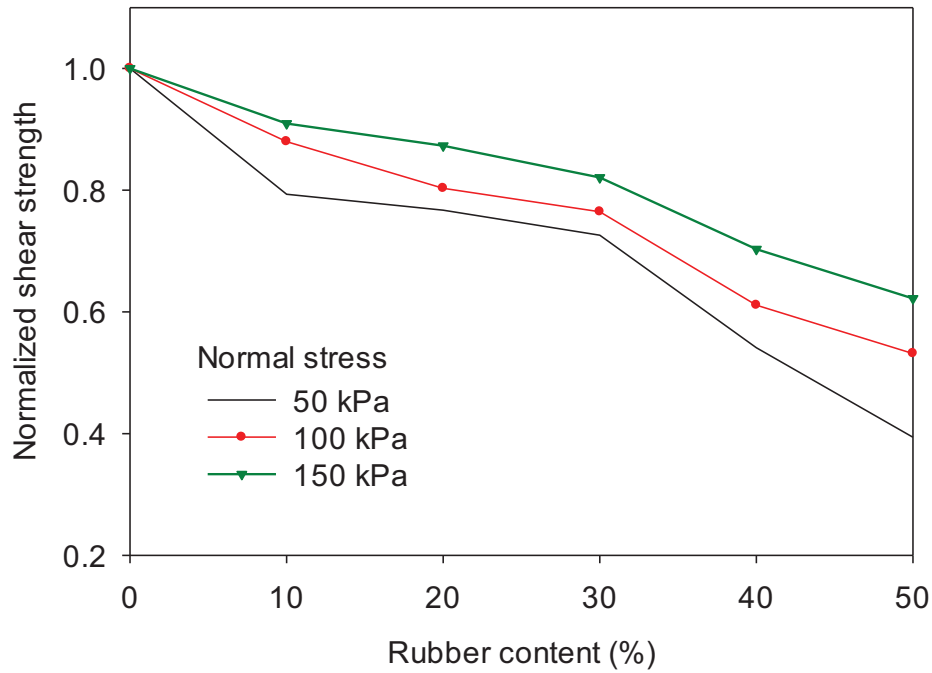


**Figure 3.10** Influence of rubber content on the shear strength of SRM (relative density- 80%)

The influence of relative density on the shear strength response of SRM was explored considering sand as well as SRM, as shown in Figure 3.11. The results show that there is a steady rise in the angle of friction when SRM is densely packed. The increment in shear strength is high for medium and high relative density SRM (65% & 80% relative density) compared to low relative density. Compared to sand, SRM with rubber content upto 30% exhibits a decrease in angle of friction of 15% for medium and high relative density mixture, while the low relative density mixture exhibits a drop in the angle of friction of upto 20%. Additionally, it can be observed that the decrease in shear strength becomes evident at a higher rubber content of 40% and above irrespective of the relative density. A similar trend on the influence of rubber content on the shear strength response of SRM was reported by Zornberg et al. (2004) and Anvari et al. (2017).

Table 3.5 summarizes the shear strength properties of the SRM and sand for the tested samples of varying rubber contents and relative densities. Upto a rubber content of 30% and relative density of 65%, the reduction in shear strength of SRM was about 25%-30%, compared to sand irrespective of the normal stress. However, at a higher relative density of 80% and normal stress

above 100 kPa, the reduction in shear strength in SRM upto 30% rubber content was about 16% while for 40% - 50% rubber content the reduction in shear strength was observed to about 37%. This indicates that normal stress and relative density heavily influence the shear strength properties of SRM.

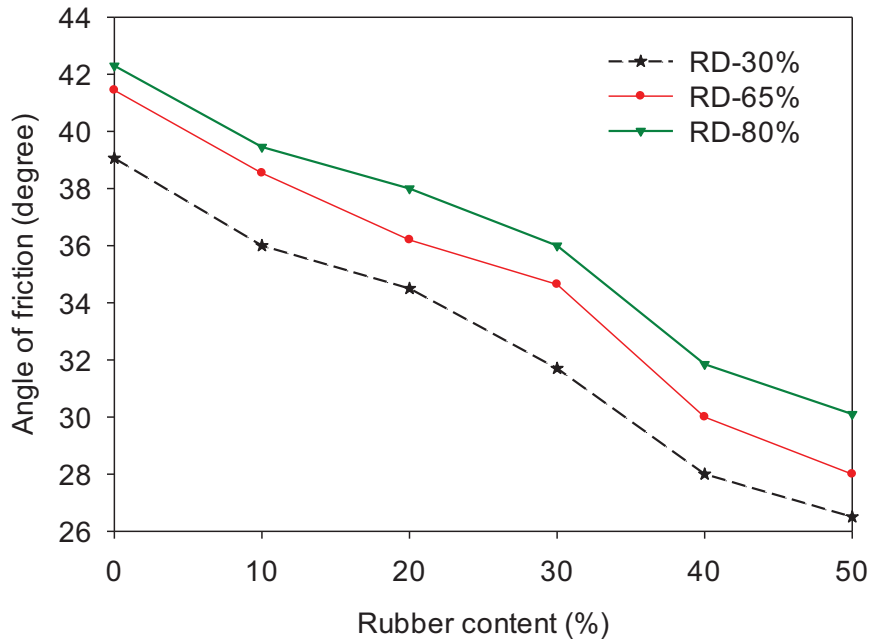


**Figure 3.11** Influence of relative density on the shear strength of SRM

The primary aim of the study is the application of SRM below the foundation of buildings for the geo-base isolation purpose. As can be seen from this section, higher rubber content reduces the shear strength of the SRM, which potentially affects the bearing capacity of the foundation resting on SRM layer. Rubber content of up to 30% in SRM exhibits reasonably low shear strength decrement with reference to pure sand. Beyond 40% rubber content, the shear strength reduces drastically since the rubber matrix becomes predominant due to the high volumetric rubber fraction. Hence it is ideal to use SRM with rubber content upto 30% as geo-base isolation material since the sand and rubber matrix contribute adequate shear strength to have required bearing capacity to support low-rise buildings. Moreover, past literature on the compression response of SRM indicates that an optimum mix proportion of upto 38% exhibits a lower void ratio, compression and settlement which can ideally be used for foundations where large settlements are a matter of concern (Ahmed 1993; Asadi et al. 2018). Further, it is advisable to use a medium to high relative density SRM to achieve the necessary bearing capacity to avoid shear failure.

**Table 3.5** Summary of the direct shear test results for sand and SRM

Relative density (%)	Sample	Peak shear strength (kPa)			Residual shear strength (kPa)		
		Normal stress			Normal stress		
		50 kPa	100 kPa	150 kPa	50 kPa	100 kPa	150 kPa
30	Sand	44.5	86.5	122.5	30.1	54.7	81.3
	SRM-10%R	35.8	72.8	110.3	29.3	62.6	98.7
	SRM-20%R	34.1	69.3	106.1	-	-	-
	SRM-30%R	29.3	62.1	86.5	-	-	-
	SRM-40%R	24.1	52.9	73.3	-	-	-
	SRM-50%R	17.5	47.2	67.5	-	-	-
65	Sand	49.9	81.5	127.8	27.6	63.2	88.1
	SRM-10%R	37.3	70.6	109.7	29.5	68.4	93.9
	SRM-20%R	34.5	65.5	102.3	-	-	-
	SRM-30%R	35.0	61.1	94.6	-	-	-
	SRM-40%R	31.7	48.8	87.5	-	-	-
	SRM-50%R	28.0	42.3	77.9	-	-	-
80	Sand	85.2	96.7	138.2	48.9	69.1	97.5
	SRM-10%R	67.6	85.1	125.7	54.5	68.1	105.7
	SRM-20%R	65.3	77.6	120.7	-	-	-
	SRM-30%R	61.8	73.9	113.5	-	-	-
	SRM-40%R	46.1	59.1	97.2	-	-	-
	SRM-50%R	33.5	51.4	86.0	-	-	-

### 3.4.2. Monotonic Triaxial Test

In this study, triaxial test was carried out to understand the monotonic behaviour of for SRM/sand as well as to evaluate the shear strength response. Consolidated drained and undrained triaxial compression tests were conducted to derive input parameters for bearing capacity analysis together with constitutive material models for the numerical analysis, which are discussed in the subsequent chapters. As indicated in the previous section, SRM with 30% rubber content exhibits adequate

shear strength and limited settlement compared to higher rubber contents that suit the static stability purpose of building-foundation systems supported on the geo-base isolation layer made of SRM. Hence further investigation is carried out in this section on triaxial samples of SRM with 30% rubber content having a high relative density. The effect of different confinement conditions for the SRM samples was also explored in the study.

### ***Sample preparation***

For the present triaxial testing, cylindrical sand/SRM specimens of 50 mm diameter and 100 mm height were considered. Since the materials used are cohesionless, samples were prepared at the pedestal of the triaxial cell in a split mould of internal diameter 50 mm, as shown in Figure 3.12a. A thin impermeable puncture resistance rubber membrane placed inside the split mould was used for holding the sample within the triaxial cell. Circular porous discs and filter papers of diameter the same as that of the sample was used to enable water flow to and fro the specimen. To start with, the cell pressure and back pressure tubes were cleared off air bubbles. The porous disc and filter paper were then mounted on the top of the triaxial pedestal, which in turn is connected to the back-pressure controller and pore pressure transducer. The rubber membrane was carefully secured into the pedestal using O-rings.

The split mould is then assembled tightly without gaps using silicone grease and is placed on the pedestal around the rubber membrane (Figure 3.12b). The rubber membrane is then stretched tightly towards the wall of the split membrane and is folded back into the outer walls of the mould. Suction pressure in the range of 10 kPa is applied to the split membrane to pull the rubber membrane tightly towards the walls of the mould. The internal height of the mould is then checked to ensure a specimen height of 100 mm.

Dry deposition method proposed by Ishihara (1996) was adopted for sample preparation of sand specimens. The sand sample is poured into the split mould using a funnel, maintaining a height of fall of 10 cm followed by tamping. A relative density of 80%-85% was maintained during sample preparation. For SRM specimens, initially, the sand and granulated tyre were mixed thoroughly to get a homogenous mixture with 30% rubber content by weight of sand. The SRM test specimens were prepared using the under-compaction method (Ladd, 1978) for a relative density of 80%-85% as described in the previous section. The pre-calculated quantity of SRM for the required relative density was divided into five equal sections and kept aside. The SRM was poured into

mould using a scoop with zero drop height in 5 equal layers and compacted to a height of 20 mm. The sample is tamped using a tamping rod of base diameter 25 mm and a weight of 0.295 kg.

The layer density was gradually increased from bottom to top to achieve uniform relative density throughout the entire depth of the sample. The percentage of under-compaction was reduced by 1.25% for each layer from the top such that the bottom-most layer will have a total under-compaction of 5%. The under-compaction ensures that the bottom layers were not over compacted due to the compaction of the top layers. Once the sample was prepared for the required depth, the top of the sample was enclosed with filter paper, porous stone and top cap. The rubber membrane was then released from the split mould and carefully secured to the top cap with O-rings using an O-ring holder. The suction pressure was removed from the split cylinder followed by careful removal of split moulds without disturbing the sample. The vertical alignment of the prepared sample was checked using a level along with the final height of the specimen. Figure 3.13 shows the SRM sample prepared for the present study along with the sample after saturation showing the segregation resistance of the mixture.

### ***Test procedure***

The VJ Tech UK-make advanced triaxial apparatus shown in Figure 3.14 was used to perform the strain-controlled monotonic triaxial loading tests in this study. The test procedure involves three stages, namely the saturation, consolidation and shearing. After the sample preparation, the triaxial cells were placed on the apparatus carefully without agitating the sample. De-aired water was filled into the triaxial chamber following which the top air vent of the chamber was closed tightly. An initial cell pressure of 20 kPa and back pressure of 10 kPa were applied to the sample. De-aired water was then allowed to permeate into the sand/SRM sample.

The top cap drainage was kept open to allow the escape of air bubbles from the sample as well as to enable saturation. The cell pressure was applied successively in increments of 50 kPa such that a difference 10 kPa was maintained at all stages. The degree of saturation is monitored at the end of each step using Skempton's pore pressure parameter B-value which is defined as the ratio between the change in specimen pore pressure to the cell pressure ( $\Delta u / \Delta \sigma_3$ ) for every increment in cell pressure. The specimen is saturated until the Skempton's pore pressure parameter B becomes greater than or equal to 0.95.



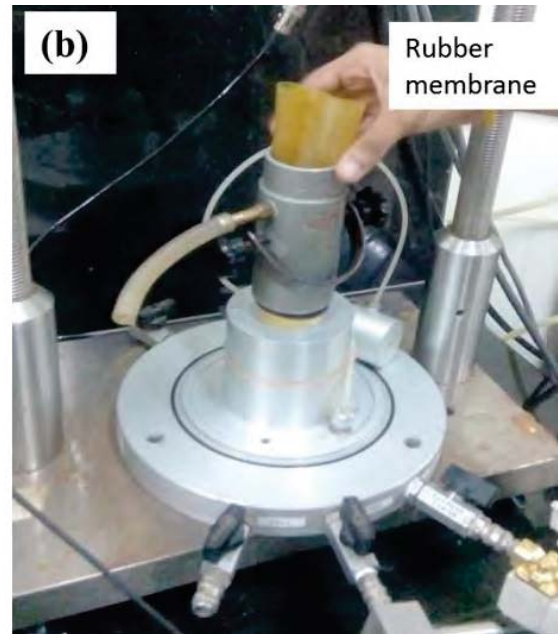
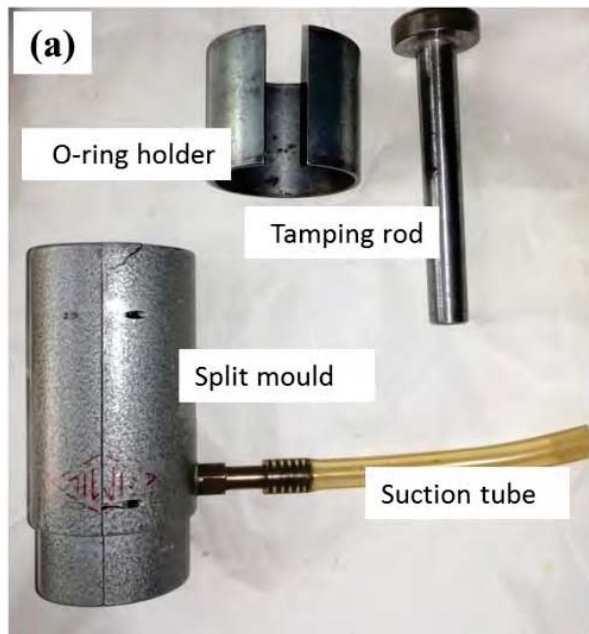


**Figure 3.12** Sample preparation (a) tools used (b) spit mould & rubber membrane to hold the sample

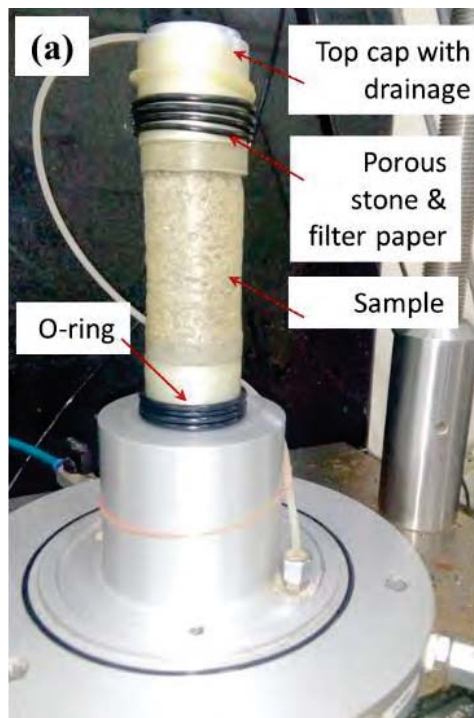


**Figure 3.13** (a) Prepared SRM sample (b) No evidence of segregation



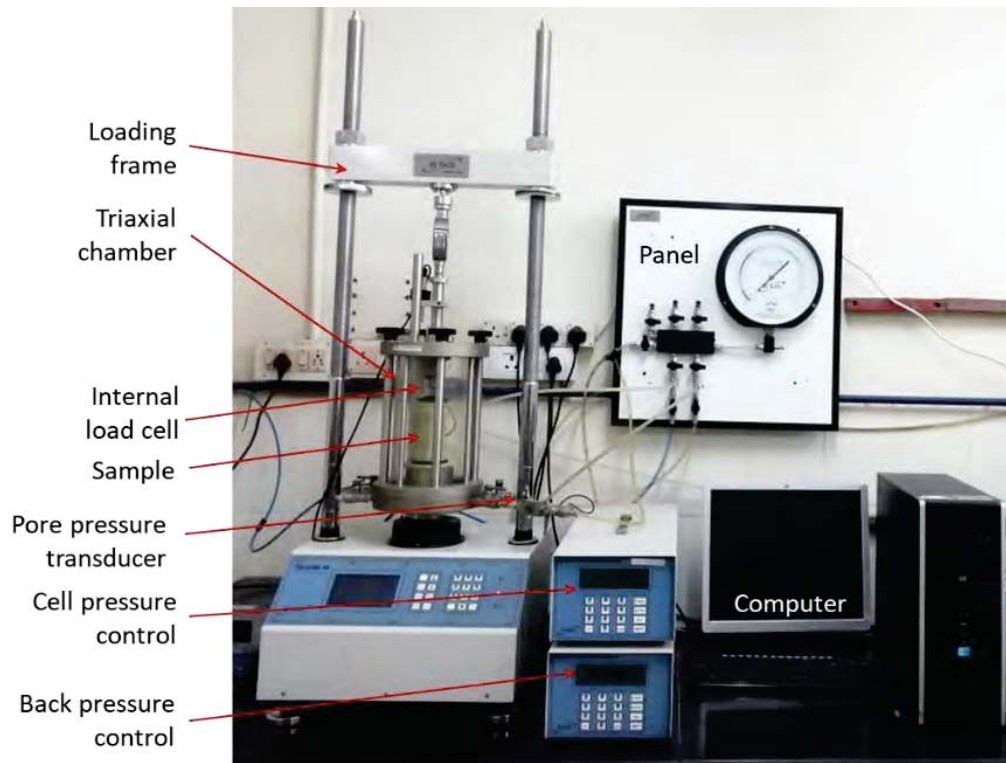


**Figure 3.14** Triaxial test setup

After saturation, the specimen was subjected to isotropic consolidation up to the desired confining pressure. The consolidation was continued until the stabilization of pore pressure such that the volume change is less than  $5 \text{ mm}^3$  in 5 min. The consolidated samples were then sheared for a constant value of confining pressure and strain rate. For the drained test, the strain rate was fixed at  $0.1 \text{ mm/min}$  for both sand/SRM to avoid pore pressure build-up during shearing of the sample considering the recommendations of Head (1998). The shearing was continued up to an axial strain of 20%. For the undrained tests on SRM, a strain rate of  $0.5 \text{ mm/min}$  was maintained. The data acquisition system present in the triaxial system was used to measure the cell pressure, pore pressure, load and displacements values during the testing. The consolidated drained triaxial test was conducted for sand and 30% SRM specimen for confining pressure of 50, 100 and 150 kPa. Further, consolidated undrained triaxial tests were also carried out for 30% SRM samples for the above confining pressures.

### ***Monotonic behaviour of SRM***

The deviator stress-axial strain curves for sand and sand-tyre mixtures obtained from the consolidated drained triaxial tests are shown in Figure 3.15. It can be noticed that sand attains peak

strength at an axial strain of 2.5%, followed by reduction to critical state. However, SRM shows an increase in shear strength without any strain softening as discussed in the previous session. The lack of any significant peak for deviator stress of SRM indicates ductile behaviour attributed to the high deformation of shredded rubber present in the mixture. The shear strength of both sand and SRM keeps increasing with added confining pressures. The angle of internal friction obtained for sand and 30% tyre content is  $42^{\circ}$  and  $35^{\circ}$  respectively.

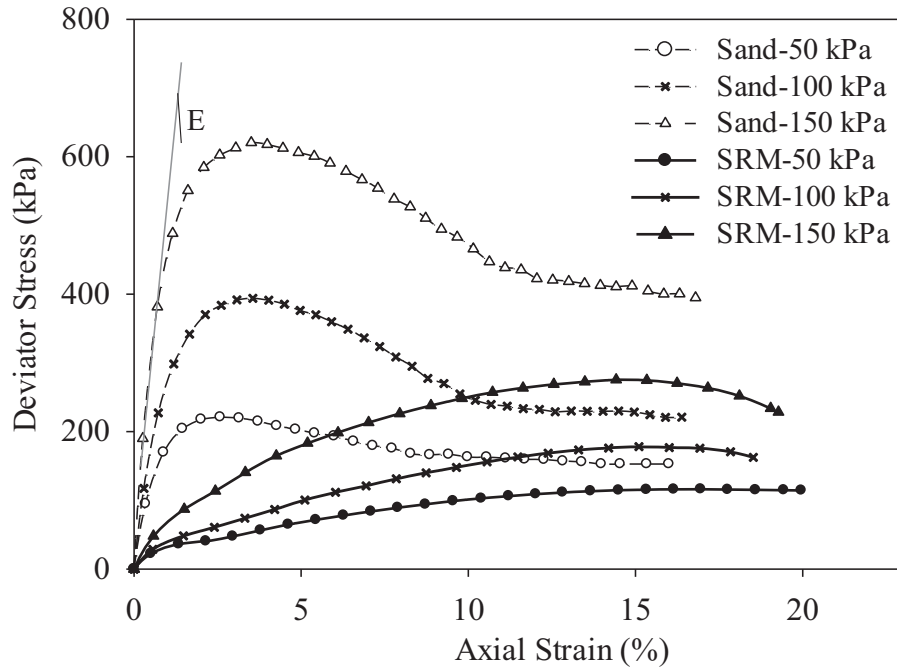


**Figure 3.15** Deviator stress-axial strain curves of sand and SRM (30% rubber) for drained conditions

The volumetric behaviour of sand and SRM is presented in Figure 3.16. It is evident from the figure that the sand shows initial compression followed by dilation, which is the typical behaviour of dense sand. However, when the granulated rubber is added to the sand, the dilative behaviour changes to compression since the rubber particles are elastic that in turn facilitates the deformation upon shearing. The effect of confining pressure on volumetric behaviour was found to be more pronounced for SRM than that for sand. The increase in confining pressure was found to increase the compressibility of both sand and SRM. The sand particles were inhibited from rolling over each other when the confining pressure is increased, which can be the reason for the dilative tendency. The SRM mixtures compress more than sand with an increase in the confining pressure

from 50 kPa to 150 kPa, which again attribute to the flexible nature of the rubber particles that deforms more at higher confining pressure (Gotteland 2005; Anvari et al. 2017).

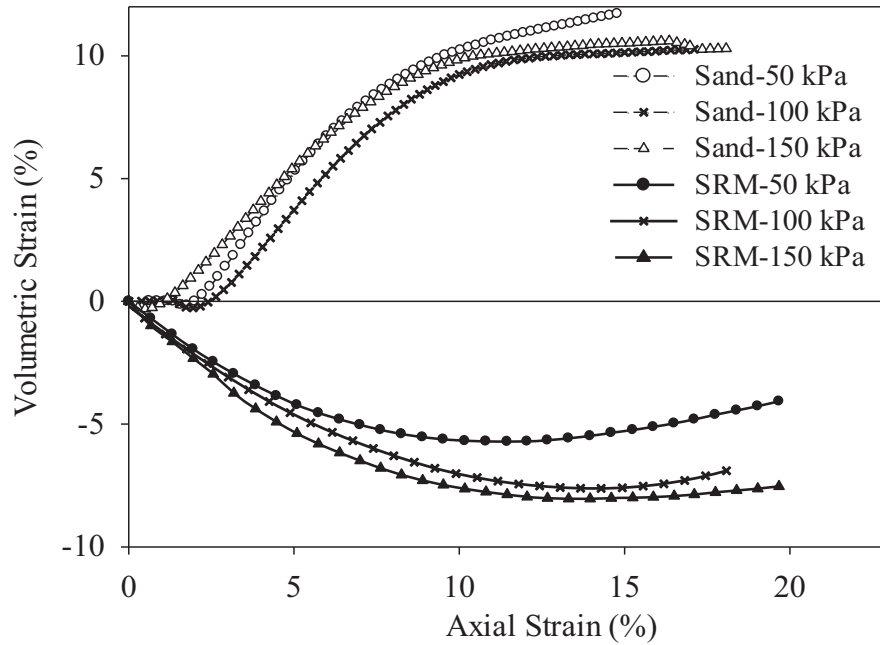


**Figure 3.16** Volume change behaviour of sand and SRM (30% rubber) under different confining pressures

The stress-strain response of SRM with 30% rubber content obtained from the consolidated undrained triaxial tests is shown in Figure 3.17. The samples exhibit evident strain hardening behaviour at all confining pressures similar to the trend reported in the consolidated drained test. The peak deviatoric stress for the undrained specimen is lower than that of drained samples for any given confining pressure. Past studies also show the inconsistency in the undrained and drained shear strength properties of granular materials with undrained strength being smaller than drained strength (Haeri et al. 2005; Baxter et al. 2011). The angle of internal friction obtained for 30% SRM under undrained conditions is  $33^\circ$ . The pore pressure variation of SRM with the increase in axial strain is shown in Figure 3.18. The excess pore pressure was observed to be positive, which prevails in the case of loose sand that try to reduce the volume upon loading since the mixtures compress with the increase in loading. The claim of increasing the confining pressure increases the compressibility many folds is again proven in Figure 3.18. It was also observed that the SRM mixtures try to dilate at large strain which is evident from both Figure 3.16 and 3.18.

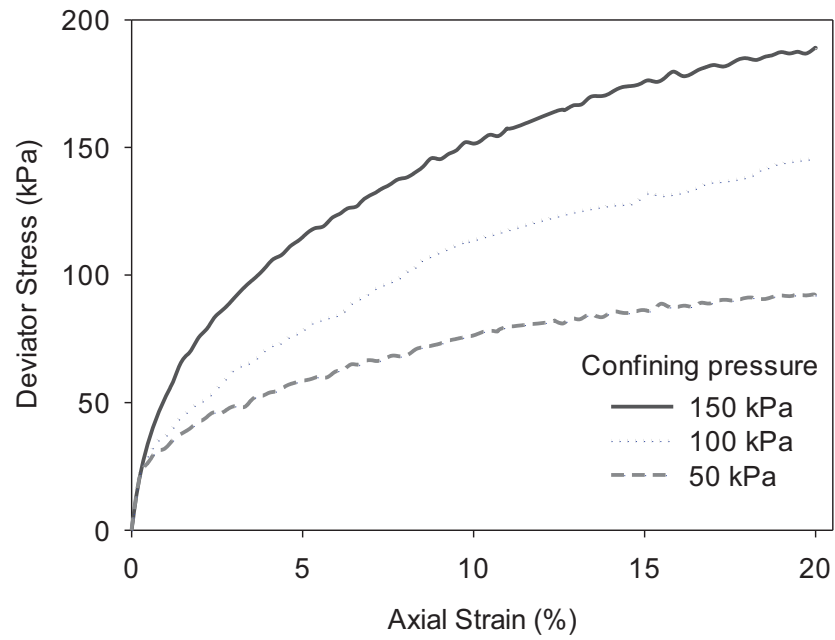


**Figure 3.17** Deviator stress-axial strain curves of SRM (30% rubber) for undrained conditions

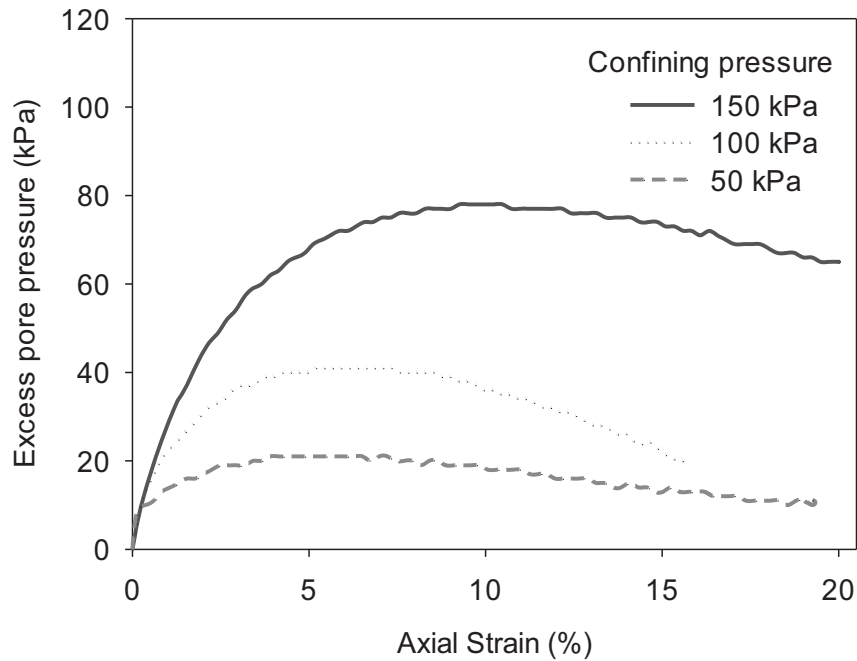


**Figure 3.18** Excess pore water pressure curves under different confining pressures for SRM (30% rubber)

### **3.5. CYCLIC TRIAXIAL TEST**

In the past, the strain-dependent dynamic response of SRM was investigated using cyclic triaxial tests and resonant column tests by few researchers (Feng and Sutter 2000; Hazarika et al. 2010; Senetakis et al. 2012; Kaneko et al. 2013). From the literature review presented in Chapter 2, it is clear that dynamic behaviour of SRM was highly dependent on rubber content, confining pressure and size of rubber present in the mixture (Feng and Sutter 2000; Anastasiadis et al. 2012). It was further found that an increase in rubber content in SRM leads to decrease in the shear modulus for rubber crumbs and granules (Nakhaei et al. 2012; Ehsani et al. 2015; Li et al. 2016). However, studies by Pamukcu and Akbulut (2006) shows an increased shear modulus of the base soil due to the addition of rubber. Besides, previous works have reported on the substantial damping of SRM, which is ideal for geo-base isolation purpose (Kaneko et al. 2013; Mashiri et al. 2015). In this section, cyclic triaxial tests carried out to evaluate the strain-dependent dynamic properties of SRM at medium to large shear strains (0.1% to 2%) are discussed. The shear modulus and damping ratio curves for SRM were obtained from the study for varying proportions of rubber content of 0%, 30%, 50% and 100%.

#### **3.5.1. Test setup and procedure**

The strain-controlled consolidated undrained cyclic triaxial tests were carried out on sand-rubber tyre mixture specimens according to ASTM D3999-11 (2011). The tests were carried out using a servo-controlled cyclic triaxial testing facility from Wykeham Farrance International (UK) make (Figure 3.19). The specimen preparation procedure is the same as that followed in triaxial study, as discussed in the previous section. Since the cyclic triaxial testing involves extension phase in addition to compression, to enable the tension stress through the loading ram, the top cap above the specimen was fitted with an additional extension top cap and rubber sleeve. Proper sealing of the top cap and extension cap without air gaps is slowly carried out during the engage phase such that suction force could be developed within the actuator and the top cap during cyclic loading. The suction helps the specimen to undergo the pull without loss of contact while the tensile stress is being applied by the actuator during the cyclic loading.

The sample was subjected to isotropic consolidation under a confining pressure of 100 kPa. Under the undrained conditions, the specimen was subjected to cyclic deviator stress in the axial direction. The tests are conducted at a frequency of 1 Hz for a constant cyclic strain rate up to 100

no. of cycles. The tests were repeated for varying cyclic strain amplitudes from 0.1% to 2%. During the testing, the axial load, axial strain and excess pore water pressure were measured. Mixtures of sand replaced with granulated tyre by dry weight in the order of 0%, 30%, 50% and 100% were used for sample preparation.



**Figure 3.19** Cyclic triaxial test setup

### 3.5.2. Cyclic behaviour of SRM

Under undrained conditions, the volumetric strain will be zero. Hence, the axial strain measured in the triaxial testing will be equal to shear strain  $\gamma_c$  and deviator stress ( $q$ ) will be equal to shear stress  $\tau_c$  (Atkinson and Bransby 1978). A typical shear stress-shear strain response of SRM specimens with 30% tyre content obtained from the cyclic triaxial tests at 1st, 3rd, 10th and 100th loading cycle is shown in Figure 3.20. The inclination of the hysteresis loop, i.e., degradation of stiffness with the increase in the number of cycles of loading can be observed from the figure. The shape of the hysteresis stress-strain loop stabilizes after three cycles. However, at a larger number of cycles (100<sup>th</sup> cycle) the hysteresis loop is found to be further inclined due to the degradation of the stiffness of soil-tyre mixture. For typical cyclic loading applications, the effect of no. of cycles diminishes beyond ten cycles (Kokusho 1980). Hence the shear modulus and damping ratio are obtained from the hysteresis loop corresponding to the 10<sup>th</sup> cycle of loading for the present study.

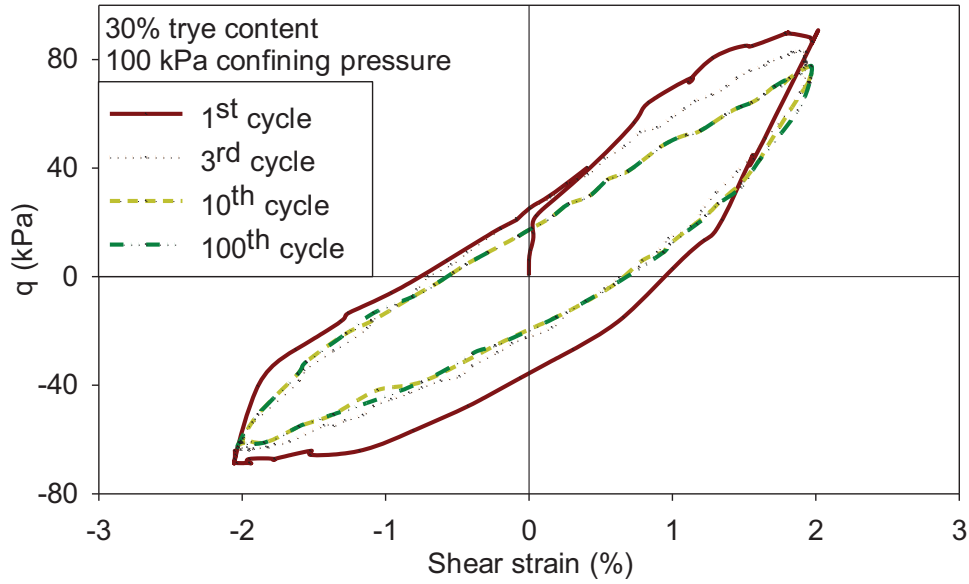


**Figure 3.20** Hysteresis loop of SRM for different cycles of loading (30% rubber content)

The equivalent linear shear modulus,  $G$  and the damping ratio,  $\xi$  of the sand/SRM are obtained from the hysteresis loop at different strain levels using equation 3.3 (Kramer 1996).

$$G = \frac{\tau_c}{\gamma_c} \quad (3.3)$$

where,  $\tau_c$  and  $\gamma_c$  are the shear stress experienced by the specimen and the shear strain amplitudes, respectively as depicted in Figure 3.21. The material damping of soil under cyclic loading can be determined from the energy lost calculated from the areas of the stress-strain hysteresis loop. The ratio of energy dissipated in one cycle and the energy stored during the loading gives the damping coefficient (Kramer 1996) as shown in equation 3.4. Mathematically, the damping ratio  $\xi$  is given by:

$$\xi = \frac{W_D}{4\pi W_s} = \frac{1}{2\pi} \frac{A_{loop}}{G\gamma_c^2} \quad (3.4)$$

where,  $W_D$  is the dissipated energy,  $W_s$  is the maximum strain energy, and  $A_{loop}$  is the area of the hysteresis loop (Figure 3.21).



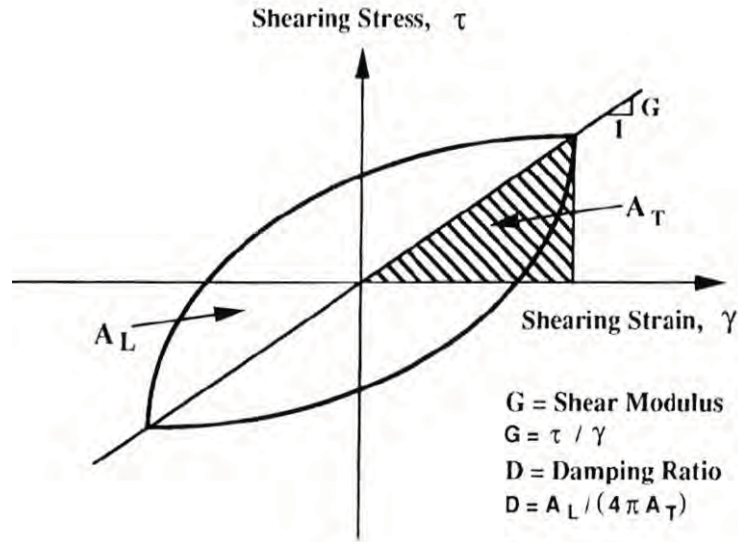


**Figure 3.21** Shear modulus and damping ratio calculation from hysteretic loop (Kramer 1996)

The variation of shear modulus with shear strain for sand and SRM with various percentage of rubber content is presented in Figure 3.22 for a confining pressure of 100 kPa. The results indicate that shear modulus decreases with increase in granulated rubber content in the SRM. The reduction in shear modulus could be attributed to the reduced stiffness of granulated rubber compared to sand grains. It was observed that for relatively small to medium strain levels, the shear modulus of the sand decreases drastically with increase in rubber content. However, for SRM specimens, the rate of degradation of shear modulus with strain level is relatively less compared to sand. Further, SRM with 30% tyre content gives a higher shear modulus value compared to the 50% and 100% granulated rubber content in the mixture. Similar trends on the influence of granulated rubber content on the reduction in shear modulus of SRM were reported by Nakhaei et al. (2012).

The variation of damping ratio with shear strain for sand and SRM with different percentage of rubber content is presented in Figure 3.23 for a confining pressure of 100 kPa. It is evident from the figure that the strain-dependent damping values of SRM increase with the increase in the granulated rubber inclusion within the mixture. It was found that at any given shear strain amplitude, SRM with 30% & 50% rubber content exhibits damping ratio increment of around 15% & 35% respectively compared to sand which is a clear indicator of the applicability of SRM for energy dissipation studies like geo-base isolation. Studies by Nakhaei et al. (2012) points out a similar trend concerning the increase in damping ratio with the addition of rubber granules as well

as at higher confining pressure. The high damping ratio can be associated with the high plastic strain endured by the SRM, resulting in bigger hysteresis loops.

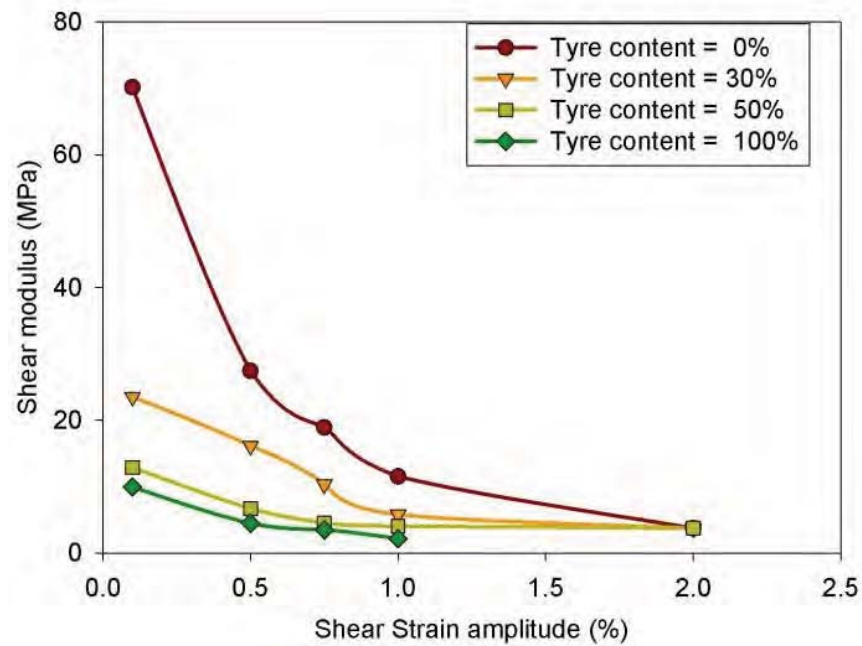


**Figure 3.22** Shear modulus degradation curve for different proportions of SRM

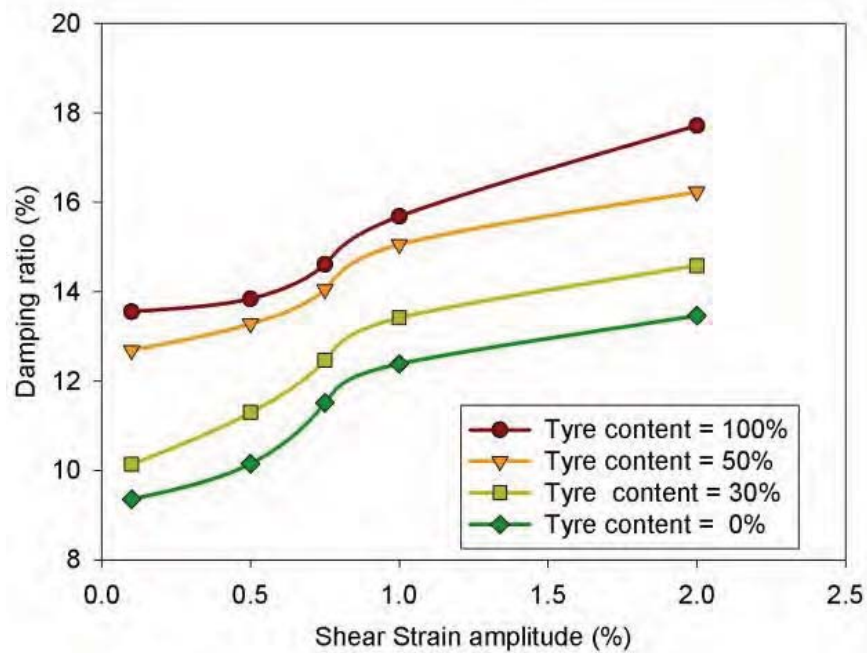


**Figure 3.23** Damping curves for different proportions of SRM

Similar to the monotonic triaxial test, the main interest of the cyclic test is on SRM with 30% rubber content compared to higher rubber contents since it possesses adequate stiffness under static loading ideal for geo-base isolation of foundations as discussed previously. The modulus reduction and damping curves obtained from the present study also points that though the shear modulus of 30% SRM is lower than sand at small strains, at strains greater than 0.5%, the difference between the values reduces drastically. The damping ratio trends for 30% SRM also seems to be satisfactory for applications involving energy dissipation purposes (Senetakis et al. 2012). Hence, for the geo-base isolation studies in the upcoming chapters, the shear strength and dynamic properties of SRM with 30% rubber content will be ideal considering the building-foundation system.

### **3.6. GEOGRIDS**

From the preceding sections, it is confirmed that though SRM possesses higher damping, the material exhibits reduced shear strength compared to sand. One way to increase the shear strength/stiffness is by using geosynthetics like geogrid, as discussed in the literature review chapter. Past works of literature substantiate the successful usage of geogrids for soil improvement under static loading by mobilising the tensile stresses (Binquet and Lee 1975; Bathurst and Jarrett 1988; Das et al. 1994; Shin et al. 2002; Ghazavi and Lavasan 2008). Further, the beneficial use of geosynthetics under dynamic loading was confirmed for various geotechnical applications like retaining walls and foundations (Sakaguchi 1996; Bathurst et al. 2007; Fakharian and Attar 2007; Taha et al. 2015; Xu et al. 2015). For the present study, the geogrid reinforcement technique was used to enhance the static and dynamic performance of SRM for geo-base isolation purposes.

The geosynthetic reinforcement used in the study is a commercially available planar biaxial geogrid (MACGRID AR) made of glass fibre strands arranged in grid shape having an aperture size of 10 mm x 10 mm (Figure 3.24). Multi-rib tensile strength test as per ASTM D-6637 (ASTM 2001) was carried out on the geogrid specimen. The properties of geogrid used in the study are listed in Table 3.6.

Since the numerical analysis procedures considered in the upcoming chapters include modelling the interface between soil/SRM and geogrids, it is necessary to find the interaction behaviour of soil/SRM and geogrids. Several studies were reported in the past to find the interface properties of soil and geosynthetics (Abramento and Whittle, 1995; Tatlisoz et al. 1998; Bergado et al. 2001).

Typically, the interaction mechanism was investigated using the pull-out test or large-scale direct shear test. Few studies available on the interaction response of geosynthetic reinforcements and SRM are mainly focussed on tyre chips of size much larger than the granulated tyre used in the current work (Bernal et al. 1997; Tatlisoz et al. 1998; Tanchaisawat et al. 2010). The interaction of sand/SRM samples were studied using regular direct shear tests in this section. The interface friction angle was obtained from direct shear tests with a horizontal layer of geogrid placed at the mid-depth of the sand/SRM sample at the shearing interface.

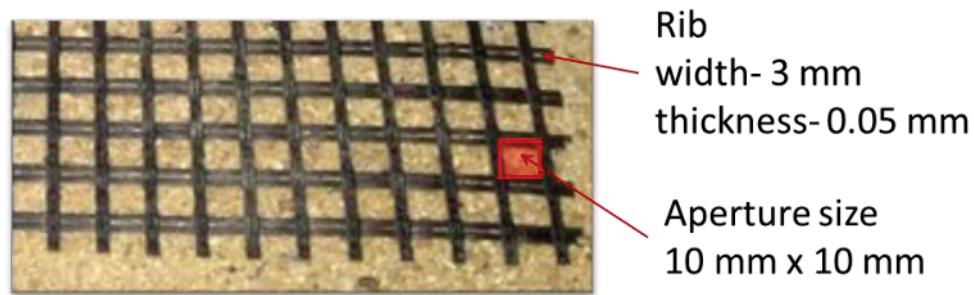


**Figure 3.24** Geogrid reinforcement used for the study

**Table 3.6** Properties of geogrid

Property	Values
Maximum tensile strength (kN/m)	11.5
Mass per unit area ( $\text{g/m}^2$ )	330
Young's modulus (GPa)	55.6
Tensile strength at 2% elongation(kN/m)	3.8
Tensile strength at 5% elongation (kN/m)	10.5

The shear testing was carried out on the direct shear test box of size 60 mm x 60 mm following the same procedure for sample preparation of sand and SRM (30% rubber content) as discussed previously in this chapter. A relative density of 80% was maintained for the specimens. The sand/SRM samples were prepared upto the bottom half of the shear box, and thereafter, the surface of the sample was levelled. Geogrid sample of size slightly larger than the shear box size was then placed on the levelled surface (Figure 3.25). The upper part of the shear box was placed above the geogrids and clamped securely in place following which the sand/SRM samples were filled till the

required height. The samples were sheared at a constant strain rate of 1 mm/ min. The direct shear testing is carried out for normal stress ranges of 50 kPa, 100 kPa and 150 kPa. The variation of shear stress with horizontal displacement for sand/SRM with geogrids at the interface (Figure 3.26) indicates that the stress-strain trends are similar to that of sand/SRM without geogrids. The interfacial angle of frictions of sand and SRM with respect to geogrids was found to be  $34^\circ$  and  $27^\circ$  respectively. The friction angles of sand/SRM decreases with the presence of geogrids since the reinforcements block the contact area at the shear plane of the samples.

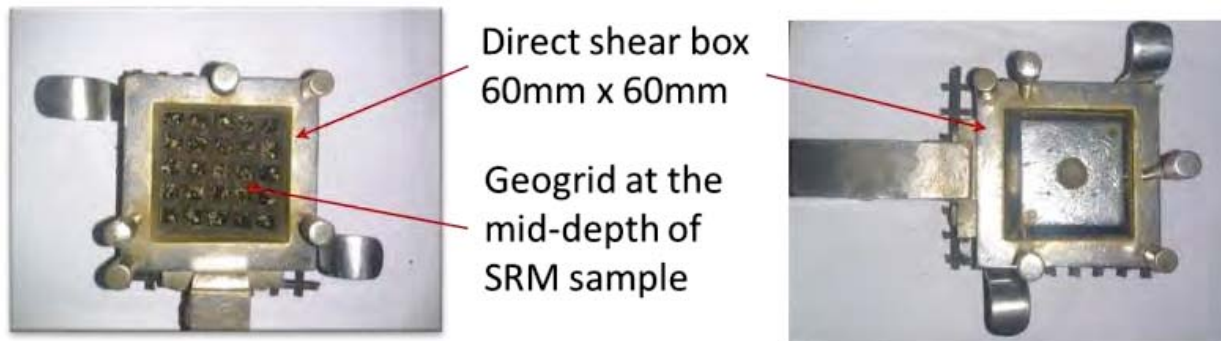


**Figure 3.25** SRM-geogrid interaction study using direct shear test

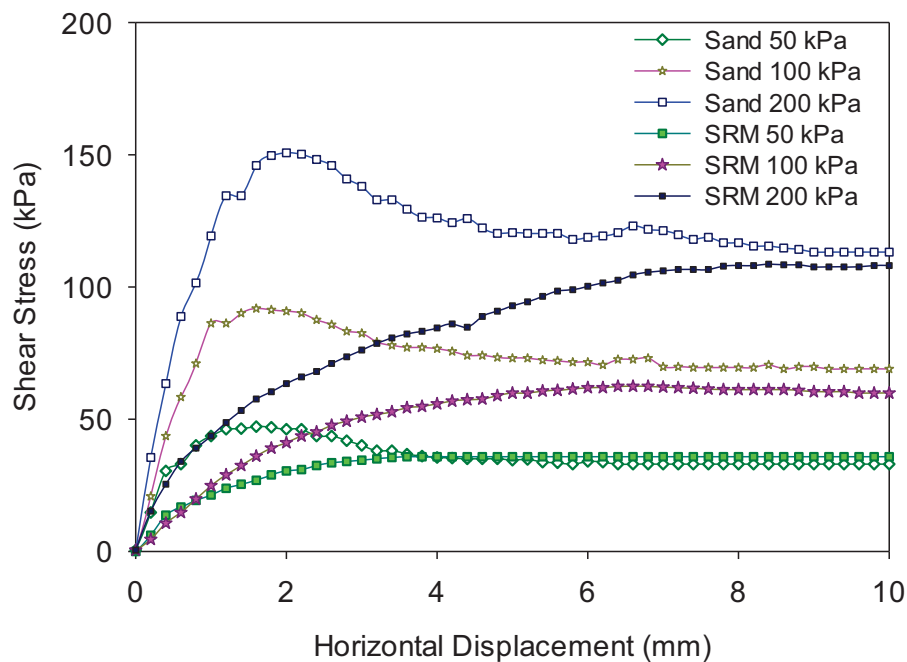


**Figure 3.26** Variation of shear stress with horizontal displacement for sand/SRM with geogrids (relative density=80%)

### 3.7. SUMMARY

This chapter presents the results of the detailed experimental investigation carried out for the material characterization of sand/SRM. Initially, the geotechnical properties of the materials were identified using routine laboratory test. The sand used in the study was classified as poorly graded (SP), whereas the granulated rubber was classified as an equivalent of poorly graded sand (SP). The granulated rubber was mixed gravimetrically with sand to get different proportions of SRM, and their minimum dry unit weight was obtained at the loosest state. The maximum dry unit weight was calculated using mini-compaction method and vibratory table method with/without surcharge. While the vibratory compaction method was found to be ideal for sand, the mini compaction method proved to be suited for SRM to achieve the maximum dry unit weight. Relative density was considered as the controlling parameter to maintain consistency for SRM with different mix proportions during sample preparation for tests. Segregation checks on SRM samples reveal that the homogeneity of the material does not get affected upto a rubber content of 50% in the mixture.

The shear strength characteristics of SRM studied using direct shear test indicates that SRM exhibits strain hardening response without distinct peaks due to its continuous densification in contrast to sand. The initial stiffness of SRM is typically lower than that of sand. At high rubber content of 40% and above, a steady drop in the initial stiffness and shear strength of SRM can be observed since the influence of rubber matrix predominates. Further, the increase in normal stress was found to increase the shear strength of the mixture, due to redistribution of rubber within the voids of sand particles. Unlike sand, which shows dilation as well as compression response depending on the relative density, for SRM samples, compression is the primary response leading to the densification of the material. At any given normal stress, the peak shear strength of the SRM is lower than that of the sand. To summarize, SRM with rubber content upto 30% exhibits optimum shear strength beyond which the shear strength of the mixture decreases rapidly. Hence, for the application of geo-base isolation, SRM with 30% rubber content can be considered since the sand and rubber matrix contributes comparably toward the shear strength response of the mixture especially at medium to high relative density which in turn is necessary for its applicability as base layer below foundations.

Monotonic tests carried out on SRM under consolidated drained conditions further confirm the compressive response of the mixture irrespective of the confining pressure. In terms of volumetric

response, SRM is influenced by the effect of confining pressure to a relatively higher extent compared to sand. The high flexibility and deformable nature of SRM attribute to the positive pore pressure developed in the mixture during consolidated undrained conditions. The cyclic triaxial tests carried out on SRM reveals that the shear modulus and damping ratio are influenced by the rubber content present in the mixture. At a given confining pressure, shear strength decreases and damping ratio increases with the addition of rubber to the SRM. Overall, SRM with 30% rubber content was found to possess adequate stiffness, shear modulus and damping properties for its use as geo-base isolation material for further studies.



## CHAPTER 4

### STATIC RESPONSE OF FOOTING ON GEOGRID REINFORCED GBI SYSTEM

#### 4.1. INTRODUCTION

In this chapter, a detailed study on the static response of foundation resting on the geogrid reinforced GBI system is carried out. The literature discussed in Chapter 3 shows the wider use of SRM for vibration isolation purposes (Hazarika et al. 2008, Kaneko et al. 2013) but for the use of SRM as an effective GBI system, it should have adequate bearing capacity to withstand the static load coming from the building foundation and superstructure. From the previous chapter, it is observed that SRM is found to exhibit strain softening behaviour and lower shear strength compared to sand. From the literature review, it was noted that reduction of initial porosity of sand-tyre mixture through compaction and preloading could reduce its compressibility to a considerable extent (Humphrey and Manion 1992; Bosscher et al. 1997). Studies by Hazarika et al. (2010) points out the compressive nature of tyre shreds as well as its high elastic deformation under vertical loads. Though the latter aspect helps in enduring higher strain by the material which is beneficial in dynamic loading conditions, the compressive nature of SRM could pose settlement issues to the footing under static loading. Consequently, the concept of soil reinforcement using geosynthetics which is primarily adopted to improve the performance of shallow foundations resting on weaker soils (Binquet and Lee 1975; Bathurst and Jarrett 1988; Das et al. 1994) can be extended to the GBI system. To address the concern related to the strength and settlement aspect of GBI system due to the compressible nature of rubber present in it, geogrid reinforcement which was frequently adopted for footing problems was incorporated into the GBI layer in the study. In the present chapter, experimental and numerical studies were carried out to investigate the effectiveness of geogrid reinforcement in addressing the low stiffness and compressibility aspects of the GBI system.

This chapter first focuses on the laboratory-based model tests that were carried out to study the load-settlement behaviour of footing resting on geogrid reinforced GBI layer. To better understand the response of GBI system, the first test was carried out in the absence of GBI system, following which the GBI layer was introduced and a series of static load tests were conducted. Subsequent series of tests were carried out with the introduction of geogrid layers into the GBI system.

Laboratory results present some highlights on the critical feature of geogrid reinforced and unreinforced GBI system under static loading conditions, which forms the basis for arriving at the framework of the factors considered for further numerical studies.

The details of finite element simulation of the response of the footing resting on geogrid reinforced GBI layer is presented in the second part of this chapter. The reliability of the numerical modelling procedure and the material model adopted for the study was ensured by comparing the computed results of the numerical analysis with that of experimental results obtained previously. Once the validation of the numerical procedure is established, this chapter then proceeds to focus on conducting a detailed FE analysis to establish the optimum parameters of the geosynthetic reinforcement, to achieve adequate bearing capacity and settlement characteristics of the footing resting on GBI system.

## 4.2. MODEL TEST

To shed insight on the understanding of shallow foundation performance with the presence of reinforced and unreinforced GBI layer, a series of laboratory model tests were carried out on scaled down model footing. Reinforced and unreinforced GBI layer were considered and test results in the form of load-displacement curves were recorded.

### 4.2.1. Scale factor for geometry and materials

It is essential to adopt proper scaling laws for small-scale physical modelling studies to obtain an accurate response of the prototype involved. Scaling laws of similitude by Wood (2004) were adopted for geometry and materials for the present study. A scale factor ( $\lambda$ ) of 10 was used to model a prototype footing of size 1 m x 1 m. The thickness of footing is arrived by equating the scaling factors of stiffness ( $K$ ) of the soil with the flexural rigidity of the footing ( $EI$ ) as shown in equation (4.1) to maintain similar values of stresses and strains in modelling (Wood 2004).

$$\lambda_{EI} = \lambda_k \lambda_L^3 \quad (4.1)$$

where,  $\lambda_L$  is the scale factor for linear dimensions,  $\lambda_{EI}$  is the scale factor for the flexural rigidity defined in terms of scale factors for Young's modulus  $\lambda_E$  and footing thickness  $\lambda_h$  (Hegde and Sitharam, 2013) as follows:

$$\lambda_{EI} = \lambda_E \lambda_h^3 \quad (4.2)$$

Also,  $\lambda_k$  is the scale factor for stiffness defined as

$$\lambda_k = \left(\frac{1}{\lambda}\right)^a \quad (4.3)$$

where,  $a$  is the material constant which is generally taken as 0.5 for sandy soil. From equations 4.1, 4.2 & 4.3, the scale factor for the thickness of the footing can be arrived as follows:

$$\lambda_h = \lambda_L \left[ \frac{(1/\lambda)^a}{\lambda_E} \right]^{1/3} \quad (4.4)$$

Accordingly, the thickness of the model footing is obtained as 12 mm, which is rounded to 10 mm for the present study based on the availability of plate. For the study, the prototype footing is made of concrete with Young's modulus ( $E$ ) of 20 GPa while the model footing is made of steel with  $E$  of 200 GPa. Assuming that the average particle size of the soil/SRM used in the model and prototype structure is identical, the scale factor for density of sand and SRM is chosen as 1 since the same material is used for the model and prototype. To avoid overestimation of test results of model geogrid reinforcement, the scale factors proposed for 1 g model test by Viswanadham and Konig (2004) was used which accounts for the scaling effects of tensile load-strain behaviour and identical frictional bond behaviour. To avoid loss of contact between soil and geogrid, the percentage opening area for model and prototype should be uniform. The percentage opening area for the model geogrid is 80%. The tensile strength-strain characteristics of the model geogrid represent the commercially available prototype geogrid Fortrac R (tensile strength 800 kN/m). The scaling laws adopted for the experimental investigation are summarized in Table 4.1.

**Table 4.1** Scale factors used for the model test (Wood, 2004; Viswanadham and Konig, 2004)

Variables	Scaling factor
Size of footing	1/10
Young's modulus	10
Stiffness	$(1/10)^{0.5}$
Stress	1/10
Geogrid length & width	1/10
Geogrid tensile strength	$1/10^2$
Geogrid strain	1

#### 4.2.2. Experimental setup

Tests were carried out on a model footing resting on geo-base isolation layer composed of sand rubber mixtures in a sand bed tank setup (Figure 4.1). The test tank used for the study was made of steel with an inside dimension of 1 m x 1 m x 1 m. The model square footing made of square steel plate having a size ( $B$ ) of 100 mm and thickness of 10 mm. The test tank was filled with sand up to a depth of 0.9 m for all the tests.



**Figure 4.1** Photograph of the test setup

The test tank is placed below the reaction frame of length 2m and height 2m made of steel beams supported by columns. Pneumatic actuators for applying loads are attached to the reaction frame, as shown in Figure 4.2. Pneumatic actuators are linear motion device, which gives a controlled motion either on load basis or displacement basis. The equipment follows the command signal from the controlled electronics through servo valve (FESTO) which in turn controls the movement of the actuator depending upon the input signal received by it. The steel plate for model footing was connected to the actuator via a steel rod of height 1 m. Vertical loading was applied on the load plate in displacement control mode using the computerized, servo-controlled pneumatic

actuator. Electronic load cell having a capacity of 20 kN was used to measure the load. Linear variable displacement transducer (LVDT) of capacity  $\pm 30$  mm was used to measure the displacement. Calibration of the load cell and LVDT are done by the equipment providers during the installation stage. The digitalized load-displacement data can be extracted from the automatically saved files after the testing.

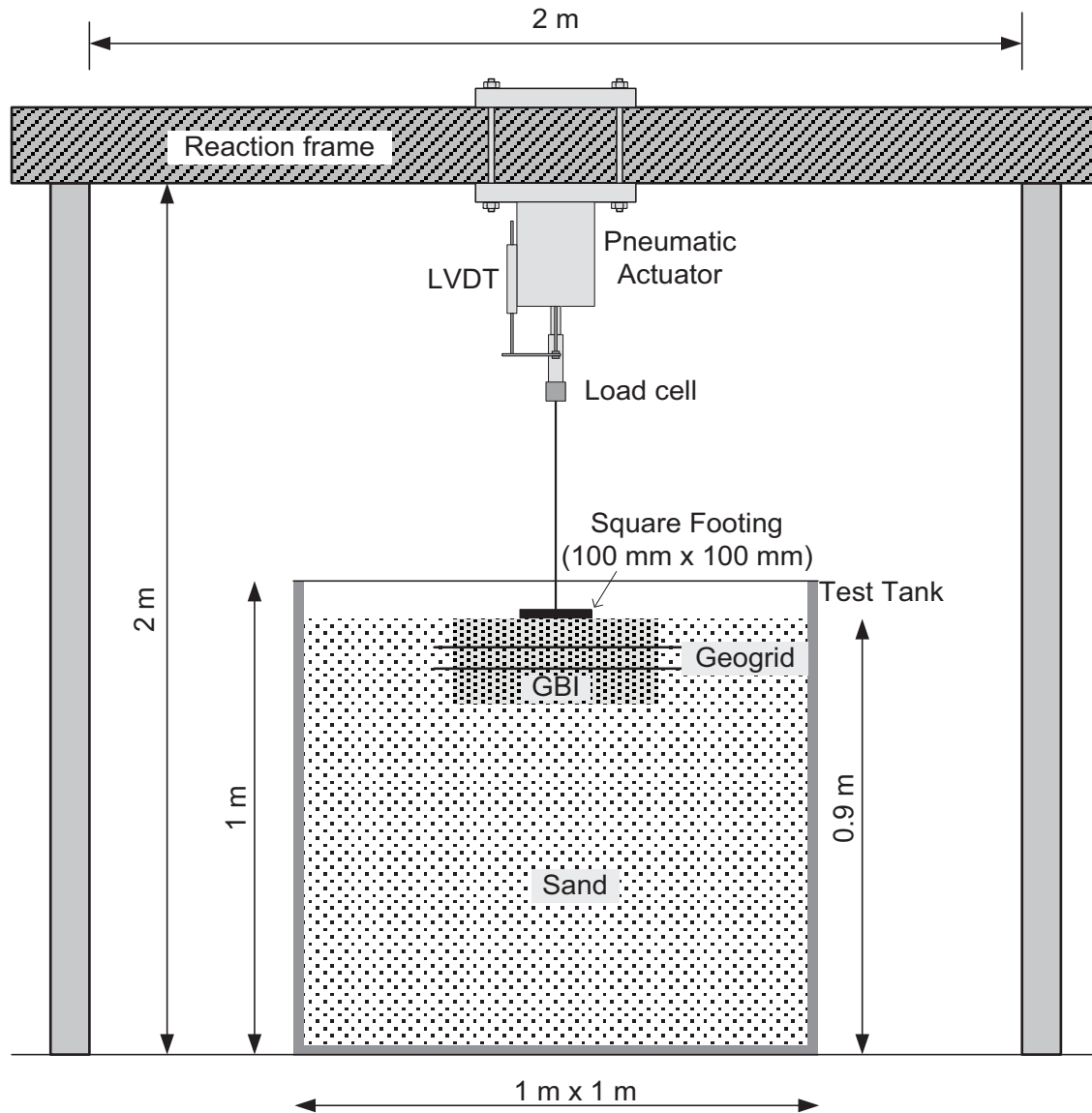


**Figure 4. 2** Schematic of the experimental setup

#### 4.2.3. Sample preparation

The first series of test was carried out on footing resting on sand bed compacted at a relative density of 85%. Sand bed was prepared using sand pluviation/rainfall technique (Cresswell et al. 1999) in

which sand was poured from a fixed height to achieve the required relative density. The relative density was calculated based on the density chart for different height of fall of sand. Also, to confirm the uniformity in density throughout the area of the sand bed, small cups of known volume were placed on different locations of the sand bed during pluviation and the density of sand falling on it was calculated. To maintain compaction control, the sand was filled in layers of 0.1 m each, and the quantity of sand required was pre-calculated for each layer. The sand was levelled before filling the following layer. To confirm the repeatability of the load testing, three preliminary trial tests using sand samples of constant relative density were carried out and comparable results of pressure-settlement curves were obtained.

The second series of tests were carried out on footing placed on GBI layer. The GBI layer was prepared by excavating the already compacted sand bed for a plan size of 300 mm x 300 mm with required thickness and backfilled with SRM (Figure 4.3a). Before the excavation, the location of excavation was marked and thin-walled rectangular aluminium sheet box with 300 mm x 300 mm size and 1 mm thickness was placed at the marked location of the sand bed (Figure 4.3b). During excavation, the aluminium box intrudes into the sand layer as the sand inside the box is removed gradually. The aluminium sheet box acts as a guide to maintain the shape and volume of the GBI layer as well as prevents caving in of sand into the excavated space. This way, ease of compaction control for SRM mixture will also be enabled. The excavated space was filled with SRM mixture weighed for the required density. Hand mixed SRM was placed in layers of 25 mm thickness and each layer is compacted by tamping using a steel template (100 mm diameter; 5 mm thickness and 0.4 kg weight) to maintain uniformity along with the required relative density. The aluminium box is lifted gently after each layer of compaction of SRM and the layer is scarified before placing the adjacent layer to ensure proper bonding. The thickness of GBI layer ( $T_{\text{GBI}}$ ) was varied as 100 mm, 200 mm and 300 mm ( $0.5B$ ,  $2B$  and  $3B$ , where  $B$  is the footing width). The width of GBI layer ( $b_{\text{GBI}}$ ) was kept constant as  $3B$ . The GBI layers were compacted to achieve a relative density of 85%.

The third series of tests were carried out on footing placed on geogrid reinforced GBI layer. Initially, sand bed and GBI layer were prepared using the procedure discussed above until the depth of placement of the geogrid is reached. The geogrids were then placed at the top of the already compacted sand and SRM layer at the desired depth (Fig 4.4) following which the



aluminium box is placed on the geogrid surface and filling of the sand and SRM for the remaining depth is carried out simultaneously to achieve the required relative density. Care is taken to prevent damage to the delicate strain gauges attached to the geogrids due to excessive twisting or bending while filling sand/SRM above the geogrids. Similarly, wires coming from the geogrids were also placed away from the footing and loading area. The geogrids were placed within a depth of  $2B$  below the footing since the effective depth of influence is within a range of  $2B$  from the bottom of footing (Guido et al. 1986; Yetimoglu et al. 1994; Omar et al. 1993; Latha and Somwanshi 2009). In the present study, single and double geogrids were used as reinforcement in the GBI system. Single layer of geogrid was placed at a depth of  $0.5B$ . Double layered geogrids were placed at depths of  $0.3B$  and  $0.5B$  (maintaining a vertical spacing of  $0.2B$ ). For all the cases, GBI layer thickness ( $T_{GBI}$ ) of  $1B$ ,  $2B$  and  $3B$  were considered.

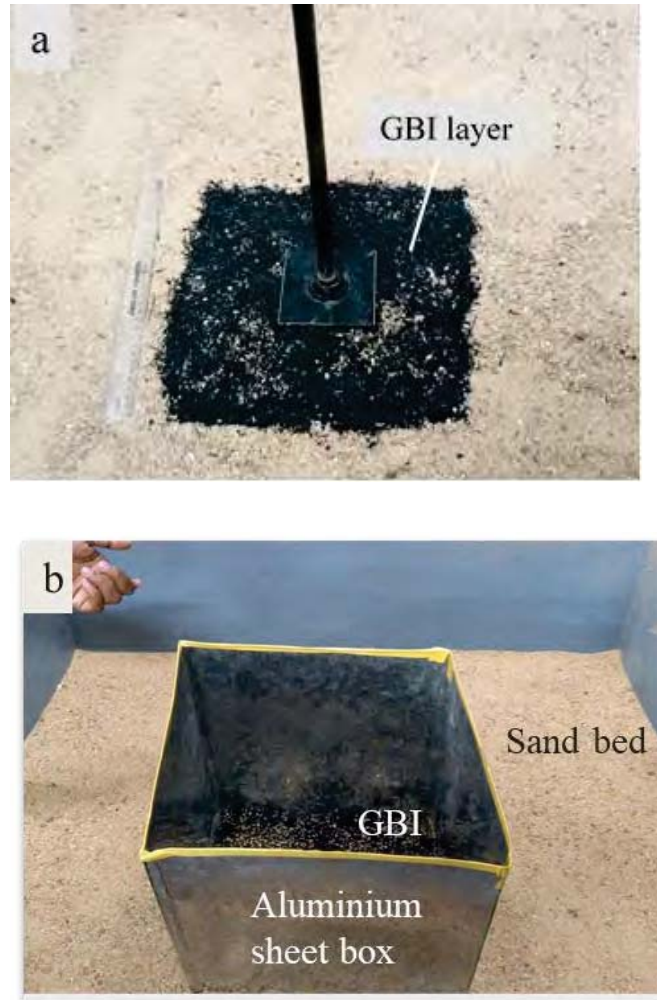


**Figure 4.3 a) Model footing on GBI layer b) Aluminium sheet box used to prepare the GBI layer**



Two strain gauges were installed in each geogrid to measure the strain developed in the geogrid below the centre of footing and at a distance of  $1.5B$  from the centre of footing. Electrical resistance type half-bridge strain gauges (HBM-LY series) of  $120\ \Omega$  resistance were adopted for the study. The strain gauges were attached to the bottom surface of the geogrid using cold curing adhesives (X60 type) to measure the bending strain in the bottom fibre (tensile zone). The outer surface of the strain gauge is coated with a protective covering putty (AK22 type) along with aluminium foil (ABM75 type) provided by the strain gauge manufacturer to prevent intrusion of sand grains into the strain gauge. The strain gauges were calibrated for electrical resistance of  $120\ \Omega$  using a multimeter each time before testing. Strain gauge data acquisition and analysis were carried out using CATMAN professional V5. (2005) software. The overall test program details are summarized in Table 4.2.

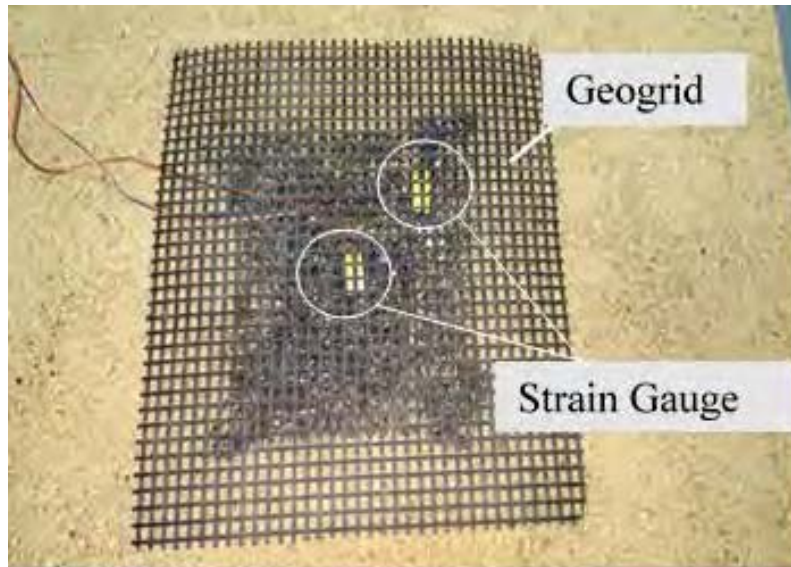


**Figure 4.4** Geogrid reinforcement used for the GBI system

#### **4.2.4. Test procedure and test program**

After preparation of the foundation bed, the model footing was placed on the level surface at the center of the prepared GBI layer and sand-bed medium (Figure 4.5). The model footing was then connected to the steel rod attached to the actuator without disturbing the sand bed. A vertical compressive load was applied to the top of the footing using the actuator at a loading rate of  $0.5\ \text{mm/min}$ . The load was applied until a distinct ultimate bearing pressure was observed, or a considerable settlement of the footing occurs for a small increment in vertical load. Readings from

the load cell, LVDT and strain gauges were collected simultaneously at a sampling rate of 5s for the entire experiment.

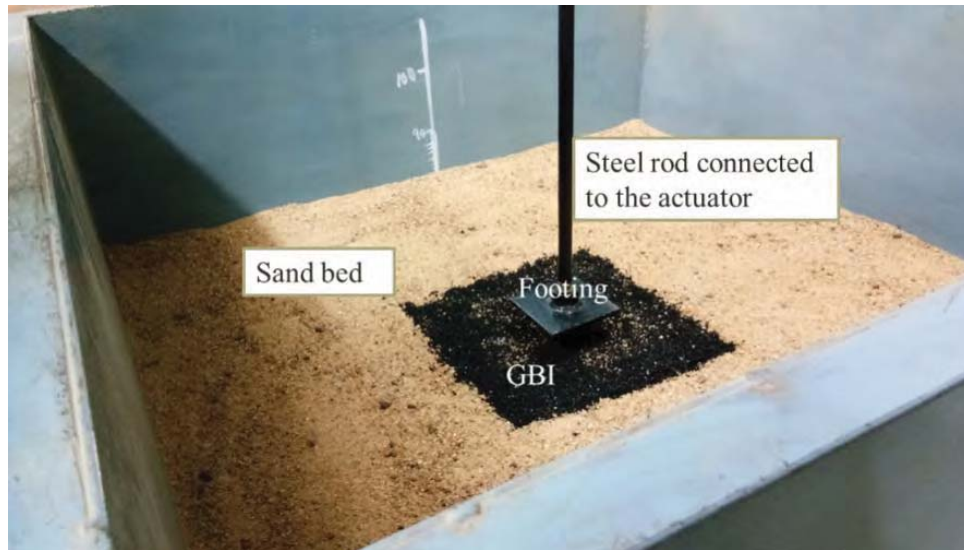


**Figure 4.5.** GBI layer and sand bed with the model footing

**Table 4.2.** Details of model tests carried out

Test Series	Description	Parameters	
		Geo-base isolation	Geogrid reinforcement
I	Pure sand (without geo-base isolation)	-	-
II	Geo-base isolation between footing and sand bed	Width ( $b_{GBI}$ ) = $3B$ Thickness ( $T_{GBI}$ ) = $0.5B$ , $1B$ , $2B$	-
III	Geogrid reinforced geo-base isolation between footing and sand bed	Width ( $b_{GBI}$ ) = $3B$ Thickness ( $T_{GBI}$ ) = $0.5B$ , $1B$ , $2B$	Width of Geogrid = $4B$ Depth of placement of geogrid below footing = $0.3B$ for single geogrid; = $0.3B$ and $0.5B$ for double geogrid

#### **4.2.5. Behaviour of footing resting on geo-base isolation layer**

The results obtained from different series of tests are plotted as bearing pressure against the footing settlement or settlement ratios. To quantify the bearing capacity improvement, due to geogrid reinforcement, the results were also discussed in terms of the bearing capacity improvement factor. Further, the strain measured along the geogrids were also discussed in the study.

The results of load tests carried out on square footing on sand with and without GBI layer is presented in Figure 4.6. The settlement of the footing ( $s$ ) is normalized by the width of the footing ( $B$ ) and is expressed as settlement ratio ( $s/B$ ) in the study. The bearing pressure-settlement curves (Figure 4.6) indicate that GBI layer exhibits a significantly larger settlement compared to that of the sand layer. It is observed that the settlement ratio corresponding to the ultimate bearing pressure is around 9% for the sand layer and 13% for GBI layer. The GBI layers exhibit initial compression due to the higher ductility of rubber content in the mixture. It is also seen that, compared to sand, there is a no considerable reduction in ultimate bearing capacity of the GBI layer. Notably, GBI layer with a thickness of  $0.5B$  exhibits bearing capacity equivalent to that of pure sand. This could be because, at lower confining pressure, the shear strength difference between sand and SRM mixture is relatively small (Figure 3.15). Although GBI layer with a thickness of  $1B$  and  $2B$  also shows an increase in the bearing capacity, the rate of increment in bearing capacity with  $s/B$  ratio reduces by 30% compared to GBI layer with  $0.5B$  width.

#### **4.2.6. Behaviour of footing resting on geogrid reinforced geo-base isolation layer**

To improve the bearing capacity and settlement aspect of GBI system, geogrid reinforcement was placed within the GBI layers beneath the footing. The load-settlement curves obtained for the footing resting on GBI layer reinforced with geogrid reinforcement is illustrated in Figure 4.7. It is evident from the figure that footing on geogrid reinforced GBI system exhibits a sharp increase in bearing capacity and reduction in the settlement. Furthermore, it is found from Figure 4.7 that the geogrid reinforced GBI system fails at higher values of settlement ratio, indicating a significant increase in ultimate capacity of footings due to reinforcement. The figure also shows that the ultimate bearing capacity of footing (corresponding to  $s/B$  ratio of 20%) on GBI system increases by three times for double geogrids and two times for single geogrid reinforcement. Previous studies by Yetimoglu et al. (1994) and Abu-Farsakh et al. (2013) on shallow footing supported by geogrid

reinforced sand also suggest that number of reinforcements is the primary parameter contributing to the increase of bearing capacity of footings.

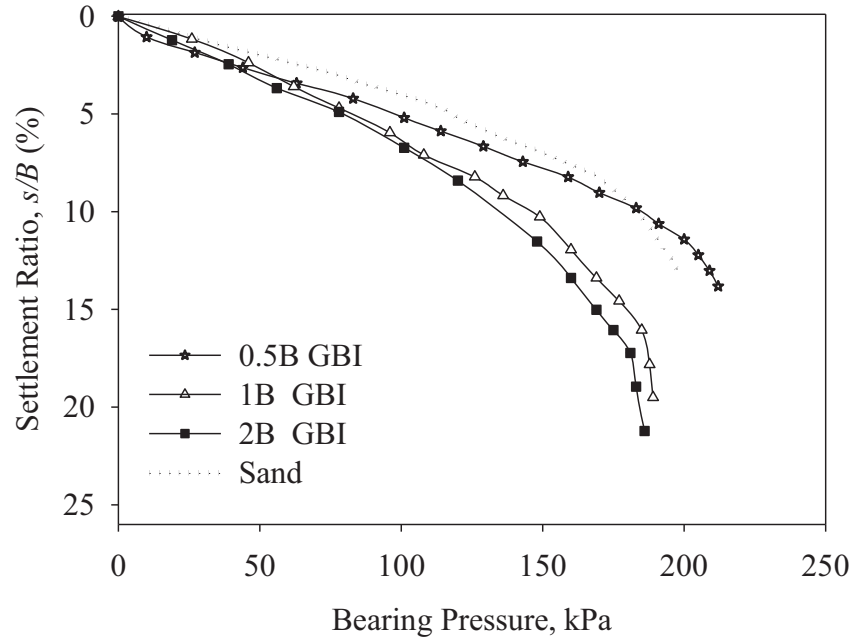


**Figure 4.6** Bearing Pressure-Settlement ratio response for footing with and without GBI layer

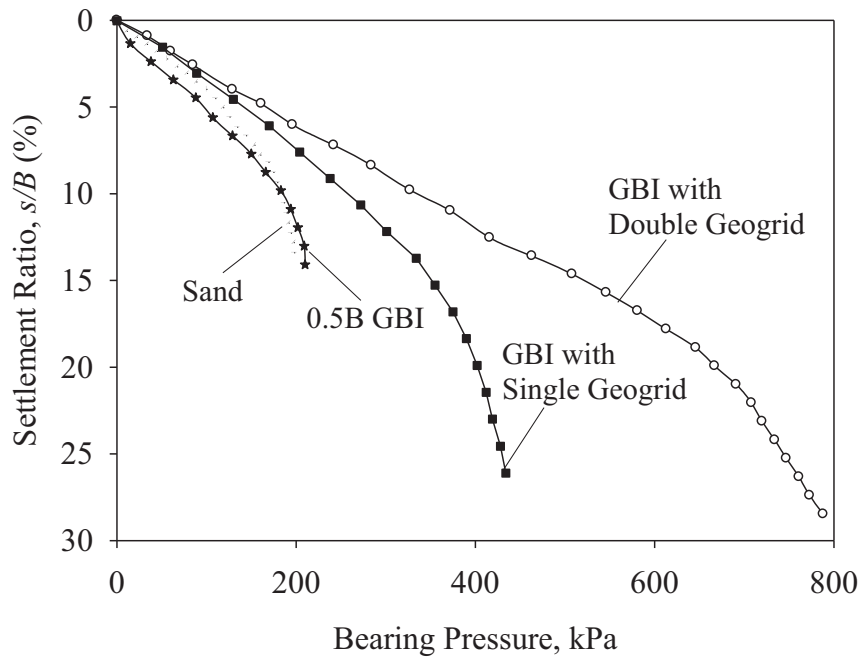


**Figure 4.7** Bearing pressure-settlement ratio curve for geogrid reinforced GBI system ( $T_{GBI}=0.5B$ )

The bearing capacity performance of the GBI system due to the inclusion of reinforcement is evaluated in terms of the dimensionless parameter, bearing capacity improvement factor ( $I_f$ ) proposed by Binquet and Lee (1975) using equation (4.5).

$$I_f = q_r / q_o \quad (4.5)$$

where,  $q_r$  is the bearing pressure of the reinforced soil foundation for given settlement, and  $q_o$  is the bearing pressure of the unreinforced soil foundation at the same settlement.

The bearing capacity improvement factor obtained from the load tests carried out on footing resting on geogrid reinforced GBI is shown in Figure 4.8. The figure shows that the bearing capacity improvement factor ( $I_f$ ) is slightly less than 1 at low values of settlement ratio but at relatively large strains i.e. beyond settlement ratio of 4%,  $I_f$  increases significantly, which implies that once the friction between geogrid and sand-rubber layer is mobilized, the bearing capacity of footing increases significantly. The GBI layer of  $0.5B$  thickness reinforced with double layered geogrid exhibits bearing capacity thrice as that of the footings on unreinforced GBI layer.

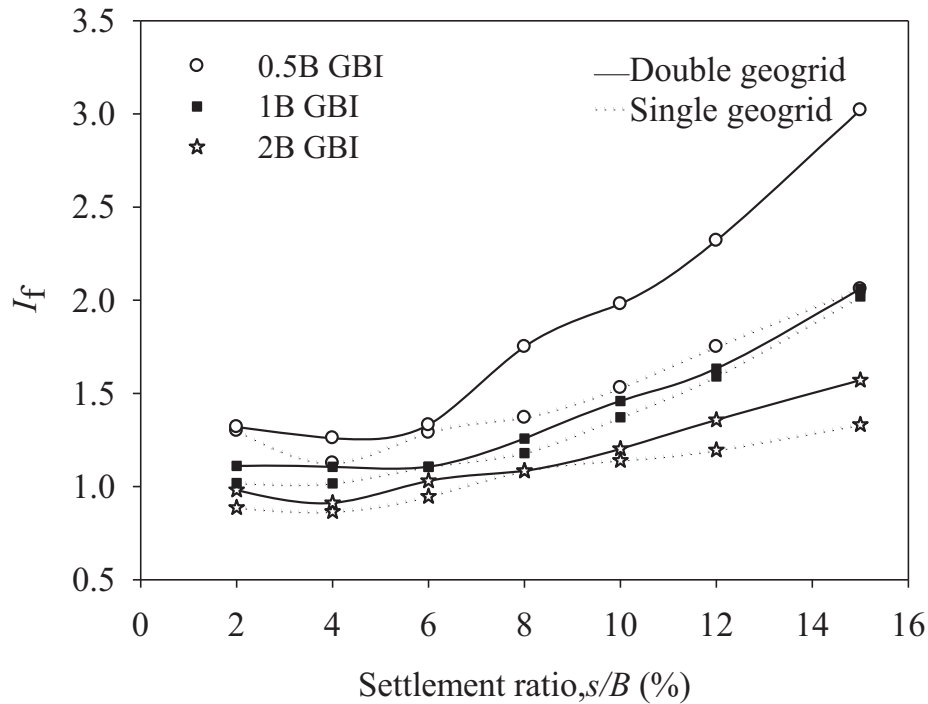


**Figure 4.8** Variation of bearing capacity factor ( $I_f$ ) with settlement ratio for geogrid reinforced-GBI system

Figure 4.9 shows the influence of thickness of GBI on the strain distribution at failure along the geogrids. In general, the strain induced in geogrids increases with the increase in thickness of GBI layer. The development of large strain is mainly due to the resistance provided by geogrid in counteracting the compressive nature of rubber in the GBI layer. The large strain measured in the geogrid also confirms the higher strength offered by the geogrid to the GBI system. However, as the distance from footing ( $x$ ) reaches  $1.5B$ , the difference in strain significantly reduces irrespective of the depth of GBI layer. This is due to the distribution of stress to a larger area by the reinforcement and reduced stress concentration. Also, Figure 4.9 shows that single-layered geogrids undergo higher strain compared to that of doubled layered geogrids.

In principle, the experimental observations approve the choice of geogrid reinforcement technique to improve the static performance of GBI system. Though the GBI layer was found to reduce the bearing capacity and increase the settlement of footing compared to the sandy layer, geogrid inclusion overall improved the performance of GBI system as high as thrice the bearing capacity of sand (for GBI with double geogrid layer). To further understand the various factors influencing the response of geogrid reinforcement GBI system, ideally, numerical studies were undertaken and focused in the upcoming section.

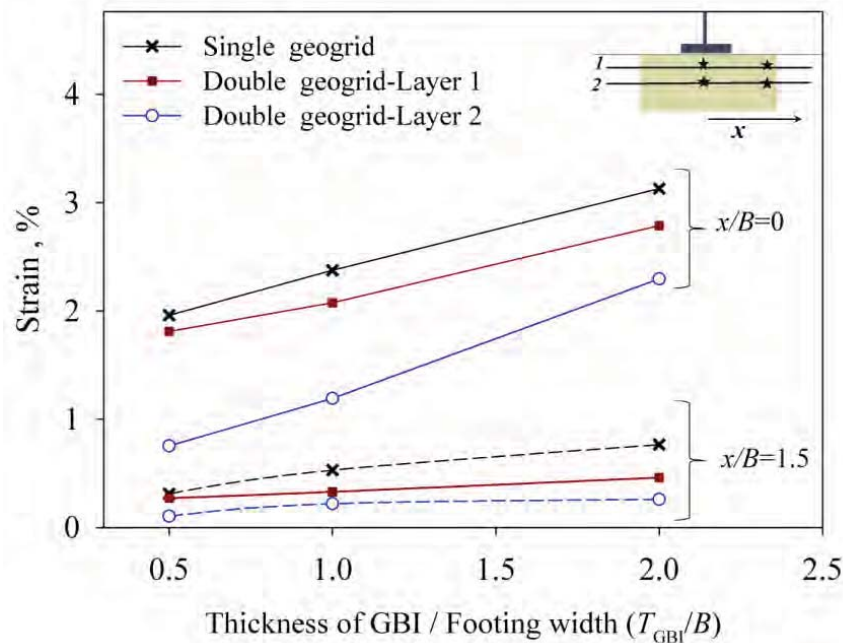


**Figure 4.9** Variation of strain developed in the geogrids with depth of GBI



### 4.3. FE MODELLING AND ANALYSIS

The experimental study on the response of model footing on GBI system gives a general idea about the bearing pressure-settlement characteristics of the GBI layer overlying sandy stratum, as well as the improvement in performance resulting from the use of geogrid reinforcement in the GBI system. As can be seen, the efficiency of reinforcement is largely dependent on the thickness of GBI layer and the depth of placement of geogrid layer. This section presents the details and results of the numerical analysis carried out to study the performance of footing resting on geogrid reinforced GBI system. Further, the numerical study also augments the finding of experiment study by considering several factors such as the width of GBI layer, depth of placement of geogrid, width of geogrid, spacing and number of geogrid layers, affecting the performance of footing resting on GBI system reinforced with geogrids.

#### 4.3.1. Model description

The numerical modelling of the footing on the GBI system was carried out using the Finite Element (FE) code ABAQUS. The numerical modelling of the footing on the GBI system was carried out using the Finite Element (FE) code ABAQUS 6.14 (2014). Though two-dimensional (2D) plane strain models are ideal for strip footings, they can be adeptly extended to simulate the response square footings with the bearing capacity being approximately 5% lower in such cases (Gourvenec et al., 2006) as well as for rectangular footings (Yetimoglu et al., 1994). In principle, the 2D plane strain model is adequate to analyze the footing-GBI response within the sand bed tank setup with suitable boundary conditions. The numerical model of the experimental study involving geogrid reinforced GBI system placed on a tank setup was created in a 2D space (Figure 4.10).

The soil domain in the study has a width of  $10B$  and height of  $9B$  similar to the sand bed used in the experimental study. The footing of width  $1B$  as in the experimental study and thickness  $0.1B$  is placed on the top surface of the GBI layer at the center of the model. The width of GBI layer ( $b_{\text{GBI}}$ ) and thickness of GBI layer ( $T_{\text{GBI}}$ ) below the footing is varied depending upon the requirements of the analysis. The geogrid layers are embedded in between the GBI layer as shown in Figure 4.10.



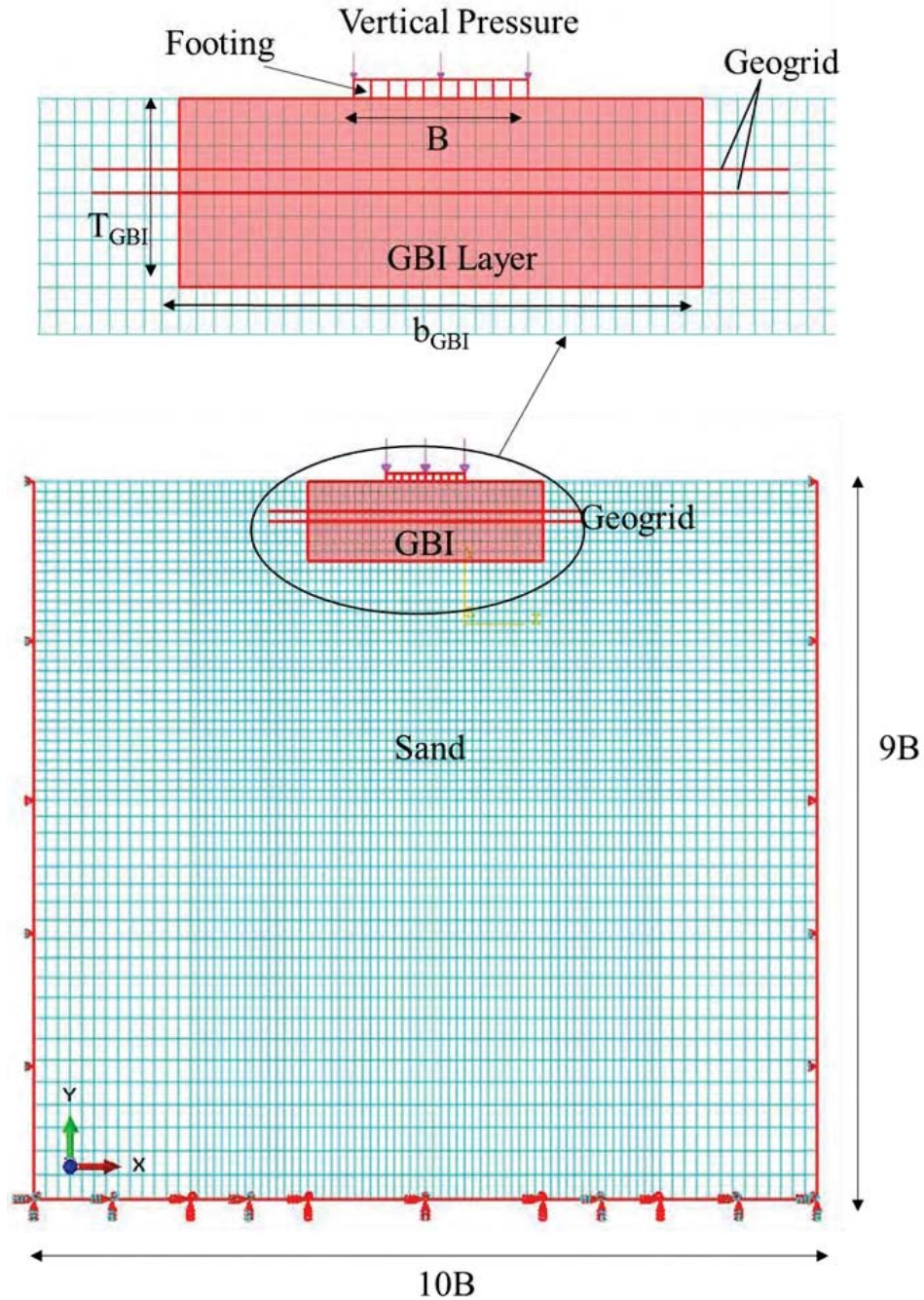


**Figure 4.10** Finite element model showing geometry and boundary conditions of geogrid reinforced GBI system

#### 4.3.2. Element type

The model footing, as well as the sand bed/GBI layer in the FE model, was discretized using 4-node plain strain continuum elements. The 4-node bilinear, reduced integration element (CPE4R)

was adopted with hourglass control (Figure 4.11). The mesh size was arrived with due emphasis to mesh convergence to ensure converged solutions in the FE analysis. The refined mesh size of the soil medium was varied from a smaller element size of 10 mm x 10 mm near the vicinity of the footing to a larger element of size 50 mm x 50 mm away from the footing for precision purpose. Geogrid elements which have a very low thickness to length ratio were modelled using the wire feature in ABAQUS Calvarano et al. (2017). Beam elements which exhibit shear flexibility and axial tension were assigned to the wire feature to model the geogrids. The final discretized mesh of the 2-D model is shown in Figure 4.10.

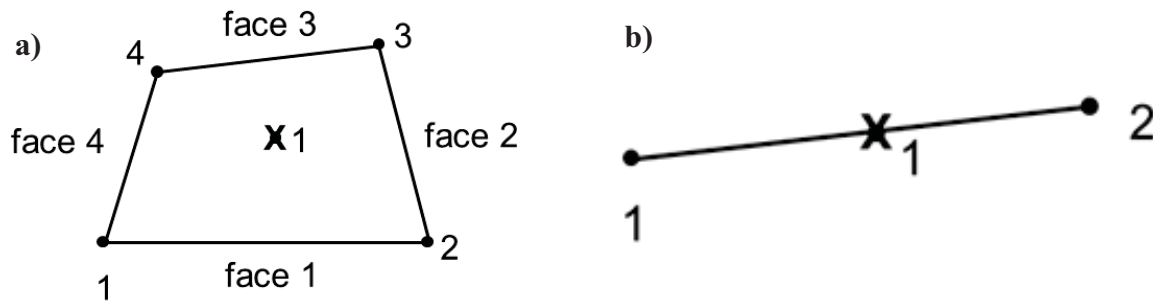


**Figure 4.11. (a) 4-node reduced integration elements (b) 2-node beam elements (ABAQUS, 2014)**

#### 4.3.3. Constitutive models

Linear elastic material model is used for modelling the footing behaviour. The geogrid is also modelled using linear elastic material model since low strain is expected as observed from the experimental study. The GBI layer made of SRM and sand medium are assumed as isotropic and homogenous and are modelled as elasto-plastic materials. The initial elastic behaviour of the sand/SRM is modelled as linear elastic using Young's modulus from the triaxial test data (Figure 1).

The linear Drucker Prager constitutive model (Drucker and Prager, 1952) with a non-associated flow rule is used to account for the failure pattern of sand/SRM. The Drucker-Prager model, which is a simplification of the Mohr-Coulomb model has a smooth yield surface which avoids singularities associated with corners as in the case of the Mohr-Coulomb model. The cylindrical cone shaped Drucker-Prager yield surface in the principal stress space is shown in Fig 4.12a. The model facilitates pressure pressure-dependent yielding primarily induced by hydrostatic pressure. The present FEM software has triaxial test data sub option and can calculate the material constants

for the Drucker-Prager model for different confining pressures. The experimental data of yield stress under plastic strain obtained from the triaxial test results (Figure 1) corresponding to sand and SRM are used in the model.

The yield criterion for the model is:

$$F = t - p \cdot \tan \beta - \delta = 0 \quad (4.6)$$

where,

$$t = 0.5q \left( 1 + \frac{1}{k} - \left( 1 - \frac{1}{k} \right) \left( \frac{r}{q} \right)^3 \right) \quad (4.7)$$

$F$  is the yield function,  $p$  is the first invariant of stress,  $\beta$  and  $\delta$  are functions of angle of friction and cohesion respectively;  $k$  is the stress ratio at yield point obtained from triaxial test;  $r$  is the third invariant of deviatoric stress and  $q$  is the Von Mises equivalent stress.

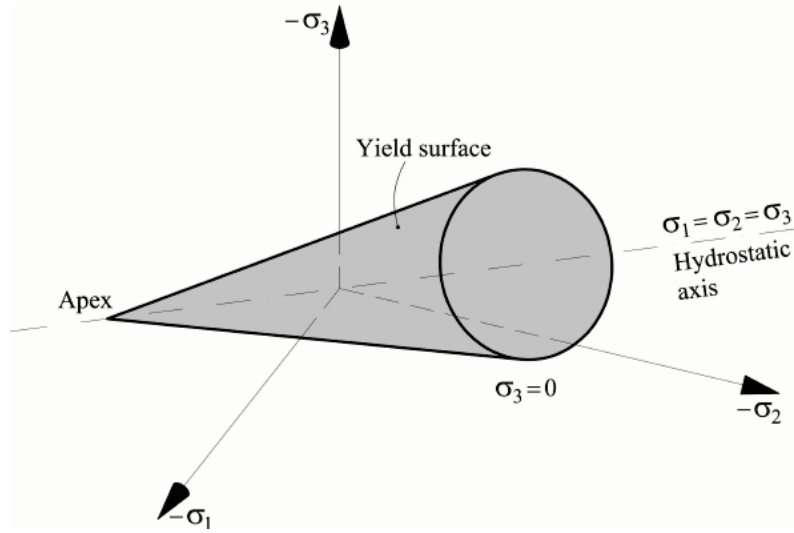
To maintain the convexity of yield surface, the flow stress ratio requires to be in the range of  $0.778 \leq k \leq 1.0$ . Fig 4.12b shows the variation of typical yield surface depending on the value of flow stress ratio.

The material properties used for the numerical analysis were obtained from the triaxial test results and basic laboratory tests, as mentioned in the previous chapter. Table 4.3 shows the material properties adopted for the different material models chosen for the present numerical simulation.

**Table 4.3** Material properties used in the FE analysis

Properties	Soil	SRM	Footing	Geogrid
Density, $\gamma$ (kg/m <sup>3</sup> )	1400	1200	2500	1100
Young's modulus, $E$ (MPa)	85	50	30000	2200
Poisson's ratio, $\mu$	0.35	0.3	0.2	0.3

a)



b)

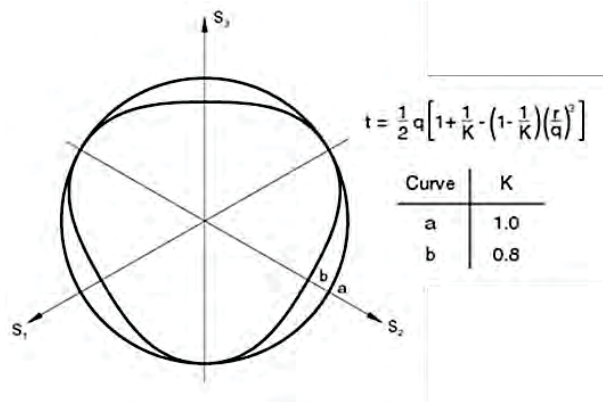


**Figure 4.12 (a)** Drucker-Prager yield surface in the stress space (Cervera et al. 2015) **(b)** Typical yield surface for the Drucker Prager model in the deviatoric plane (ABAQUS, 2014)

#### 4.3.4. Interface modelling

The numerical simulation of interface behaviour between different surfaces should consider aspects such as choice of contact models, surfaces of interaction and suitable contact control checks. For the present study, surface to surface contact discretization was used to model the interface between different surfaces (Figure 4.13) since it avoids the chances of largely localized penetrations (Nguyen et al. 2016). Also, this method is not sensitive to the mesh size between surfaces, choice of master and slave roles and can predict the contact stresses reliably. The shear interaction between geogrid and the soil/GBI layer was ensured using surface to surface contact pairs above and below the soil-geogrid interface. Geosynthetic elements were considered as master surface and the corresponding contact surface (which is sand or GBI layer) was assumed as slave

surface. In ABAQUS, the mechanical properties of the contact surface were defined in terms of normal and tangential behaviour. The normal behaviour at the contact interface is defined using ‘hard’ contact where penetrations of surfaces are not allowed at the constraint levels (Nguyen et al. 2016). The tangential behaviour of the contact surface is modelled using Coulomb friction model (equation 4.8) where the interaction friction coefficient ( $\mu$ ) and an elastic slip tolerance ( $E_{slip}$ ) were the parameters used for defining the soil-geogrid interaction.

$$\mu = \tau / \sigma = \tan (\phi) + c / \sigma \quad (4.8)$$

where,  $\tau$  is the shear strength;  $\sigma$  is the normal stress;  $c$  and  $\phi$  are cohesion and angle of internal friction corresponding to the failure envelope of Mohr circle.

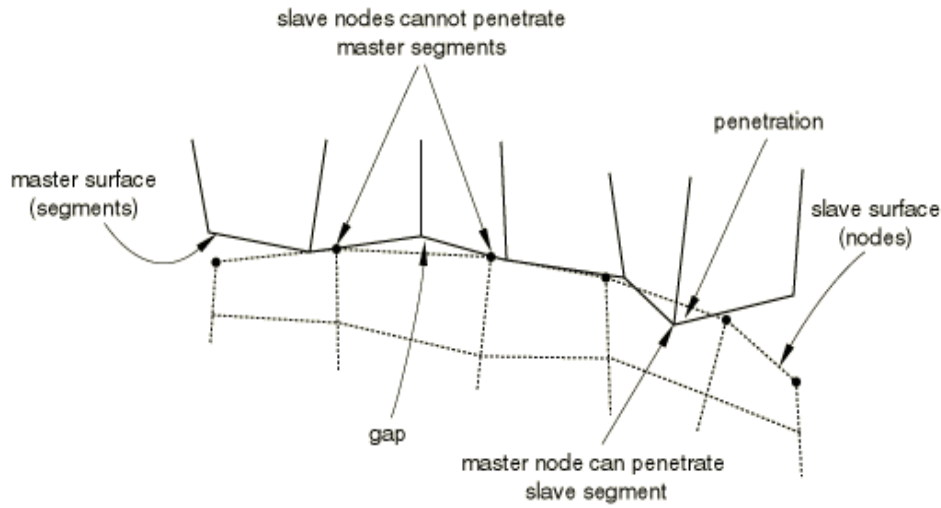


**Figure 4.13** Typical Surface to surface interface configuration (ABAQUS, 2014)

The interface friction angle between sand/SRM and geogrid used for the study was obtained from direct shear tests carried out on sand and SRM with a horizontal layer of geogrid placed at the mid-depth of the sample at the shearing interface as mentioned in the previous chapter. The interfacial angle of frictions of sand and SRM with respect to geogrids was found to be  $34^\circ$  and  $27^\circ$  respectively. Correspondingly, friction coefficients of 0.65 and 0.5 respectively were used to model tangential contact of soil-geogrid and SRM-geogrid interfaces, respectively. An  $E_{slip}$  value of 0.005 was also adopted for the slip tolerance between surfaces.

#### 4.3.5. Boundary conditions and modelling procedure

Boundary conditions were established by applying roller supports to the sides such that horizontal displacement was restricted and vertical movements were permitted ( $U1 = UR2 = 0$ ). Fixed support

at the base of the soil model ensures that displacement was restricted in all directions ( $U1 = U2 = UR1 = UR2 = 0$ ). The footing was considered at the center of the model to avoid boundary effects. To simulate the static loading experienced by the footing, geometric surface-based uniformly distributed loading is applied on the top surface of the footing.

Geostatic stress conditions were established initially on the numerical model based on the unit weight of the material. Gravity load was applied in the initial step followed by vertical pressure on the top of the footing. Vertical loading was applied in equal increments of 20 kPa. Since the strain experienced by the geogrids in the experimental study is lesser than 5% (Figure 4.9), the numerical modelling is carried out using Eulerian solution scheme. After the analysis, stresses, displacements and rotations were extracted at the desired nodal points for different directions using field output variables. Finite element study of compressive loading conditions yields results in the form of bearing pressure and displacement at different nodal points on the numerical model.

#### **4.4. VALIDATION OF FE RESULTS WITH EXPERIMENTAL RESULTS**

To calibrate the analysis procedure and the material model used in the numerical study, the experimental results obtained from the model test on the tank was compared with a series of results computed from the numerical analysis of the same problem. This ensures accuracy of the parametric study carried out in the succeeding session. The pressure-settlement curves obtained from the experimental results were used to compare with the finite element study for GBI system with and without reinforcement as shown in Figure 4.14.

For the unreinforced GBI system, pressure-settlement curves of GBI layer with thickness  $0.05B$  (Figure 4.6) was compared. Similarly, for the reinforced GBI system, the pressure-settlement curve of the double-layered geogrid reinforced GBI system (Figure 4.7) was compared. The numerical and experimental results match comparably with a deviation of 5%. Slight differences in the numerical studies compared to the experimental results could be due to the selection of material model. From the above comparisons, it is clearly visible that the numerical studies using ABAQUS can simulate the response of geogrid reinforced GBI system reasonably well.



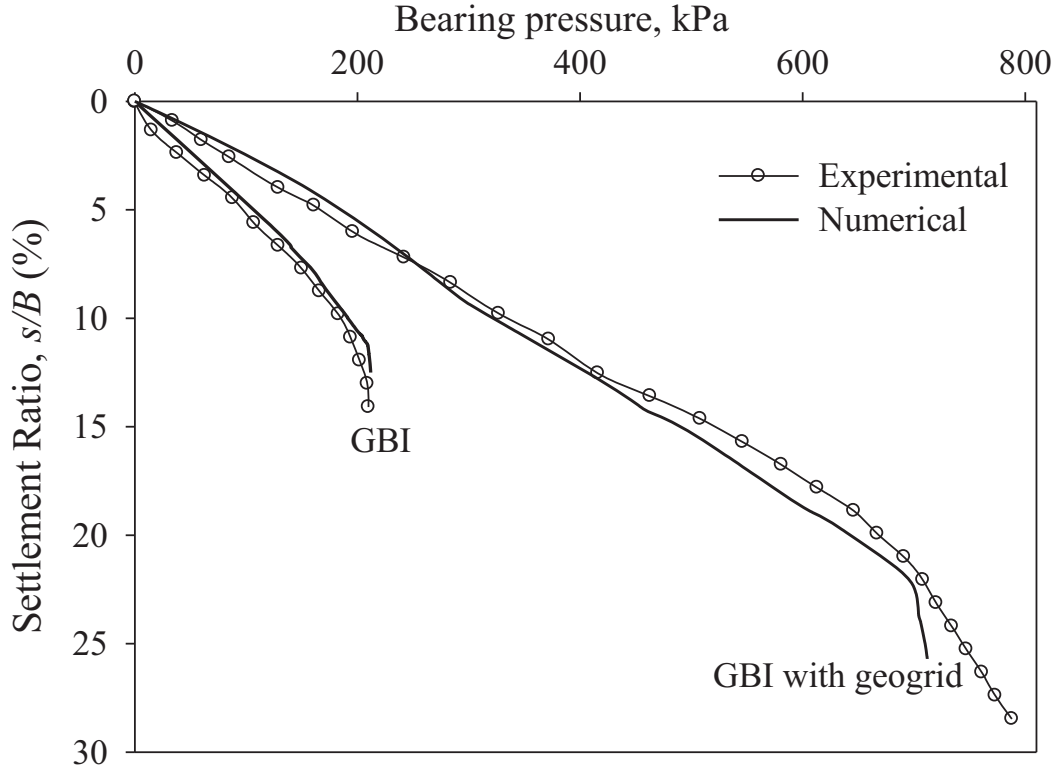


**Figure 4.14** Comparison of bearing pressure to settlement ratio as obtained from numerical study with experimental results

#### 4.5. PARAMETRIC STUDIES

The developed numerical model was used for parametric studies to explore the response of GBI layer in the presence of geogrid reinforcement. The parameters studied were the depth of placement of first geogrid below the footing ( $u$ ), number of geogrid layers ( $N$ ), length of geogrid ( $L$ ), thickness of GBI layer ( $T_{\text{GBI}}$ ), width of GBI layer ( $b_{\text{GBI}}$ ). The parameters were normalized with the width of footing ( $B$ ) as  $u/B$ ,  $L/B$ ,  $T_{\text{GBI}}/B$  and  $b_{\text{GBI}}/B$ . The thickness of GBI system was varied as  $0.5B$  to  $2B$  and the width of GBI layer in the range of  $1B$  to  $4B$  was considered. For the geogrids, the depth of placement of the top-most geogrid was varied as  $0.2B$  to  $0.5B$  below the footing and the length of the geogrid was varied as  $1B$  to  $6B$ . Up to 5 layers of geogrid reinforcement ( $N=5$ ) with a spacing of  $0.2B$  and  $0.3B$  were investigated in the present study.



#### 4.5.1. Effect of depth of placement of top geogrid

The depth ' $u$ ' which is the location of placement of the top-most geogrid below the footing has a considerable influence on the performance of geogrid in improving the bearing capacity of soil as it directly affects the tensile force mobilized in the geosynthetics (Abu-Farsakh et al. 2013). The experimental study demonstrates that the influence of geogrid in improving the performance of the GBI system is strongly dependent on the thickness of the GBI layer. Therefore, the optimum depth ( $u$ ) of placement of the first layer of geogrid was investigated along with the thickness ( $T_{\text{GBI}}$ ) of GBI system. In the study, a single layer of geogrid ( $N=1$ ) was placed at varying depths ( $0.2B$ ,  $0.3B$ ,  $0.4B$  and  $0.5B$ ) below the footing. The thickness of GBI system was varied as  $0.5B$ ,  $1B$  and  $2B$ . The typical variation of  $I_f$  with  $u/B$  ratio corresponding to  $s/B$  ratio of 0.1 is shown in Figure 4.15.

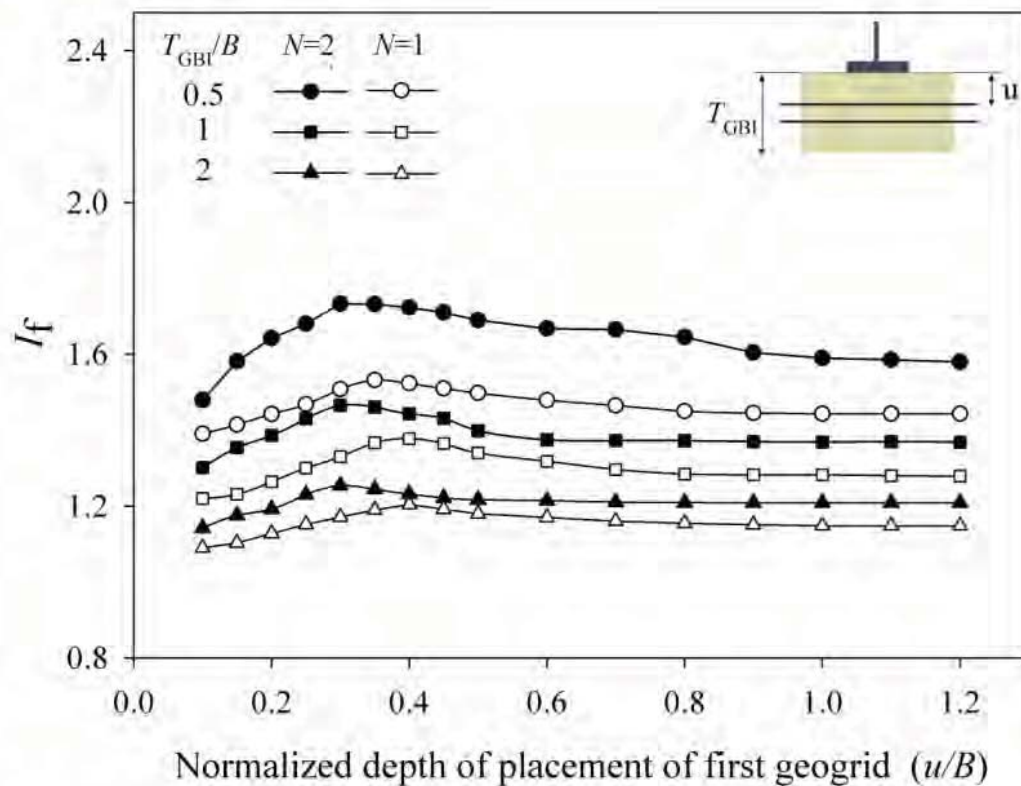


**Figure 4.15** Effect of the depth of placement of first geogrid on bearing capacity improvement factor ( $I_f$ )

The results clearly indicate that the  $I_f$  value increases gradually up to  $0.35 \leq u/B \leq 0.4$  irrespective of the thickness of GBI layers. It is to be noted that, at a higher thickness of GBI, the depth of placement of the top reinforcement can be optimized as  $0.4B$ . This could be due to the low rigidity

of the GBI layer which causes the reinforcement to perform satisfactorily at a higher  $u/B$  ratio thereby avoiding punching of the geogrid. For two layered geogrid systems, the value of  $I_f$  increases in the range  $0 \leq u/B \leq 0.3$ , following which it maintains peak value at  $0.3 \leq u/B \leq 0.35$  and subsequently reduces. Moreover, beyond  $u/B$  of 1,  $I_f$  remains constant for all the cases. It must be noted that the depth of placement of the top reinforcement is arrived considering static loading conditions. However, in the event of dynamic loading, the top layers of geogrids are highly susceptible to displacement due to foundation rocking and eccentric loading. Hence, in such cases, the position of top geogrids should be also calculated considering the dynamic loading conditions also.

#### 4.5.2. Effect of length of geogrid

The variation of the bearing capacity improvement factor ( $I_f$ ) with the length of geogrid ( $L$ ) was studied considering single layered geogrid with  $u/B$  ratio of 0.3 and  $L/B$  ratio varying from  $1B$  to  $6B$ . Since geogrid was resting partially on the GBI layer and sand, the influence of width of GBI layer ( $b_{GBI}$ ) is also considered for the study. The thickness of GBI layer was kept constant as  $0.5B$  since  $I_f$  is higher at this thickness and the width of the layer was varied from  $1B$  to  $4B$ .

Figure 4.16 shows the variation of the bearing capacity improvement factor ( $I_f$ ) with the normalized length of geogrid layer corresponding to  $s/B$  ratio of 20%. It can be observed that there is a gradual increase of  $I_f$  with  $L/B$  ratio followed by a stable trend. As the width of GBI layer reduces, the increase in bearing capacity is predominant at a smaller length of geogrid itself. The bearing capacity improvement factor ( $I_f$ ) increase significantly when  $L/B \geq b_{GBI}/B$  indicating that the geogrids perform satisfactorily when the width of the reinforcement is higher than the width of the GBI system. This could be due to the higher stiffness of the surrounding sand which offers higher fixity and pull-out resistance to the geogrids. The higher interface friction between sand and geogrid also contributes to the additional resistance. In all cases, the  $I_f$  value reaches peak corresponding to  $3 \leq L/B \leq 5$  depending on the width of the geogrid. It can also be noted that the use of stiffer reinforcements below the footing could reduce the need for longer reinforcements for sand layers (Huang and Tatsuoka 1990). Hence for higher  $b_{GBI}/B$  ratio of GBI layer, stiffer geogrids could be used to reduce the effective length of geogrids.

Past studies on geogrid reinforced soil by Abu-Farsakh et al. (2012), Das and Omar (1994), Omar et al. (1993) and Prasad et al. (2016) also points out at the increase in  $I_f$  with the increase in length

of the reinforcement up to an effective  $L/B$  ratio following which the variation gradually becomes constant. An effective length of  $4B$  to  $6B$  was suggested by Shin et al. (2002) and Abu-Farsakh et al. (2012) for geogrid reinforced soil.

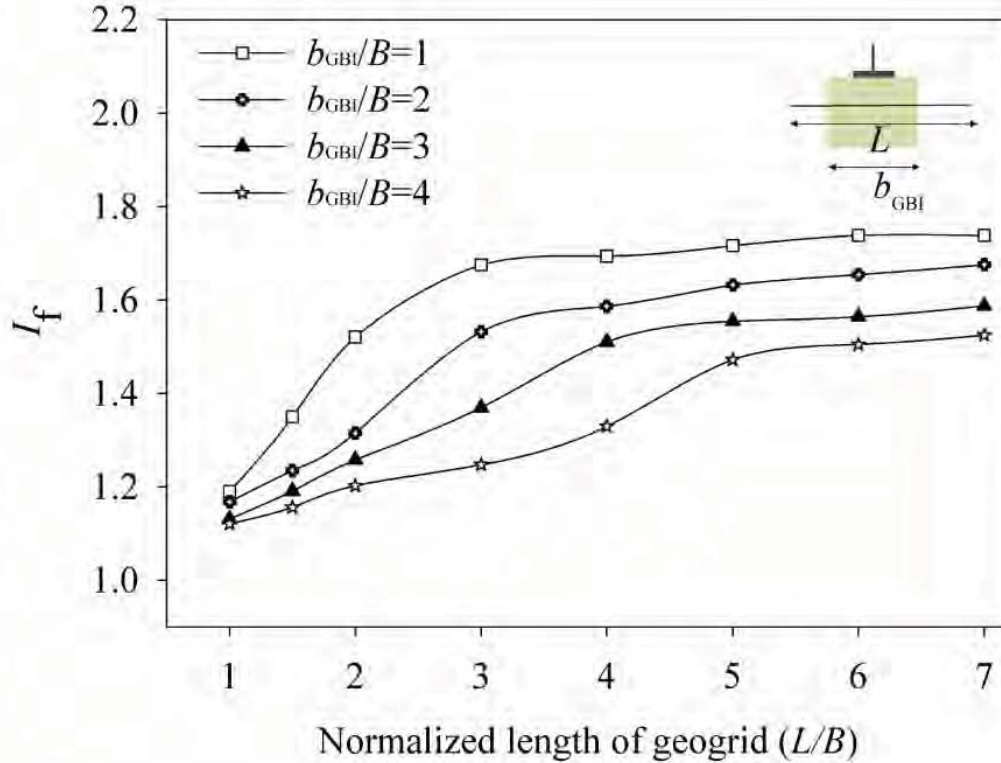


**Figure 4.16** Effect of length of geogrid on the bearing capacity improvement factor ( $I_f$ )

#### 4.5.3. Effect of number and spacing of reinforcement

A series of numerical analysis was carried out to find the optimum number of reinforcement ( $N$ ). The number of reinforcements is largely dependent on the influence depth of the soil, i.e. the depth of placement of geogrid below the footing beyond which the presence of geogrids contributes negligibly to the increase in bearing capacity. For the present study, an influence depth of  $2B$  was assumed for the placement of geogrids (Omar et al. 1993). The  $L/B$  ratio was kept constant as 3 and  $T_{GBI}/B$  ratio was varied from 0.5 to 4. The GBI system was reinforced with 1 to 5 layers of geogrids placed at distinct intervals below the footing. The spacing of the geogrid was varied as  $0.2B$  and  $0.3B$ . Single layered geogrid was placed at  $u/B$  ratio of 0.35 and the rest of the geogrids were placed at  $u/B$  ratio of 0.3. The influence of the bearing capacity improvement factor ( $I_f$ ) for

varying  $N$  values (corresponding to  $s/B = 20\%$ ) was plotted for different thickness of GBI and spacing of geogrid as shown in Figure 4.17.

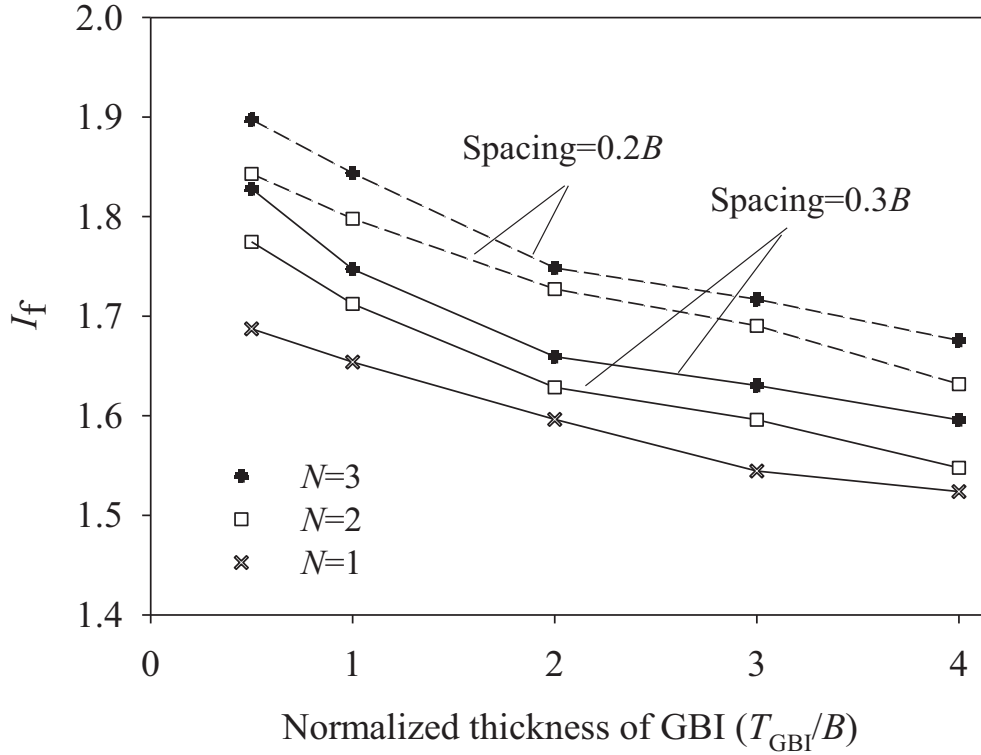


**Figure 4.17** Effect of number of layers ( $N$ ) and spacing of geogrid on bearing capacity improvement factor ( $I_f$ )

Increase in the number of reinforcement layers is found to increase the bearing capacity of GBI system (Figure 4.17). For spacing of  $0.2B$ , the increment in bearing capacity is not significant beyond top two layers of geogrid. On the other hand, for spacing of  $0.3B$ , the optimum number of reinforcements is 3. This is reasonable since closer reinforcement spacing reduces footing settlement by creating a soil-geogrid composite which acts like a quasi-rigid earth slab (Huang and Menq 1997). The reinforcement beyond  $N=3$  (for spacing of  $0.2B$ ) and  $N=4$  (for spacing of  $0.3B$ ) is placed below the influence depth and hence its contribution to  $I_f$  will be negligible. For the present study, the influence depth is observed at around  $1.25B$  irrespective of the thickness of GBI layer. It could also be noted that at  $T_{GBI}/B=0.5$ , the rate of increase of  $I_f$  is high due to the high frictional resistance offered by the top layer of reinforcement. An optimum  $N$  value of 3 for spacing of  $0.2B$  was suggested by Yetimoglu et al. (1994) and Abu-Farsakh et al. (2013) for shallow

footing resting on sandy soil. Comparable results with  $N=3$  were suggested by Das et al. (1994) for both sandy and clayey soils. Saha Roy and Deb (2017) also points out that the value of  $N$  should be more than 1 for a multilayer soil system.

#### 4.5.4. Strain distribution across the geogrids

The strain distribution along the reinforcements, obtained for the load corresponding to the ultimate load capacity of the reinforced GBI system was analysed. Single and double layered geogrid (spacing  $0.2B$ ) with  $T_{GBI}/B=1$  and  $b_{GBI}/B=1$  were used for the study. The variation of strain for different layers of geogrid reinforcement along the centre line of footing for sand and GBI system is shown in Figure 4.18. As observed in the experimental study, the maximum tensile strain value occurs below the footing, which gradually reduces and becomes compressive in nature.

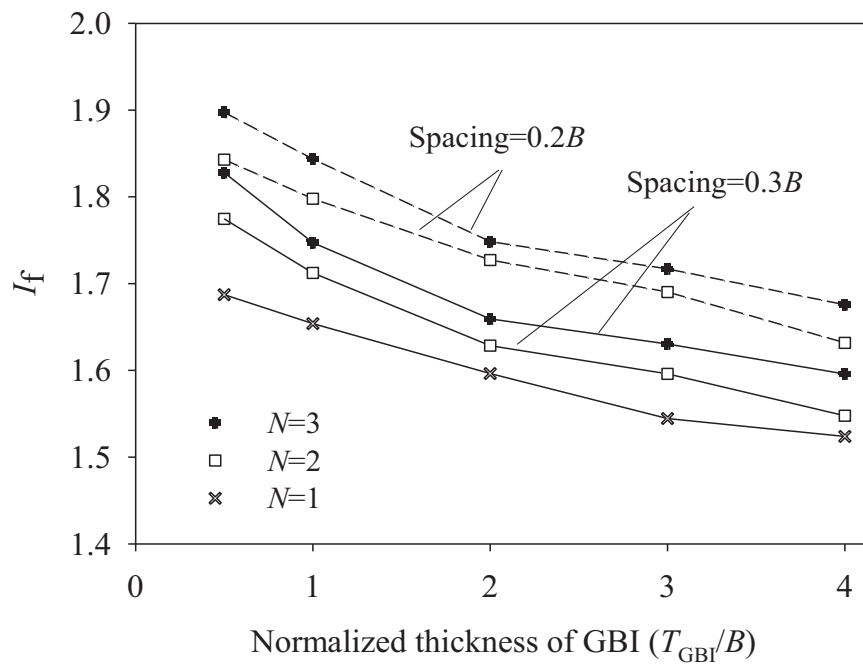


**Figure 4.18** Effect of number of layers ( $N$ ) and spacing of geogrid on bearing capacity improvement factor ( $I_f$ )

The value of  $x/B$  from 1.5 to 2 is the transition zone of strain from tension to compression gives a clear idea about the length of reinforcement to be used. Beyond  $x/B$  of 2, the compressive strain reduces gradually and becomes constant at  $x/B$  of 2.5. The compressive strain experienced by the geogrids beyond  $x/B$  of 2 is primarily due to the compressive strain exerted by the soil surrounding

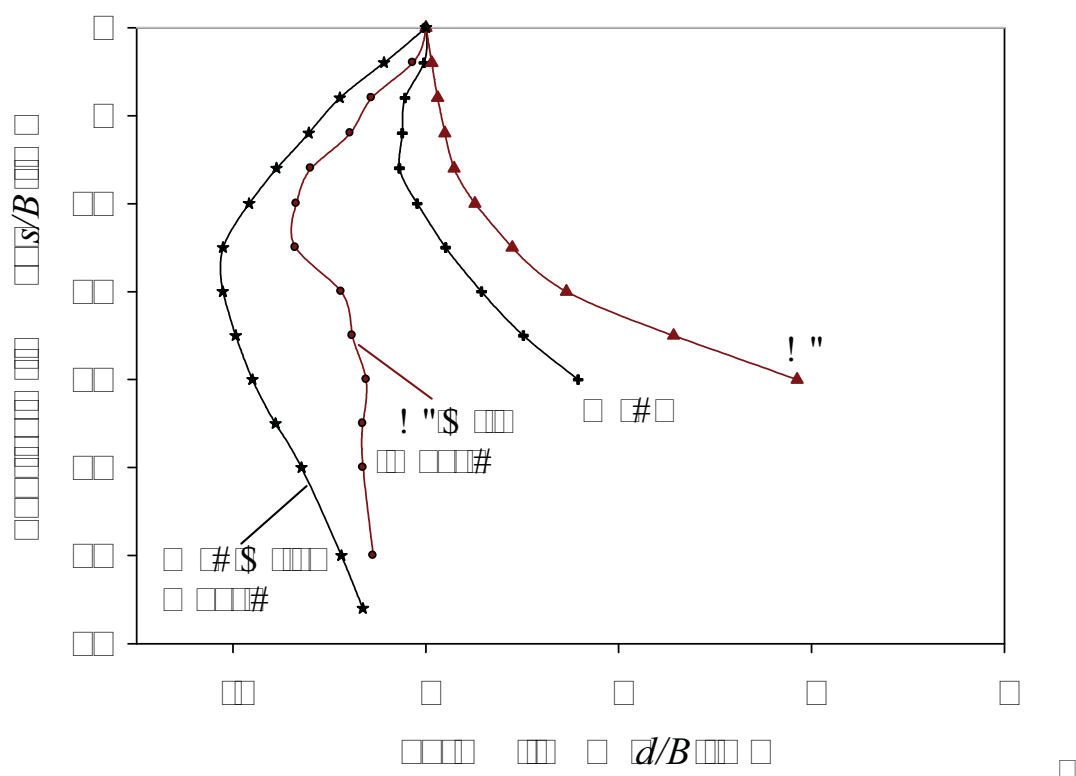
the geogrids in the horizontal direction as reported in the literature ( Michalowski 2004; Abu-Farsakh et al. 2013). The minimal value of strain beyond  $x/B$  of 2.5 indicates a negligible contribution of geogrid for bearing capacity increment of soil. Accordingly, the length of reinforcement layers in reinforced soil foundation should be greater than  $2.5B$  for full mobilization of tensile force in the reinforcements.

Similar trends of transition zones were reported by Huang and Tatsuoka (1990) on sand and Abu-Farsakh et al. (2012) on crushed limestone for reinforced shallow footings. Moreover, the first reinforcement layer usually experiences the higher strain, while the last reinforcement layer experiences the lowest strain. As the width of GBI system ( $b_{\text{GBI}}$ ) increases, the transition zone distance (from the centre of footing) for tensile force mobilization also increases. This could be due to the grip and interlocking provided by the surrounding sand compared to sand rubber mixture.

#### **4.5.5. Surface deformation in the reinforced GBI system**

The surface heave behaviour of GBI layer for reinforced and unreinforced case was analyzed to understand the failure pattern of the GBI system. Deformation at the surface ( $d/B$ ) was measured from the centreline of the footing ( $x/B$ ). Past studies (Chummar 1972; Latha and Somwanshi 2009; Hegde and Sitharam 2013) suggest that isolated footing placed on unreinforced soils exhibit maximum heave at  $1.5B$  from the centre of footing and the heave further extend up to  $2B$ . In Figure 4.19, the surface deformations near the footing measured at  $1.5B$  from the centre line of the footing are plotted for different settlement ratios.

For unreinforced case, as expected, GBI system exhibits significant heaving at the surface level compared to sand. The surface heave exhibited by the unreinforced GBI system is about 36% higher than that of sand. For the reinforced case, the heave has significantly reduced and has not extended well to the surface. Compared to the unreinforced sand layer, the surface heave of the reinforced sand layer reduces by about 2.25 times. Similarly, for the GBI system, the surface heave of the reinforced GBI layer reduces by about 2.5 times compared to the unreinforced GBI layer. This further confirms that the reinforcement and the sand/GBI layer act as a coherent and composite body enabling it to withstand well the effects of footing loading. In short, introduction of geogrid significantly arrests the surface heave of both GBI layer and sand layers.



%         \$    ! "  &  #  #&  &

0000 0 0000000000 0000 00\$ 00000# 0000000000'0 0 #0( 00\$ 0000 0000000#00000000 0 0000# ' 00000000 0  
 0 0000 00 0 000000 # ' 0000000 ( # 00000000 0000000000D\_0\$ 00000 0 000000# 0( 0000000 0 0  
 000000 0( 000000 ' 0&00000000000( 0#0000000# #0( 000000 ' 0&0) 0 00000\*00000 00 0000 0000  
 0000000000000000000000000000 00 ( ## #0000000000( 0000000( 000000 ' 0&00000 00) 000#0  
 0 0000 00000 0000000000s/B00 0000+s/B00 00000 0000'0 0#0000000000 0000 0( 000000 ' 0&\$ 000( 0  
 0 ' 00000\*, 0 00#0-' 00 00 00000#00000000 00( 00000 00000000 000000 0 0000 ( # 00# ' 0000  
 000000000000000000000000 #00 0#&000000000000 00\*000000\*0\_0\$ 0 00000000 00 000000 #0 !"0  
 0&0 000 000000 0 00000 ( # 00# ' 00000000\$ 0000# 0000#\*0000000'000 00000#&0000000&0  
 00 000000 0 00000 ( # 00# ' 00000000 000000 #00 0#&00&0\$ 0000 0& #00#000 ' 0#0\$ 000000 00  
 0000-' 00 000000 000000( 0&000000 00\*00000000000000( 000000 ' 0&0 ' 0000 000000 000000  
 # 0 0( #00000) 0 0000000\*0\*000000 00000 00 000 0&0 0\$ 00 000#0000000000 00 000000 #0 !"0



system for a range of embedment depth varying from 0.2B to 1B. Since Shin et al., (2002) considers  $s/B < 5$ , the present study considers an  $s/B$  of 4% as limited settlement level.

$$\left( \frac{I_{f(s)}}{I_{f(u)}} \right) = \frac{\text{Bearing capacity ratio at limited settlement level}}{\text{Bearing capacity ratio at ultimate load}} \quad (4.9)$$

Figure 4.20 shows the variation of bearing capacity improvement factor ratio ( $I_{f(s)}/I_{f(u)}$ ) for varying embedment ratios, where ( $I_{f(s)}$ ) and ( $I_{f(u)}$ ) are bearing capacity factors corresponding to  $s/B$  ratio of 4% and ultimate load (for  $s/B=20\%$ ) respectively. The study is carried out for GBI layer with  $N=1$ ;  $u/B=0.35$ ;  $L/B=3$ ;  $b_{GBI}/B=1$  and  $T_{GBI}/B=0.5$ . The results are presented along with those reported by Shin et al. (2002) for strip footings on sandy layer, corresponding to  $N=1$ ;  $s/b < 5\%$ ;  $u/b=0.4$  and  $L/B=6$ . The results of numerical study for sandy layer (without GBI) for the above parameters of Shin et al. (2002) are also plotted in Figure 4.20.

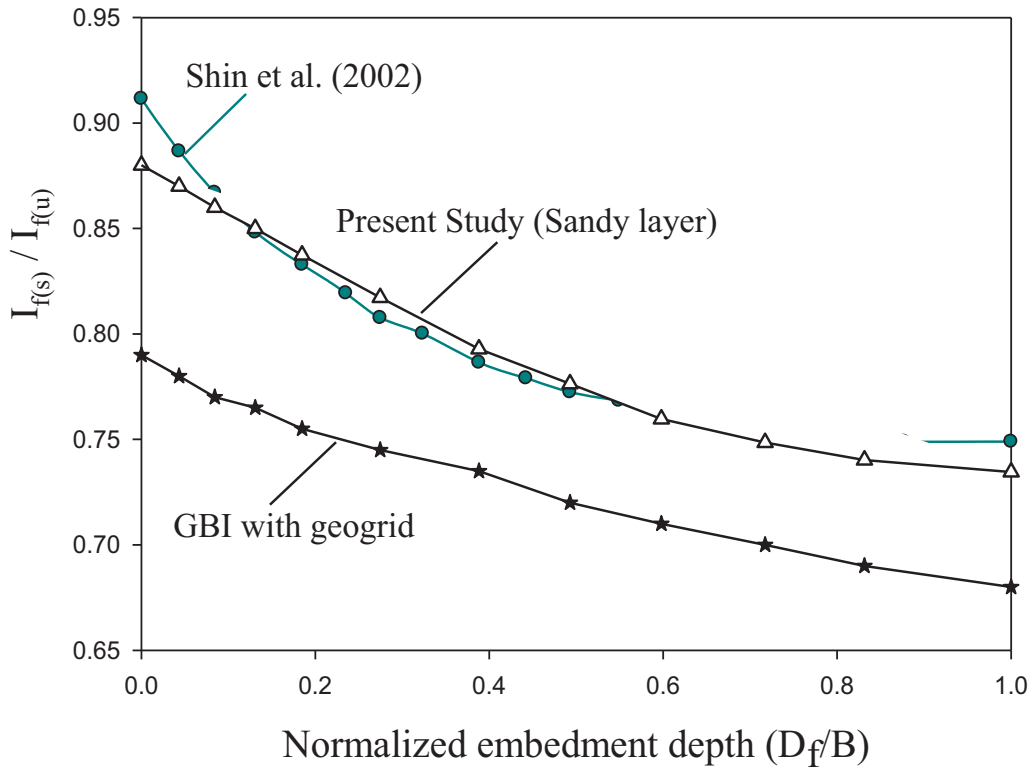


**Figure 4.20** Influence of embedment depth on the bearing capacity

It is clearly seen that the bearing capacity trends of sandy soil from the present study and Shin et al. (2002) are in good agreement. The bearing capacity factor ratio of GBI system is seen to reduce

gradually with the embedment ratio similar to that of sandy layer. This is because, at higher embedment depths, the bearing capacity of unreinforced GBI system increases, resulting in a low bearing capacity improvement factor.

#### **4.6. SUMMARY**

The experimental studies and numerical investigations discussed in this chapter offers some key directions about the effectiveness of the use of geogrid in improving the performance of a footing of resting on GBI system made of sand rubber mixture under static loading conditions as well as the basic failure mechanism of GBI system with and without geogrid reinforcement. Experimental observations indicate that the introduction of the proposed geo-base isolation layer placed between footing and sandy strata reduces bearing capacity and increases settlement. Provision of geogrids to the geo-base isolation system was found to increase the bearing capacity by two times for single geogrid layer and three times for double geogrid layer. The larger strain on geogrids measured during the experimental study shows the development of interlocking frictional resistance offered by geogrid, which counteracts the compressive nature of rubber in the GBI layer.

The FE analysis carried out on footing on geogrid reinforced GBI system shows that the number, position and length of geogrids along with the width of GBI layer are the primary parameters influencing the increase in bearing capacity and reduction in settlement of the footing. The length of reinforcement shall be greater than the width of the GBI layer. In addition to the better performance in terms of bearing capacity and settlement, the geo-base isolation using the geogrid reinforcement can also arrest the surface heave of the footing.

This chapter confirms that geogrid reinforced GBI system performs well under static loading conditions and can sustain foundation loading sufficiently with adequate bearing capacity and reduced settlement. Once the static load demand is satisfied, the dynamic load response aspect of the geogrid reinforced GBI system needs to be explored. The next chapter discusses in detail about the performance of a typical low-rise building placed on geogrid reinforced GBI system under seismic loading conditions.

## **CHAPTER 5**

### **DYNAMIC FE MODELLING AND ANALYSIS OF A LOW-RISE BUILDING RESTING ON GEOGRID REINFORCED GBI SYSTEM**

#### **5.1. INTRODUCTION**

The main aim of the present chapter is to understand the applicability of the geogrid reinforced GBI system to a typical low rise building by assessing its performance under dynamic loading conditions. The results of the static study presented in Chapter 4 indicates that the reduced stiffness of GBI system and the associated settlement concerns are well taken care of with geogrid reinforcement. Moreover, the static study emphasizes that the isolated footing resting on geogrid reinforced GBI system bears foundation loading effectively like any other typical reinforced soil beds. Studies from the literature review chapter also point out that higher normal stress and confining pressure can significantly reduce the plastic compression of SRM (Humphrey and Manion 1992; Edil and Bosscher, 1994). Hence, for a superstructure-foundation system placed on GBI layer, in addition to the geogrid reinforcement, the presence of structure itself can provide sufficient surcharge to the GBI layer, thereby reducing deformation to a considerable extent. Further, the beneficial effects of geosynthetics in the protection of structures such as foundations, retaining walls and soil walls subjected to dynamic loading is well established by several researchers (Sakaguchi 1996; Bathurst et al. 2007; Basha and Babu 2011; Taha et al. 2015; Xu et al. 2015; Kalpakci et al. 2018; Xu and Fatahi 2018a, b). In view of this, the present chapter focuses on the combined response of GBI system with geogrid reinforcement for low-rise buildings subjected to seismic loading through a series of numerical investigation and parametric studies.

To comprehend the seismic response of GBI system, the initial part of the chapter deals with developing an SSI based FE model using ABAQUS 6.14 (2014) considering a conventional low-rise building-foundation system resting on soil/GBI layer. The chapter also examines the selection of appropriate constitutive models for the materials and boundary conditions suitable for numerical simulation under seismic loading conditions. The study considers the seismically active Indo-Gangetic plain region of India for choosing seismic design load factors considering typical soil profile in the region. The recently recorded earthquake ground motions (acceleration time histories) in the Indian subcontinent with low to high-frequency content is chosen for the input

motion in the analysis. The seismic SSI analysis is carried out by the direct approach in the time domain analysis. The ensuing part of the chapter focuses on confirming the accuracy of the numerical modelling procedure by comparing the FE results with the results of laboratory shake table tests on SRM by Bandyopadhyay et al. (2015).

Similar to the static settlement of GBI system, the seismic settlement is an important aspect that influences the deformation response of the building in an earthquake event. The next part of the chapter focuses on the seismic settlement aspect of GBI system with and without the presence of geogrid reinforcement. Besides, the geogrid parameters were also optimized for further studies in the chapter.

Further, the free-field response of the geogrid reinforced GBI system at the foundation depth due to the seismic excitation applied at the bottom level of the soil model was initially considered without the influence of the structure in terms of acceleration time history and transfer functions. Subsequently, the foundation-structure system was introduced into the system, and the behaviour of geogrid reinforced GBI system under seismic loading condition was studied at the foundation level. In this way, a basic understanding of the influence of SSI in the present study can be obtained.

Finally, in this chapter parametric studies were carried out to address the influence of the thickness of GBI layer ( $T_{\text{GBI}}$ ), frequency content and PGA of earthquake input motions on the seismic response of the structure placed on the geogrid reinforced GBI layer. The structural response in terms of acceleration time history and response spectra were calculated at desired locations. In addition, the base shear and inter-storey drift experienced by the structure with and without the presence of the GBI system were compared.

## **5.2. PROBLEM STATEMENT**

The present study is aimed at implementation of the GBI technique to the rural area as a low-cost alternative for the conventional base isolation technique. That being the case, to study the dynamic performance of the GBI system, a conventional low-rise building with shallow footing is considered. The current study adopts a typical moment resisting framed structure supported on raft footing for the numerical modelling and analysis. The GBI layer is placed below as well as at the sides of the raft footing for the desired thickness. The geogrid reinforcement is placed within the

GBI layer for its added advantages to the GBI system under static and dynamic loading conditions, as discussed previously in Chapter 2 and 4. The present study is region specific, hence layered soil domain pertaining to a typical site in the highly seismic Indo-Gangetic plain basin is considered for the numerical investigation. Figure 5.1 presents the schematic illustration of the framed structure placed on the proposed GBI layer.

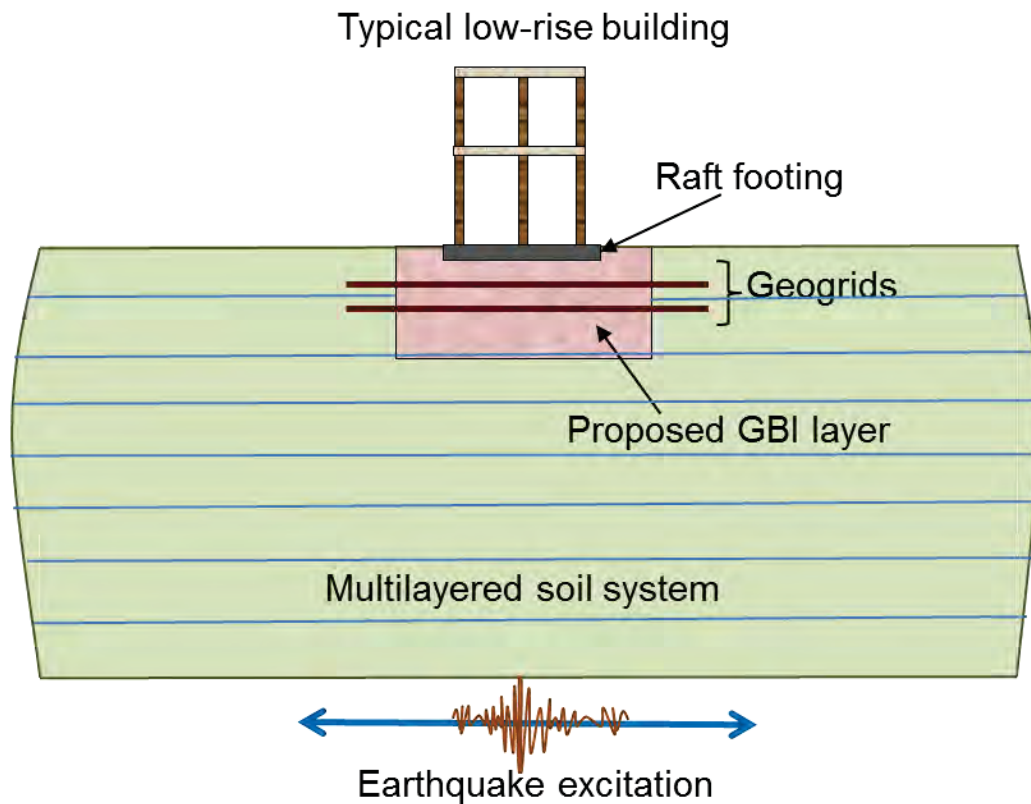


**Figure 5.1** Schematic of the soil-structure system with geogrid reinforced GBI layer

### 5.2.1. Seismicity of the region considered

For the present study, the Indo-Gangetic plain region (Figure 5.2) which is the most seismically active region in the Indian subcontinent with a dense population is considered. The Himalayan tectonic trends have given rise to the formation of Indo-Gangetic plain basin lying in the southern side of Himalaya along the Himalayan Frontal Thrust. The basin encompasses several ridges and faults running transversely and obliquely across the Himalayan seismic belt (Valdiya 1976, 2016). An estimated 16 seismically active faults exist in this region including the Moradabad fault and the Great Boundary fault (Dasgupta et al. 2000) with most of the faults being strike-slip in nature

(Gupta 2006). The Indo-Gangetic plain is primarily a sedimentary basin formed by the deposits of three major rivers namely the Ganges, Brahmaputra and Indus. This region lies at an average elevation of around 200 m above mean sea level (Raghukanth and Kavitha 2014). The sedimentary deposit in the basin sometimes extends up to 5 km depth. The plain is 150 km to 500 km wide with an area of 2.5 million km<sup>2</sup> to 3 million km<sup>2</sup> comprising major parts of northern India, Himalayan foothill regions, parts of Nepal, Bangladesh & Pakistan including major cities like Delhi and Karachi.

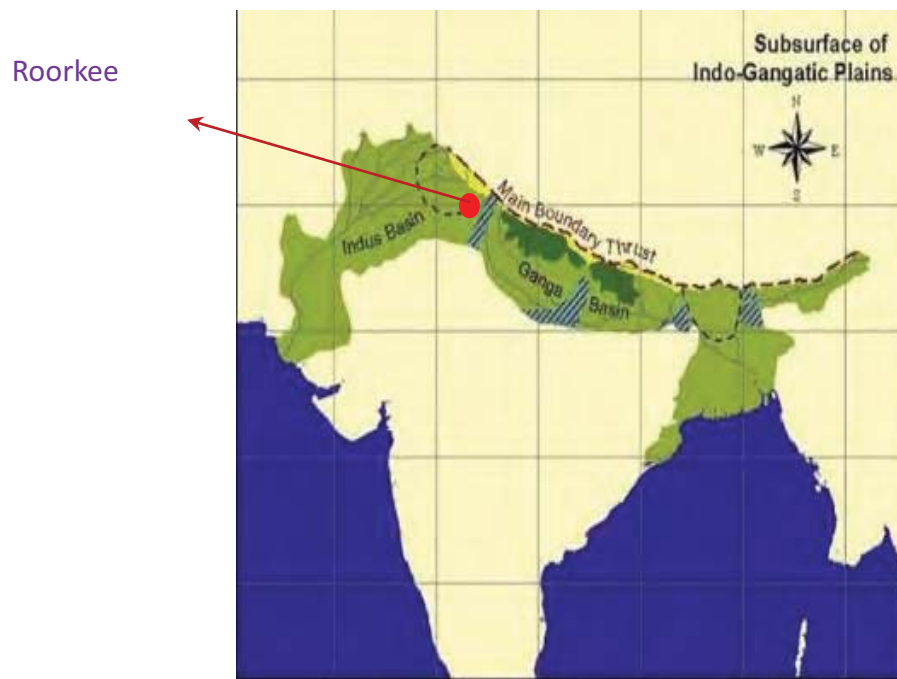


**Figure 5.2** Indo-Gangetic plain region (source: [www.iitk.ac.in/gangetic/intro\\_gallerie/subsurface\\_indo-gang](http://www.iitk.ac.in/gangetic/intro_gallerie/subsurface_indo-gang))

The past earthquakes, in the Indo-Gangetic plain and the surrounding Himalayan regions, such as the 1905 Kangra ( $M_w=8.6$ ), 1934 Bihar ( $M_w= 8.0$ ), 1950 Assam ( $M_w= 8.7$ ), 1988 Bihar-Nepal ( $M_w= 6.9$ ), 2005 Kashmir ( $M_w=7.6$ ), 2015 Nepal ( $M_w=7.8, 7.3$ ), 2015 Hindu Kush ( $M_w=7.5$ ), etc. show the seismicity of the region and the existence of potential seismic zones that could trigger future earthquakes (Kattri 1987; Bilham and England 2001). The Indo-Gangetic plain falls under zone IV and V that contains regions of high seismic intensity as per the Indian Standard (IS) code IS 1893 Part 1 (2016). Demographically, a massive population of about 125 million in this region ([www.censusindia.gov](http://www.censusindia.gov).) living in buildings poorly adhering to earthquake design practices further adds to the vulnerability to earthquake hazards. Besides, the basin effect arising from thick soil

sediments increases the ground amplification potential in the region (Bagchi and Raghukanth 2019). The 2015 Nepal earthquake ( $M_w=7.8$ ) in the Himalayan belt with a casualty of around 9000 people indicates the ongoing tectonic activities in the region asserting the necessity of preparedness for building safety arising from earthquake crisis in the near future. In the present study, recorded ground motions of major earthquakes that occurred in the Indian subcontinent in the past two decades were considered to study the response of typical low-rise building resting on GBI layer in the Indo-Gangetic plain region.

### 5.2.2. Geotechnical properties

The soil profile of a typical site in the Roorkee town/region located at the Indo-Gangetic plain was considered for the study. Though the sedimentary deposits of Indo-Gangetic plain may extend to few kilometers depth (Raghukantha and Kavitha 2014), for the present study, geotechnical properties from the soil profile of Roorkee site up to 32 m depth was considered. This region is prone to major earthquakes since it is classified as Zone IV as per IS 1893 part 1 (2016) with a zone factor of 0.24. The typical soil profile of the site consists of top layers of low to medium dense sand followed by dense soil. The Standard Penetration Test (SPT) data obtained from the Roorkee site is shown in Figure 5.3. The shear wave velocity ( $V_s$ ) profile for the site (Figure 5.3) was calculated from empirical correlation between  $V_s$  and SPT  $N$  values for sandy soils proposed for Roorkee region by Kirar et al. (2016) as follows:

$$V_s = 100.3 N^{0.338} \quad (5.1)$$

### 5.2.3. Superstructure details

Two storied residential apartment buildings classified as A-4 type as per the National Building Code (NBC) of India (2016) was adopted to represent the conventional low-rise building. The framed structure considered for the study has a height of 4.5 m at the ground floor (including plinth level) and 3 m for the top floor. Two equal bays with a width of 4 m each was assigned to the framed structure. The beams and columns were assigned a cross-section of 0.35 m x 0.4 m and 0.35 m x 0.45 m respectively. The details of the superstructure considered in the present study are illustrated in Figure 5.4.



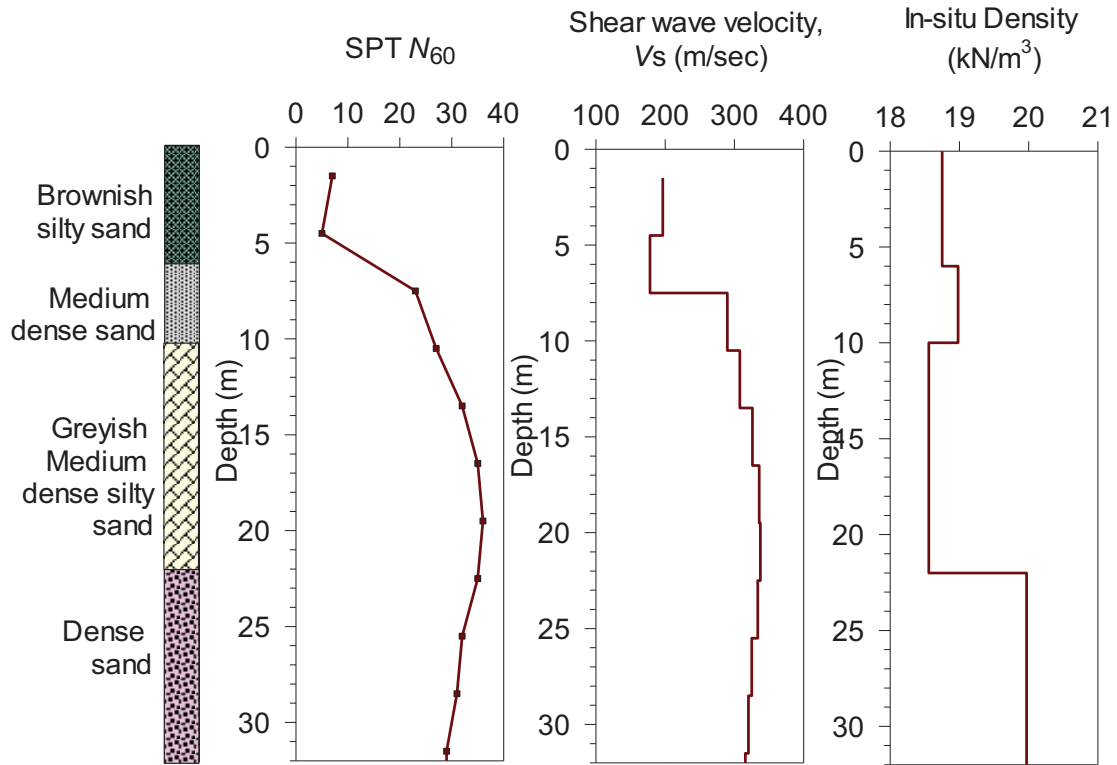


**Figure 5.3** Details of typical soil profile for the Indo-Gangetic plain region

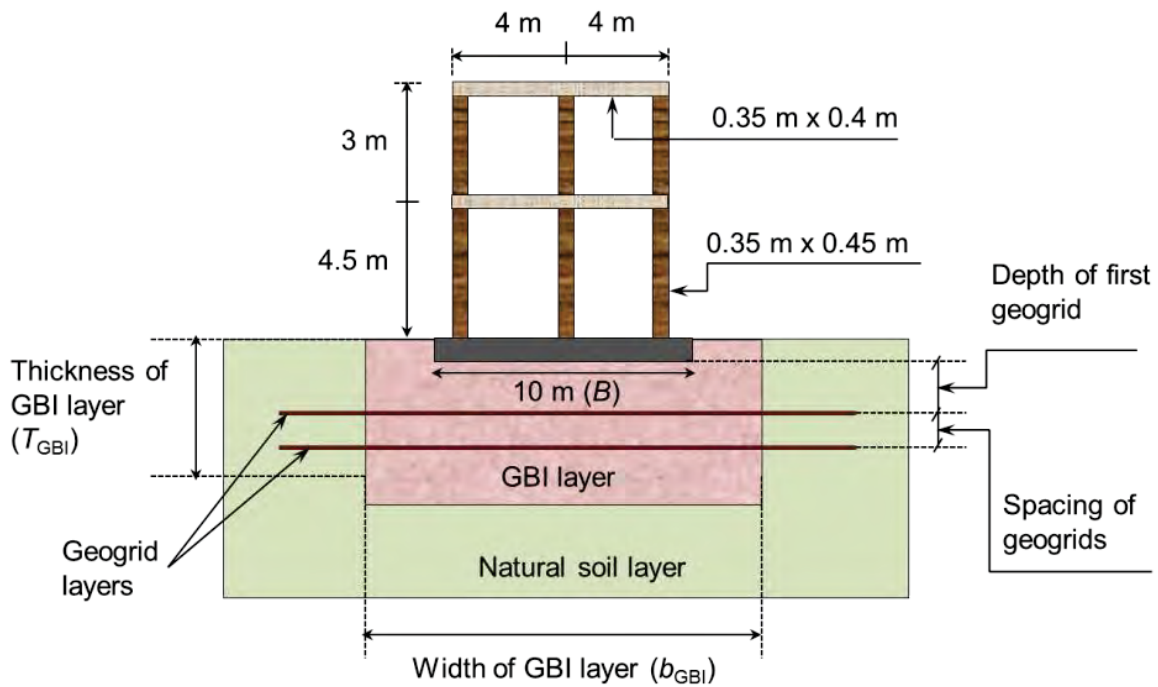


**Figure 5.4** Details of the building structure-footing system

The dead load and live load coming on the structure was calculated based on the code provision, IS 875:1987 Part 1 & II (2008). The live load coming on each floor slab was applied as a uniformly distributed load on the beam. The framed structural elements made of M30 grade concrete and the raft footing made of M40 grade concrete were designed for safety using IS 456 (2016). GBI layers were placed surrounding the raft footing at varying thickness. Geogrid reinforcement was included within the GBI layer to improve its performance. The frame span was considered as 3m and the dead load due to the slab was calculated as 11.25 kN/m. The live load, including floor finish from the slab, was considered as 12 kN/m for the analysis. The stability of the building frame under static and seismic conditions was checked using standard SAP2000 (CSI 2010) following Indian building standards (IS 456 2016; IS 1893 2016) as shown in Figure 5.5.

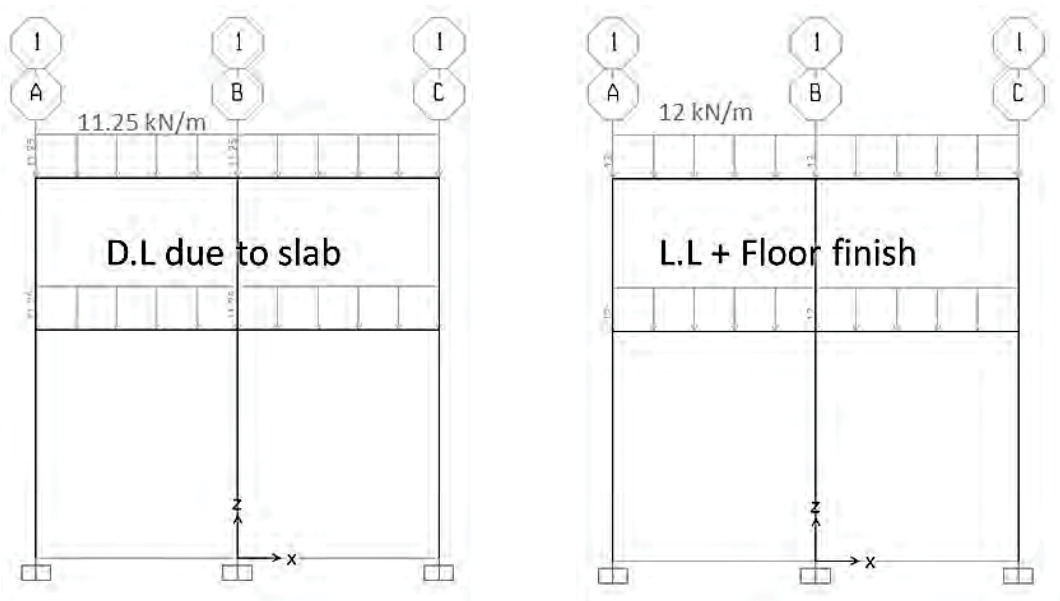


**Figure 5.5.** Details of the framed structure analysis

#### 5.2.4. Foundation details

The shallow foundation considered for the study is raft footing (Figure 5.4) to support the building frame for the safe transfer of building load to the underlying soil/SRM medium. Routine engineering procedure was adopted to design the raft footing based on bearing capacity and settlement criteria for safe load transfer (Bowles 2001; IS 2950:1981). Accordingly, the raft footing was designed having a width of 10 m and a depth of 1.5 m to support the framed structure. The bearing capacity of the raft footing was calculated based on specifications by IS 6403 (1981) and net safe bearing capacity of 715 kPa and 628 kPa was calculated for raft on natural soil and

GBI layer respectively. The raft is classified as rigid based on the rigidity factor suggested by ACIC 336 (1988). The settlement calculations for the footing considering the elastic theory as per IS 8009 Part 1 (1976) and a maximum settlement of 27mm and 38mm were calculated for the raft on natural soil and GBI layer respectively.

### 5.3. FE MODELLING AND ANALYSIS

A series of two-dimensional FE analysis was carried out using Abaqus 6.14 (2014), to investigate the seismic response of GBI layer made of SRM for low-rise buildings in the Indo-Gangetic plain region of India. Since modelling the soil-structure interaction problem involving the governing equations of motion as well as arriving at solutions for the equations is a complex issue, the present study uses the direct method of SSI analysis where the whole soil-structure-foundation system is modelled together as a finite element model. The equation of motion for the soil-structure system is shown below:

$$[M]\{\ddot{u}\} + [C]\{\dot{u}\} + [K]\{u\} = -[M]\{\ddot{u}_g\} \quad (5.2)$$

where,  $[M]$ ,  $[C]$  and  $[K]$  are the mass, damping and stiffness matrix respectively for the structure;  $\ddot{u}$ ,  $\dot{u}$  and  $u$  are the acceleration, velocity and displacement at the nodes for the soil-foundation system;  $\ddot{u}_g$  is the earthquake acceleration applied to the system.

The soil medium is assumed as an inelastic continuum for the present analysis and is modelled as a rectangular soil domain with appropriate boundary conditions. The soil domain of depth 32 m was chosen for the study. Initially, a homogenous soil profile of 32m depth is subjected to sinusoidal input motion at the base of the soil domain, and the corresponding transfer function is obtained at the ground surface level. The transfer functions obtained are cross-checked with the analytical solutions for the transfer function of uniform soil proposed by Kramer (1996) for different widths of the soil domain. To fix the optimum width of the soil medium, the transfer function at different locations along the width of the ground surface is compared for uniform results throughout the ground surface to ensure free-field response. The width of the soil domain was fixed as  $30B$  ( $B$  is the width of footing), with infinite boundaries to prevent reflection of waves back into the system. Figure 5.6 shows the rectangular soil domain with the structure-foundation system, with appropriate boundary conditions.

### 5.3.1. FE meshing and element types

Plane strain quadrilateral grids with four-node iso-parametric elements were used to model the soil, GBI layer and footing. The mesh size was determined based on CFL criteria (Courant et al. 1967) considering the shear wave velocity and time step adopted for the wave propagation. According to CFL criteria, the mesh size should be lesser than the distance travelled by the wave in each time step to ensure proper transfer of information from one element to the next along with the stability for wave propagation. The maximum frequency adopted in the study was 8 Hz. Therefore, a mesh size of 1 m x 1 m was chosen for the foundation, GBI layer and soil mass near the vicinity of the building. The mesh size of the soil domain gradually varies from 1 m x 1 m at the centre of the soil model to 1 m x 5 m at the far-field region as illustrated in Figure 5.6. The geogrids used in the study was modelled using two-node beam elements having shear flexibility and axial load carrying capacity. The beams and columns of the structure were modelled using the two-node beam elements. Common nodes with mechanical interaction were established between the frame and footing to prevent slippage and to allow uniform movement during seismic loading conditions.

### 5.3.2. Constitutive models and material properties

#### *Sand*

Soils subjected to small to medium range of strain arising from seismic loadings commonly exhibit non-linear elastic stress-strain behaviour. Hypoelastic materials exhibit reversible stress-strain response even at small strains and are commonly adopted for plasticity theories to model the load response beyond the elastic limit. The non-linear hypoelastic formulation (Fung 1965) considers the strain-dependent modulus reduction behaviour of the material and is ideal for modelling sand under seismic loading conditions (Coon and Evans 1971; Corotis et al. 1974; Chen 1985). The hypoelastic formulation used in the modelling of natural soil is shown below:

$$d\sigma = D^{el} d\epsilon^{el} \quad (5.3)$$

where  $d\sigma$  is the rate of change of stress;  $d\epsilon^{el}$  is the rate of change of elastic strain;  $D^{el}$  is the tangent elasticity matrix defined as functions of strain invariants  $I_1$ ,  $I_2$  and  $I_3$  expressed in terms of the elastic strain  $\epsilon^{el}$  as follows:

$$I_1 = trace \epsilon^{el} \quad (5.4)$$

$$I_2 = \frac{\varepsilon^{el} \cdot \varepsilon^{el} - I_1^2}{2} \quad (5.5)$$

$$I_3 = \det(\varepsilon^{el}) \quad (5.6)$$

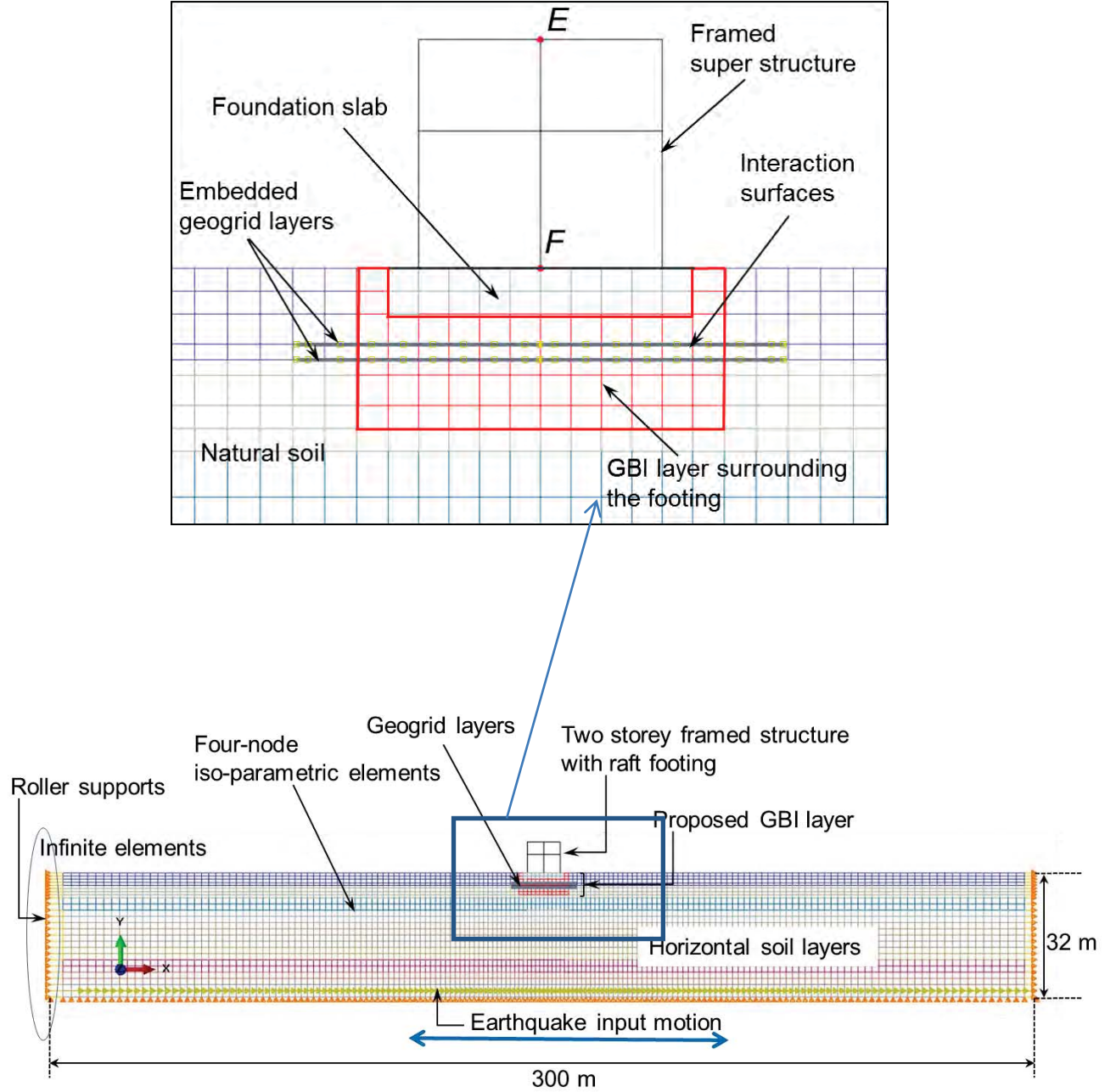


**Figure 5.6** Finite element model of the soil-structure system with the proposed GBI layer

The soil is divided into 11 layers, the bottom-most layer being 2 m thickness and the rest of the layers 3 m thickness each. The modulus reduction curves for sand proposed by Ishibashi (1992)

for non-plastic soils (Figure 5.7) were used for modelling soil layers depending on the depth and corresponding confining pressures. The maximum shear modulus was calculated from the  $V_s$  and density profiles (Figure 5.3) at the mid-depth of each soil layer. The soil parameters such as Young's modulus (obtained from  $V_s$  profile and density), Poisson's ratio and Rayleigh damping coefficients were also used for defining the material behaviour.

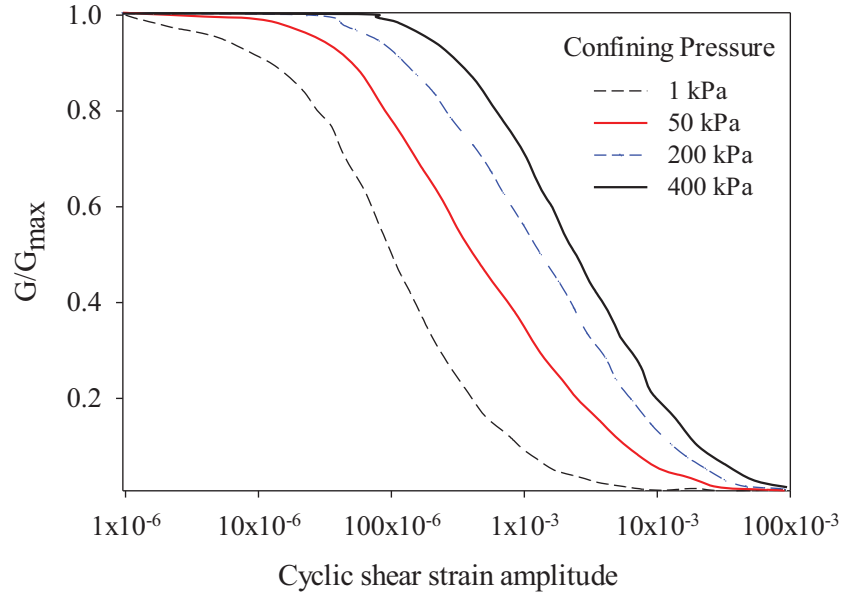


**Figure 5.7** Modulus reduction curves for non-plastic soils under varying confining pressure (Ishibashi 1992)

### ***SRM***

Hyperelastic models were widely used as the constitutive model for rubber, elastomeric bearings and vibration isolators, which exhibits nonlinear elastic response even at higher strains (Brinson and Brinson 2008). Hyperelastic models based on strain energy potentials (Houlsby et al. 2005) were used to define the non-linear stress-strain response and hysteresis energy loss of materials under cyclic loading. The strain energy potential  $W$  can be derived in terms of the principal Cauchy stresses ( $\sigma_i$ ) as below (Sasso et al. 2008):

$$\sigma_i = \lambda_i \frac{dW}{d\lambda_i} - p \quad (5.7)$$

where, the first term represents the deviatoric part of the stress;  $p$  represents the hydrostatic part of stress and  $\lambda_i$  is the principal stretch ratio. Further, strain-energy potential can be considered as a function of the strain invariants  $I_1, I_2, I_3$ .

$$W = U(I_1, I_2, I_3) \quad (5.8)$$

Unlike soil, SRM exhibits substantial flexibility and behaves more like a hyperelastic material due to highly elastic deformations. The present numerical study adopts the hyperelastic material model to represent the stress-strain response of SRM. It was noted from the literature that SRM with an optimum rubber content of 30% exhibits adequate stiffness and high damping ratio compared to higher rubber content (Senetakis et al. 2012). Therefore, in the present study, SRM with 30% rubber content was considered. The material constants to define the optimal strain energy potential of the first-order polynomial were automatically calculated by ABAQUS from the data of stress-strain curves obtained from triaxial tests (Figure 3.4). Poisson's ratio of 0.4 was chosen for SRM (Mashiri 2015) to account for the compressibility of the material.

The applicability of the hyperelastic constitutive model was validated by comparing the results obtained from the triaxial test on SRM samples with that computed from the numerical simulations. To simulate triaxial testing, a 2D plane strain model of 25 mm x 100 mm was created having 600 mesh elements. Axisymmetric boundary conditions with roller supports were assumed for the model at one of the lateral boundaries. The bottom boundary of the model was considered to be fixed. Figure 5.8 displays the details of the FE numerical model adopted to simulate the triaxial compression test for SRM. The material properties obtained from triaxial testing for SRM (Figure 5.9) in the form of stress-strain curves were applied to the model depending on the confining pressure for each numerical analysis.

After establishing initial stress conditions, back pressure and confining pressure were applied. Deviator stress was applied in steps of 10 kPa each. Figure 5.9 shows the stress-strain response obtained in an element at the centre of the numerical model for confining pressures of 50 kPa, 100 kPa and 150 kPa. It is apparent that the initial elastic deformation stage of the stress-strain response is predicted well by the adopted hyperelastic material model. Further, it can be observed that the present model can simulate the stress-strain distribution of SRM from experimental results with reasonable accuracy.



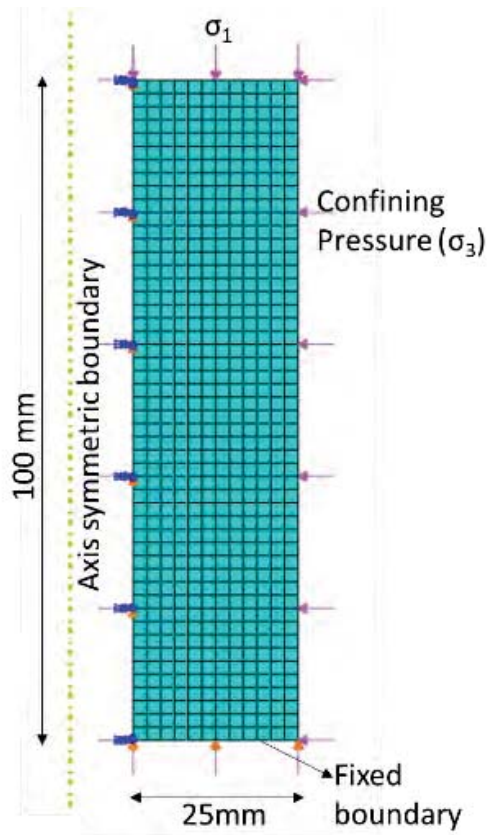


**Figure 5.8** FE mesh for triaxial test simulation

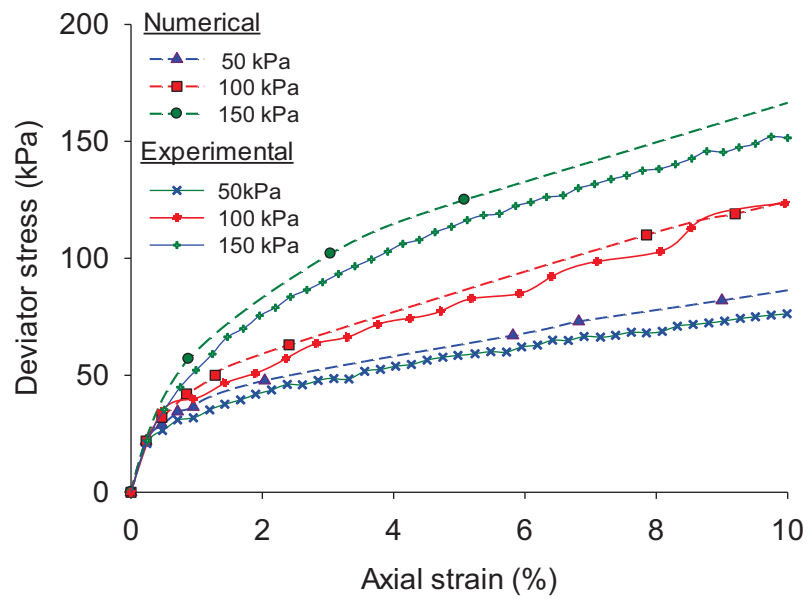


**Figure 5.9** Hyper-elastic model validations for SRM (30% rubber content) under varying confining pressure

### ***Geogrid***

Uniaxial geogrids adopted for the 2D model was assumed to be isotropic and homogenous. Elastic-perfectly plastic material constitutive behaviour was assumed for geogrids modelled using beam elements. The material exhibits linear-elastic behaviour until the ultimate tensile strength is reached, beyond which the tensile stress remains constant with further deformation, as shown in Figure 5.10. The geogrid layers were embedded inside the soil region. Surface to surface contact pairs was used to ensure shear interaction between geogrid and the soil/GBI layer above and below the soil-geogrid interface as well as to avoid pull out failure. The properties of the contact surface were defined using Coulomb's friction model with friction angles  $34^\circ$  and  $27^\circ$  for sand and SRM respectively as discussed in Section 4.3.4. Table 5.1 depicts the material properties of commercially available uniaxial PET100 grade geogrids used for the study. A Poisson's ratio of 0.3 was adopted for geogrids based on studies by Liu et al. (2007).

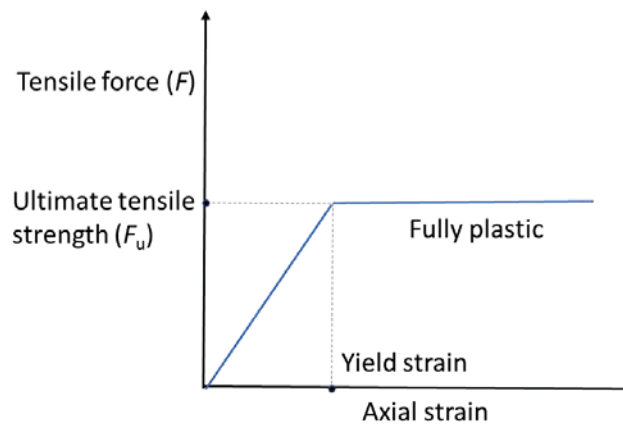


**Figure 5.10** Constitutive model adopted for geogrid behaviour

The concrete sections used for footing and building frame were modelled assuming elastic-perfectly plastic material behaviour such that each element behaves linearly elastic until it reaches the plastic moment beyond which deformation happens without any added resistance. The material properties used for designing the concrete structures in the FE model are listed in Table 5.2. M30 grade of concrete was used for the framed structure while M40 grade was used for the foundation. The Young's modulus of concrete was calculated based on the characteristic compressive strength of concrete as per IS 456 (2016). A structural damping ratio of 5% was assigned to the building for dynamic analysis. The fundamental period of the framed structures under fixed base condition

was found to be 0.24 s by extracting Eigenvalues from free vibration analysis to calculate the natural frequency.

**Table 5.1** Material properties of geogrid

Properties	PET geogrid
Ultimate tensile strength (kN/m)	100
Poisson's ratio	0.3
Density (kg/m <sup>3</sup> )	450
Strain at ultimate tensile strength (%)	10
Mass per unit area (g/m <sup>2</sup> )	450
Tensile stiffness (kN/m)	1000
Thickness (mm)	10

**Table 5.2** Material properties of concrete

Properties	Frame	Footing
Compressive strength (MPa)	30	40
Density (kg/m <sup>3</sup> )	2500	2500
Young's modulus (MPa)	27400	31650
Poisson's ratio	0.2	0.2

The footing-soil interaction was incorporated using surface to surface contact pairs. The normal behaviour at the interface was modelled using a hard contact and the tangential behaviour was modelled using Coulomb friction model using friction coefficient and a slip tolerance parameter (Nguyen et al. 2016) as discussed in Section 4.3.4. The master surface was defined as the outer surface of footing due to the rigidity of the footing compared to the surrounding soil/GBI and the slave surface was defined as the inner surface of soil/GBI layer.

### 5.3.3. Damping mechanism

To simulate the energy loss due to damping in the soil-structure system under seismic loading the classical Rayleigh damping, which is viscous damping was commonly adopted to model energy dissipation (Wood 2004; Jia 2018). For the present time-domain analysis, Rayleigh damping with

modal coefficients  $\alpha$  and  $\beta$  was used to model the damping mechanism for the FE system. The damping matrix ( $C$ ) in Rayleigh damping was assumed to be linearly proportional to mass ( $M$ ) and stiffness ( $K$ ) matrices (Chopra 2007) as mentioned below:

$$C = \alpha M + \beta K \quad (5.9)$$

where, the Rayleigh coefficients  $\alpha$  and  $\beta$  can be determined from the solutions of first and second mode vibration frequencies ( $\omega_i$ ) and for specified damping ratios ( $\zeta$ ) using equation 5.10.

$$\zeta_n = \frac{\alpha}{2\omega_i} + \frac{\beta\omega_i}{2} \quad (5.10)$$

#### 5.3.4. Boundary conditions

The soil domain was divided into homogenous horizontal layers. Boundary conditions were assigned to the model such that reasonable prediction for the static and dynamic analysis is achieved. The bottom boundary was assumed to be fixed by constraining movements in all directions (Dutta and Roy 2002). The side boundaries were provided with roller supports restraining movements in the horizontal direction and allowing vertical movements. To simulate unbounded soil media and to prevent reflection of waves from coming back to the system, transmitting boundaries made of infinite elements (Figure 5.11a) were used (Wolf and Song 1996). Infinite element artificial boundaries are used in conjunction with regular finite elements (Figure 5.11b). They act as quiet boundaries under dynamic loading conditions by suppressing the stiffness matrix of the element and allowing the effects of damping matrix.

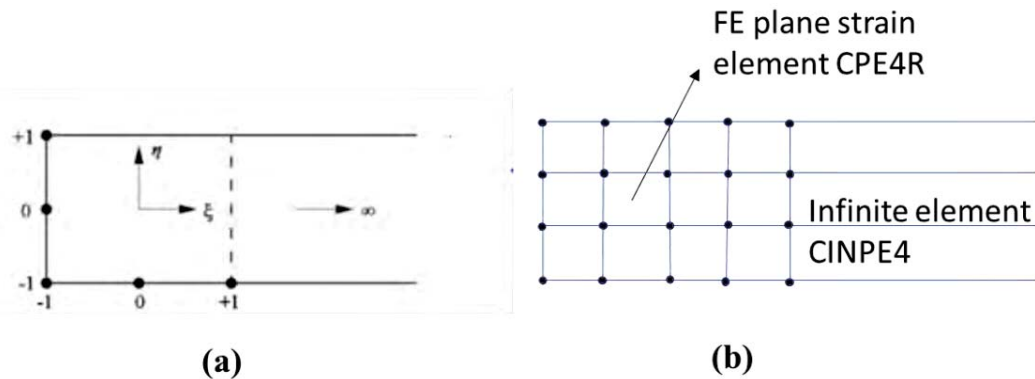


**Figure 5.11 (a)** Geometry of typical infinite element (Bettess 1980) **(b)** Infinite element used in ABAQUS 2D model

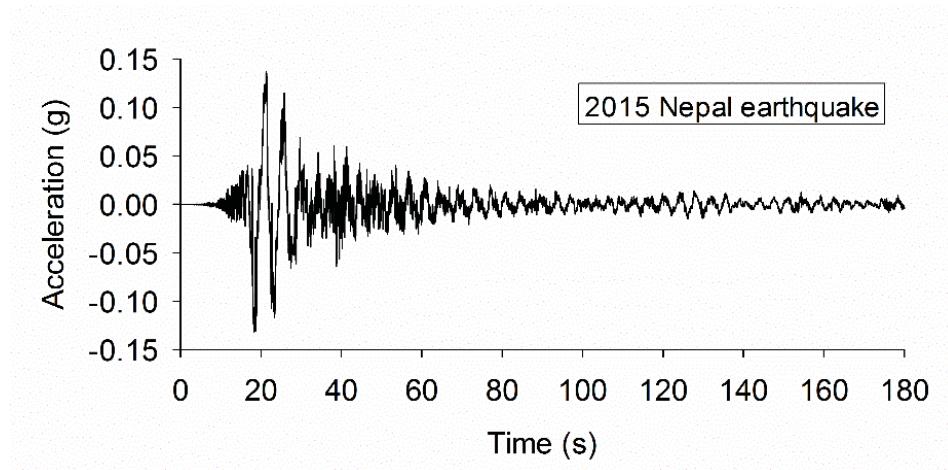
It should be noted that the infinite elements neither alters the eigenmodes of the system, nor does it changes the static forces developed in the system at the beginning of the dynamic analysis. Infinite elements introduce boundary damping constants in the form of normal and shear tractions to minimize reflection of shear waves at the boundary. The current numerical model adopts infinite elements (CINPE4) with linear elastic material properties applied at the side boundaries in the periphery of the finite element to transmit the seismic energy out of the FE mesh (Figure 5.6).

### 5.3.5. Input motion

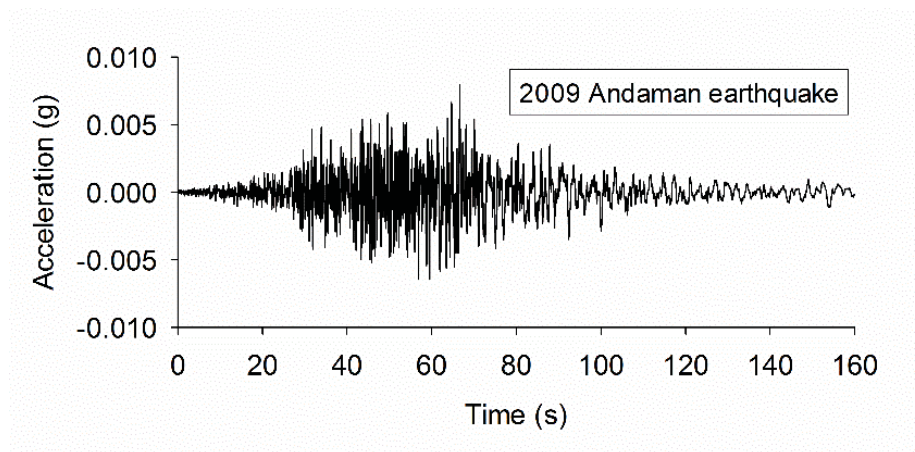
Input motions considered for the dynamic analysis involves five acceleration-time histories of recent major earthquakes that have occurred in the Indian subcontinent in the past two decades. Table 5.3 shows the details of the earthquake input motions used in the study namely the 2001 Bhuj earthquake ( $M_w=7.7$ ), 2009 Andaman earthquake ( $M_w=7.8$ ), 2011 Sikkim earthquake ( $M_w=6.9$ ), 2015 Nepal earthquake ( $M_w=7.8$ ) and 2016 Myanmar earthquake ( $M_w=6.9$ ) covering predominant frequencies ranging from 0.1 Hz to 10 Hz. The strong-motion data were collected from COSMOS Virtual Data Center. The acceleration-time history plots for all the five earthquakes are shown in Figure 5.12. The input motions were applied at the base of the soil model in the horizontal direction for the time domain analysis. In the present study, the selected recorded ground motions are scaled to IS 1893 (2016) specified PGA value of 0.24g for the Indo-Gangetic plain region considered. The scaling based on PGA value is justified since the PGA is well correlated to damage in short period structures such as low-rise buildings (Matsumara 1992).

**Table 5.3** Details of earthquake input motions used in the study

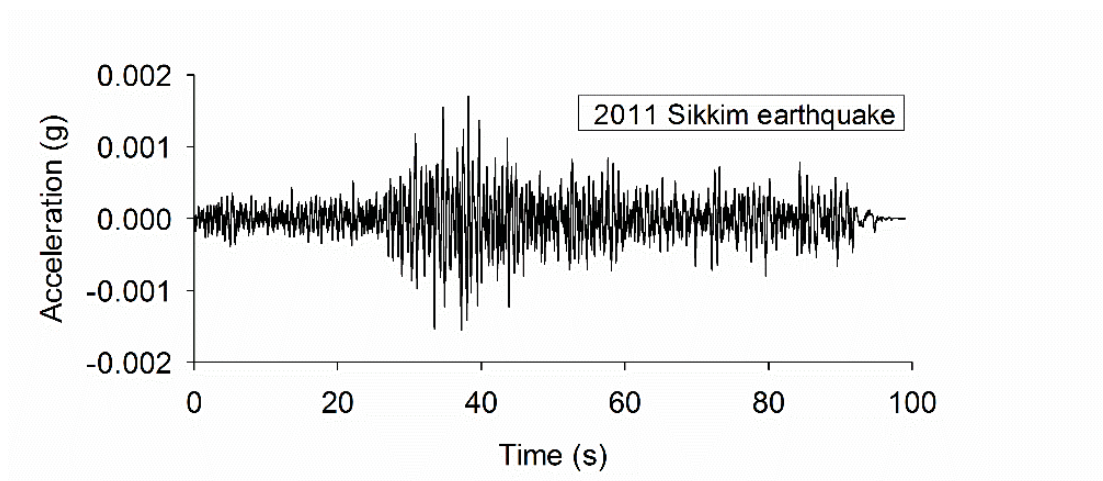
Earthquakes	Year	Recording station	Magnitude ( $M_w$ )	Peak acceleration (g)	Predominant frequency (Hz)
Nepal (NE)	2015	Kathmandu	7.8	0.14	0.2
Andaman (EW)	2009	Port Blair	7.8	0.008	0.3
Sikkim (EW)	2011	Chamoli	6.9	0.002	1.5
Bhuj (NE)	2001	Bhuj	7.7	0.102	3.5
Myanmar (NE)	2016	Roorkee	6.9	0.12	8



(a)

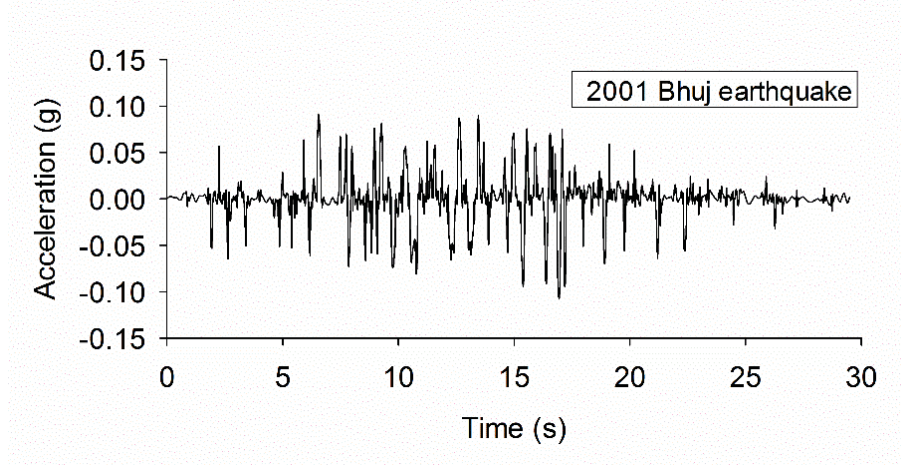


(b)

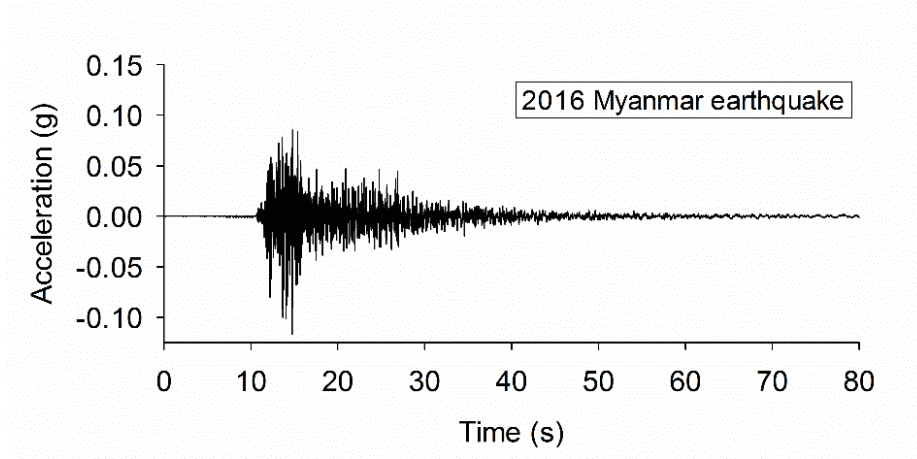


(c)





(d)



(e)

**Figure 5.12** Acceleration-time histories of earthquakes **(a)** 2015 Nepal ( $M_w=7.8$ ) **(b)** 2009 Andaman ( $M_w=7.8$ ) **(c)** 2011 Sikkim ( $M_w=6.9$ ) **(d)** 2001 Bhuj ( $M_w=7.7$ ) **(e)** 2016 Myanmar ( $M_w=6.9$ )

### 5.3.6. Analysis

Dynamic implicit FE analysis using Newton-Raphson iteration scheme was used to calculate the stiffness matrix for each increment steps in the present investigation. The convergence criteria were ensured by considering numerical damping for the model for the given mesh sizes and time increment steps adopted in the study. The SSI model was analyzed initially for static stress conditions followed by the dynamic loading. Initially, while considering static loading conditions,



the bottom boundary of the numerical model was assumed to be fixed. For the static analysis, the initial condition was established followed by the gravity loading, which includes self-weight of the framed structure and foundation system. In the following step, the live load acting on the building was applied as a uniformly distributed load on the top surface of the beams. Dynamic response of the GBI system was analysed in the time domain, considering the direct method of SSI. During the dynamic analysis, the horizontal constraint in the bottom boundary was removed. Infinite elements at the side boundaries ensure the simulation of free field conditions for the FE model. Seismic excitation in the form of acceleration-time history was applied at the base of the soil model at a depth of 32 m. The corresponding outputs in the form of stress, strain and acceleration-time histories were obtained at nodes/ elements at desired locations of soil and building within the model.

#### **5.4. VALIDATION OF THE NUMERICAL ANALYSIS WITH 1G SHAKE TABLE STUDIES (BANDYOPADHYAY ET AL. 2015)**

Since there is no experimental test data available on the seismic response of framed structure placed on SRM layer, the results computed from the current numerical model was compared with that obtained from the shake table studies by Bandyopadhyay et al. (2015) on model footing isolated with SRM layer. The model footing of size 200 mm x 200 mm and thickness 40 mm was placed on a sand bed layer inside the shake table setup. The base isolator made of SRM was placed between the foundation block and the sand layer. The whole shake table setup in the study was subjected to sinusoidal motions and the output response was obtained from accelerometers mounted on the footing.

In the present study, FE simulation of the above shake table study Bandyopadhyay et al. (2015) was carried out with the constitutive models a modelling/analysis procedure and as discussed in the previous section to the dynamic response of model footing resting on SRM/ sand layer. The numerically computed time history of acceleration obtained at the top level of the foundation was compared with the shake table experiment results to confirm the suitability of modelling criteria/procedure adopted in the present study.

The geometry of the shake table FE model was the same as in the experimental study (Bandyopadhyay et al. 2015) and the footing was placed at the centre of the model. Four noded

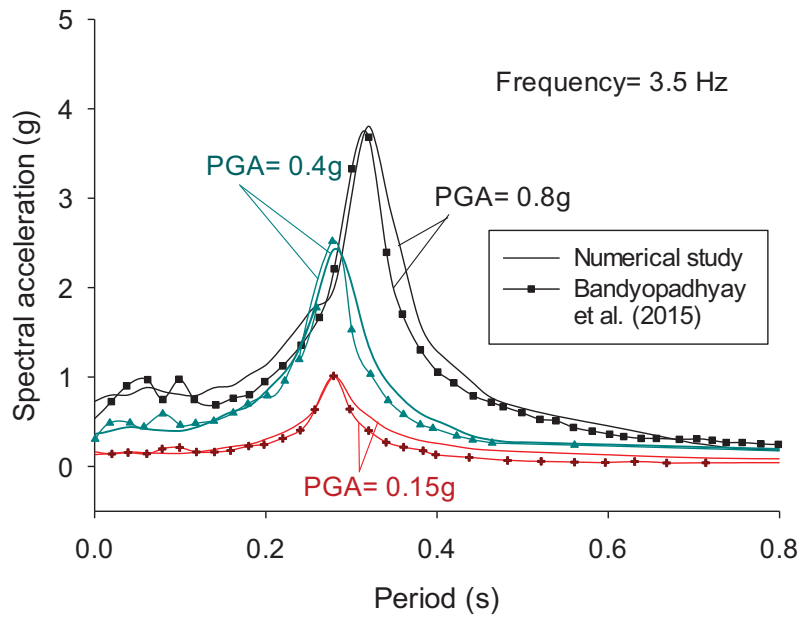
iso-parametric plane strain elements were used to model soil, SRM and footing assuming hypoelastic model for sand and hyperelastic model for SRM with the same boundary conditions as explained in the previous section. Sinusoidal input motion was applied to the shake table FE model at the bottom level of sand-bed and the resulting acceleration time history was noted at the top nodes of the foundation.

The response spectra curves for sand and SRM mixture obtained from the numerical study were compared with that of Bandyopadhyay et al. (2015). Figure 5.13a shows the response of footing resting on the sand while Figure 5.13b shows the response of footing resting on GBI layer made of SRM (30% rubber content). The results of the numerical study reflect the experimental trends reported by Bandyopadhyay et al. (2015) quite well. Hence the same numerical modelling procedure can be extended to study the response of a framed structure placed GBI layer as discussed in the subsequent sections.

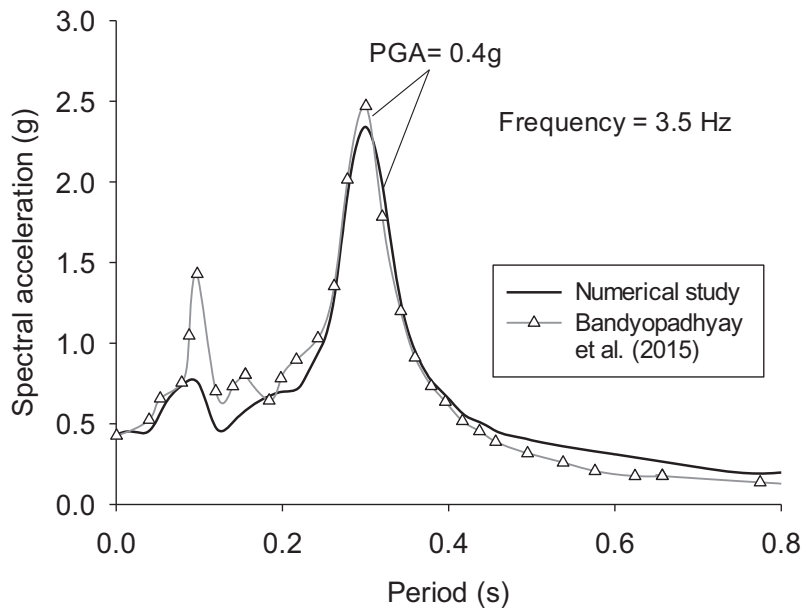
## **5.5. SEISMIC SETTLEMENT OF GBI SYSTEM WITH GEOGRID REINFORCEMENT**

In the present study, the settlement aspects of the low-rise building placed on GBI layer under seismic loading conditions in the Indo Gangetic plain region was numerically analysed considering the effect of geogrid reinforcement on GBI layers. The maximum depth of replacement of soil with GBI layer was limited to 2 m ( $0.2B$ ) considering practicality and cost efficiency under field conditions. The width of the GBI layer ( $b_{\text{GBI}}$ ) was maintained as  $1.2B$  constantly throughout. For the study, the thickness of GBI layer ( $T_{\text{GBI}}$ ) was considered as  $0.2B$  below the footing of the low-rise building. Upto three layers of geogrid, placed at a spacing of  $0.05B$  were included between the GBI layers. The first layer of geogrid was placed at a depth of 0.5 m below the ground surface. The length of the geogrid layer was limited to  $2B$  to avoid an increase in the base shear of the building (Xu and Fatahi 2018a). It should be noted that the energy dissipation process can be affected by the geogrid, which introduces additional stiffness to the whole system (Xu and Fatahi 2018a).

From this point onwards, the notations  $\text{GBI}_{\text{ur}}$  and  $\text{GBI}_{\text{r}}$  will be used to represent the reinforced and unreinforced GBI cases, respectively. Similarly, the unreinforced natural soil will be represented as  $S_{\text{ur}}$ .



(a)



(b)

**Figure 5.13** Comparison of response spectra as obtained in the present study with that reported by Bandyopadhyay et al. (2015) for **(a)** GBI layer **(b)** sand layer



reduction in foundation rocking. Hence double layered geogrid reinforcement can be satisfactorily included within the GBI layers for better performance under seismic loading conditions. Based on the present findings, further numerical analyses carried out in the subsequent sections will have geogrid reinforcement with two layers; spacing=  $0.05B$  & length =  $2B$  placed between the GBI layers.

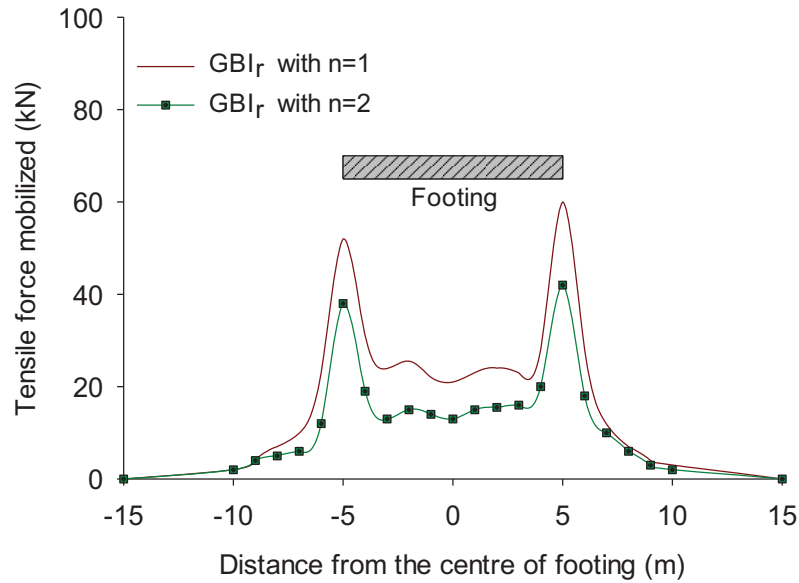


**Figure 5.15** Maximum mobilized tensile force along the top geogrid layer (2015 Nepal earthquake,  $M_w=7.8$ ;  $PGA=0.14g$ )

## 5.6. SEISMIC RESPONSE OF FRAMED STRUCTURE RESTING ON GEOGRID REINFORCED GBI LAYER

In this section, a detailed discussion of the results of the numerical analysis carried out on GBI layer as an isolating media for a low-rise framed structure is presented. The free-field condition was considered initially to assess the site response of the GBI system without the influence of building. The numerical study then explores the response of the GBI system with the presence of the building-foundation system. To evaluate the effect of geogrid reinforced/unreinforced GBI layer on the seismic response of the low-rise building, several response parameters were investigated. Parametric studies were conducted in terms of the thickness of GBI layer, frequency content and peak acceleration of earthquake input motion for building foundation resting on layer of GBI<sub>r</sub>, GBI<sub>ur</sub> and S<sub>ur</sub>. In addition to the base shear experienced by the building, engineering

demand parameters such as the maximum inter-storey drift and footing rotation were also investigated. Seismic isolation factor ( $SIF_a$ ), a parameter defined in equation 5.11 is used to quantify the degree of isolation effect by GBI isolation for the present study.

$$SIF_a = \frac{PA_{GBI} - PA_{NI}}{PA_{NI}} \quad (5.11)$$

where  $PA_{GBI}$  and  $PA_{NI}$  are the peak acceleration value for GBI isolated system and non-seismic isolated system respectively. The seismic isolation factor in equation 5.11 can be further extended as  $SIF_{sa}$  in terms of peak spectral acceleration using the peak spectral acceleration value for GBI system and non-seismic isolated system. Furthermore, the period shift between the fundamental period of the non-isolated system and GBI isolated system is a key factor to identify the efficiency of GBI system in benefiting the structural seismic response.

### 5.6.1. Free field response

In order to study the free-field response of the GBI system with and without geogrid reinforcement, the numerical model without the framed-structure foundation system was considered. GBI layer with  $T_{GBI}$  of  $0.1B$  and  $b_{GBI}$  of  $1.2B$  with double layered geogrid reinforcement was located at the center of the soil model. This particular analysis was carried out for the earthquake input motion of the recorded 2015 Nepal earthquake ( $M_w=7.8$ ;  $PGA=0.14g$ ) applied at a depth of 32 m below the ground surface. Acceleration time histories were computed at the free surface (point  $P$ ) and at depths of 0.5 m, 1 m & 2 m, i.e. point  $Q$ ,  $R$  &  $S$  respectively below the ground level (Figure 5.16) considering with and without GBI system.

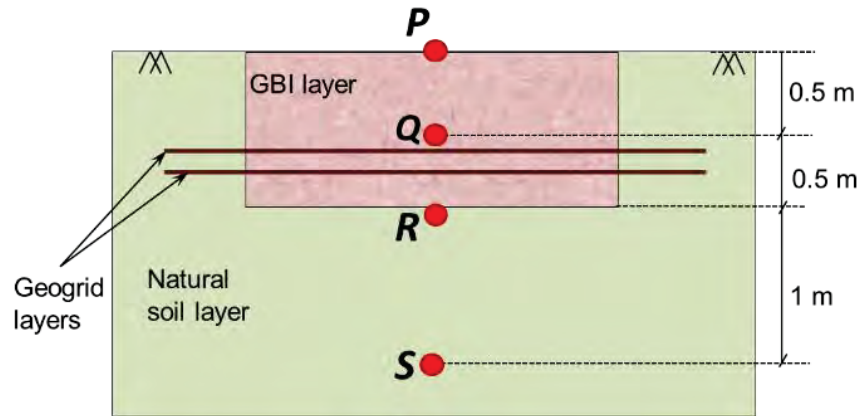
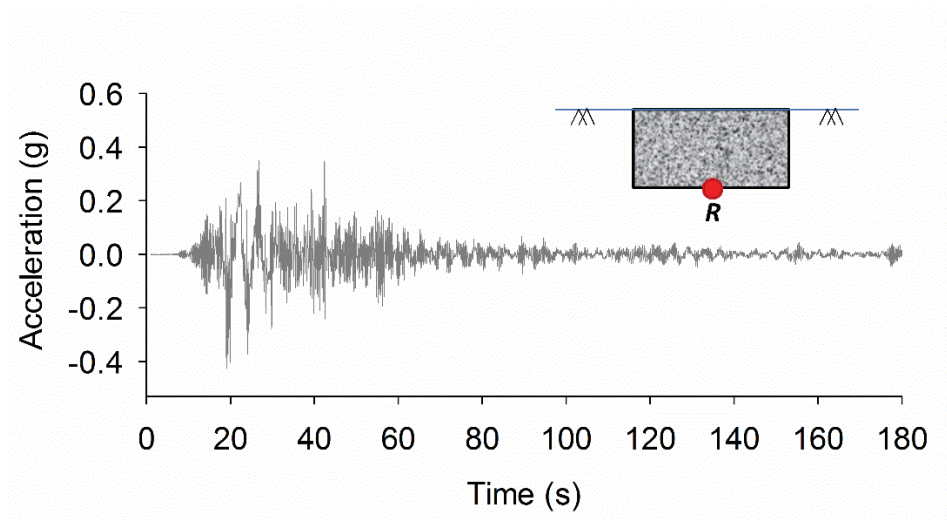
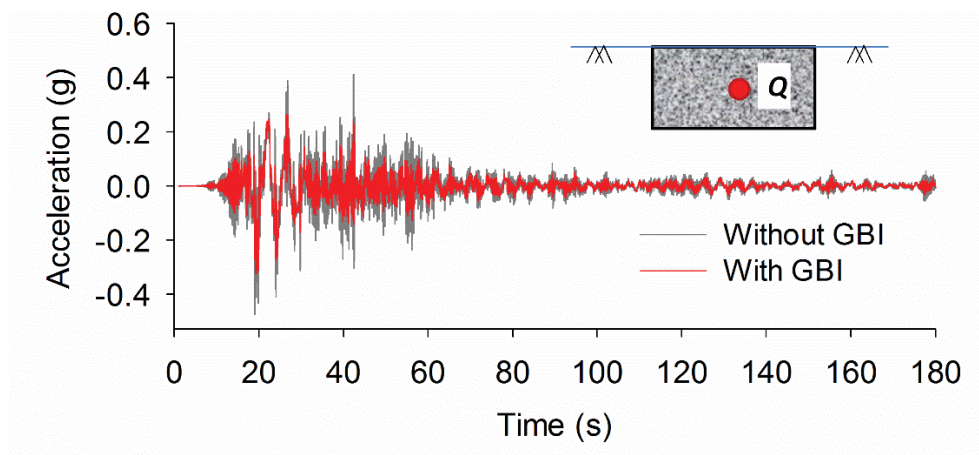


**Figure 5.16** Schematic of different points considered for the analysis output

Figure 5.17 presents the acceleration-time history plots obtained from the free-field analysis for the GBI system at different locations. Figure 5.17a shows the acceleration-time history obtained from the analysis at the boundary of GBI and natural soil (point *R*). As we move towards the middle of the GBI layer, at point *Q* (Figure 5.17b), there is a clear trend of reduction in the amplitude of acceleration for the GBI system compared to the natural soil. The degree of amplitude reduction for the GBI system further increases towards point *P* compared to natural soil (Figure 5.17c). This can be attributed to the higher damping nature of GBI layer, which acts as a vibration screener as the waves pass through it. On the other hand, the addition of geogrid in the GBI system is found to be less influencing the acceleration amplitude reduction (Figure 5.17d). This could be due to the higher stiffness of the geogrid material, which does not contribute significantly to the seismic wave filtering process compared to the SRM layer.

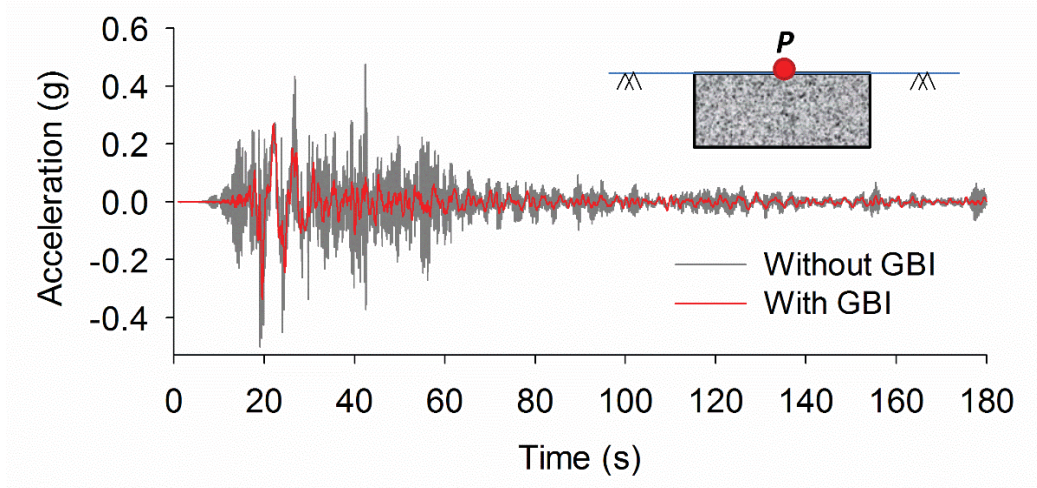


(a)

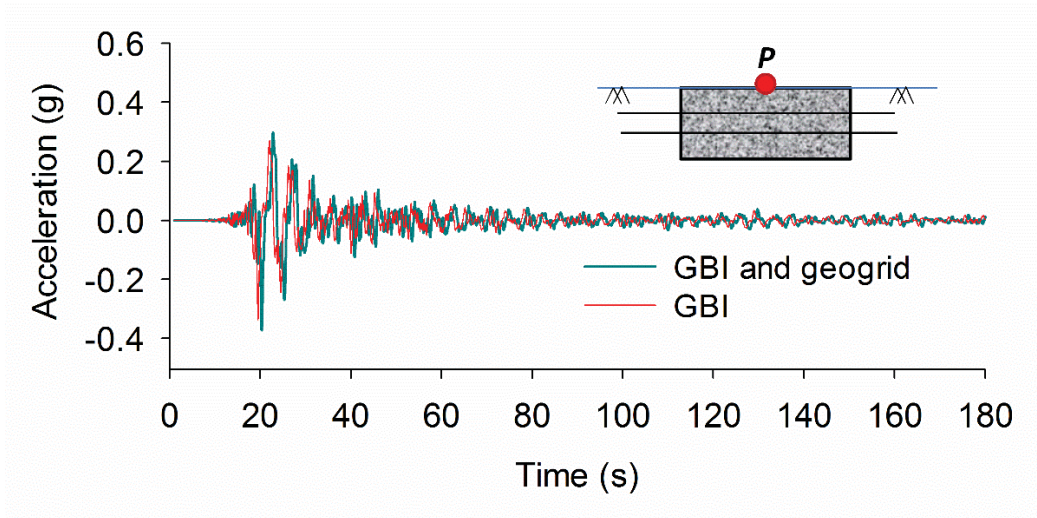


(b)





(c)

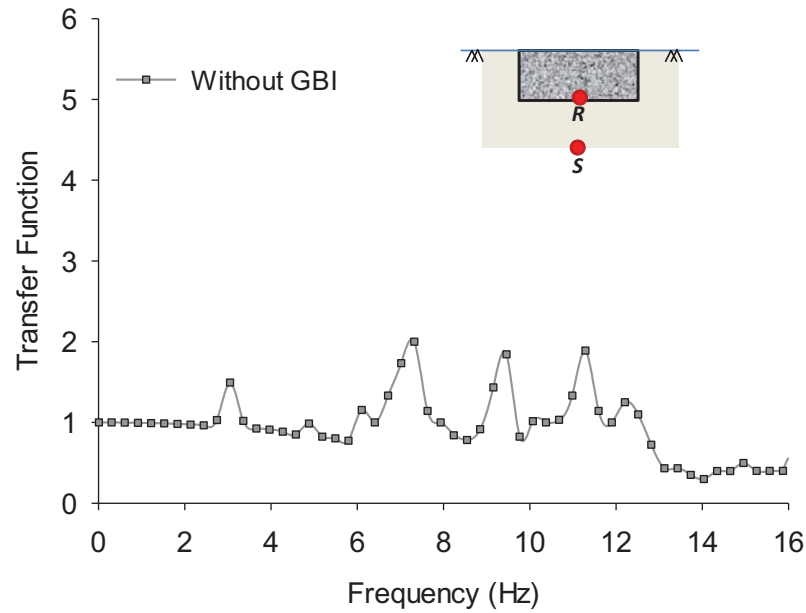


(d)

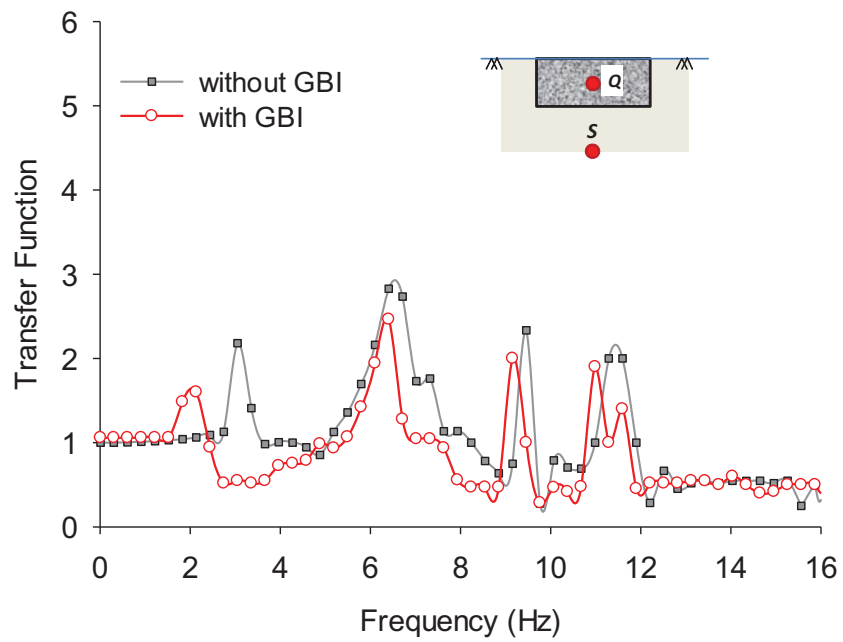
**Figure 5.17** Acceleration-time history **(a)** below GBI layer at *R* **(b)** middle of GBI layer at *Q* **(c)** ground surface at *P* **(d)** ground surface at *P* for GBI with geogrids (2015 Nepal earthquake,  $M_w=7.8$ ;  $PGA=0.14g$ )

Transfer functions were generally calculated as ratios of time series in the frequency domain. In the present study, transfer functions were considered as the ratio between the Fourier spectra obtained at distinct locations (points *P*, *Q* & *R*) and the Fourier spectra computed at point *S*. Figure 5.18 shows the transfer functions at different locations for  $S_{ur}$ ,  $GBI_{ur}$  and  $GBI_r$  cases. Initially, the transfer function values are calculated between point *R* and point *S* as presented in Figure 5.18a.

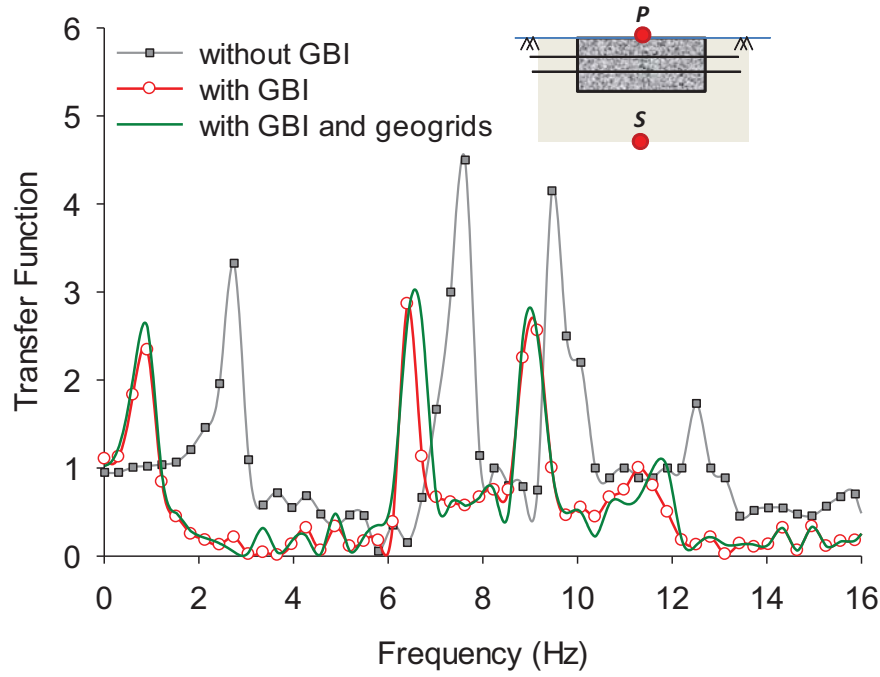
The transfer function plot at point  $Q$  (Figure 5.18b) indicates the reduction in the peaks for the GBI layer. As mentioned earlier, the decrease in peak for GBI layer is more pronounced at point  $P$  (Figure 5.18c) indicating the influence of thickness of the GBI layer for isolation purpose.



(a)



(b)



(c)

**Figure 5.18** Transfer functions: **(a)** below GBI layer at  $R$ , **(b)** middle of GBI layer at  $Q$ , and **(c)** ground surface at  $P$  (2015 Nepal earthquake,  $M_w=7.8$ ;  $PGA=0.14g$ )

The reduction in the transfer function of  $GBI_{ur}$  system is significant for the first three peaks compared to  $S_{ur}$  system. Regardless of the presence of geogrids,  $GBI_r$  tends to show a similar amplitude reduction in transfer function curves as  $GBI_{ur}$  case. The influence of GBI layer in altering the fundamental period of the system can be well observed from Figure 5.18. For example, the soil layer at point  $R$  shows a fundamental period of 0.33 s (Figure 5.18a) which increases to 0.5 s and 1.1 s at points  $Q$  and  $P$  respectively for  $GBI_{ur}$  system (Figure 5.18b & c). However, for  $S_{ur}$  system, the fundamental period increased only to 0.36 s at point  $P$  (Figure 5.18c). In addition, Figure 5.18c depicts that the introduction of the geogrid reinforcement in the GBI system has an insignificant effect on the fundamental period of the isolation system.

Further insight on the seismic response of GBI system is achieved through analyzing the response spectra at the ground surface with and without GBI layer under free-field condition. Figure 5.19 shows the response spectra plot at the ground surface (point  $P$ ) for  $S_{ur}$ ,  $GBI_{ur}$  and  $GBI_r$  cases. As expected, the reduction in peak spectral acceleration values is apparent for  $GBI_r$  and  $GBI_{ur}$  system

compared to  $S_{ur}$  case. Both reinforced and unreinforced GBI layers tend to show a significant period shift away from the natural period of the site. The presence of geogrid is of little influence on the peak spectral acceleration and the fundamental period of the GBI system.

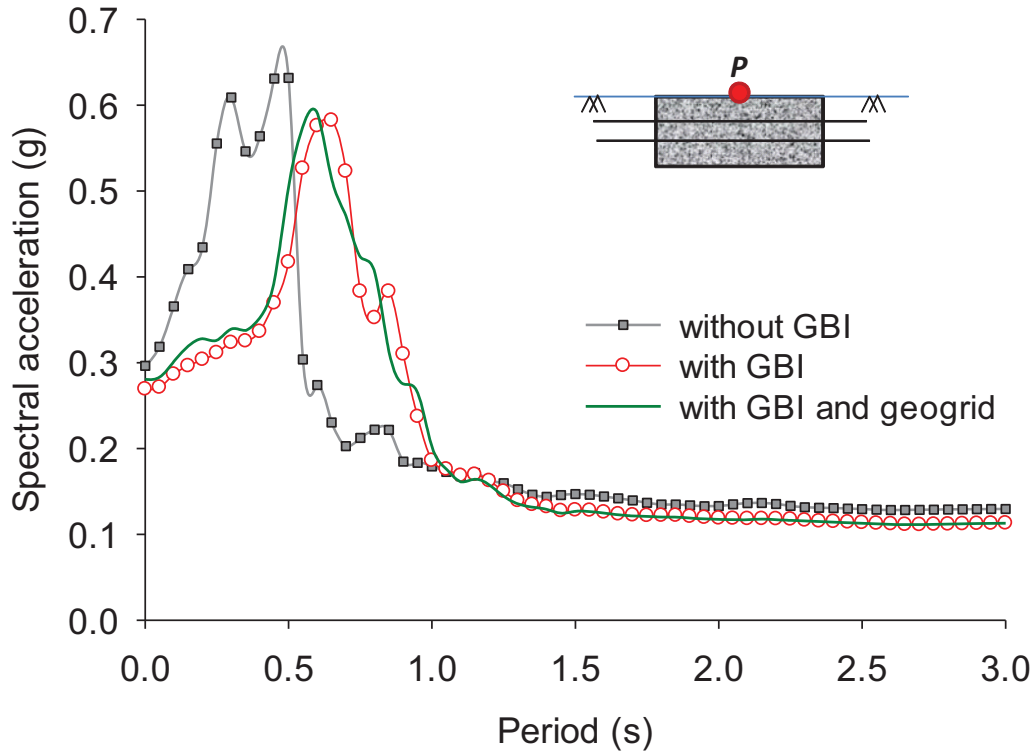


**Figure 5.19** Response spectra at the ground surface at  $P$  for the 2015 Nepal earthquake ( $M_w=7.8$ ;  $PGA=0.14g$ )

### 5.6.2. Framed structure response

In this section, the building structure-foundation system was introduced into the FE model to evaluate the response of geogrid reinforced GBI system for a low-rise framed structure. The typical response of the geo-base isolated building for the recorded 2015 Nepal earthquake ( $M_w=7.8$ ;  $PGA=0.14g$ ) is initially studied, following which a detailed parametric study ensued. Double layered geogrid was adopted and the geogrid configurations were maintained constant throughout the study as briefed earlier in Section 5.4.2. For the GBI layer, the thickness ( $T_{GBI}$ ) was varied as  $0.05B$ ,  $0.1B$  and  $0.2B$  keeping width of GBI layer ( $b_{GBI}$ ) constant. The frequency content of the earthquake input motion was varied from 0.1 Hz to 10 Hz, while the peak acceleration was varied

from 0.01g to 0.5g. The results were analyzed in terms of PGA, response spectra, base shear and inter-storey drift at different levels of the structure to identify the optimum parameters for maximizing the seismic isolation efficiency of the GBI system.

Figure 5.20 shows the typical acceleration-time history obtained at the top of the footing corresponding to natural soil and GBI layer of thickness 0.05B for the input motion of the 2015 Nepal earthquake. The reduction in the amplitude of acceleration is evident for the GBI layer compared to the  $S_{ur}$  system with regard to horizontal accelerations at the footing top. A fair idea about the characteristics of the acceleration response spectra (5% damping) for building resting on GBI<sub>r</sub> layer at the top of the footing (point *E*) can be obtained from Figure 5.21. The reduction in spectral acceleration is apparent for the GBI system compared to natural soil layer. The reduction in a spectral acceleration of GBI layer is more pronounced at the mid-period range of 0.3 s to 1 s, whereas for the period range less than 0.3 s & greater than 1 s, the reduction in spectral acceleration is less evident. The presence of GBI layer marginally shifts the predominant period of the system to a higher value compared to the natural soil system. This leads to a reduction of spectral acceleration in low rise buildings, which will have lesser natural period such as 0.24 s in the present case.

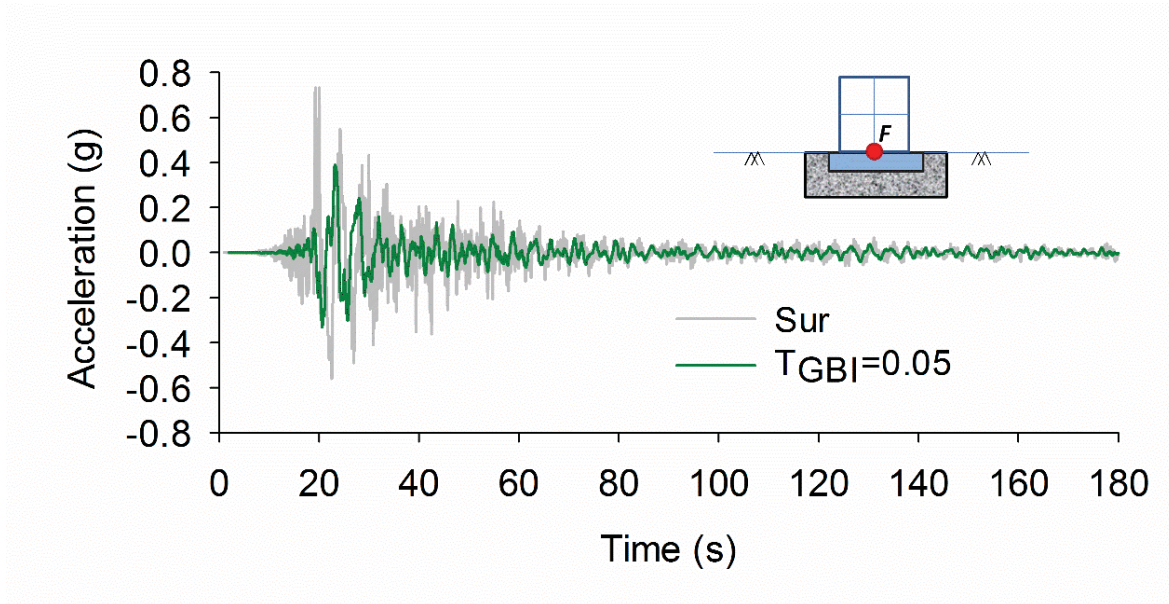


**Figure 5.20** Acceleration time history at the footing top for the 2015 Nepal earthquake ( $M_w=7.8$ ; PGA= 0.14g)

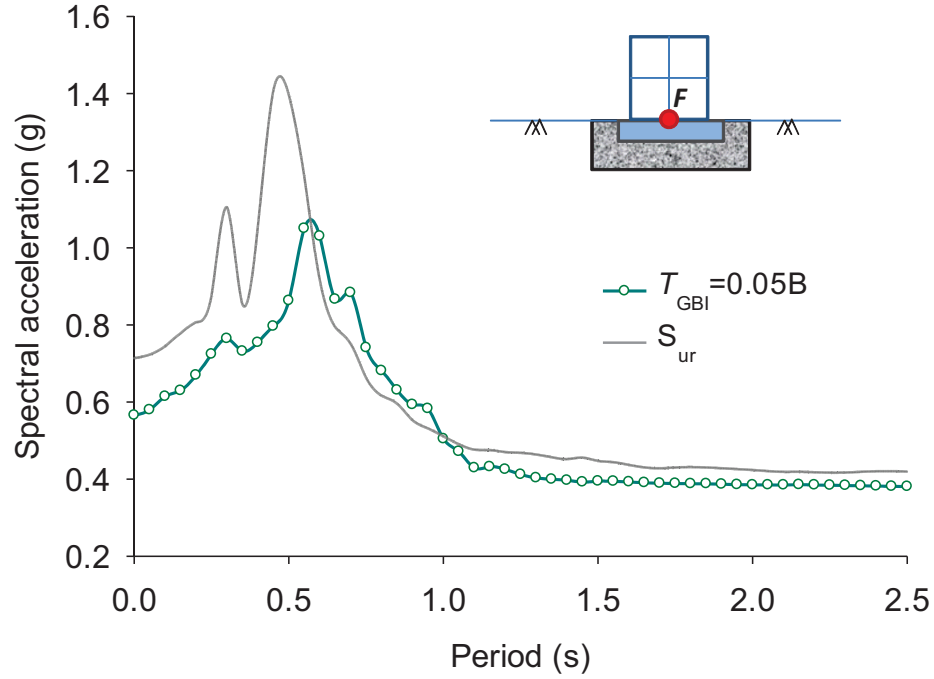


**Figure 5.21** Response spectra at the footing top for the 2015 Nepal earthquake ( $M_w=7.8$ ; PGA=0.14g)

#### ***Effect of thickness of GBI layer***

As previously discussed in Section 5.4.3.1, the degree of reduction in amplification of earthquake input motion is sensitive to the thickness of the GBI system. Numerical analysis was carried to arrive at an optimum thickness of the GBI layer for satisfactory seismic isolation of the proposed building. The GBI layer thickness was varied as  $0.05B$ ,  $1B$  and  $2B$ . Double layer geogrid reinforcement was provided to the system. The earthquake motion was scaled to 0.24g considering the IS code recommended PGA value for the Roorkee region (IS 1893, 2016) chosen for the study. The scaled acceleration-time history of the 2015 Nepal earthquake ( $M_w=7.8$ ) was used as the input motion. The results of the dynamic analysis computed in the form of acceleration-time histories were extracted from nodes at the top of the building (point  $E$ ) and footing (point  $F$ ). The corresponding values in the form of  $SIF_a$ , peak spectral acceleration and predominant period are presented in Table.5.4.

The  $SIF_a$  values for the  $GBI_r$  system keep increasing with the increase in the thickness of the GBI layer indicating the high energy absorption induced by thicker layer of GBI system. For example,



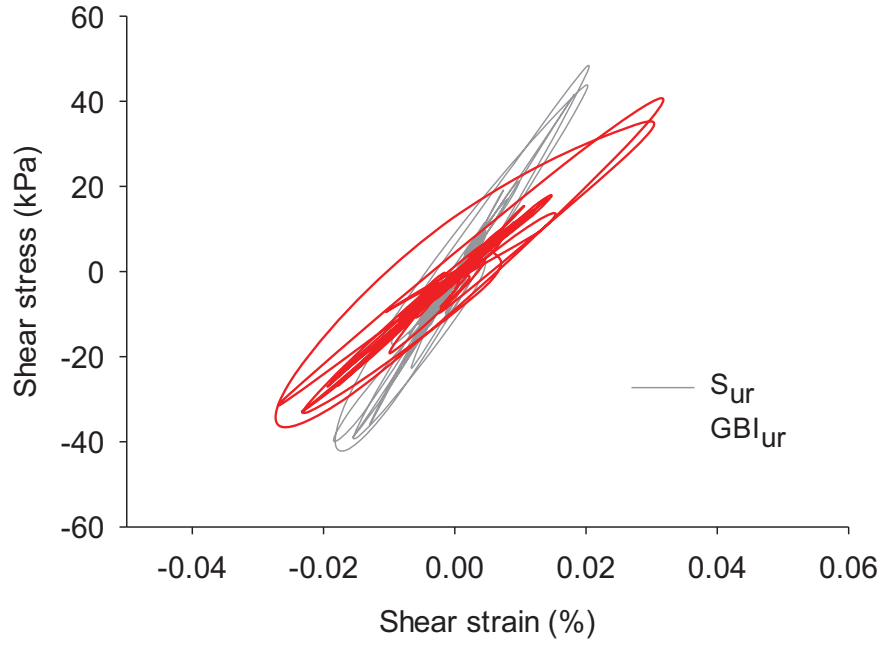
at the top of the building, the isolation factor increased by 37% when the thickness of the GBI layer was increased from  $0.05B$  to  $2B$ . An isolation factor of 0.35 obtained at the footing top indicates that the peak ground acceleration of incoming seismic waves reduced by around 35% due to the presence of GBI<sub>r</sub> layer ( $T_{\text{GBI}}=2B$ ). Peak spectral acceleration values computed from the response spectra plots at point *E* and *F* highlights that the reduction in the peak values of the spectral acceleration due to the presence of GBI<sub>r</sub> is evident for all thickness of GBI layer (Table 5.4). Though the isolation effect increases with increase in  $T_{\text{GBI}}$  initially,  $SIF_a$  values for  $0.1B$  and  $0.2B$  are more or less similar indicating that use of  $0.1B$  thickness of GBI layer itself is enough to achieve the necessary energy dissipation. Moreover, the shift in the fundamental period of the system is more significant for  $T_{\text{GBI}}$  of  $0.1B$  and  $0.2B$  compared to  $0.05B$ .

**Table 5.1.** Effect of thickness of GBI layer on peak spectral acceleration and predominant period  
(Scaled 2015 Nepal earthquake,  $M_w=7.8$ ; PGA= 0.24g)

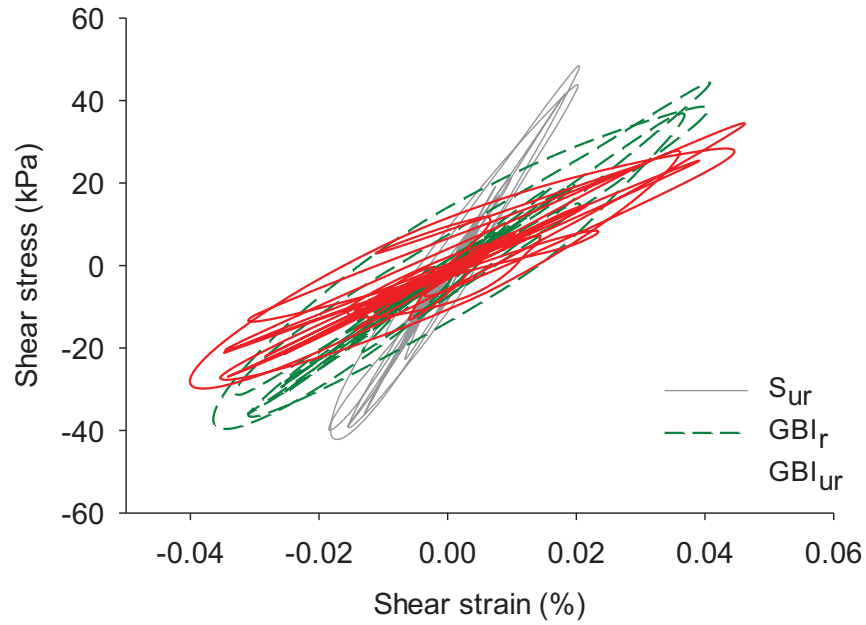
Description	$SIF_a$		Peak spectral acceleration (g)		Predominant period (s)	
	Footing top	Building top	Footing top	Building top	Footing top	Building top
Natural soil ( $S_{ur}$ )	-	-	2.39	2.75	0.47	0.67
Reinforced $T_{\text{GBI}}=0.05B$	0.24	0.27	1.72	2.27	0.6	0.85
GBI layer $T_{\text{GBI}}=0.1B$	0.32	0.34	1.59	1.73	0.67	0.90
(GBI <sub>r</sub> ) $T_{\text{GBI}}=0.2B$	0.35	0.37	1.46	1.69	0.7	0.95

Further insight into the response of GBI system can be attained by examining the typical characteristics of the shear stress-shear strain plots for the  $S_{ur}$ , GBI<sub>ur</sub> and GBI<sub>r</sub> cases. Figure 5.22 depicts the hysteresis stress-strain loops developed in the soil and GBI layer with  $T_{\text{GBI}}$  of  $0.05B$  and  $0.1B$  respectively, at point *Q*. Overall, the computed results capture the non-linear response of soil and GBI system to a reasonable extent. It is apparent from Figure 5.22 that the GBI layers can sustain higher strain compared to natural soil. The shear strains increase by about 2 times for GBI<sub>ur</sub> layer and 2.5 times for GBI<sub>r</sub> layer ( $T_{\text{GBI}} = 0.1B$ ) compared to the  $S_{ur}$  case.





(a)



(b)

**Figure 5.22** Hysteresis loop for GBI isolated and non-isolated system: **(a)**  $T_{GBI}$  of  $0.05B$  **(b)**  $T_{GBI}$  of  $0.1B$  (2015 Nepal earthquake)

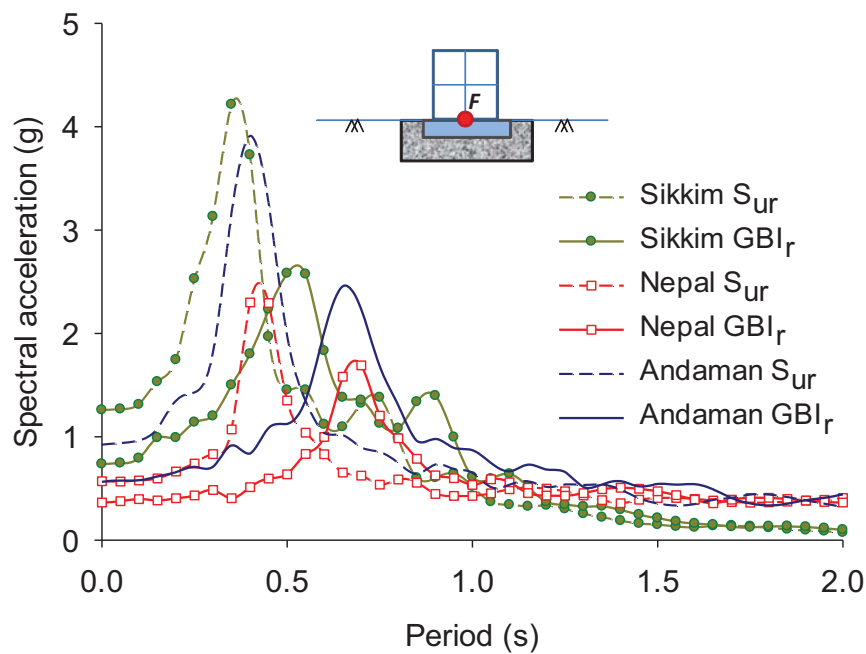
As far as the size of the hysteresis loops is concerned, for the natural soil, the loop is essentially narrow as evident from Figure 5.22a. The area of the hysteresis loop widens for  $T_{\text{GBI}}$  of  $0.05B$ . For thicker GBI layer ( $T_{\text{GBI}}=0.1B$ ), the size of the loop widens as well as elongates, thereby exhibiting larger area as shown in Figure 5.22b. The larger size of the loop indicates the higher energy dissipative nature of the GBI layer. Also, it has been noticed that the area of the loop for  $T_{\text{GBI}}$  of  $0.05B$  is around 1.15 times as that of the  $S_{\text{ur}}$  case (Figure 5.22a). Whereas in case of  $T_{\text{GBI}}$  of  $0.1B$ , for both  $\text{GBI}_{\text{ur}}$  and  $\text{GBI}_{\text{r}}$  system, area of the loop was found to be around 1.5 times as that of the  $S_{\text{ur}}$  case (Figure 5.22b). Although the initial stiffness of the natural soil system reduces with the introduction of GBI layer primarily due to the reduced shear modulus of SRM (Figure 5.22a), the addition of geogrid is largely found to contribute in increasing the shear stiffness of the GBI layer (Figure 5.22b). However, the area of hysteresis loops remains same for both reinforced and unreinforced GBI layer indicating that the contribution of geogrid in terms of damping is less significant for the GBI layer.

#### ***Effect of characteristics of earthquake input motion***

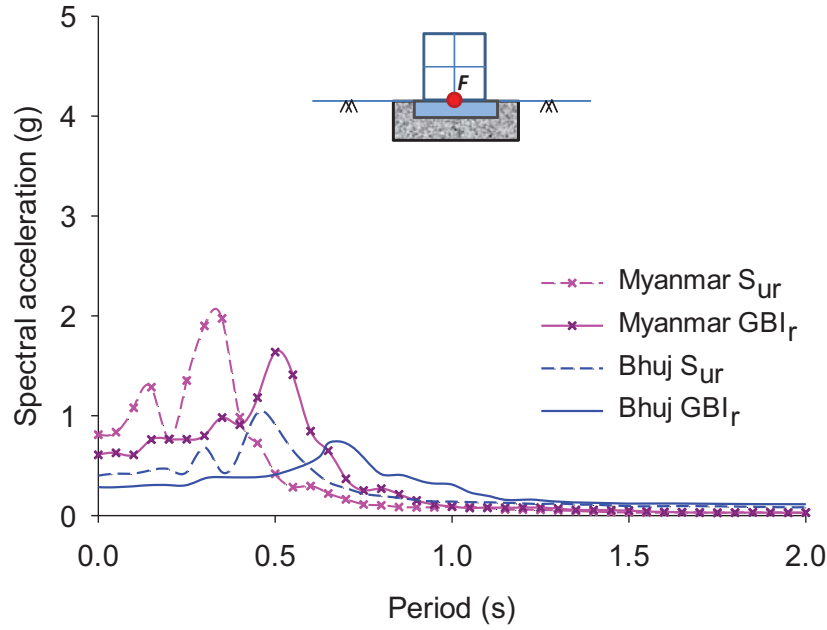
The influence of ground motion characteristics on the response of the GBI system was studied considering the two perspectives, namely the predominant frequency content of input motion and peak acceleration of the earthquake. In view of this, the influence of frequency content of earthquake input motion was studied considering five earthquakes of varying predominant frequency ( $f$ ) mentioned in Table 5.3. The input motions were scaled to a peak acceleration of  $0.24g$  considering the zone factor for Roorkee region. In the present study, the earthquake records are considered as low frequency ( $f < 0.5$  Hz), medium frequency ( $0.5 \text{ Hz} \leq f \leq 2 \text{ Hz}$ ) and high frequency ( $f > 2 \text{ Hz}$ ). Accordingly, 2015 Nepal ( $M_w=7.8$ ) and 2009 Andaman ( $M_w=7.8$ ) earthquakes are considered as low-frequency earthquakes, 2011 Sikkim earthquake ( $M_w=6.9$ ) is considered as medium frequency earthquake and 2001 Bhuj ( $M_w=7.7$ ) & 2016 Myanmar ( $M_w=6.9$ ) earthquakes are considered as high-frequency earthquakes. For this particular study, the framed structure-footing system was supported on  $\text{GBI}_{\text{r}}$  layer, maintaining constant  $T_{\text{GBI}}$  of  $0.01B$  and  $b_{\text{GBI}}$  of  $1.2B$ .

Figure 5.23 shows the resulting acceleration response spectra curves at the top of the footing subjected to different earthquake input motions. For low-frequency earthquakes, the results

indicate that  $GBI_r$  layer induced lower peak for spectral acceleration amplitude (1.5g - 2.5g) at the footing top compared to the  $S_{ur}$  case which is consistent with the trends discussed in previous sections. However, for medium frequency earthquake, the acceleration response spectra (Figure 5.23a) shows a sharp increase in peak spectral acceleration for the  $S_{ur}$  case (4.3g). This could be because the natural frequency of the structure on the reinforced  $GBI$  system matches with the frequency of input motion. A clear benefit of  $GBI_r$  system in bringing down the peak spectral acceleration value to 2.8g for the above medium frequency earthquake can be observed in Figure 5.23a. Moving to high-frequency earthquakes, an overall decline in the peak spectral acceleration values could be observed (Figure 5.23b) for both  $S_{ur}$  and  $GBI_r$  cases. In all the cases, the introduction of  $GBI_r$  layers caused significant reduction in peak spectral acceleration and shifting of the fundamental period of the structure. The reduction in spectral acceleration amplitude of the geogrid reinforced  $GBI$  layer and the period shift is more robust between a period of 0.3 s to 1 s for low and high-frequency earthquakes, while for medium frequency earthquake this period range lies from 0.2 s to 0.6 s. It is clearly evident that low and medium-frequency earthquakes are more sensitive to geogrid reinforced  $GBI$  layer compared to the high-frequency case in terms of period shift and spectral acceleration amplitude reduction.



(a)



(b)

**Figure 5.23** Response spectra at the top of footing for unreinforced natural soil and reinforced GBI system **(a)** low & medium frequency earthquakes **(b)** high frequency earthquakes (scaled PGA=0.24g)

Apart from the SSI study, the fixed base response of the structure is also carried out keeping the bottom of the footing fixed, maintaining rigid boundary conditions. In this way, the seismic response of the framed structure under both fixed base and geo base-isolated conditions could be examined. The influence of frequency content of earthquake input motion quantified in terms of peak acceleration and peak spectral acceleration at the top of footing are listed in Table 5.5 & 5.6, respectively. Table 5.5 shows that the peak acceleration of building on  $S_{ur}$  layer is lower than that computed for fixed base conditions due to SSI effect. The reduction in peak acceleration for  $GBI_r$  layers are evident for all predominant frequencies of input motions considered. Compared to natural soil,  $GBI_r$  layer can dampen the peak acceleration by 40% for low and medium frequency earthquakes. However, for high-frequency earthquakes, the reduction in peak acceleration is only 30%. It is evident from Table 5.6 that  $SIF_{sa}$  for the  $GBI_r$  system is more prominent for medium-frequency earthquakes compared to low and high-frequency earthquakes. In addition, low-frequency earthquakes exhibit significant shift of period compared to medium and high frequency

earthquakes. The high period shift for  $GBI_r$  layer with respect to fixed base condition indicates the contribution of SSI in period shifting and damping for all cases of input motions considered.

**Table 5.2.** Effect of peak acceleration on predominant frequency of input motions (scaled  $PGA=0.24g$ ) at the top of the footing

Earthquake	Peak acceleration (g)		
	Fixed base	Natural soil, $S_{ur}$	Reinforced GBI, $GBI_r$
2015 Nepal ( $M_w=7.8$ )	0.58	0.57	0.36
2009 Andaman ( $M_w=7.8$ )	0.95	0.92	0.56
2011 Sikkim ( $M_w=6.9$ )	1.29	1.25	0.74
2001 Bhuj ( $M_w=7.7$ )	0.47	0.40	0.31
2016 Myanmar ( $M_w=6.9$ )	0.87	0.81	0.61

**Table 5.3.** Effect of peak spectral acceleration on predominant frequency of input motions (scaled  $PGA=0.24g$ ) at the top of the footing

Earthquake	Peak spectral acceleration (g)			Isolation factor, $SIF_{sa}(\%)$	Period shift for $GBI_r$ (s)	
	Fixed Base	Natural soil, $S_{ur}$	Reinforced GBI, $GBI_r$		*w.r.t. fixed base	w.r.t. $S_{ur}$ layer
2015 Nepal ( $M_w=7.8$ )	2.51	2.39	1.59	33.47	0.40	0.32
2009 Andaman ( $M_w=7.8$ )	4.03	3.9	2.47	36.9	0.35	0.28
2011 Sikkim ( $M_w=6.9$ )	4.78	4.25	2.60	40	0.30	0.25
2016 Myanmar ( $M_w=6.9$ )	2.07	1.97	1.40	28.9	0.26	0.20
2001 Bhuj ( $M_w=7.7$ )	1.29	1.03	0.73	29.6	0.3	0.21

\*w.r.t. (with respect to)

--	--	--	--

### 5.6.3. Shear force and inter-storey drift

The effect of seismic isolation on the base shear of the framed structure was analyzed and the results were compared between the fixed base structure and  $S_{ur}$ ,  $GBI_{ur}$  &  $GBI_r$  structure considering SSI effects. Figure 5.25 shows the plot of base shear ratio, which is the ratio of shear force developed in the SSI structure to that of the fixed base structure. A constant scaled PGA of 0.24g was maintained for the earthquake input motions in the study. It can be inferred from the figure that SSI effects prove to be beneficial for GBI system by reducing the base shear compared to the fixed base system. Further, Figure 5.25 shows that the observed reduction in base shear is predominant for building placed on  $GBI_{ur}$  system compared to  $GBI_r$  system. This could be due to the decrease in stiffness of the soil beneath the building foundation. The non-isolated system ( $S_{ur}$ ) showed higher base shear ratio due to its relatively stiff nature compared to the GBI system. For instance, in case of the 2015 Nepal earthquake ( $M_w=7.8$ ), the base shear ratio is 0.47 for  $S_{ur}$  system which got reduced to 0.3 for  $GBI_{ur}$  system. Moreover, the flexible-base rendered by the GBI layer influences the SSI effects resulting in lower base shear compared to the fixed base.

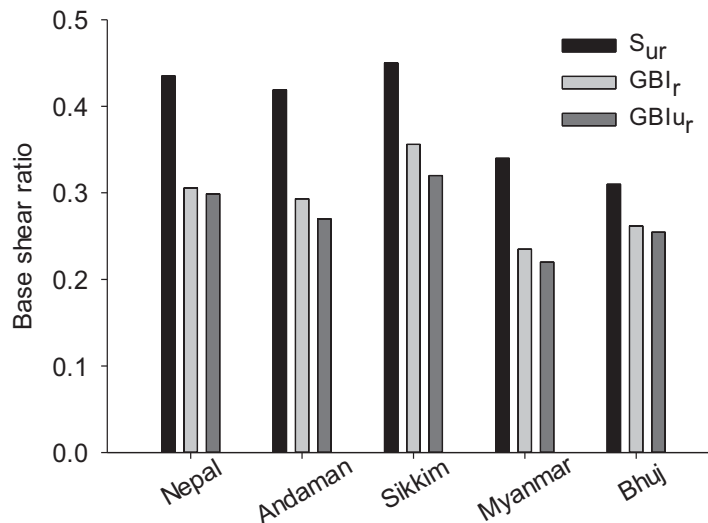


**Figure 5.25** Base shear ratios for different earthquakes for the building (scaled)

The lateral deformation of the structure under earthquake loading is a key factor in evaluating the performance of GBI isolated structure. The maximum lateral displacement experienced by different floors of the building for isolated and non-isolated cases were obtained for different



earthquakes input motions and their Inter-storey Drifts ( $ID$ ) were computed as per IS 1893 Part 1 (2016) using equation 5.12.

$$ID = \frac{(d_{j+1} - d_j)}{H} \quad (5.12)$$

where,  $d_j$  is the lateral deflection in the  $j^{\text{th}}$  storey;  $d_{j+1}$  is the lateral displacement in the  $(j+1)^{\text{th}}$  storey of the building and  $H$  is the storey height.

For the study, maximum displacement in the lateral direction are noted at the rightmost nodes of the framed structure at each floor level to calculate the  $ID$ . Table 5.7 summarizes the variation of maximum storey drift at the 1st floor and 2nd floor of the building for different ground motions ( $PGA=0.24g$ ) for the  $S_{ur}$ ,  $GBI_{ur}$  &  $GBI_r$  cases. It is noted from the table that  $S_{ur}$  layer exhibit higher inter-storey drift due to high lateral displacement compared to  $GBI_{ur}$  layer. This is primarily due to the high amplitude of the seismic waves reaching the structure. The lateral displacement of  $GBI_{ur}$  layers can be further reduced by introducing geogrids. The presence of geogrids creates a confining effect, thereby restraining the lateral displacement of the structure placed on the  $GBI$  system. Considering the case of 2015 Nepal earthquake, the maximum lateral displacement of the  $GBI_{ur}$  system was found to reduce by 20% due to the geogrid reinforcement. According to IS 1893 Part I (2016), the maximum inter-storey drift should be within  $0.004H$  for the overall structural safety of the building. In this study, all the cases of  $GBI_{ur}$  and  $GBI_r$  system and few of  $S_{ur}$  systems are within the prescribed safety limit.

**Table 5.4.** Maximum inter-storey drift of the building for different earthquake motions

Earthquake	Maximum storey drift (mm)					
	Natural soil, $S_{ur}$		Unreinforced $GBI, GBI_{ur}$		Reinforced $GBI$ , $GBI_r$	
	1 <sup>st</sup> floor	2 <sup>nd</sup> floor	1 <sup>st</sup> floor	2 <sup>nd</sup> floor	1 <sup>st</sup> floor	2 <sup>nd</sup> floor
2015 Nepal ( $M_w=7.8$ )	9.4	10.5	7.7	8.6	6.1	6.6
2009 Andaman ( $M_w=7.8$ )	12.4	12.6	10.5	10.6	8.7	8.6
2011 Sikkim ( $M_w=6.9$ )	14.7	16.4	11.5	12.3	9.7	10.4
2016 Myanmar ( $M_w=6.9$ )	6.1	6.4	5.4	5.6	4.4	4.4
2001 Bhuj ( $M_w=7.7$ )	3.6	5.1	3.2	4.5	3.0	4.2

Furthermore, foundation rotation induced by rocking motion of the structure due to the inertial force developed in it during earthquake excitation was computed for the low-rise building in the study. Table 5.8 shows the maximum base rotation experienced by the building at the footing level. The middle node at the bottom of the footing was chosen to extract the rotational displacement experimented by the footing due to seismic loading. The maximum angular rotation for raft foundations shall not exceed 1:400 as per IS 1904 (1986). Since the building is low-rise, the foundation rotations are well below the permissible limit for all the five chosen earthquakes. Because of the presence of geogrids, GRI system showed reduced foundation rotation compared to the unreinforced GBI system since the foundation rotation induced by soil deformation and failure is well curtailed by geogrid layers. Thus, the contribution of geogrids in resisting foundation deformation is pivotal during earthquake loading conditions in terms of settlements and rotation.

**Table 5.5.** Rotation of the building

<b>Earthquake</b>	<b>Maximum base rotation (rad)</b>	
	<b>Unreinforced GBI, GBI<sub>ur</sub></b>	<b>Reinforced GBI, GBI<sub>r</sub></b>
2015 Nepal ( $M_w=7.8$ )	0.00065	0.00043
2009 Andaman ( $M_w=7.8$ )	0.00059	0.00031
2011 Sikkim ( $M_w=6.9$ )	0.00086	0.00043
2001 Bhuj ( $M_w=7.7$ )	0.00021	0.00011
2016 Myanmar ( $M_w=6.9$ )	0.00037	0.00015

## 5.7. SUMMARY

The numerical study explored in this chapter sheds significant light on the use of GBI layer made of SRM and reinforced with geogrids for seismic isolation of low-rise buildings in the Indo-Gangetic plain region. From the numerical simulations, it was inferred that the proposed hyper-elastic model could be used to represent the stress-strain response of the SRM reasonably well. The accuracy of the numerical modelling procedure adopted was confirmed by comparing the FE results with that of the shake table test results on footing isolated using SRM by Bandyopadhyay et al. (2015). One of the engineering implications arising from this study is that the geogrid

reinforcement, which primarily controls the static bearing capacity and settlement issues of the GBI system can be significantly beneficial under seismic loading conditions. Geogrid reinforcement arrests the seismic settlement and rotation arising in the GBI layer considerably. Double layered geogrid systems are recommended for effective settlement reduction of GBI layers subjected to static and seismic loading.

The chapter further discusses the response of the GBI system in the free-field condition and with the presence of the building. Under free-field conditions, there is a gradual reduction in the amplitude of earthquake waves as it passes through the GBI layer due to the high damping nature of SRM present in it. The presence of geogrid does not contribute to acceleration amplitude reduction owing to the higher stiffness of the geogrid compared to the surrounding SRM. The free-field response reveals modification in the amplitude of seismic waves at different depths of the GBI layer along with alteration in the ground response for the GBI system in comparison to the natural soil. In view of this, further investigation with the low-rise framed structure focuses on factors such as the thickness of the GBI layer, earthquake input motion characteristics, and its influence on PGA, spectral acceleration, base shear & interstorey drift of the building.

For the two-storied building supported on GBI layer, one of the main conclusions is that an optimum thickness of  $0.1B$  is deemed to be sufficient for effective seismic isolation beyond which the rate of increase in damping and period shift is not significant. Further, the GBI layer exhibits a bigger hysteresis loop and shear strain endurance compared to natural soil. The presence of geogrid contributes to the increase in shear stiffness for the GBI system.

Since the influence of SSI and earthquake characteristic significantly affects the performance of the GBI system, further studies were undertaken with five different earthquake input motions. Firstly, for GBI layer of  $0.1B$  thickness, the results conclude that low and medium frequency earthquakes exhibit significant acceleration reduction of 40% while high-frequency earthquakes exhibit a 30% reduction in peak acceleration compared to the natural soil. The presence of GBI layer marginally shifts the predominant period of the system to a higher value compared to the natural soil system leading to a reduction of spectral acceleration in low rise buildings. Secondly, the GBI thickness of  $0.1B$  is adequate for peak accelerations of  $0.01g$  to  $0.4g$ .

The combination of SRM and GBI lowers the base shear developed in the low-rise building compared to natural soil due to the lower stiffness of SRM as well as SSI effects. Presence of

geogrids in the GBI system plays a vital role in reducing the inter-storey drift of the building by providing additional confinement thereby restraining the lateral displacement of building significantly. Further, Geogrids prove to be beneficial in arresting foundation rotation.

The results and recommendations for the proposed GBI layer for low-rise framed structure suits well for soil profile similar to the Roorkee region considered in the analysis. In conclusion, since the ground motion characteristics and site conditions greatly affect the performance of GBI layer, due consideration should be given to these factors while considering the GBI isolation system for earthquake-prone areas. The study can be extended to buildings of varying height, foundation conditions for different soil conditions considering different types of geogrids to get a wider understanding of its seismic isolation efficiency.

## CHAPTER 6

### CONCLUSIONS AND RECOMMENDATIONS

#### 6.1. SUMMARY

The present study explores the use of geo-base isolation system made of sand-rubber mixture as a vibration isolation layer below the foundation system as an alternative to the prevalent base-isolation technique for seismic protection of buildings. While the conventional base-isolation reduces the seismic demand to the building superstructure, the proposed engineered layer of GBI system specially aims at reducing transmission of vibratory energy to the foundation of buildings. As reviewed in Chapter 2, most of the experimental studies reported in the literature on this area are focused on the material characterization of SRM baring few shake table model studies using SRM as vibration absorbing system below footings. Limited numerical investigation on the use of SRM layer below building foundations focuses on idealized soil conditions with little emphasis on site-specific cases considering different characteristics of earthquake induced ground motion. Further, there is limited information available on settlement problems for foundations posed by the low stiffness of SRM during static loadings.

The details of the static and seismic response analysis carried out on low-rise building resting on geogrid reinforced GBI system are presented in the thesis. Based on the material characterization of SRM carried out using laboratory tests such as direct shear, monotonic and cyclic triaxial tests as described in Chapter 3, the optimum rubber content considering the shear strength, stiffness and damping properties required for geo base isolation is arrived. The series of laboratory element test performed in this study for the material characterization of sand/SRM encompass routine laboratory test, direct shear test, triaxial test and cyclic triaxial tests. In chapter 4, the effectiveness of geogrid reinforcement in improving the performance of a footing of resting on GBI system under static loading condition is studied by carrying out laboratory model tests and finite element based numerical analysis. The fundamental failure mechanism of the GBI system with and without geogrid reinforcement was studied concerning the bearing capacity and settlement of the footing. The numerical model of the footing on the GBI system with geogrid is developed using the FE code ABAQUS. The results obtained from numerical studies were compared with the experimental findings of the model test and are found to be in good agreement. The parametric

study with different variables of geo-base isolation system and geogrid is carried out to arrive at optimal values of parameters for attaining maximum bearing capacity and reduced settlement.

The final aim of the research was to investigate the use of GBI layer made of SRM reinforced with geogrids for seismic isolation of full-scale low-rise buildings with raft footing in the Indo-Gangetic plain region. Two-dimensional FE studies were carried out to analyze the seismic response of a two-storey building supported on raft footing resting on GBI layer as discussed in Chapter 5. The present study uses the direct method of SSI analysis which accounts for the inertial and kinematic interactions simultaneously with the entire soil-structure where the whole soil-structure-foundation system is modelled together as a finite element model. The accuracy of the numerical modelling procedure adopted was confirmed by comparing the FE results with that of the shake table test results on footing isolated using SRM by Bandyopadhyay et al. (2015). Geogrid reinforcement was added to the GBI layers to reduce settlement and footing rotation during seismic loading. The free-field response of the GBI layer was further investigated. Factors affecting the performance of the GBI system such as the thickness of GBI layer and earthquake input motion characteristics were investigated, and its influence on PGA, spectral acceleration, base shear and inter storey drift of the building were analyzed.

## **6.2. CONCLUSIONS**

The main conclusions arrived from the present study can be summarized as follows:

### **6.2.1. Static and cyclic response of SRM**

One of the major findings from the results of the present laboratory tests on the shear strength characteristics of SRM is that dense SRM exhibits strain hardening response in contrast to the behaviour of dense sand which exhibits brittle behaviour with a prominent peak followed by strain-softening behaviour. It is also found that the contribution of sand and rubber to the material matrix is predominant at rubber content below 40% higher than which the influence of rubber matrix prevails.

The volumetric response of SRM is typically compressive, unlike sand which exhibits both dilative and compressive response. The study concludes that, for SRM with rubber content higher than 30%, the shear strength of the mixture decreases rapidly. Keeping in mind the geo-base isolation

application of SRM, 30% rubber content at medium to high relative density was found to optimally contribute both sand and rubber matrix response towards the shear strength.

The monotonic triaxial tests further reaffirm the compressive response of the SRM (30% rubber content) irrespective of the confining pressure under consolidated drained conditions and positive pore pressure development in the mixture during consolidated undrained conditions. Segregation checks on SRM samples reveal that the homogeneity of the material remains unaffected up to a rubber content of 50%.

In addition, the findings from cyclic triaxial tests carried out on SRM suggest that at a given confining pressure, shear strength decreases and damping ratio increases with the addition of rubber to the SRM. One of the more significant findings in the study is that SRM with 30% rubber content possesses adequate stiffness, shear modulus and damping properties ideal for its use as geo-base isolation material.

#### **6.2.2. Static response of model footing resting on geogrid reinforced GBI layer**

One of the main aims of the present study was to assess the contribution of geogrid reinforcement in reducing the settlement problem associated with the compressibility of SRM. In this regard, studies on the bearing capacity-settlement response of a model footing resting on GBI layer with and without geogrid reinforcement was explored considering a series of laboratory model tests.

The introduction of the proposed GBI layer between the footing and the underlying sandy strata reduces bearing capacity and increases settlement. Provision of geogrids to the geo-base isolation system was found to increase the bearing capacity by two times for single geogrid layer and three times for double geogrid layer. Further, single and double layered geogrid reinforcement reduces the settlement of GBI system up to 30% and 45% respectively. The larger strain on geogrids measured during the experimental study shows the development of interlocking frictional resistance offered by geogrid, which counteracts the compressive nature of rubber in the GBI layer.

The finite element analysis carried out on footing on geogrid reinforced GBI system indicate that the number, position and length of geogrids along with the width of GBI layer are the primary parameters influencing the increase in bearing capacity and reduction in settlement of the footing.

The optimum depth of placement of the first layer of geogrid below the isolated footing is found to be  $0.35B$  to  $0.4B$  for single geogrid and  $0.3B$  to  $0.35B$  for double layered geogrid system. The



optimum length of geogrid is found to be varying from  $4B$  to  $6B$ . Moreover, the length of reinforcement shall be greater than the width of the GBI layer. In the case of double layer reinforcement, the optimum geogrid spacing was found to be  $0.2B$ . The most prominent finding to emerge from this study is that double layer reinforcement within the GBI layer is suitable for satisfactory performance in terms of bearing capacity and settlement of the footing.

### **6.2.3. Seismic response of a low-rise building resting on geogrid reinforced GBI system**

The following conclusions have been drawn based on the numerical studies carried out on the dynamic response of GBI layer reinforced with geogrids for seismic isolation of a low-rise framed structure with raft footing in the Indo-Gangetic plain region.

- Geogrid inclusion arrests the seismic settlement arising in GBI layer significantly. Double layered geogrid systems are recommended for effective settlement reduction of GBI layers under static and seismic loading.
- Under free-field conditions, there is a gradual reduction in the amplitude of earthquake waves as it passes through the GBI layer due to the high damping nature of SRM present in it. The presence of geogrid does not contribute to acceleration amplitude reduction owing to the higher stiffness of the geogrid compared to the surrounding SRM.
- For the two-storied building supported on GBI layer, a seismic isolation factor ( $SIF_a$ ) of about 0.4 and a period shift of 0.4 s were obtained with GBI thickness of  $0.1B$  for the 2015 Nepal earthquake input motion. An optimum thickness of  $0.1B$  is deemed to be sufficient for effective seismic isolation beyond which the rate of increase in damping and period shift is not significant. The GBI thickness of  $0.1B$  is effective for peak accelerations upto 0.4g.
- GBI layer exhibits a larger hysteresis loop compared to that of natural soil. Though there is a reduction in the shear modulus of the GBI layer, the presence of geogrid contributes to the increase of shear stiffness. Geogrid reinforced GBI layers can endure shear strain up to 2.3 times as that of natural soil due to its ductile nature.
- The influence of SSI and earthquake characteristic significantly affects the performance of the GBI system. For GBI thickness of  $0.1B$ , an acceleration reduction of 40% was obtained for low and medium frequency earthquakes. For high-frequency earthquakes, a 30% reduction in peak acceleration was obtained.

- The presence of GBI layer marginally shifts the predominant period of the system to a higher value compared to the natural soil system. This period shift leads to a reduction of spectral acceleration in low rise buildings
- The shear force developed in the low-rise building decreases by around 45% to 55% compared to the fixed base structure due to the introduction of GBI layer. The reduced stiffness of the GBI layer, as well as SSI effects, benefits in the reduction of shear force.
- Presence of geogrids in the GBI system plays a vital role in reducing the inter-storey drift of the building by upto 20% by providing additional confinement, thereby restraining the lateral displacement of building significantly. Further, geogrids prove to be beneficial in arresting foundation rotation
- It is recommended to adopt the geo-base isolation system for seismic protection of low-rise symmetric buildings in the seismically active Indo Gangetic region of India with the following parameters: GBI layer with a width of  $1.2B$  and thickness of  $0.1B$  reinforced with two layers of geogrid having a spacing of  $0.05B$  and length of  $2B$ .

### 6.3. RECOMMENDATIONS FOR FUTURE STUDIES

Some recommendations for further research are suggested below:

- In the present study, the effect of the water table and liquefaction implications were not considered given that the SRM has high permeability. However, further studies need to be carried out to understand the seismic response of such geo-base isolated foundation response incorporating water table effects.
- The study region described in this thesis considers a typical soil profile from Roorkee region in the Indo Gangetic plain. However, it is recommended to carry out further studies for other typical site conditions prevailing in the Indo Gangetic plain.
- Since the ground motion characteristics and site conditions may significantly affect the performance of the GBI layer, due consideration should be given to these factors while considering the GBI isolation system for earthquake-prone areas.
- The present study is confined to symmetric building geometry. However, since modern buildings are mostly asymmetric in geometry, 3D numerical studies should be undertaken to study the influence of such shape effects on the seismic response of the GBI system.

- The study can be extended to buildings of varying height, foundation conditions for different soil conditions to get a more comprehensive understanding of its seismic isolation efficiency. Moreover, further research is necessary to explore the different type of geosynthetic reinforcement available or preloading techniques to eliminate the plastic compression of the SRM.
- The laboratory model test in the present study only explores the static loading response of geosynthetic reinforced GBI system. To examine the seismic response associated with geosynthetic reinforced GBI system, shake table and centrifuge model tests can be undertaken in the future.

## REFERENCES

- ABAQUS 6.14.** (2014). ABAQUS/CAE User's Manual, Dassault systems, USA.
- Abdelhaleem, A. M.** (2012). Evaluation of rubber sand mixtures as replacement soils to mitigate earthquake induced ground motions. *Proceedings of the 18th International Conference on Soil Mechanics and Geotechnical Engineering*, Paris, 3163–3166.
- Abichou, T., Tawfiq, K., Edil, T. and Benson, C.** (2004). Behaviour of a soil-tire shreds backfill for modular block-wall, *Recycled Materials in Geotechnics*. Geotechnical Special Publication, ASCE, **127**, 162-172.
- Ab-Malek, K. and Stevenson, A.** (1986). The effect of 42 year immersion in sea-water on natural rubber. *Journal Of Materials Science*, **21**, 147-154.
- Abramanto, M. and Whittle, A. J.** (1995). Experimental evaluation of pullout analyses for planar reinforcements. *Journal of Geotechnical Engineering*, **121**(6), 486–492.
- Abu-Farsakh, M., Chen, Q. and Sharma, R.** (2013). An experimental evaluation of the behaviour of footings on geosynthetic-reinforced sand. *Soils and Foundations*, **53**(2), 335–348. DOI: 10.1016/j.sandf.2013.01.001.
- Abu-Farsakh, M., Gu, J., Voyiadjis, G. and Chen, Q.** (2012). Finite element parametric study on the performance of strip footings on reinforced crushed limestone over embankment soil. *Electronic Journal of Geotechnical Engineering*, **17**, 723–742.
- ACIC 336** (1988). *Analysis and Design Procedures for Combined Footings and Mats*. Reapproved (2002). American Concrete Institute, Detroit.
- Adamu, M. and Uche, O. A. U.** (2014). Durability properties of concrete containing scrap tyre as fine & coarse aggregate in concrete. *International Journal of Scientific and Engineering Research*, **5**(11), 126-133.
- Ahmed, I.** (1993). *Laboratory Study on Properties of Rubber Soils*. Ph.D. thesis, School of Civil Engineering, Purdue University, West Lafayette, IN. Report No. FHWA/IN/JHRP – 93/4.
- Ahmed, I. and Lovell, C.** (1993). Use of rubber tyres in highway construction. *Utilization of Waste Material in Civil Engineering Construction*, ASCE, New York, 166–181.

- Ahn, I. and Cheng, L.** (2014). Tire derived aggregate for retaining wall backfill under earthquake loading. *Construction and Building Materials*, **57**, 105–116.
- Akbulut, S. and Pamukcu, S.** (2010). Evaluation of dynamic properties of geosynthetic reinforced clay samples for environmental impact practices. *Environmental Earth Sciences*, **61**(7), 1449–1456.
- Alavi, E. and Alidoost, M.** (2012). Soil structure interaction effects on seismic behaviour of base isolated buildings. *Proceedings of the 15th World Conference on Earthquake Engineering*, Lisboa.
- Altun, S., Goktepe, A. B. and Lav M. A.** (2008). Liquefaction resistance of sand reinforced with geosynthetics. *Geosynthetics International*, **15**(5), 322–332.
- Anastasiadis, A., Senetakis, K. and Pitilakis, K.** (2012). Small-strain shear modulus and damping ratio of sand-rubber and gravel-rubber mixtures. *Geotechnical and Geological Engineering*, **30**(2), 363–382. DOI: 10.1007/s10706-011-9473-2.
- Ansari, Y., Richard, M., Yamamoto, H. and Daichao, S.** (2011). Computers and geotechnics numerical analysis of soilbags under compression and cyclic shear. *Computer and Geotechnics*, **38**(5), 659–68. DOI: 10.1016/j.compgeo.2011. 02.002.
- Anvari, S. M., Shooshpasha, I., and Kutanaei, S. S.** (2017). Effect of granulated rubber on shear strength of fine-grained sand. *Journal of Rock Mechanics And Geotechnical Engineering*, **9**(5), 936–944.
- Asadi, M., Thoeni, K. and Mahboubi, A.** (2018). An experimental and numerical study on the compressive behaviour of sand-rubber particle mixtures. *Computers and Geotechnics*, **104**, 185–195.
- ASTM D 6270** (1988). *Standard Practice for use of Scrap Tires in Civil Engineering Applications*. ASTM International, West Conshohocken, PA: 2008-1.
- ASTM D 6637** (2001). *Standard Test Method for Determining Tensile Properties of Geogrids by Single or Multi-Rib Tensile Method*. West Conshohocken, PA.
- ASTM D3999-11** (2011). *Standard Test Methods for the Determination of the Modulus and Damping Properties of Soils Using the Cyclic Triaxial Apparatus*. ASTM International, West Conshohocken, PA.

**ASTM D4253** (2016). *Standard test methods for maximum index density and unit weight of soils using a vibratory table*. ASTM International, West Conshohocken, PA.

**Atkinson, J. H. and Bransby, P. L.** (1982), *The mechanics of soil: An introduction to Critical State Soil Mechanics*. McGraw Hill Book Company, U.K, 1982.

**Attom, M. F.** (2006). The use of shredded waste tires to improve the geotechnical engineering properties of sands. *Environmental Geology*, **49**(4), 497–503.

**Australian Government** (2011). Product stewardship for the end of life tyres, Department of the Environment.. *Protection and Heritage Council (EPHC)* website, (<http://www.environment.gov.au/settlements/waste/tyres/index.html>).

**Badakhshan, E. and Noorzad, A.** (2015). Load eccentricity effects on behaviour of circular footings reinforced with geogrid sheets. *Journal of Rock Mechanics and Geotechnical Engineering*, **7**(6), 691–699. 10.1007/s10706-011-9473-2.

**Bagchi, S. and Raghukanth, S. T. G.** (2019). Seismic response of the central part of Indo-Gangetic plain. *Journal of Earthquake Engineering*, **23**(2), 183–207. DOI: 10.1080/13632469.2017.1323044.

**Balachowski, L., and Gotteland, P.** (2007). Characteristics of tyre chips-sand mixtures from triaxial tests. *Archives of Hydro-Engineering and Environmental Mechanics*, **54**(1), 3–14.

**Bali Reddy, S., Pradeep K. D. and Murli K. A.** (2016). Evaluation of the optimum mixing ratio of a sand-tire chips mixture for geoengineering applications. *Journal of Materials in Civil Engineering*. **28** (2): 06015007. DOI: 10.1061/(ASCE)MT.1943-5533.0001335.

**Bandyopadhyay, S., Sengupta, A. and Reddy, G. R.** (2015). Performance of sand and shredded rubber tire mixture as a natural base isolator for earthquake protection. *Earthquake Engineering and Engineering Vibration*, **14**(4), 683–693. DOI: 10.1007/s11803-015-0053-y.

**Basha, B. and Babu, G. S.** (2011). Seismic reliability assessment of internal stability of reinforced soil walls using the pseudo-dynamic method. *Geosynthetics International*, **18**(5), 221–241. DOI: 10.1680/gein.2011.18.5.221.

**Basu, U. and Chopra, A. K.** (2003). Perfectly matched layers for time harmonic elasto-dynamics of unbounded domains: Theory and finite element implementation. *Computer Methods in Applied*

*Mechanics and Engineering*, **192**(11-12), 1337-1375.

**Bathurst, R. J. and Jarrett, P. M.** (1988). Large-scale model tests of geocomposite mattresses over peat subgrades. *Transportation Research Record*, **1188**, 28–36.

**Bathurst, R. J., Zarnani, S. and Gaskin, A.** (2007). Shaking table testing of geofoam seismic buffers. *Soil Dynamics and Earthquake Engineering*, **27**(4), 324–332. DOI: 10.1016/j.soildyn.2006.08.003.

**Baxter, C. D. P., Sharma, M. S. R., Moran, K., Vaziri, H. and Narayanasamy, R.** (2011). Use of  $\bar{A}=0$  as a failure criterion for weakly cemented soils. *Journal of Geotechnical and Geoenvironmental Engineering*, **137**(2), 161–170.

**Bergado D. T., Youwai S. and Rittirong A.** (2005). Strength and deformation characteristics of flat and cubical rubber tyre chip-sand mixtures, *Geotechnique*, **55**(8), 603–606. DOI: 10.1680/geot.2005.55.8.603.

**Bergado, D. T., Voottipruex, P., Srikongsri, A. and Teerawattanasuk, C.** (2001) Analytical model of interaction between hexagonal wire mesh and silty sand backfill. *Canadian Geotechnical Journal*, **38**, 782–795.

**Bernal, A., Salgado, R. and Lovell, C.** (1996). *Laboratory Study on the Use of Tire Shreds and Rubber -sand in Backfills and Reinforced Soil Applications*. Final Report Indiana Department of Transportation, Joint Highway Research Project Report No. FHWA/IN/JHRP-96. Purdue University, West Lafayette, Indiana, U.S.A.

**Bernal, A., Salgado, R., Swan, R. H., Jr. and Lovell, C. W.** (1997). Interaction between tire shreds, rubber-sand and geosynthetics. *Geosynthetics International*, **4**(6), 623–643.

**Bettess, P.** (1980). More on infinite elements. *International Journal for Numerical Methods in Engineering*, **15**(11), 1613–1626.

**Bilham, R.** (2019). Himalayan earthquakes: a review of historical seismicity and early 21st century slip potential. *Himalayan Tectonics: A Modern Synthesis*, Geological Society, London, Special Publications, 483.

**Bilham, R. and England, P.** (2001). Plateau pop up in the great 1897 Assam earthquake. *Nature*, **410**, 806-809. DOI: 10.1038%2F35071057.



- Binquet, J. and Lee, K.** (1975). Bearing capacity tests on reinforced earth slabs. *Journal of the Geotechnical Engineering Division*, ASCE, **101**, 1241–1255.
- BMTPC.** (2019). *Vulnerability Atlas of India*. Third Edition. Ministry of Housing & Urban Affairs, Government of India, New Delhi.
- Boominathan, A. and Hari, S.** (2002). Liquefaction strength of fly ash reinforced with randomly distributed fibers. *Soil Dynamic Earthquake Engineering*, **22**(9), 1027–1033.
- Booth, E. D. and Key, D.** (2006). *Earthquake Design Practice for Buildings*. 3rd Edition. ICE Publishing 2019. Scotland.
- Bosscher, P. J., Edil, T. B. and Eldin, N.** (1993). Construction and performance of shredded tire test embankment. *Transportation Research Record*, 1345, Transportation Research Board, Washington, D.C., 44–52.
- Bosscher, P. J., Edil, T. B. and Kuraoka, S.** (1997). Design of highway embankments using tire chips. *Journal of Geotechnical and Geoenvironmental Engineering*, **123**(4), 295–304. DOI: 10.1061/(ASCE)1090-0241(1997)123:4(295).
- Bowles, J. E.** (2001). *Foundation Analysis and Design*. McGraw-Hills, 5<sup>th</sup> Edition, Civil Engineering Series. New York, USA.
- Brinson H. and Brinson L.** (2008). *Polymer Engineering Science and Viscoelasticity: An Introduction*. Evanston: Springer Verlag. DOI: 10.1007/978-1-4899-7485-3.
- Cabalar, A. F.** (2011). Direct shear tests on waste tires-sand mixtures. *Geotechnical and Geological Engineering*, **29**(4), 411–418. 10.1007/s10706-010-9386-5.
- Calvaranoa, L. S., Leonardi, G. and Palamara, R.** (2017). Finite element modelling of unpaved road reinforced with geosynthetics. *Procedia Engineering*, **189**, 99–104.
- Calvi, G., Ceresa, P., Casarotti, C., Bolognini, D. and Auricchio, F.** (2004). Effects of axial force variation in the seismic response of bridges isolated with friction pendulum systems. *Journal of Earthquake Engineering*, **8**(01), 187–224.
- Catman professional V5.** (2005). *Operating manual Catman professional 5*, Hottinger baldwin messtechnik GMBH, Germany.
- Cervera, M., Chiumenti, M., Benedetti, L. and Codina, R.** (2015). Mixed stabilized finite

element methods in nonlinear solid mechanics. Part III: Compressible and incompressible plasticity. *Computer Methods in Applied Mechanics and Engineering*, **285**, 752–775.

**Chadwick, E., Betree, P. and Langhrouche, O.** (1990). Diffraction of short wave modelled using new mapped wave envelopes finite and infinite elements. *International Journal for Numerical Methods in Engineering*, **45**(3), 335–354.

**Chen, C. F.** (1985). *Mechanics of Geomaterials*, In: Z. Bazant; editor. John Wiley & Sons Ltd, 65-86.

**Chen, Q., Abu Farsakh, M., Sharma, R., and Zhang, X.** (2007). Laboratory investigation of behaviour of foundations on geosynthetic reinforced clayey soil. *Transportation Research Record, Journal of The Transportation Research Board*, 28–

**Cheng, D.** (2016). *Usage Guide for Tire derived Aggregates (TDA)*. Report DRRR 2016-01545, California Department of Resources Recycling and Recovery (CalRecycle).

**Choobbasti, A. J., Vafaei, A. and Kutanaei, S. S.** (2015). Mechanical properties of sandy soil improved with cement and nanosilica. *Open Engineering*, **5**(1), 111–116.

**Chopra, A. K.** (2007). *Dynamics of Structures: Theory and Applications to Earthquake Engineering*, 3<sup>rd</sup> Edition, Prentice-Hall, Englewood Cliffs, N.J.

**Christopoulos, C. and Filiatrault, A.** (2006). *Principles of passive supplemental damping and seismic isolation*, IUSS Press, Pavia, Italy.

**Chummar, A. V.** (1972). Bearing capacity theory from experimental results. *Journal of Soil Mechanics and Foundation Division*, **98**(12), 1257–1276.

**Cicek, E., Guler, E. and Yetimoglu, T.** (2018). Stress distribution below a continuous footing on geotextile-reinforced soil. *International Journal of Geomechanics*, **18**(3), 6018005.10.1061/(ASCE)GM.1943-5622.0001095.

**Coon, M. D. and Evans, R. J.** (1971). Recoverable deformation of cohesionless soils, *Journal of the Soil Mechanics and Foundations*, **97**(2), 375-391.

**Corotis, R. B., Farzin, M. H. and Krizeck, R. J.** (1974). Nonlinear stress-strain formulations for soil, *Journal of the Geotechnical Engineering Division*, **100**(9), 993-1008.

- Courant, R., Friedrichs, K. and Lewy, H.** (1967). On the partial difference equations of mathematical physics, IBM. *Journal of Research and Development*, **11**(2), 215–234.
- Cresswell, A., Barton, M. E. and Brown, R.** (1999). Determining the maximum density of sands by pluviation. *Geotechnical Testing Journal*, **22**(4), 324-328.10.1520/GTJ11245J.
- CSI** (2010). *SAP2000 V14 Analysis Manual: Inelastic Time History Analysis*. CSI (Computers and Structures Inc.), Berkley, USA.
- Das, B. M. and Omar, M. T.** (1994). The effects of foundation width on model tests for the bearing capacity of sand with geogrid reinforcement. *Geotechnical and Geological Engineering*, **12**, 133-141. DOI: 10.1007/BF00429771.
- Das, B. M., Shin, E. C. and Omar, M. T.** (1994). The bearing capacity of surface strip foundations on geogrid-reinforced sand and clay- a comparative study. *Geotechnical and Geological Engineering*, **12**, 1-14. DOI: 10.1007/BF00425933.
- Dasgupta, S., Mukhopadhyay, M. and Nandy, D. R.** (1987). Active–transverse features in the central portions of the Himalaya. *Tectonophysics*, **136**, 255264.
- Dasgupta, S., Pande, P., Ganguly, D., Iqbal, Z., Sanyal, K., Venkatraman, N. V., Dasgupta, S., Sural, B., Harendranath, L., Mazumdar, K., Sanyal, S., Roy, A., Das, L. K., Misra, P. S. and Gupta, H.** (2000). *Seismotectonic Atlas of India and its Environs*. Geological survey of India.
- Demir, A., Yildiz, A., Laman, M., and Ornek, M.** (2014). Experimental and numerical analyses of circular footing on geogrid reinforced granular fill underlain by soft clay. *Acta Geotechnica*, **9**(4), 711–723.
- Derham, C. J., Kelly, J. M. and Thomas, A.** (1985). Nonlinear natural rubber bearings for seismic isolation. *Nuclear Engineering and Design*, **84**(3), 417-428. DOI: 10.1016/0029-5493(85)90258-4.
- Drucker, D. C. and Prager, W.** (1952). Soil mechanics and plastic analysis or limit design. *Quarterly of Applied Mathematics*. **10**, 157–165. DOI: 10.1090/qam/48291.
- Dutta, S. C. and Roy, R.** (2002). A critical review on idealization & modeling for interaction among soil–foundation–structure system. *Computers and Structures*, **80**, 1579–1594. DOI: 10.1016/s0045-7949(02)00115-3.

- Ealangi, I.** (2010). Earthquake protection of buildings by seismic isolation. Devices and concepts. *Young Researchers Conference*, Technical University of Civil Engineering Bucharest.
- Edeskar, T.** (2004). *Technical and Environmental Properties of Tyre Shreds Focusing on Ground Engineering Applications*, Ph. D. thesis, Lulea University of Technology, Sweden.
- Edeskar, T.** (2006). *Use of tyre shreds in civil engineering applications technical and environmental properties*. PhD Dissertation. Lulea University of Technology, Department of Civil and Environmental Engineering, Division of Mining and Geotechnical Engineering, Sweden.
- Edil, T. and Bosscher, P.** (1994). Engineering properties of tire chips and soil mixtures. *Geotechnical Testing Journal*, **17**, 453–464. DOI: 10.1520/GTJ10306J.
- Edinçliler, A. and Ayhan, V.** (2010). Influence of tire fiber inclusions on shear strength of sand. *Geosynthetics International*, **17**(4), 183–192. DOI: 10.1680/gein.2010.17.4.183.
- Edinçliler, A., Baykal, G. and Dengili, K.** (2004). Determination of static and dynamic behaviour of recycled materials for highways. *Resources Conservation and Recycling*, **42**(3), 223–237.
- Ehsani, M., Shariatmadari, N., and Mirhosseini, S. M.** (2015). Shear modulus and damping ratio of sand granulated rubber mixtures. *Journal of Central South University*, **22**(8), 3159–3167.
- El Sawwaf, M. A.** (2007). Behaviour of strip footing on geogrid reinforced sand over a soft clay slope. *Geotextiles and Geomembranes*, **25**(1), 50–60.
- El-Sherbiny, R., Youssef, A. and Lotfy, H.** (2013). Triaxial Testing on Saturated Mixtures of Sand and Granulated Rubber. Proceedings of the *Geo-Congress 2013-Stability and Performance of Slopes and Embankments III*, ASCE, 82–91, 2013.
- Esmaeili, M., Zakeri, J. A., Ebrahimi, H. and Sameni, M. K.** (2016). Experimental study on dynamic properties of railway ballast mixed with tire derived aggregate by modal shaker test. *Advances in Mechanical Engineering*, **8**(5), 1–13. DOI: 10.1177/1687814016640245.
- European Tyre and Rubber Manufacturers Association ETRMA (2012).** *Information+Enforcement+Consumer Protection—Annual Report (2011–2012)*. August (2012), Brussels, ([http://www.etrma.org/uploads/Modules/Documentsmanager/etrma-annual-report-2012\\_8\\_def.pdf](http://www.etrma.org/uploads/Modules/Documentsmanager/etrma-annual-report-2012_8_def.pdf)).

- Fakharian, K. and Attar, I. H.** (2007). Static and seismic numerical modeling of geosynthetic-reinforced soil segmental bridge abutments. *Geosynthetics International*, **14**(4), 228–243. DOI: 10.1680/gein.2007.14.4.228.
- Feng, Z. Y. and Sutter, K. G.** (2000). Dynamic properties of granulated rubber / sand mixtures. *Geotechnical Testing Journal*, **23**(3), 338–344. DOI: 10.1520/GTJ11055J.
- Foose, G. J., Benson, C. H. and Bosscher, P. J.** (1996). Sand reinforced with shredded waste tires. *Journal of Geotechnical Engineering*, **122**, 760–767. DOI: 10.1061/(ASCE)0733-9410(1996)122:9(760).
- Fu, R., Coop, M. R. and Li, X. Q.** (2017). Influence of particle type on the mechanics of sand–rubber mixtures. *Journal of Geotechnical and Geoenvironmental Engineering*, **143**(9), 04017059.
- Fu., R., Coop, M. R. and Li, X. Q.** (2014). The mechanics of a compressive sand mixed with tyre rubber, *Geotechnique Letters*, **4**(3), 238–243.
- Fung, Y. C.** (1965). *Foundations of Solid Mechanics*. Englewood Cliffs, NJ: Prentice Hall.
- Garga, V. K. and Shaughnessy, V.** (2000). Tire reinforced earthfill. Part 1: Construction of a test fill, performance, and retaining wall design. *Canadian Geotechnical Journal*. **37**(1), 75–96.
- Gazetas, G.** (1991). Formulas and charts for impedances of surface and embedded foundations. *Journal of Geotechnical Engineering*, **117** (9), 1361- 1381.
- Genan Business & Development A/S.** (2012). Scrap tyres. (<http://www.genan.eu/tyres-2.aspx>) (Apr. 18, 2013).
- Gharehbaghi, S., Salajegheh, E., and Khatibinia, M.** (2012). Evaluation of seismic energy demand of reinforced concrete moment resistant frames considering soil structure interaction effects. Proceedings of the *Eleventh International Conference on Computational Structures*, Croatia.
- Ghazavi, M. and Lavasan, A. A.** (2008). Interference effect of shallow foundations constructed on sand reinforced with geosynthetics. *Geotextiles and Geomembranes*, **26**(5), 404–415. DOI: 10.1016/j.geotexmem.2008.02.003.
- Ghazavi, M. and Sakhi, M. A.** (2005). Influence of optimized tire shreds on shear strength parameters of sand. *International Journal of Geomechanics*, **5**, 58–65. DOI:

10.1061/(ASCE)1532-3641(2005)5:1(58).

**Goswami, P. K., Pant, C. C. and Pandey, S.** (2009). Tectonic controls on the geomorphic evolution of alluvial fans in the Piedmont Zone of the Ganga Plain, Uttarakhand, India. *Journal Earth System Science*, **118**, 245-259.

**Gotteland, P. G.** (2005). Strength characteristics of tyre chips – sand mixtures. *Studia Geotechnica et Mechanica*, **27**(1-2), 55-56.

**Gourvenec, S., Randolph, M. and Kingsnorth, O.** (2006). Undrained bearing capacity of square and rectangular footings. *International Journal of Geomechanics*, **6**(3), 147–157.

**Guido, V. A., Dong, K. G. and Sweeny, A.** (1986). Comparison of geogrid and geotextiles reinforced earth slabs. *Canadian Geotechnical Journal*, **23**(1), 435–440. 10.1139/t86-073.

**Gupta, I. D.** (2006). Delineation of probable seismic sources in India and neighbourhood by a comprehensive analysis of seism tectonic characteristics of the region, *Soil Dynamics and Earthquake Engineering*, **26**, 766–790. DOI: 10.1016/j.soildyn.2005.12.007.

**Haeri, S.M., Hosseini, S.M., Toll, D.G. and Yasrebi, S.S** (2005). The behaviour of an artificially cemented sandy gravel. *Geotechnical and Geological Engineering*, **23**(5), 537–560.

**Han, G., Gong, Q. and Zhou, S.** (2015). Soil arching in a piled embankment under dynamic load. *International Journal of Geomechanics*, **15**(6), 1–7.

**Hardin, B.O. and Drnevich, V.P.** (1972). Shear modulus and damping in soils, design equations and curves. *Journal of the Soil Mechanics and Foundations Division*, ASCE, **98**(SM7), 667-692.

**Harris, D. A.** (1991). *Vibration Isolation Materials BT, Noise Control Manual, Guidelines for Problem Solving in the Industrial / Commercial Acoustical Environment*. Springer, Boston, USA.

**Hazarika, H., Igarashi, N. and Yamada, Y.** (2011). Behaviour of Granular and Compressible Geomaterial Under Cyclic Loading. *5th International Conference on Earthquake Geotechnical Engineering*, Santiago, Chile.

**Hazarika, H., Kohama, E. and Sugano, T.** (2008). Underwater shake table tests on waterfront structures protected with tire chips cushion. *Journal of Geotechnical and Geoenvironmental Engineering*, **134**(12), 1706-1719. DOI: 10.1061/(ASCE)1090-0241(2008)134:12(1706).



- Hazarika, H., Kohama, E., Suzuki, H. and Sugano, T.** (2006). Enhancement of earthquake resistance of structures using tire chips as compressible inclusion. *Report-Port and Airport Research Institute*, **45**(1), 3–28.
- Hazarika, H., Yasuhara, K., Karmokar, A. K. and Mitarai, Y.** (2007). Shake table test on liquefaction prevention using tire chips and sand mixture. *Scrap Tire Derived Geomaterials- Opportunities and Challenges*, Taylor Francis, London, 215–222.
- Hazarika, H., Yasuhara, K., Kikuchi, Y., Karmokar, A. K. and Mitarai, Y.** (2010). Multifaceted potentials of tire-derived three-dimensional geosynthetics in geotechnical applications and their evaluation. *Geotextiles and Geomembranes*, **28**, 303–315. DOI: 10.1016/j.geotexmem.2009.10.011.
- Head, K. H.** (1998). *Manual of Soil Laboratory Testing Volume 3 Effective Stress Tests (Second edition)*. John Wiley, and Sons, Inc., West Sussex.
- Hegde, A. and Sitharam, T. G.** (2013). Experimental and numerical studies on footings supported on geocell reinforced sand and clay beds. *International Journal of Geotechnical Engineering*, **7**, 346–354. DOI: 10.1179/1938636213Z.000000000043.
- Heimdahl, T. and Drescher, A.** (1998). Deformability parameters af shredded tire lightweight fills. Proceedings of the *International Conference on Cold Regions Engineering*, Duluth, MN.
- Houlsby, G. T., Amorosi, A. and Rojas, E.** (2005). Elastic moduli of soil dependent on pressure: A hyperelastic formulation. *Geotechnique*, **55**(5), 383–392. DOI: 10.1680/geot.2005.55.5.383.
- Huang, C. C. and Menq, F. Y.** (1997). Deep-footing and wide-slab effects in reinforced sandy ground. *Journal of Geotechnical and Geoenvironmental Engineering*, **123**, 30–36. DOI: 10.1061/(ASCE)1090-0241(1997)123:1(30).
- Huang, C. C. and Tatsuoka, F.** (1990). Bearing capacity of reinforced horizontal sandy ground. *Geotextiles and Geomembranes*, **9**, 51-82. DOI: 10.1016/0266-1144(90)90005-W.
- Humphrey, D.** (2004). Effectiveness of design guidelines for use of tire derived aggregate as lightweight embankment fill. *Recycle Master Geotechnical*, 61–74.
- Humphrey, D. and Manion, W.** (1992). Properties of tire chips for lightweight fill. Grouting, *Soil Improvement and Geosynthetics*, ASCE, **2**, 1344–1355.



**Humphrey, D. N. and Sandford, T. C.** (1993). Tire shreds as lightweight subgrade fill and retaining wall backfill. Proceedings of the *Symposium on Recovery and Effective Reuse of Discarded Materials and By-Products for Construction of Highway Facilities*, Federal Highway Administration, Washington, DC, pp. 5–87 to 5– 99.

**Humphrey, D. N., Sandford, T. C., Cribbs, M. M., Gharegrat, H. and Manion, W. P.** (1993). Shear strength and compressibility of tire chips for use as retaining wall backfill. *Transportation Research Record No. 1422*, Transportation Research Board, 29–35.

**Hyodo, M., Yamada, S., Orense, R. P., Okamoto, M. and Hazarika, H.** (2007). Undrained cyclic shear properties of tire chip sand mixtures. Proceedings of the *International Workshop on Scrap Tire Derived Geomaterials-Opportunities and Challenges*. Hazarika and Yasuhara Eds. Taylor and Francis, UK, 187–196.

**IS 1498** (1970). *Classification and Identification of Soils for General Engineering Purpose*. Bureau of Indian Standards, New Delhi.

**IS 1904** (1986). *Code of Practice for Design and Construction of Foundations in Soils: General Requirements*. Third Revision. Bureau of Indian Standards, New Delhi.

**IS 2720: Part 13** (1983). *Methods of Test for Soils: Direct Shear Test*. Bureau of Indian Standards (BIS) New Delhi

**IS 2950: Part I** (1981). *Code of Practice for Design and Construction of Raft Foundations- Part I: Design*. Reapproved (2008), Second Revision, Bureau of Indian Standards, New Delhi.

**IS 456: 2000** (2016): *Plain and Reinforced Concrete-Code of Practice*. Bureau of Indian Standards, New Delhi.

**IS 6403** (1981). *Indian Standard Code of Practice for Determination of Breaking Capacity of Shallow Foundations*, First revision, Reapproved (2002), Bureau of Indian Standards, New Delhi.

**IS 8009: Part I** (1976). *Code of Practice for Calculation of Settlements of Foundations - Part I: Shallow Foundations Subjected to Symmetrical Static Vertical Load*, Reapproved (2003), Bureau of Indian Standards, New Delhi.

**IS 875: 1987 Part 1** (2008). *Code of Practice for Design Loads (Other than Earthquake) For Buildings and Structures. Part 1: Dead Loads-Unit Weights of Building Materials and Stored Materials*. Bureau of Indian Standards, New Delhi.

**IS 875: 1987 Part 2** (2008). *Code of Practice for Design Loads (Other than Earthquake) For Buildings and Structures. Part 2: Imposed Loads*. Bureau of Indian Standards, New Delhi.

**IS 1893: Part 1** (2016). *Criteria for Earthquake Resistant Design of Structures: General Provisions and Buildings*. Bureau of Indian Standards (BIS) New Delhi.

**Ishibashi, I.** (1992). Discussion, effect of soil plasticity on cyclic response. *Journal of Geotechnical Engineering*, **118**(5), 830-832.

**Ishihara, K.** (1996). *Soil Behaviour in Earthquake Geotechnics (First edition)*. Oxford Clarendon Press, New York, 1996.

**Jain, S. K.** (2016). Earthquake safety in India: achievements, challenges and opportunities. *Bulletin of Earthquake Engineering*, **14**(5), 1337–1436.

**Jain, S. K. and Thakkar, S. K.** (2004). Application of base isolation for flexible buildings. *13th World Conference on Earthquake Engineering*, Vancouver, B.C, Canada, August, Paper no. 1924.

**Jewell, R. A., Milligan, G. W. E., Sarsby, R. W. and Dubois, D.** (1984). Interaction between soil and geogrids. Proceedings of the *Conference on Polymer Grid Reinforcement*, Thomas Telford Publishing, London, 18-30.

**Jia, J.** (2018). Dynamic and Cyclic Properties of Soils. *Soil Dynamics and Foundation Modeling*, Chapter 2, 75-108. DOI: 10.1007/978-3-319-40358-8\_2.

**Kalpakci, V., Bonab, A. T., Özkan, M. Y. and Gülerce, Z.** (2018). Experimental evaluation of geomembrane/geotextile interface as base isolating system. *Geosynthetics International*, **25**(1), 1–11. DOI: 10.1680/jgein.17.00025.

**Kaneda, K., Hazarika, H. and Yamazaki, H.** (2007). The numerical simulation of earth pressure reduction using tire chips in backfill. In: Hazarika, and Yasuhara (Eds.), *Proceedings of the International Workshop on Scrap Tire Derived Geo- materials opportunities and Challenges*, Yokosuka, Japan, 245-251.

- Kaneko, T., Orense, R. P., Hyodo, M. and Yoshimoto, N.** (2013). Seismic response characteristics of saturated sand deposits mixed with tire chips. *Journal of Geotechnical and Geoenvironmental Engineering*, **139**(4), 633–643. DOI: 10.1061/(ASCE)GT.1943-5606.0000752.
- Karmokar, A.** (2007). Use of scrap tire derived shredded geomaterials in drainage application. Proceedings of the *International Workshop on Scrap Tire Derived Geomaterials—Opportunities and Challenges*, In: Hazarika and Yasuhara (eds), Yokosuka, Japan, 127–138.
- Kawata, S., Hyodo, M., Orense, P., Yamada, S. and Hazarika, H.** (2007). Undrained and drained shear behaviour of sand and tire chips composite material. In: Hazarika and Yasuhara (eds). Proceedings of the *International Workshop on Scrap Tire Derived Geomaterials-Opportunities and Challenges*, Yokosuka, Japan, 277–283.
- Kelly, J. M.** (1991). *Shake table tests of long period isolation system for nuclear facilities at soft soil sites*. UBC/EERC-91/03, University of California at Berkeley.
- Kelly, J. M.** (1996). *Earthquake Resistant Design with Rubber*, 2nd edition, Springer, Verlag, London.
- Kelly, J. M.** (2002). Seismic isolation systems for developing countries. *Earthquake Spectra*, **18**, 385–406.
- Khattari, K. N.** (1987). Great earthquakes, seismicity gaps and potential for earthquake disaster along the Himalayan plate boundary. *Tectonophysics*, **138**(1), 79–92. DOI: 10.1016/0040-1951(87)90067-9..
- Khing, K. H., Das, B. M., Puri, V. K., Cook, E. E. and Yen, S. C.** (1993). The bearing capacity of a strip foundation on geogrid-reinforced sand. *Geotextiles and Geomembranes*, **12**(4), 351–361. DOI: 10.1016/0266-1144(93)90009-d.
- Kim, D. and Yun, C. B.** (2000) Time domain soil structure interaction analysis in two dimensional medium based on analytical frequency dependent infinite elements. *International Journal For Numerical Methods In Engineering*, **47**(7), 1241–1261.
- Kim, H. K., and Santamarina, J. C.** (2008). Sand–rubber mixtures (large rubber chips). *Canadian Geotechnical Journal*, NRC Research Press, **45**(10), 1457–1466.
- Kim, Y. T. and Kang, H. S.** (2011). Engineering characteristics of rubber-added lightweight soil

as a flowable backfill material. *Journal of Materials in Civil Engineering*, **23**(9), 1289–1294.

**Kirar, B., Maheshwari, B. K. and Muley, P.** (2016). Correlation between shear wave velocity ( $V_s$ ) and SPT resistance (N) for Roorkee region. *International Journal of Geosynthetics and Ground Engineering*, **2**(9), 1-11. DOI: 1-11 10.1007/s40891-016-0047-5.

**Kirzhner, F., Rosenhouse, G. and Zimmels, Y.** (2006). Attenuation of noise and vibration caused by underground trains using soil replacement. *Tunneling and Underground Space Technology*, **21**(5), 561-567.

**Kokusho, T.** (1980). Cyclic triaxial test of dynamic soil properties for wide strain range. *Soils and Foundations*, **20**(2), 45–60.

**Konagai, K. and Kim, D.** (2001). Simple evaluation of the effect of seismic isolation by covering a tunnel with a thin flexible Material. *Soil Dynamics and Earthquake Engineering*, **21**, 287–95.

**Kramer, S. L.** (1996). *Geotechnical Earthquake Engineering*. Prentice Hall, New Jersey (NJ).

**Kramer, S. L. and Stewart, J.** (2004). Geotechnical aspects of earthquake hazards in earthquake engineering. *Engineering Seismology to Performance Based Engineering*, by Bozorgnia Y. and Bertero V.V., CRC Press, Chapter: 4.

**Krishnaswami, N. R. and Isaak, N. T.** (1995). Liquefaction analysis of saturated reinforced granular soils. *Journal of Geotechnical Engineering*, **121**(9), 645–651.

**Kuwano, J., Miyata, Y. and Koseki, J.** (2014). Performance of reinforced soil walls during the 2011 Tohoku earthquake. *Geosynthetics International*, **21**(3), 179–196. DOI: 10.1680/gein.14.00008.

**Ladd, R. S.** (1978). Preparing test specimens using under compaction. *Geotechnical Testtesting Journal*, **1**(1), 16–

**Latha, G. M. and Somwanshi, A.** (2009). Effect of reinforcement form on the bearing capacity of square footings on sand. *Geotextiles and Geomembranes*, **27**, 409–422. DOI: 10.1016/j.geotexmem.2009.03.005.

**Lavasan, A. A., Ghazavi, M. and Schanz, T.** (2017). Analysis of interfering circular footings on reinforced soil by physical and numerical approaches considering strain-dependent stiffness. *International Journal of Geomechanics*, **17**(11), 1–14. DOI: 10.1061/(ASCE)GM.1943-

5622.000099.

**Lee, H. J. and Roh, H. S.** (2007). The use of recycled tire chips to minimize dynamic earth pressure during compaction of backfill. *Construction and Building Materials*, **21**(5), 1016-1026.

**Lee, J. H., Salgado, R., Bernal, A. and Lovell, C. W.** (1999). Shredded tires and rubber-sand as lightweight backfill. *Journal of Geotechnical and Geoenvironmental Engineering*, **125**(2), 132–141. DOI: 10.1061/(asce)1090-0241(1999)125:2(132).

**Lee, J., Dodds, J. and Santamarina, J. C.** (2007). Behaviour of rigid-soft particle mixtures. *Journal of Materials in Civil Engineering*, **19**(2), 179–184.

**Li, B., Huang, M. and Zeng, X.** (2016). Dynamic behaviour and liquefaction analysis of recycled-rubber sand mixtures. *Journal of Materials in Civil Engineering*, **28**(11), 1-14. DOI: 10.1061/(ASCE)MT.1943-5533.0001629.

**Li, W., Kwok, C. Y., Sandeep, C. S. and Senetakis, K.** (2019). Sand type effect on the behaviour of sand-granulated rubber mixtures: Integrated study from micro to macro scales. *Powder Technology*, **342**, 907–916.

**Li, Y., Li, J., Tian, T. and Li, W.** (2013). Corrigendum: A highly adjustable magnetorheological elastomer base isolator for applications of real-time adaptive control (2013 Smart Mater. Struct. 22 095020). *Smart Materials and Structures*, **23**(12), 129501. DOI: 10.1088/0964-1726/23/12/129501

**Liu, H. L., Ng, C. W. and Fei, K.** (2007). Performance of a geogrid-reinforced and pile-supported highway embankment over soft clay: Case study. *Journal of Geotechnical and Geoenvironmental Engineering*, **133**(12), 1483–1493. DOI: 10.1061/(ASCE)1090-0241 (2007)133:12(1483).

**Liu, S., Gao, J., Wang, Y. and Weng, L.** (2014). Experimental study on vibration reduction by using soil bags. *Geotextiles and Geomembranes*, **42**(1), 52–62.

**Lysmer, J. and Kuhlemeyer, A. M.** (1969). Finite dynamic model for infinite media. *Journal of Engineering Mechanics Division*, ASCE, 859-877.

**Madhusudhan, B. R., Boominathan, A. and Banerjee, S.** (2017). Static and large-strain dynamic properties of sand–rubber tire shred mixtures. *Journal of Materials in Civil Engineering*, **29**(10), 04017165. DOI: 10.1061/(ASCE)MT.1943-5533.0002016.

- Maheshwari, B. K., Singh, H. P., and Saran, S.** (2012). Effects of reinforcement on liquefaction resistance of solani sand. *Journal of Geotechnical and Geoenvironmental Engineering*, **138**(7), 831–840.
- Masad, E., Taha, R., Ho, C. and Papagiannakis, T.** (1996). Engineering properties of tire/soil mixtures as a lightweight fill material, *Geotechnical Testing Journal*, **19**, 297–304. DOI: 10.1520/GTJ10355J.
- Mashiri, M. S.** (2014). *Monotonic and cyclic behaviour of sand-tyre chip (STCh) mixtures*. Ph.D. thesis, University of Wollongong.
- Mashiri, M. S., Vinod, J. S. and Sheikh, M. N.** (2015). Constitutive model for sand – tire chip mixture. *International Journal of Geomechanics*, **16**(1), 1–10. DOI: 10.1061/(ASCE)GM.1943-5622.0000472.
- Mashiri, S., Vinod, J. S. and Sheikh, M. D.** (2016). Liquefaction potential and dynamic properties of sand-tyre chip (STCh) mixtures. *Geotechnical Testing Journal*, **39**, 69-79.
- Matsumura, K.** (1992). On the intensity measure of strong motions related to structural failure. *Proceedings of the 10th World Conference on Earthquake Engineering*, **1**, 375–380.
- Matsuoka, H., Muramatsu, D. and Liu, S. H.** (2005). Reduction of traffic induced vibration by soil bags. *Proceedings of 16th International Conference on Soil Mechanics and Geotechnical Engineering*, Japan, 1381- 1384.
- Mavronicola, E., Komodromos, P. and Charmpis, D.** (2010). Numerical investigation of potential usage of rubber soil mixtures as a distributed seismic isolation approach. In: Topping, B. H. V., Adam, J. M., Pallares, F. J., Bru, R. and Romero, M.L. (Eds.), *Proceedings, Tenth International Conference on Computational Structures Technology*. Civil-Comp Press, Stirlingshire, Paper no.168. DOI: 10.4203/ ccp.93.168.
- Mayes, R. L. and Naeim, F.** (2001). *Design of Structures with Seismic Isolation: The Seismic Design Handbook*. Springer, USA. 723-755.
- Medeot, R.** (2004). Re-centering capability evaluation of seismic isolation systems based on energy concepts. *13th World Conference on Earthquake Engineering*, Vancouver, B.C, Canada, paper no. 3106.



- Michalowski, R. L.** (2004). Limit loads on reinforced foundation soils. *Journal of Geotechnical and Geoenvironmental Engineering*, **130**(4): 381-390. DOI: 10.1061/(ASCE)1090-0241(2004)130:4(381).
- Mittal, S. and Chauhan, R.** (2013). Liquefaction behaviour of reinforced saturated sand under dynamic conditions. *International Journal of Geotechnical Engineering*, **7**(1), 109–114.
- Mokha, A., Constantinou, M. C., Reinhorn, A. M. and Zayas, V. A.** (1991). Experimental study of friction-pendulum isolation system. *Journal of Structural Engineering*, **117**(4), 1201–1217.
- Murali-K, A., and Madhavi, L. G.** (2012). Modeling the dynamic response of wrap faced reinforced soil retaining walls. *International Journal of Geomechanics*, **12**(4), 439–450.
- Murillo, C., Thorel, L. and Caicedo, B.** (2009). Ground vibration isolation with geofoam barriers: Centrifuge modeling. *Geotextiles and Geomembranes*, **27**(6), 423–434.
- Naeim, F. and Kelly, J. M.** (1999). *Design of Seismic Isolated Structures: From Theory to Practice*, 1st Edition, John Wiley Sons and Hoboken, NJ, USA.
- Nakagawa, Y., Chen, G.L., Tatsui, T. and Chida, S.** (2009). Verification of vibration reduction characteristics with soil bag structure. Proceeding of *4th Asia Regional Conference on Geosynthetics*, China, 603-608.
- Nakhaei, A., Marandi, S. M., Kermani, S. S., and Bagheripour, M. H.** (2012). Dynamic properties of granular soils mixed with granulated rubber. *Soil Dynamics and Earthquake Engineering*, **43**(4), 124–132.
- NBC** (2016). *National Building Code of India*. Bureau of Indian Standards (BIS) New Delhi.
- Ngo, A. T. and Valdes J. R.** (2007). Creep of sand-rubber mixtures. *Journal of Materials in Civil Engineering*, **19**(12): 1101–1105. DOI: 10.1061/(ASCE)0899-1561(2007)19:12(1101).
- Nguyen, Q. Van, Fatahi, B. and Hokmabadi, A. S.** (2016). The effects of foundation size on the seismic performance of buildings considering the soil-foundation-structure interaction. *Structural Engineering and Mechanics*, **58**(6), 1045–1075. DOI: 10.12989/sem.2016.58.6.1045.
- Novak, M. and Henderson, P.** (1989). Base-isolated buildings with soil-structure interaction. *Earthquake Engineering and Structural Dynamics*, **18**, 751-765.



- Okamoto, M., Orense, R., Hyodo, M. and Kuwata, J.** (2008). Monotonic shear behaviour of sand tyre chips mixtures. *Proceedings of 18th NZGS Geotechnical Symposium on Soil Structure Interaction*. Ed. CY Chin, Auckland.
- Okur, D. V. and Umu, S. U.** (2018). Dynamic properties of clean sand modified with granulated rubber. *Advances in Civil Engineering*, 5209494,1- 11. DOI: 10.1155/2018/5209494
- Omar, M. T., Das, B. M., Puri, V. K. and Yen, S.C.** (1993). Ultimate bearing capacity of shallow foundations on sand with geogrid reinforcement. *Canadian Geotechnical Journal*, **30**, 545–549.
- Pamukcu, S. and Akbulut, S.** (2006). Thermoelastic enhancement of damping of sand using synthetic ground rubber. *Journal of Geotechnical and Geoenvironment Engineering*, **132**(4), 501–510.
- Perez, J. C. L., Kwok, C. Y. and Senetakis, K.** (2017). Micromechanical analyses of the effect of rubber size and content on sand-rubber mixtures at the critical state. *Geotextiles and Geomembranes*, **45**(2), 81–97.
- Perez, L. J. C., Kwoka, C.Y. and Senetakis, K.** (2016). Effect of rubber size on the behaviour of sand-rubber mixtures: A numerical investigation. *Computers and Geotechnics*, **80**,199–214.
- Pitilakis, D., Razavi, M. F. A. and Clouteau, D.** (2013). Equivalent linear dynamic impedance functions of surface foundations. *Journal of Geotechnical and Geoenvironmental Engineering*, **139**, 1130–1139.
- Pitilakis, K., Karapetrou, S. and Tsagdi, K.** (2015). Numerical investigation of the seismic response of RC buildings on soil replaced with rubber-sand mixtures. *Soil Dynamics and Earthquake Engineering*, **79**, 237–252. DOI: 10.1016/j.soildyn.2015.09.018.
- Poh, P. S. H. and Broms, B. B.** (1995). Slope stabilization using old rubber tires and geotextiles. *Journal of Performance of Constructed Facilities*, **9**(1), 76–79. DOI: 10.1061/(ASCE) 0887-3828(1995).
- Prasad, B. D., Hariprasad, C. and Umashankar, B.** (2016). Load-settlement response of square footing on geogrid reinforced layered granular beds. *International Journal of Geosynthetics and Ground Engineering*, **2**, 1-28. DOI: 10.1007/s40891-016-0070-6.
- Promptthangkoon, P. and Hyde, A. F. L.** (2007). Compressibility and liquefaction potential

of rubber composite soils. Proceedings of *International Workshop on Tire Derived GeoMaterials*, Kurihama, Japan.

**Raghukanth, S. T. G.** (2008). Simulation of strong ground motion during the (1950) great Assam earthquake. *Pure and Applied Geophysics*, **165**(9-10), 1761-1787.

**Raghukanth, S. T. G. and Kavitha, B.** (2014). Ground motion relations for active regions in India. *Pure and Applied Geophysics*, **171**(9), 2241–2275. DOI: 10.1007/s00024-014-0807-x.

**Rao, G. V. and Dutta, R. K.** (2006). Compressibility and strength behaviour of sand-tire chip mixtures. *Geotechnical and Geological Engineering*, **24**(3), 711–724. DOI: 10.1007/s10706-004-4006-x.

**Reddy, K. R. and Saichek, R. E.** (1998). Characterization and performance assessment of shredded scrap tires as leachate drainage material in landfills. Proceedings of the *14th International Conference on Solid Waste Technology and Management*, Philadelphia, USA.

**Roeder, C. W., Stanton, J. F. and Taylor, A. W.** (1990). Fatigue of steel-reinforced elastomeric bearings. *Journal of Structural Engineering*. **116**(2), 407–26.

**Rowe, R. and McIsaac, R.** (2005). Clogging of tire shreds and gravel permeated with landfill leachate. *Journal of Geotechnical and Geoenvironmental Engineering*, **131**(6).

**Saha Roy, S. and Deb, K.** (2017). Bearing capacity of rectangular footings on multilayer geosynthetic-reinforced granular fill over soft soil. *International Journal of Geomechanics*, **17**(9), 04017069. DOI: 10.1061/(ASCE)GM.1943-5622.0000959.

**Sakaguchi, M.** (1996). A study of the seismic behaviour of geosynthetic reinforced walls in Japan. *Geosynthetics International*, **3**(1), 13–30. DOI: 10.1680/gein.3.0051.

**Sasso, M., Palmieri G., Chiappini, G. and Amodio, D.** (2008). Characterization of hyperelastic rubber-like materials by biaxial and uniaxial stretching tests based on optical methods. *Polymer Testing*, **27**(8), 995-1004. DOI: 10.1016/j. polymertesting.2008.09.001.

**Senetakis, K. and Anastasiadis, A.** (2015). Effects of state of test sample, specimen geometry and sample preparation on dynamic properties of rubber–sand mixtures. *Geosynthetics International*, **22**(4), 301–310. DOI: 10.1680/gein.15.00013.

- Senetakis, K., Anastasiadis, A. and Pitilakis, K.** (2012). Dynamic properties of dry sand/rubber (SRM) and gravel/rubber (GRM) mixtures in a wide range of shearing strain amplitudes. *Soil Dynamics and Earthquake Engineering*, **33**(1), 38–53. DOI: 10.1016/j.soildyn.2011.10.003.
- Senetakis, K., Anastasiadis, A., Trevelopoulos, K. and Pitilakis, K.** (2009). Dynamic response of SDOF systems on soil replaced with sand/rubber mixture. Proceedings of the *ECOMAS Thematic Conference on Computation Methods in Structural Dynamics and Earthquake Engineering*, Rhodes, Greece.
- Senthen Amuthan, M., Boominathan, A. and Banerjee, S.** (2018). Density and shear strength of particulate rubber mixed with sand and fly ash. *Journal of Materials in Civil Engineering*, **30**(7), 1–13. DOI: 10.1061/(ASCE)MT.1943-5533.0002322.
- Sheikh, M. N., Mashiri, M. S., Vinod, J. S. and Tsang, H. H.** (2013). Shear and compressibility behaviours of sand-tyre crumb mixtures. *Journal of Materials in Civil Engineering*, **25**(10). 1366–1374. DOI: 10.1061/(ASCE)MT.1943-5533.0000696.
- Shin, E. C., Das, B. M., Lee, E. and Atalar, C.** (2002). Bearing capacity of embedded strip foundation on geogrid-reinforced sand. *Geotextiles and Geomembranes*, **20**, 169–180. DOI: 10.1016/j.geotextmem.2005.02.001.
- Shrestha, S., Ravichandran, N., Raveendra, M. and Attenhofer, J.A.** (2016) Design and analysis of retaining wall backfilled with shredded tire and subjected to earthquake shaking. *Soil Dynamics and Earthquake Engineering*, **90**, 227-239.
- Skinner, R. I., Robinson, W. H. and McVerry, G. H.** (1993). *An introduction to Seismic Isolation*, Wiley, New York.
- Sridharan, A. and Sivapullaiah, P. V.** (2005). Mini compaction test apparatus for fine grained soils. *Geotechnical Testing Journal*, **28**(3), 240–246.
- Sukontasukkul, P., and Tiamlom, K.** (2012). Expansion under water and drying shrinkage of rubberized concrete mixed with crumb rubber of different sizes. *Construction and Building materials*, **29**, 520-526.
- Tafreshi, S. N. M. and Dawson, A. R.** (2010). Comparison of bearing capacity of a strip footing on sand with geocell and with planar forms of geotextile reinforcement. *Geotextiles and Geomembranes*, **28**(1), 72–84.

- Taha, A., Naggar, M. H. E and Turan, A.** (2015). Experimental study on the seismic behaviour of geosynthetic-reinforced pile-foundation system. *Geosynthetics International*, **22**(2), 183–195. DOI: 10.1680/gein.15.00004.
- Tanchaisawat, T., Bergado, D. T., Voottipruex, P. and Shehzad, K.** (2010). Interaction between geogrid reinforcement and tire chip sand lightweight backfill. *Geotextiles and Geomembranes*, **28**(1), 119–127.
- Tatliso, N., Edil, T. B. and Benson, C. H.** (1998). Interaction between reinforcing geosynthetics and soil-tire chip mixtures. *Journal of Geotechnical and Geoenvironmental Engineering*, **124**(11), 1109–1119. DOI: 10.1061/(ASCE)1090-0241(1998)124:11(1109).
- Thompson, A. C. T.** (1998). High damping rubber seismic isolation bearings – behaviour and design implications. CE299 Report, University of California, Berkeley.
- Torunbalci, N.** (2004). Seismic isolation and energy dissipating systems in earthquake resistant design. *13<sup>th</sup> World Conference on Earthquake Engineering, 13WCEE*, Vancouver, Canada, Paper no. 3273.
- Tsang, H. Ho., Sheikh, M. and Lam, N.** (2007). Rubber-soil cushion for earthquake protection. *Australian Earthquake Engineering Society Conference*, 1-8.
- Tsang, H., Lo, S. H., Xu, X and Sheikh, M. N.** (2012). Seismic isolation for low-to-medium-rise buildings using granulated rubber – soil mixtures: numerical study. *Earthquake Engineering and Structural Dynamics*, **41**, 2009–2024. DOI: 1002/eqe.2171.
- Tsoi, W.Y. and Lee, K. M.** (2011). Mechanical properties of cemented scrap rubber tyre chips. *Geotechnique*, **61**(2), 133-141.
- Uchumira, T., Chi, N., Nirmalan, S., Sato, T., Meidani, M. and Towhata, I.** (2007). Shaking table tests on effect of tire chips and sand mixture in increasing liquefaction resistance and mitigating uplift of pipe. In Hazarika, and Yasuhara (Eds.), *Proceedings, International Workshop on Scrap Tire Derived Geomaterials opportunities and Challenges*, Yokosuka, Japan, 179-186.
- Umashankar, B., Yoon, S., Prezzi, M. and Salgado, R.** (2014). Pullout response of uniaxial geogrid in tire shred-sand mixtures. *Geotechnical and Geological Engineering*, **32**(2), 505–523. DOI:10.1007/s10706-014-9731-1.

- Valdiya K. S.** (2016). Indo-Gangetic Plains: Evolution and Later Developments. *The Making of India*, Society of Earth Scientists Series, Springer. DOI: 10.1007/978-3-319-25029-8\_22.
- Valdiya, K. S.** (1976). Himalayan transverse faults and folds and their parallelism with subsurface structures of North Indian plains. *Tectonophysics*, **32**, 353–386. DOI: 10.1016/0040-1951(76)90069-x.
- Vercueil, D., Billet, P. and Cordary, D.** (1997). Study of the liquefaction resistance of a saturated sand reinforced with geosynthetics. *Journal of Soil Dynamic and Earthquake Engineering*, **16**(7–8), 417–425.
- Viswanadham, B. V. S. and König, D.** (2004). Studies on scaling and instrumentation of a geogrid. *Geotextiles and Geomembranes*, **22**(5), DOI: 307–328. 10.1016/S0266-1144(03)00045-1.
- Wang, C., Deng, A. and Taheri, A.** (2018). Digital image processing on segregation of rubber sand mixture. *International Journal of Geomechanics*, **18**(10), 1–13. DOI: 10.1061/(ASCE)GM.1943-5622.0001269.
- Webster, A. C.** (1994). *Technological Advance in Japanese Building Design and Construction*. ASCE Press. DOI: 10.1061/9780872629325.
- Wiszniewski, M and Cabalar A. F.** (2016). Applications of permeability, oedometer and direct shear tests to the sand mixed with waste tire crumb. *Acta Scientiarum Polonorum*, **15**(1), 69–82.
- Wolf, J. P.** (1997). Spring dashpot mass models for foundation vibrations. *Earthquake Engineering and Structural Dynamics*, **26**, 231–949.
- Wolf, J. P. and Song, C.** (1996). *Finite-Element Modeling of Unbounded Media*, John Wiley & Sons, West Sussex: England.
- Wood, D. M.** (2004). *Geotechnical Modelling*. Taylor & Francis. DOI: 10.4324/9780203477977.
- Woods, R. D.** (1968). Screening of surface waves in soils. *Journal of the Soil Mechanics and Foundations Division*, ASCE, **94** (SM4), 951–979.
- Wu W. Y., Benda, C. C. and Cauley, R.F.** (1997) Triaxial determination of shear strength of tire chips. *Journal Geotechnical and Geoenvironment Engineering*, **123**(5), 479–482.

- Xiao, H., Butterworth, J. W. and Larkin, T.** (2004). Low-technology techniques for seismic isolation. *NZSEE Conference*, Auckland, New Zealand.
- Xiong, W. and Li, Y.** (2013). Seismic isolation using granulated tire–soil mixtures for less-developed regions: experimental validation. *Earthquake Engineering and Structural Dynamics*, **42**, 2187–2193. DOI: 10.1002/eqe.2315.
- Xu, C., Song, S. and Han, J.** (2015). Scaled model tests on influence factors of full geosynthetic reinforced pile supported embankments. *Geosynthetics International*, **23**, 140–153.
- Xu, R. and Fatahi, B.** (2018a). Influence of geotextile arrangement on seismic performance of mid-rise buildings subjected to MCE shaking. *Geotextiles and Geomembranes*, **46**(4), 511–528. DOI: 10.1016/j.geotexmem.2018.04.004.
- Xu, R. and Fatahi, B.** (2018b). Geosynthetic-reinforced cushioned piles with controlled rocking for seismic safeguarding. *Geosynthetics International*, **00**, DOI: 1–21.10.1680/ jgein.18.00018.
- Xu, X., Lo, S. H., Tsang, H. H. and Sheik, M. N.** (2009). Earthquake protection by tire-soil mixtures numerical study, Proceedings of the *New Zealand Society for Earthquake Engineering*, New Zealand.
- Yamamoto, K. and Otani, J.** (2002). Bearing capacity and failure mechanism of reinforced foundations based on rigid plastic finite element formulation. *Geotextiles and Geomembranes*, **20**(6), 367–393.
- Yazici, G.** (2014). Parametric study of the seismic response of base isolated liquid storage tanks with lead-core elastomeric bearings. *Acta Physica Polonica Series*, **125**, 382–384.
- Yegian, M. K. and Kadakal, U.** (2004). Foundation isolation for seismic protection using a smooth synthetic liner. *Journal of Geotechnical and Geo-Environmental Engineering*, **130**(11), 1121–1130.
- Yetimoglu, T. Wu, J. T. H. and Saglamer, A.** (1994). Bearing capacity of rectangular footings on geogrid-reinforced sand. *Journal of Geotechnical Engineering*, **120**, 2083–2099. DOI: 10.1061/(ASCE)0733-9410(1996)122:4(326).

- Youwai, S. and Bergado, D. T.** (2003). Strength and deformation characteristics of shredded rubber tire – sand mixtures. *Canadian Geotechnical Journal*, **40**, 254–264. DOI: 10.1139/T02-104.
- Youwai, S., Bergado, D. T. and Supawiwat, N.** (2004). Interaction between hexagonal wire reinforcement and rubber tire chips with and without sand mixture. *Geotechnical Testing Journal*, **27**(3), 1–9.
- Zarnani, S. and Bathurst, R. J.** (2008). Numerical modeling of EPS seismic buffer shake table tests. *Geotextiles and Geomembranes*, **26**(5), 371-383.
- Zayas, V.** (1987). The FPB earthquake resisting system. *Report No. UCB/EERC-87/01*, Earthquake Engineering Research Center, Berkley, Canada.
- Zhou F. L., Stiemer, S. F. and Cherry, S.** (1990). A new isolation and energy dissipating system for earthquake resistant structures. *Proceeding of 9th European Conference on Earthquake Engineering*, Moscow, 223-230.
- Zienkiewicz, O. C., Bando, K., Betress, P., Emson, C. and Chiam, T. C.** (1985). Mapped infinite elements for exterior wave problems. *International Journal for Numerical Methods in Engineering*, **21**(7), 1229–1251.
- Zornberg, J. G., Cabral, A. R. and Viratjandr, C.** (2004). Behaviour of tire shred-sand mixtures. *Canadian Geotechnical Journal*, **41**, 227–241. DOI: 10.1139/t03-086.
- .



## LIST OF PUBLICATIONS BASED ON THIS THESIS

### REFEREED JOURNALS

- (a) **Dhanya, J. S.**, Boominathan, A. & Banerjee, S. (2019). Performance of geo-base isolation system with geogrid reinforcement, *International Journal of Geomechanics*, ASCE, 19(7), 1-13. DOI:10.1061/(ASCE)GM.1943-5622.0001469.
- (b) **Dhanya, J. S.**, Boominathan, A. & Banerjee, S. Geogrid reinforced geo-isolation layer for seismic protection of low-rise building in the Indo-Gangetic plain. *Geosynthetics International* (under review).

### CONFERENCE PROCEEDINGS AND CHAPTERS INTERNATIONAL

- (a) Boominathan, A., Banerjee, S. and **Dhanya, J.S.** (2019). Geo-base isolation system with geogrid reinforcement for low-rise buildings. *Proceeding in Earth and Geosciences: Geotechnics Fundamentals and Applications in Construction*, CRC Press, Taylor and Francis, Vol.2, 86-92.
- (b) **Dhanya, J.S.**, Boominathan, A. and Banerjee, S. (2018). SSI study of low-rise building placed on sand-rubber mixture isolation layer, *16th European Conference on Earthquake Engineering*, Thessaloniki, Greece, June 2018, Paper no. 11712.
- (c) **Dhanya, J.S.**, Boominathan, A. and Banerjee, S. (2017). Response of soil-tyre mixture subjected to cyclic loading, *16th World Conference on Earthquake Engineering*, Santiago, Chili, 9-13 January 2017, Paper no. 1662.
- (d) Boominathan, A., Banerjee, S. and **Dhanya, J.S.** (2015). Performance of soil-rubber tyre scrap mixture as seismic base isolators for foundations, *Proceedings of the 6<sup>th</sup> International Conference on Earthquake Geotechnical Engineering*, Christchurch, New Zealand, Paper no.593.

### NATIONAL

- (a) Boominathan, A., Madhusudhan B.R., **Dhanya, J.S** (2018). An innovative geomaterial for seismic isolation of low-rise buildings. *16th Symposium on Earthquake Engineering*, IIT Roorkee, India.
- (b) **Dhanya, J.S.**, Boominathan, A. and Banerjee, S. (2018). FE study on the seismic response of geo-isolated RC buildings, *Indian Geotechnical Conference 2018*, Guwahati. Paper no. 654.

## **DOCTORAL COMMITTEE**

### **CHAIRPERSON**

Dr. K. Ramamurthy  
Professor and Head  
Department of Civil Engineering

### **GUIDE**

Dr. Boominathan A.  
Professor  
Department of Civil Engineering

Dr. Subhdeep Banerjee  
Associate Professor  
Department of Civil Engineering

### **MEMBERS**

Dr. Arun Menon  
Associate Professor  
Department of Civil Engineering

Dr. Rupen Goswami  
Associate Professor  
Department of Civil Engineering

Dr. Sujatha C  
Professor  
Department of Applied Mechanics

## CURRICULUM VITAE

Name : Dhanya J S

Date of birth : May 27, 1988

### **Educational qualifications**

**2010 : Bachelor of Engineering (B.E.)**

Institution : Thiagarajar College of Engineering  
Madurai, Tamil Nadu, India

Specialization : Civil Engineering

**2012 : Master of Engineering (M.E.)**

Institution : Anna University: College of Engineering Guindy,  
Chennai, India

Specialization : Geotechnical Engineering

**2019 : Doctor of Philosophy (Ph.D.)**

Institution : Indian Institute of Technology Madras,  
Chennai, India

Specialization : Soil Dynamics and Earthquake Engineering  
Civil Engineering